The University Of Sheffield.

Identification and characterisation of novel molecular players in mechanotransduction

Pei Li Tseng

A thesis submitted in partial fulfilment of the requirements for the degree of

Doctor of Philosophy

The University of Sheffield

Faculty of Science

Department of Biomedical Science

December 2021

Abstract

Cells sense and respond to the stiffness of the surrounding extracellular matrix (ECM) or sense and respond to forces elicited from adjacent cells and convert them into biological signals in a process known as mechanotransduction. In addition to propagating mechanical cues through remodelling of cytoskeleton stress fibres, cells rely on mechano-activated shuttling of proteins between the nucleus and the cytosol regulating gene expression that underpins multiple cellular behaviours such as proliferation, differentiation and migration. Already several proteins, including transcriptional regulators YAP/TAZ, have been identified to shuttle between the nucleus and cytosol depending on the presence of specific mechanical stimuli. However, the regulators and mechanisms of mechanotransduction are not fully understood.

In this project, we established a screen by manipulating RhoA activity coupled with nuclear proteome specific proximity biotinylation and mass spectrometry analysis to search for mechanotransducers with nuclear function. This screen revealed 102 proteins significantly enriched in the nucleus after RhoA activation. A Gene Ontology analysis showed that most of the proteins are correlated with RNA regulation at both transcriptional and translational level such as RNA splicing and gene translation. Immunoblot analysis of selected protein candidates including the RNA splicing regulators PCBP1 and PTBP1 verified their nuclear enrichment was promoted by RhoA activity. The further investigation of PCBP1 and PTBP1 showed that the subcellular localization of PCBP1 and PTBP1 are regulated by ECM stiffness and cell density. Furthermore, RT-PCR experiments indicated that ECM stiffness may regulate alternative splicing through PCBP1 and PTBP1 activity. We therefore suggest that PCBP1 and PTBP1 are potential mechanoregulators and play a role in ECM stiffness-mediated alternative splicing.

Acknowledgement

I would like to express my deepest gratitude to my supervisor, Dr Kai Erdmann, who has always given his brilliant insight and guidance that inspire me and keep me moving on the way becoming a scientist. The procedure is not easy, fulling of challenge and stress, but Kai's unwavering support and patience has helped me overcome numerous obstacles, one after another. As a supervisor, his stimulating scientific discussion has always driven me to explore more profound idea of my research. He is also a mentor and a friend that helped me gradually build up confidence. Without Kai's support and guidance, I would not go through my PhD and complete my thesis.

I would also like to warmly thank my advisor Dr Mark Collins and Dr Ivana Barbaric whose support and continuous advice were invaluable during my PhD. My particular thank goes to Mark, who's been a tremendous help to my mass spectrometry experiments and data analysis. In addition, I would like to thank Dr Chun Guo for his encouragement and cheerful chatting that gave me a lot of fun, especially at my weekend work. I would also thank him for kindly letting me use his UV light for our pilot experiments, which is very useful for my subsequent study.

I would like to acknowledge all the advice and help from Dr Jason King and Dr Andrew Peden as well as their lab members. Thank you for providing a friendly and supportive environment on D-floor to work in. I would also like to thank all the people from Biomedical Science department of University of Sheffield who are happy to help, providing reagents or giving advice for solving technical issue.

My heartfelt thank goes to our past and current lab members, Agnieszka, Claire, Toni, Sindhu, Kinga, Andrew, Ahmed, Mubarak and Weiwei for their emotional and moral support during my PhD. I particularly like to thank Claire Murzeau for teaching me all the techniques and providing me constructive advice. Having discussion with her always gave me great inspiration and imaginative thinking in my project. In addition, my deepest appreciation goes to my amazing lab mate, Andrew Wood, with whom I shared most of the good and bad times

through my PhD. I also want to thank Andrew for sharing the numerous happy lunches with me, which really added a lot of fun to my challenging while sometimes tough days

This work would not have been easy without the unwavering support of my husband Chun-Lin Yeh. I would like to express my huge thank to him for taking care of our children and organizing all important family schedules. I also like to acknowledge his contribution to editing of the content lists of my thesis.

Finally, my deepest heartfelt thanks go to my parents and sister whose constant, selfless love a strongest support for me to pursue my dream. Especially my parents, who always encourage me never give up when I encounter a challenge. They are the role models for me in the past, present, and future. Without their love and support, I would not complete my PhD.

Declaration

I declare that my thesis entitled "**Identification and characterisation of novel molecular players in mechanotransduction**" is entirely composed by myself. All the results in the thesis have been carried out by myself unless otherwise stated by reference or acknowledgement. Figures acquired from other publications or sources have been clearly acknowledged. I confirm that this work has been done in my candidacy for a research degree at The University of Sheffield. Neither any part of this work has been submitted or published.

Pei-Li Tseng
September 2021

Table of Contents

List of Figures

List of Tables

Abbreviation

3'UTR: 3' untranslated region

5'UTR: 5' untranslated region

AJs: Adherens junctions

ANOVA: Analysis of Variance

APS: Ammonium persulfate

AS: Alternative splicing

CA-RhoA: constitutively active RhoA

CIP: Calf intestinal alkaline phosphatase

Dab2: Disabled-2

DC assay: Detergent compatible protein assay

DMEM: Dulbecco's Modified Eagle Medium

DMSO: Dimethyl sulfoxide

DN-RhoA: Dominantly negative RhoA

DNA: Deoxyribonucleic acid

dNTPs: Deoxynucleotide triphosphates

E. coli: Escherichia coli

ECM: Extracellular matrix

EDB-FN: Extradomain B fibronectin

EDTA: Ethylenediaminetetra acetic acid

EGF: Epidermal growth factor

EMT: Epithelial-mesenchymal transition

EtOH: Ethanol

FAK: Focal-adhesion kinase

FAs: Focal adhesions

FBS: Focal bovin serum

FWD: Forward

GFP: Green fluorescence protein

HBSS: Hanks' Balanced Salt Solution

HF: High fidelity

hnRNPs: Heterogeneous nuclear ribonucleoproteins

HS: Horse serum

IF: Immunofluorescence

ILEI: Interleukin-like EMT inducer

IRES: Internal ribosome entry site

KD: Knockdown

KH domain: K Homology domain

Lat A: Latrunculin A

LATS1/2: Large tumour suppressor homolog ½

LINC: Linker of Nucleocytoskeleton and Cytoskeleton

MDCK: Madin-Darby canin kidney cell line

MeOH: Methanol

mM: mmol/L

MST1/2: Mammalian sterile 20-like ½

MW: Molecular weight

NES: Nuclear export signal sequencez1uju8

NLS: Nuclear localization signal sequence

NP-40: 4-Nonylphenyl-polyethylene glycol, Nonidet PTM 40

Oligo: Oligonucleotides

PAA gel: Polyacrylamide gel

PAK-1: Serine/threonine-protein kinase1

PBS: Phosphate buffered saline

PBST: Phosphate buffered saline with Tween 20

PCBP1: Poly(rC) Binding Protein 1

PCR: Polymerase chain reaction

PDMS: Polydimethylsiloxane

PI3K: Phosphoinositide 3-kinase

PKA: Protein kinase A

PKM1: Pyruvate kinase M isoform 1

PKM2: Pyruvate kinase M isoform 2

PRR: Proline-rich region

PTBP1: Polypyrimidine Tract Binding protein 1

RE: Restriction enzyme

REV: Reverse

RhoA: Ras homolog gene family A

RIPA: Radioimmunoprecipitation assay

RNA-seq: RNA sequencing

RNA: Ribonucleic acid

ROCK: RhoA kinase

RRM: RNA recognition motif

SDS-PAGE: Sodium dodecyl sulphate polyacrylamide gel electrophoresis

Ser: Serine

SFK: Src family kinase

siRNA: Small interfering RNA

SRp40: Serine arginine rich protein 40

TAZ: Transcriptional co-activator with PDZ binding motif

TGF-β: Transforming growth factor β

Thr: Threonine

VEGF: Vascular endothelial growth factor

YAP: Yes associated protein

1. Chapter 1 – Introduction

1.1 Cellular Mechanotransduction-overview

Under physiological conditions, cells not only perceive chemical signals but also continuously experience a myriad of mechanical forces from the microenvironment. The process in which cells sense and convert the mechanical stimuli into biochemical signalling which elicit various cell behaviours is known as mechanotransduction. The overall process of mechanotransduction is carried out by mechanosensing eliciting a mechanoresponse. Through sensor molecules, cells detect mechanical forces from neighbouring cells, sense the physical properties of extracellular matrix (ECM), or respond to fluid shear stress caused by blood flow. The mechanical signals are then propagated within cells by inducing alterations of cytoskeletal filament structures. The mechanical force from extracellular environment is also coupled to the nucleus through the Linker of Nucleoskeleton and Cytoskeleton (LINC) complex, inducing nuclear deformation and activating mechanosensitive genes related to multiple cellular and developmental processes [1, 2]

Many cellular functions and tissue homeostasis are tightly orchestrated by the crosstalk between cells and physical properties arising from their microenvironment. It has been recognized that many facets of cellular and developmental processes such as morphology, proliferation, differentiation and migration are closely correlated to cell's sensing and interpreting the mechanical characteristics from its microenvironment [3-5]. Aberrant mechanosignalling is often implicated in various diseases such as cancer, fibrosis and atherosclerosis [6-8]. However, the regulators and mechanisms of mechanotransduction are not fully understood.

Chapter 1 of my thesis gives an overview of cellular mechanotransduction, which includes the molecular components and mechanisms underlying mechanical perception at the level of cell-ECM and cell-cell interactions. We discuss how mechanical forces lead to the dynamical changes of cytoskeletal stress fibres, in which RhoA/ROCK pathway plays a key role in the remodelling of actin cytoskeletal stress fibres. With respect to conversion of mechanical stimuli to cell-specific genetic programmes, we also highlight the role of YAP/TAZ as mechanotransducers as they shuttle between the nucleus and cytoplasm to regulate multiple genes in response to mechanical stress.

1.2 Mechanotransduction at Cell-ECM interaction site

Most cells are anchorage dependent and need to adhere to the combination of their adjacent cells and surrounding extracellular matrix (ECM) to prevent inappropriate cell proliferation and apoptosis. ECM is a three-dimensional, non-cellular network that presents between cells and tissues. In addition to providing essential mechanical support for the cellular assembly and tissue integrity, the dynamic and constant remodelling structure of ECM also impose mechanical stimuli to cells [9].

Cells probe physical properties of the ECM through mechanosensitive complexes named focal adhesions (FAs). FAs are the direct contact sites of cells to their surrounding ECM, act as bridge between the ECM and intracellular actomyosin machinery [9]. The mechanosensitive properties of FAs enable cells to respond and transfer mechanical cues from the ECM to cytoskeletal stress fibres [9]. The structures of FAs are mainly composed of transmembrane receptors termed integrins and a variety of adaptor and signalling proteins. Upon changes of ECM rigidity, the mechanical signals from the ECM induce activation and clustering of integrins, which in turn leads to recruitment of other adaptor and signalling proteins. These proteins aggregate at integrin-ECM binding sites to form a dense and dynamic structure termed adhesomes which also link to the termini of actin stress fibres, causing reorganization of cytoskeleton and triggering multiple signalling pathways which eventually determine cell fate [1, 2, 10, 11].

1.2.1 Integrin mediates formation of mechanical force-dependent adhesion structure

Integrins are the major receptors of the ECM which mediate the physical connection of the extracellular and intracellular compartments. Integrins are transmembrane heterodimers composed of α and β subunits. There are at least 18 α and 8 β subunits in mammals, generating 24 distinct integrins through different combination of the α and β subunits [12]. Integrin receptors have distinct domain structures. The extracellular domains of each subunit recognize specific sets of ECM ligands such as RGD tripeptide in fibronectin, collagen, and laminin, while the cytoplasmic tails connect to actin cytoskeleton and intermediate filaments through a number of signalling proteins [1, 12]. Activation of integrin usually occurs by ligand binding to the extracellular domains, causing conformational changes in integrin domain structure, leading downstream events including integrin clustering and adhesion components assembly [10, 13].

Notably, integrins coordinate extracellular and intracellular environments in a bidirectional manner, in which integrin-mediated signalling pathways can be activated by extracellular or intracellular factors. Such events have been demonstrated in previous studies describing the activation of αvβ3 integrins by ECM ligand binding through extracellular domains [14, 15], or talin binding to integrin via its β-subunit intracellular tail is final step to control integrin activation [15]. The bidirectionality of integrins known as outside-in and inside-out signalling is particularly highlighted in the integrin-mediated mechanosensing machinery. In outside-in signalling, cell quickly responds to external mechanical force like rigid substrate by bringing integrins at the leading edge of cell protrusions where they can bind the matrix [10, 16]. Upon ligand binding, a large number of proteins are recruited to cytoplasmic integrin tails where they assemble nascent adhesions. When a cell is exposed to substrate of high rigidity, force is transduced on nascent adhesions, accelerating integrins conformational change, strengthening the bond between ECM ligand and integrins. Subsequently, nascent adhesions undergo further maturation to grow into larger focal adhesions, which cause the binding of the integrin cytoplasmic tails to the actin cytoskeleton and regulating the polymerization of actin stress fibre through Rho GTPase [17].

Intracellularly, coupling of integrins to actin cytoskeleton through focal adhesions causes cells to generate actomyosin-mediated contractile force which pulls themselves over the adhesion sites. The cell-generated contractile force, which is directly proportional to substrate rigidity, has been shown to activate multiple biological signalling pathway as a way to respond to the stiffness of their microenvironment in a process coined inside-out signalling pathway [16, 17]. The intracellular tensile forces have been shown to affect ECM architecture via focal adhesions. This has been evidenced by a previous study that RhoA-medaited contractility promotes fibronectin assembly, and impairing contractility by an actin inhibitor can reduce fibronectin level [18]. In addition, Han et al. demonstrated that cell contractility stiffens their surrounding environment [19]. As such, the outside-in and inside-out mechanotransduction provides a rapid feedback loop at integrin-ECM adhesion sites, by which the mechanical forces can be transmitted through integrin-mediated focal adhesions and translated into biochemical information to control ECM architecture as well as fundamental processes that determine cell fate (Figure 1.1).

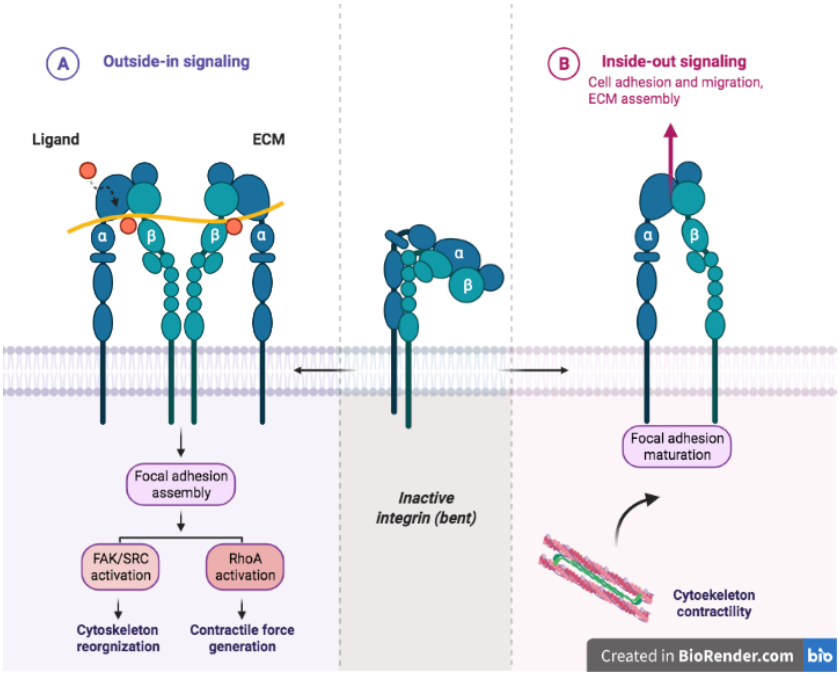

Figure 1.1 | Outside-in and Inside-out signalling

A. In outside-in signalling, mechanical stimuli from ECM activates integrin and causes conformational change of its extracellular domains, strengthening the bond between integrin and ECM ligands. Activated Integrin triggers assembly of focal adhesion and activation of downstream signaling e.g., RhoA/ROCK and FAK/SRC, which in turn promote cytoskeleton remolding and cellular contractility.

B. In inside-out pathway, the dynamic change of cytoskeletal stress fibre and contractile forces regulate ECM architecture and rigidity via focal adhesion. The stiffened ECM by inside-out signaling then promotes more integrin-ligand interaction, triggering more outside-in signaling.

1.2.2 Structure and organization of focal adhesions

The ECM ligand-integrin binding recruits numerous proteins to the adhesion sites to modulate the linkage of integrin to the actin cytoskeleton. The highly dynamic focal adhesion composition was summarised in a previous review which depicted a complex network of 156 proteins as well as 690 interactions [20]. Another study further integrated several integrin adhesome proteomic datasets to established a consensus adhesome in which 60 proteins are identified and represented as the core components of the integrin adhesion machinery [21]. Of note, though focal adhesions are of a high degree of complexity with respect to their component structures and molecular interactions, these proteins are organized in a hierarchical manner rather than being randomly assembled at integrin-ligand interaction sites. This observation was demonstrated by Kanchanawong et al. who utilized super-resolution fluorescence microscopy (interferometric photoactivated localization microscopy, iPALM) to

show that integrins and actin cytoskeleton are vertically separated by three partially overlapped protein-specific layers of focal adhesion core region; an integrin signalling layer, a force transduction layer, and an actin-regulatory layer (Figure 1.2) [22]. Each component within the three functional layers occupies a distinct vertical position and exert characteristic function to regulate focal adhesion.

Figure removed because of copyright

Figure 1.2 | A schematic model of focal adhesion molecular architecture based on iPALM analysis

The model depicts that the focal adhesion components form an organised structure that links integrins to actin stress fibres. Figure reproduced from Ref. [19]

1.2.2.1 Integrin signalling layer

The integrin signalling layer is closest to plasma membrane, containing integrin cytoplasmic tail, focal adhesion kinase (FAK) and paxillin. FAK is one of the first proteins recruited to adhesion sites in response to external mechanical cues and acts as a key regulator for further maturation of focal adhesions. Upon integrin attachment to rigid microenvironment, FAK is first activated by autophosphorylation on tyrosine residue 397, creating a binding site for several Src-homology (SH)2 domain-containing proteins such as Src and Shc [23]. The binding of Src to FAK induces further phosphorylation of FAK on several tyrosine sites including Tyr576, 577 and 861. This process is needed for formation and full activation of FAK-Src signalling complex and facilitates subsequent phosphorylation of various FAK-targeted proteins [23, 24].

The two major target proteins of FAK-Src complex are p130 Crk-associated substrate (p130Cas) and paxillin. FAK-Src complex catalyses tyrosine phosphorylation of p130Cas, further enhances SH3 domain-mediated binding of p130Cas to FAK and promotes interaction between SH2 domain of Crk adaptor protein and p130Cas. Despite not being observed in consensus adhesome [25], p130Cas has been defined as a mechanosensor in focal adhesion. Sawada et al. provide evidence that stretching of cells or traction force induces Src-dependent tyrosine phosphorylation of p130Cas and the phosphorylation of p130Cas is responsible for force-dependent Rap1 activation, suggesting a role of p130Cas as a force transducer [26].

Paxillin, like p130Cas, is a cellular target of tyrosine kinase in focal adhesion. Paxillin is suggested to integrate ECM-derived mechanical cues due to its association with actin-binding proteins such as vinculin and actopaxin [27]. This protein contains a number of domains like LD, LIM, SH2-binding site and SH3-binding site, which serve docking sites to other cytoskeletal and signalling proteins [27]. The binding ability of paxillin to vinculin and actopaxin relies on the phosphorylation of this protein. Paxillin is tyrosine-phosphorylated by FAK and Src on Tyr31 and 118 under physiological condition as well as integrin-dependent cell adhesion, thus induces the binding of vinculin and actopaxin to LD motifs of paxillin and stabilizes FA-cytoskeleton interaction [27, 28]. The phosphorylated paxillin also exposes two binding sites for the SH2 domain of Crk adaptor protein and promotes the formation of paxillin-Crk complex, which plays an important role in integrin-mediated cell motility [29].

1.2.2.2 Force transduction layer

Next to integrin signalling layer is a broad central zone which is known as an intermediate force transduction layer, where talin and vinculin are the main components observed in this layer [22]. Talin is a 270 kDa protein composed of a globular N-terminal integrin-binding FERM and a flexible C-terminal rod domain consisting 13 helical bundles (R1-R13). Kanchanawong et al. who conducted super-resolution microscope studies have addressed a highly polarized orientation of talin, showing its N-terminal head close to cell membrane and the sites of FAK while C-terminal tail occupies an area overlapped with actin-regulatory layer [22]. Thus, talin forms tethers that span the stratified focal adhesion. This may also explain that the binding partners of talin cover multiple components that constitute focal adhesion, including integrin, FAK, vinculin and actin [30]. Though being traditionally defined as mechanosensor, however, talin is held inactive by an autoinhibitory bond between R9 of rod domain and F3 of FERM [9, 31]. The mechanical properties of talin relies on its stepwise unfolding dynamics of C-terminal

rod domains. The application of mechanical force initiates stretching of talin rod domains to expose cryptic binding sites for vinculin (VBS) [31, 32]. This activates vinculin and forms subsequent talin-vinculin system which has been evidenced to stabilize interaction between adhesion sites and actin stress fibre [33].

Vinculin is one of the core focal adhesion proteins as well as the major binding partner of talin. Structurally, vinculin consists of a globular N-terminal head and C-terminal tail domain separated by a short proline-rich neck region [33]. Similar to talin, vinculin exhibits a default inactive state in the cytoplasm by high-affinity intramolecular interaction between the head and tail domains, masking multiple ligand-binding sites in vinculin [34]. Activation of vinculin happens when it is translocated from cytoplasm to focal adhesions. Case et al. have shown that phosphorylated paxillin recruits vinculin to lower integrin signalling layer, where the vinculin head domain binds to VBS of talin, a process that in turn triggers conformational changes in vinculin and activates this protein. Consequently, talin binding of vinculin promotes the upward localization of this protein from lower integrin signalling layer to force transduction layer, where vinculin engages focal adhesion maturation and stabilization [35]. For the role of vinculin in force transmission, Dumbauld et al. demonstrated a differential contribution of vinculin head and tail domains. The head domain intensifies adhesion strength by increasing ECM-bound integrin-talin complexes, while the tail domain physically linking to head domain is required for propagating traction forces to actin stress fibres [36].

1.2.2.3 Actin-regulatory layer

The uppermost region of focal adhesions comprises zyxin, vasodilator-stimulated phosphoprotein (VASP) and α-actinin [22]. Zyxin is a zinc-binding phosphoprotein containing three LIM motifs in the C-terminal sites. The presence of LIM motifs potentiates this protein to localize at force-bearing focal adhesions where they interact with a number of FA proteins. In a previous review, Hirata et al. discussed the role of zyxin as a mechanotroansducer element in the regulation of actin polymerization at focal adhesions and adherens junctions [37]. Zyxin mechanosensing activity is dependent on its dynamic translocation through varying cellular compartments. It has been shown that actin polymerization highly occurs at zyxin-rich focal adhesion sties. Removal of mechanical load such as inhibiting cell contractility by blebbistatin or culturing cells on soft gel causes zyxin to release from focal adhesions and consequently decreases force-mediated actin polymerization at focal adhesions. Conversely, mechanical stretch restores accumulation of zyxin in the focal adhesions and facilitates actin polymerization [38, 39]. Furthermore, zyxin has been found to recruit and interact with

another focal adhesion protein, VASP, to actin filaments after mechanical stimulation such as cyclic stretch [40]. These observations suggest the role of zyxin and its binding partner VASP in regulation of force-dependent actin polymerization in focal adhesions.

Despite being regarded as a focal adhesion component, α-actinin is also defined as an actin-binding protein which is localized along the actin stress fibres that cross-links actin filaments. Through its NH2-terminal 27-kD domain, α-actinin interacts with zyxin. Thus, α-actinin serves as physical linker between integrin and cytoskeleton [41]. A previous study has shown that α-actinin is required for the establishment of stress fibres as well as the maturation of focal adhesion [42]. In addition, Meacci, G. et al. demonstrated that α-actinin plays an important role in the control of rigidity sensing. The depletion of α-actinin results in aberrant rigidity sensing and loss of contractility that allows cell to proliferate on soft substrate [43].

1.3 Mechanotransduction at cell-cell junction

In a multicellular assembly, the mechanical stimuli exerted from physical properties of their surrounding environment are transmitted to neighbouring cells. Cells adhere to each other through the formation of adherens junctions (AJs) and desmosomes. This review will focus on the role of adherens junction in mechanotransduction.

1.3.1 Structure and organization of adherens junctions

AJs are specialized cell-cell adhesion structures formed by interaction between the extracellular domains of classic cadherins. Cadherins are Ca^{2+}-dependent transmembrane proteins featured with an N-terminal extracellular domain, a transmembrane domain, and a highly conserved C-terminal domain that links actin filaments to cell adhesions through the binding of catenin proteins [44]. Classic cadherins include several different family members whose expression is cell-type specific. E-cadherin is preferentially expressed in epithelia, whereas VE-cadherin is vascular endothelial-specific and N-cadherin is located in non-epithelial cells [45]. At cell-cell adhesion, cadherins of adjacent cells form trans dimers through their N-terminal extracellular domains. Inside the cells, the cytoplasmic domain of cadherin binds to p120 catenin and β-catenin. β-catenin in turn binds to α-catenin to AJs, forming the cadherin-catenin core complex (Figure 1.3).

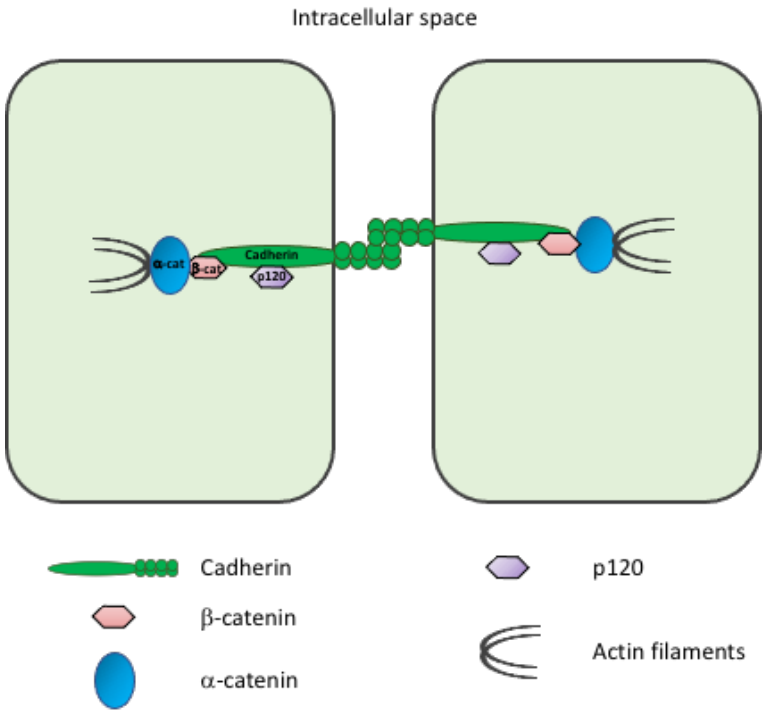

Figure 1.3 | A schematic representation of adherens junction

Adherens junction is a protein complex structure that mainly consists of cadherin and catenin. The extracellular domains of cadherins from adjacent cells form homophilic cell-cell interaction. The cytoplasmic domain of cadherins bind to b-catenin which engages actin filaments to adherens junction through α-catenin.

1.3.2 Mechanosensing and mechanotransduction at adherens junction

1.3.2.1 Tension generation at adherens junction

The mechanical coupling of cadherin to actin filaments through α-catenin can be observed when cells first establish adhesive contacts with each other. The initial adhesion between adjacent cells strengthens the physical association between cadherins and their engagement with the cortical stress fibre. This has been shown to further promote the remodelling of cortical stress fibres through Arp2/3 and RhoA activity (Figure 1.4). Kovacs et al. showed that E-cadherin adhesion interacts with actin nucleator Arp2/3 and activates local actin assembly [46]. Arp2/3 induces polymerization of branched actin fibres at adhesion sites, which has been suggested to contribute the establishment of junctional tension [47]. On the other hand, cadherin adhesion also promotes activation and recruitment of myosin II to cell-cell contact sites, a process regulated by Rho kinase-dependent signalling [48]. Importantly, activated myosin II and RhoA are also essential for cells to concentrate cadherins at cell-cell contacts and maintain cell adhesiveness [48, 49]. Thus, these active cellular mechanisms not only

reinforce junctional tension but also provide a feedback loop to stabilize cadherin localization at cell-cell adhesion.

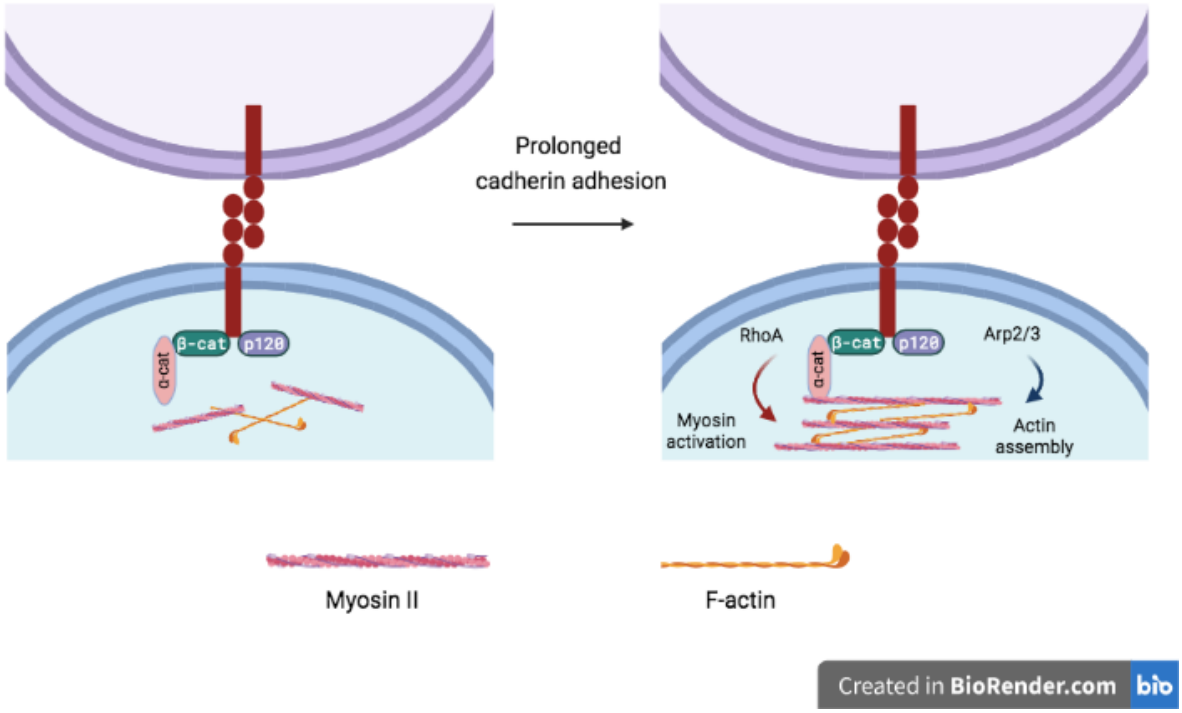

Figure 1.4 | Tension force generation at cell-cell junction

When cells first contacts with each other may generate junction tension through the engagement of cadherin-catenin complex to cortical stress fibre. This process also recruits myosin II to cell adhesion sites and promotes actin assembly, which reinforces junction tension and stabilizes cadherin localization at cell junctions.

1.3.2.2 Tension-sensing through the a-catenin/vinculin complex

In cadherin complex-based mechanotransduction, α-catenin is the most well studied protein known as a core mechanosensor at the core of AJs. α-catenin is an actin-binding protein which couples adhesion receptors to the contractile cortical actomyosin. α-catenin consists of three key domains: the N-terminal domain that binds to b-catenin, the central modulatory domain containing the vinculin-binding site for its interaction with vinculin, and C-terminal actin-binding domain [50]. Yonemura et al. demonstrated that the binding of α-catenin with both β-catenin and actin cytoskeleton causes α-catenin to undergo a force-dependent change in its conformation, expose vinculin-binding site and promote the recruitment of vinculin [51].

The accumulation of vinculin, in turn, leads to the recruitment of more actin filaments to associate with AJs [52]. Furthermore, Seddikiet al. showed that vinculin/α-catenin interaction promotes tension-dependent cell-cell contact stability and controls collective cell dynamics [53]. The model of force sensing through cadherin adhesion is depicted in Figure 1.5.

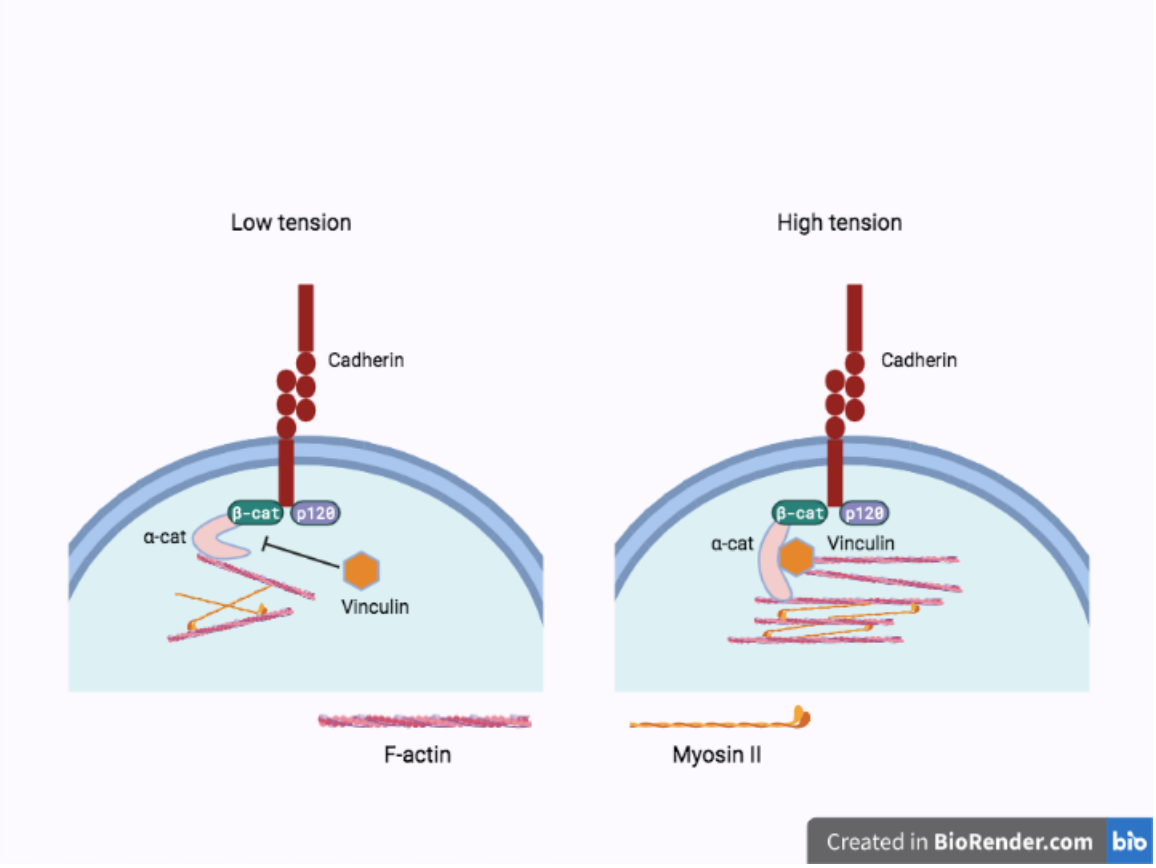

Figure 1.5 | Schematic representation of tension sensing at adherens junction
Cell adhesion leads to the binding of α-catenin to β-catenin and actin fibre through its N-terminal and C-terminal domains respectively. Then the junction tension induces the conformational change of α-catenin, exposing its central modulatory domain for its association of vinculin. The binding of vinculin to cadherin-catenin complex also recruits more actin filaments to adherens junction.

1.4 Cytoskeleton and mechanotransduction

When experiencing mechanical forces from the microenvironment, cells are not simply force receivers in a passive manner but instead, dynamically generate an opposed cellular force to pull on the substrate or neighbouring cells. This process requires assembly of actomyosin contractile network and remodeling of cytoskeletal stress fibres. Through the

regulation of cytoskeleton tension, the external mechanical forces can be propagated throughout the cells and further modulate downstream factors which will control cell behaviours [1].

Stress fibres are dynamic structures composed of cytoskeletal filaments and stress fibre-associated proteins. There are three major types of cytoskeletal polymers: F-actin fibre, microtubules and intermediate filaments (IFs), which differ in the magnitude of their mechanical stiffness and dynamics of their assembly [54]. All three components display a highly organized networks that provide physical support to the cell and contribute to maintain intracellular compartment integrity. Together, they control cell shape, motility and tension homeostasis. (Figure 1.6).

Figure moved because of copyright

Figure 1.6 | Schematic representation of the three major cytoskeleton system

Mammalian cytoskeleton is mainly composed of three major cytoskeletal polymers. Microtubules are the hollow cylinders with diameter of approximately 25 nm, consisting of repeating units of α- and β-tubulin subunits. Microtubules are the stiffest of the thress polymers, providing rigid and organized cytoskeletal components that maintains cell shape. Actin filaments are the smallest type of the cytoskeleton system, with a diameter of only bout 7 nm. Actin filaments are composed of actin along with numerous crosslinkng proteins and contribute to cell flexibility and motility. Intermediate filaments are assembled from elongated fibrous proteins, with the size normally 8-10 nm in diameter. Intermediate filaments mainly function to support mechanical strength of cells.
Figure reproduced from https://www.mechanobio.info/cytoskeleton-dynamics/what-is-the-cytoskeleton/

1.4.1 Major components of cytoskeleton

1.4.1.1 F-actin cytoskeleton

The actin fibres consist of filamentous actin (F-actin), globular actin (G-actin) and numerous crosslinking proteins. With the binding of crosslinking proteins such as α-actinin and filamin, actin fibres are orgnized into stiff, complex structures known as stress fibres [54, 55]. The actin cytoskeleton is highly dynamic, polar helical structure, where its reorgnization is modulated by rapid turnover of actin molecules in its filament. The constant assembly and disassembly of actin filament is controlled by local activity of signalling systems. For example, the binding of chemoattractants to its receptors triggers a signalling cascade that induces

polymerization and assembly of actin filaments at the leading edge of cells, causing cellular polarization and movement [56].

Actin filaments are well known for its role in sensing and responding to external mechanical forces by generating contractile forces. In these cases, actin filaments are held together with motor protein myosin II to form actomyosin bundles and assemble at cell-ECM contact sites upon adhesion receptors integrins bind ECM ligands [57]. The contractile forces generated from actin stress fibres have profound effect on focal adhesion functions and cell behaviours.

1.4.1.2 Microtubules

Microtubule network is present in all eukaryotic cells and is recognized for its role in various cellular processes. The microtubules are the stiffest of the three cytoskeleton components, composed of α- and β-tubulin heterodimers that associate in a head-to-tail orientation to form a hollow, cylindrical polymer called protofilament [54]. Previous reviews described that microtubules are highly dynamic structures, where its assembly and disassembly constantly occurs. This dynamic instability of microtubules particullarly plays a critical role in chromosome alighment and segregation during mitosis, where microtubules rearrange themselves into mitotic spindle. The disassembly and reassembly of spindle fibres provide a pulling force that separate chromosome toward opposing spindle poles [58].

1.4.1.3 Intermediate filaments

The third type of cytoskeleton are intermediate filaments. Inermediate filaments are the least stiff among the three major cytoskeletal components. Unlike F-actin filaments and microtubules that are made of globular proteins, intermediate filaments are assembled from elongated coiled-coils fibrous proteins that form a long central α-helical rod domain flanked by non α-helical N-and C- terminus [59]. Intermediate filaments cross with each other through anchor proteins called plectin. There are two distinct intermediate filament systems, one is in the nucleus while the other is in cytoplasm. In both cases, the major function of intermediate filaments is assumed to be a 'buffer' of mechanical stress and to maintain cytoskeleton integrity [60].

Inside the nucleus, inermediate filaments form a layer of proteins called lamins, which is associated with a number of transmembrane as well as chromatin-binding proteins to form nuclear lamina. While in the cytoplasm, intermediate filaments couple to the outer nuclear membrane through plectin and nesprin-3. These filaments also connect to cell-ECM junctions

by plakin-type molecules such as plectin and BPAG1, and to cell-cell junction through desmoplakin and plakoglobin that links to desmosomal cadherin. Furthermore, intermdate filaments can crosslink to actin filaments and microtubules through plakin-type molecules. Thus, together with other actin-binding proteins and microtubule-associated molecules, these three interconnected cytoskeleton networks contribute significantly to mechanical homeostasis and cell integrity.

1.4.2 Cytoskeletal stress fibres transmit mechanical signals

Among the three cytoskeleton networks, actin filaments are well recognized as a mechanical messenger to transmit external and internal physical forces through an actomyosin contractile network. Actin filaments associate with the motor protein myosin II to form actomyosin bundles called stress fibres, the major contractile network in many animal cells [61]. The assembly of actomyosin contratile network occurs when cells encouter physical forces from their microenvironment. For example, as described in **1.1.2**, stiff substrate or mechanical stress leads to clusterring of integrin receptors and activation of focal adhesion kinase as well as Src tyrosine kinase, which in turn promotes stress fibre growth and stability [26]. The stress fibre contractility is attributed to the movement of myosin II along actin filaments. How myosin II together with actin filaments generate contractile force has left a considerable controversy. A major model is the power stroke, also known as contraction cycling [62]. Power stroke is based on the binding and hydrolysis of ATP by myosin II, which in turn causes the conformational change of this protein and generate forces on actin filaments, leading to contraction of actin cytoskeleton [62] (Figure 1.7).

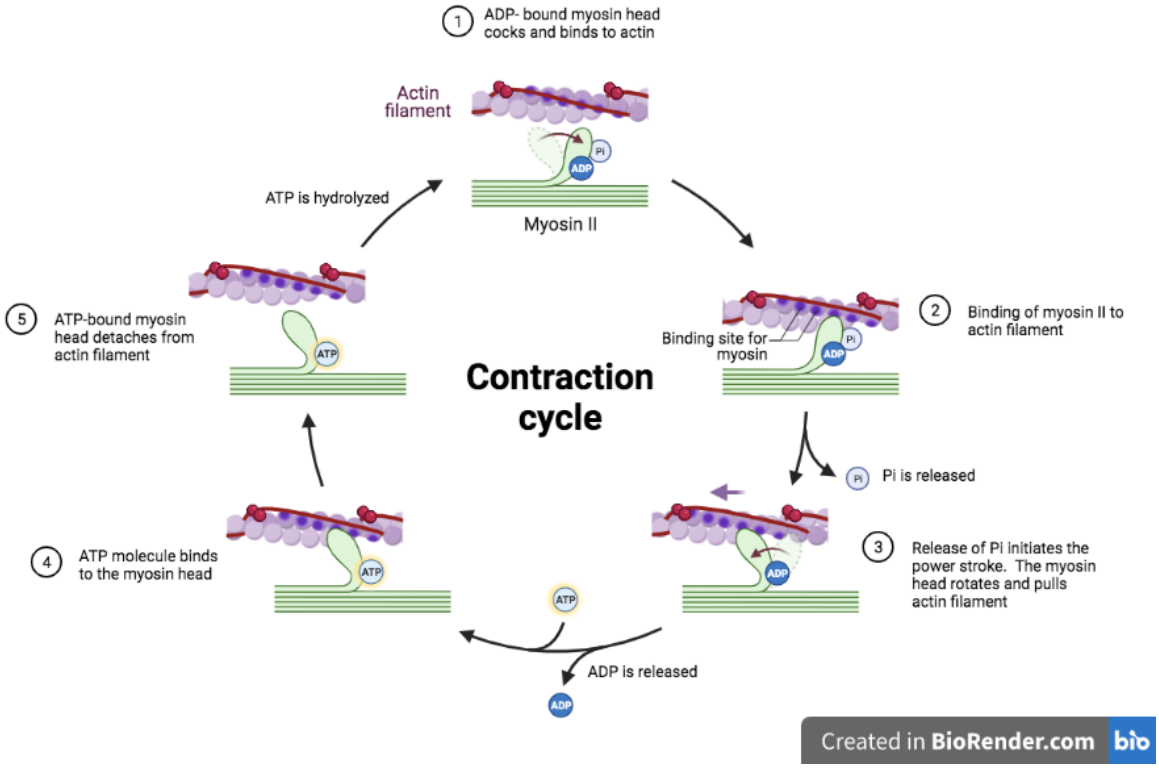

Figure 1.7 | A schematic model of contraction cycle (power stroke)

Contractile cycle is a series of conformational changes of myosin II driven by hydrolysis of ATP. At the start of next cycle, Myosin II hydrolyzes ATP to ADP and inorganic phosphate (Pi), resulting energized ADP-bound myosin head cocks and binds to actin (1). The binding of ADP-myosin head to actin forms a cross bridge (2). The contact of ADP-myosin head to actin causes conformational change of myosin that induces the release of Pi. The release of Pi initiates the power stroke, making myosin head rotates toward its original conformation and pulls actin filament (3). ADP is released from myosin II, but myosin head remains attached to actin filament to form a short-lived conformaiton until another ATP binds to myosin II (4). The binding of ATP to myosin II reduces its affinity to actin filament and causes its head to bend into a position further along the actin filament (5). ATP is then hydrolyzed by myosin II which starts the next cycle.

Of note, based on their different structural organization and association with focal adhesions, the actomyosin stress fibres can be divided into several different subtypes: dorsal stress fibres, transverse arcs, ventral stress fibres, and perinulcear actin cap [63]. Dorsal stress fibres are anchored to the focal adhesions at the leading edge while with the other end rise toward the dorsal side. Dorsal stress fibres lack myosin II, as a result, they cannot contract. Dorsal stress fibres also function as a platform to connect other types of stress fibres to focal adhesions [64]. Transverse arcs, on the contrary, are curved-shaped actomyosin bundles of a periodic α-actinin and myosin II structure that is typical for contractile actomyosin network. Transverse arcs are indirectly attached to focal adhesions through

dorsal stress fibres. Thus, through the mechanical coupling, contractile forces generated by the arcs are transferred to the surrounding environment [63, 65]. Ventral stress fibres are contractile actomyosin bundles that are rich of both α-actinin and myosin II. Ventral stress fibres are often confined to the cell base, with both ends connected to focal adhesions [66]. Perinuclear actin cap, on the other hand, is recently identified as a subtype of stress fibres. Perinuclear actin cap fibres wraps around the nucleus and link to the nuclear envelope through LINC (linker of nucleoskeleton and cytoskeleton) complex. As being extended from the dorsal to ventral side of cells, perinuclear actin cap also connect the nuclear envelope to focal adhesions [66].

Importantly, during the mechanotransduction focal adhesions and cytoskeletal stress fibres cooperate and stabilize each other in a tighly controlled feedback loop [61]. Focal adhesions work as sensory system where integrin receptors interact with mechanical cues generated from surronding microenvironment. Activation of integrin receptors then initiate a series of signalling cascades that trigger maturation of focal adhesion, which results in assembly of stress fibres and generation of contractile forces . The mechanical contractility generated from stress fibres, in turn, lead to further growth and maturation of focal adhesions. Thus, the increased size of focal adhesion further reinforces actin stress fibres and promotes cytoskeletal tension, which affect multiple cellular behaviour such as cell proliferation and migration [67, 68]. The close relastionship between focal adhesions and cytoskeletal fibres have been demonstrated by several groups. For example, Yamashita et al. showed that strss fibres increases the level of vinculin to localize at focal adhesions [69]. Similarly, Balaban et al. demonstrated that inhibition of actomyosin contraction led to disruption of focal adhesions [70]. These studies suggest that focal adhesion only assemble and grow when they encouter contractile forces through their actin connections. Thus, the mechanical crosstalk between ECM-sensing machinery and cytoskeletal stress fibres plays also a major role in determining the corresponding cellular behaviours.

1.4.3 The role of Rho signalling in mechanotransduction

It has been shown that a signalling cascade involving RhoA regulates the assembly of stress fibres. RhoA belongs to the small GTPase Rho-family, and along with Rac1 and Cdc42, are the most ubiquitous members in the family. All the three Rho-family members are key regulators of cytoskeleton dynamics [71]. With respect to mechanotransduction, we focus here on RhoA

as many efforts have been directed to clarify the role of RhoA in the promotion of actin fibres assembly and generation of intrecallular contractile forces.

RhoA exists with two different forms, active GTP-bound state and inactive GDP-bound state. Cycling of RhoA between its active and inactive states is regulated by several classes of proteins: guanine nucleotide exchange factors (GEFs), GTPase-activating proteins (GAPs), and guanine nucleotide dissociation inhibitors (GDIs). GEFs activate RhoA by catalyzing exchange of GDP for GTP and keep RhoA to interact with plasma membrane while GAPs inactive RhoA by hydrolyzing the bound GTP to GDP. In addition, Rho-specific guanine nucleotide dissociation inhibitors (GDIs) forms a complex with inactive GDP-RhoA and maintain a stable pool of inactive RhoA in the cytoplasm [72]. How GDP-RhoA release from GDI has not been completely defined. One possible mechanism involves the function of GDI dissociation factor (GDF), which has been postulated to interact with RhoA-GDI and trigger dissociation of this protein complex [73]. RhoA cycle is depicted in Figure 1.8.

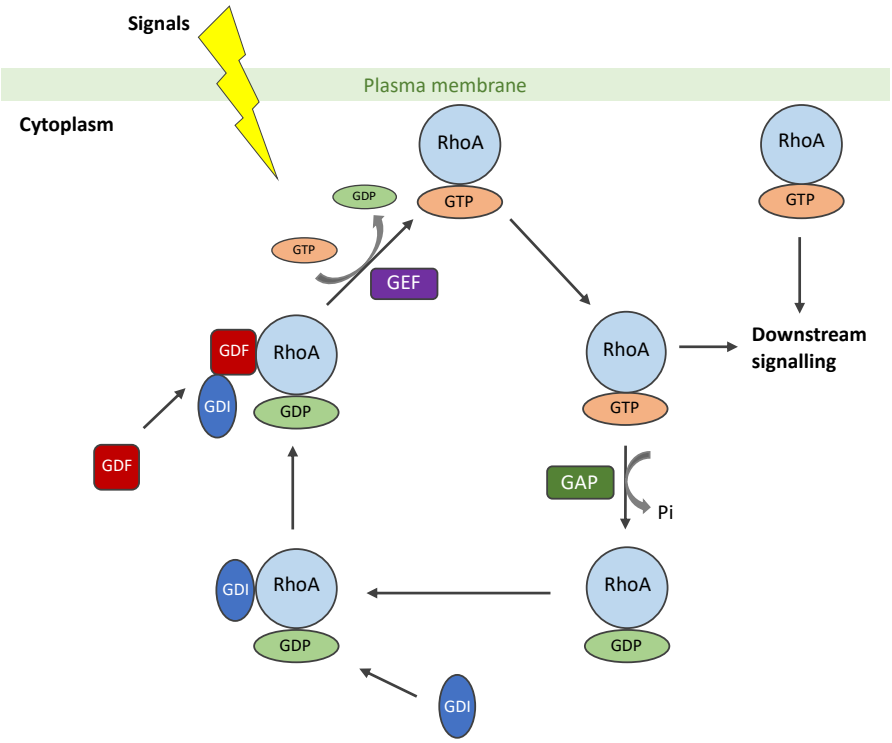

Figure 1.8 | RhoA cycle

RhoA activity is regulated by its GTP-bound or GDP-bound state. RhoA is inactive in the GDP-bound form which usually remains in the cytoplasm with the interaction of GDI. The association of GDF with GDI detaches GDI from RhoA-GDP, allowing GEF to activate RhoA by catalysing the exchange of GDP/GTP. The active RhoA-GTP is localized at plasma membrane and triggers a series of downstream signalling. GAP inactivates RhoA by hydrolysing GTP to GDP and inorganic phosphate. GDI then sequesters the inactive RhoA-GDP in the cytoplasm before next cycle.

Several groups have demonstrated that RhoA engages in the focal adhesions-mediated actomyosin contraction. Guilluy et al. showed that force on integrins activates RhoA through stimulation and recruitment of two GEFs, LARG and GEF-H1, to adhesion complexes [74]. Following activation by signals from focal adhesion, the GTP-bound RhoA directly activates the remodeling of cytoskeletal stress fibres through its effectors [75]. One of the critical effectors of RhoA is Rho kinase (ROCK). Activation of ROCK by RhoA induces myosin regulatory light chain (MLC) activity by direct phosphorylation of MLC or by inhibition of MLC phosphatase (MLP) [76]. The phosphorylated MLC, in turn, induces assembly of myosin II to actin filaments and promotes generation of contractile forces [62]. Active ROCK also phosphorylates and activates LIM domain kinase (LIMK), therefore, inhibits F-actin severing protein cofilin and maintains the integrity of actin stress fibre [77]. RhoA also facilitates the polymerization of long actin filaments e.g., dorsal stress fibres, through its binding to mammalian Diaphanous (mDia), a member of the formin family that plays a role in promoting actin nucleation [64] (Figure 1.9).

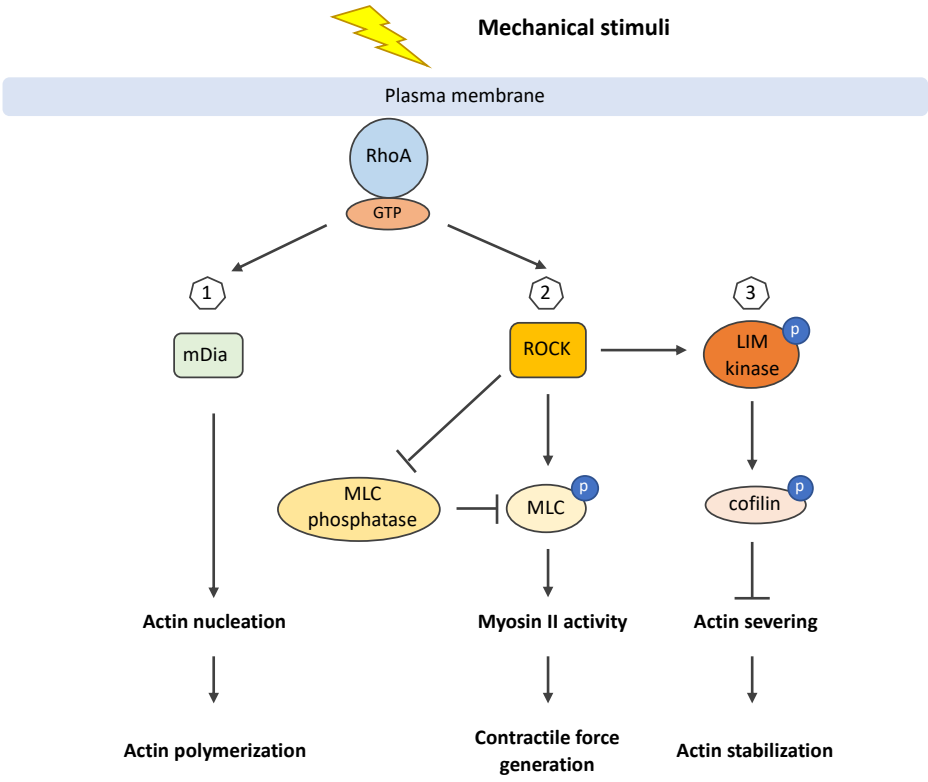

Figure 1.9 | RhoA signalling downstream of mechanical cues.
Activated RhoA by mechanical stimuli interacts with effector proteins such as mDia, which promotes actin nucleation and leads to actin polymerization. RhoA also activates ROCK signalling that enhances contractile force generation through phosphorylation of MLC and inhibitition of MLC phosphatase. ROCK promotes actin stabilization by phosphorylating LIM kinase, which in turn inactivates cofilin-mediated actin severing.

1.5 Mechanotransduction from cytoplasm to nucleus

Regulation of transcription events as a response to mechanical stimuli from cellular microenvironment has been shown to play a critical role in tissue homeostasis. Previous studies have demonstrated the transduction of mechanical cues from the cellular microenvironment to the nucleus through the cytoskeleton networks, which link focal adhesions and cell-cell adhesions to the nucleus by the linker of nucleoskeleton and cytoskeleton (LINC) [78].

The major components entail in nucleocytoplasmic mechanical coupling are outer nuclear membrane protein nesprins and inner nuclear membrane proteins SUN. Nesprins family are KASH transmembrane-domain proteins and are part of the LINC complex [79]. Among the protein family, nesprin-1/2 directly interact with actin filaments with their N-terminal actin-binding domain, while nesprin-3 binds to intermediate filaments through plectin and nesprin-4 connecting nucleus and microtubules via its interaction with kinesin [78, 79]. The C-terminal KASH domain of nesprin family also interact with another LINC component, SUN, which spans the inner nuclear membrane, in turn connects to the nuclear lamina and chromatin inside the nucleus. Thus, the nucleo-cytoskeletal coupling bridge plasma membrane and nucleus, providing a direct transmission of extracellular mechanical signals across the cytoskeleton to the nucleus [78, 79] (Figure 1.10).

Figure removed because of copyright

Figure 1.10 | Schematic representation of LINC complex

LINC complex is mainly composed of outer nuclear membrane protein nesprins and inner nuclear membrane proteins SUN. Different nesprin isoforms connect various cytoskeleton to the nucleus. Nesprin-1/2 directly interact with F-actin filaments, while nesprin-3 and nesprin-4 connect to intermediate filaments (IFs) and microtubules (MTs) respectively. Nesprins are coupled to lamin A/C and chromatin through the interaction with SUN protein which spans the inner nuclear membrane. Figure reproduced from Ref. [2].

Mechanical forces generated by contraction of adherent cells or changes of cell geometry have been shown to be associated with the remodelling of actin cytoskeleton, which in turn cause deformation of the nucleus [80]. Apical actin stress fibres, which are the actin filaments wrapping around the apical outer surface of the nucleus and forming the perinuclear actin cap, have been shown to tightly control nuclear shape as a response to mechanical signals [81]. For example, cells grown on stiff substrates display stronger apical actin stress fibres which compress the nucleus into a flat ellipse, while the relaxed and thin actin structures possessing less mechanical force lead to a spherical nucleus when cells are adhesive to soft substrates [78].

The physical homeostasis of the nucleus partly depends on the architecture of the nuclear membrane. The supportive structural components which contribute to the biophysical and mechanical properties of the nucleus are laminas, a protein network of lamin and lamin-binding proteins lining the inner surface of nuclear envelope [81]. Lamina network with elastic extensibility has been shown to function as a load-bearing element that is necessary for protection of nuclear envelope from rupture [25]. Lamin A/C are tension sensitive proteins and have been implied to affect chromatin anchoring and modulate gene expression, while lamin B filaments provide mainly elastic properties which function to determine the mechanical resilience against nuclear deformation [82]. In addition, a related study has shown that lamin A/C levels and phosphorylation are tension-dependent. For example, lamin A/C levels increase and influence differentiation of mesenchymal stem cells when experience stiff matrices, while lamin A/C is rapidly phosphorylated when subjected to soft matrices, leading to nuclear softening and lower lamin A/C levels [83]. Together, these studies indicate the role of lamin in the regulation of nuclear morphology downstream of matrix mechanics.

One of the important events in cells responding to mechanical cues is the regulation of gene expression. Mechanical signals transmitted to the nucleus through nucleo-cytoskeleton coupling result in alteration of several nuclear biophysical properties, including heterochromatin movement, phosphorylation of nuclear proteins such as Src and emerin, and activation of DNA repair pathway when nuclear envelope rupture induced by substantial mechanical challenge [84]. Mechanical forces also regulate nuclear import of various transcriptional factors. YAP/TAZ are particularly highlighted as the mechanoregulation of transcriptional cofactors, which will be reviewed in the following section.

Another important example is the crosstalk between stiffness substrates, MRTF, and NF-κB pathway [78]. Cells grown on rigid matrices displaying actin polymerization disassociate G-actin-bound transcription cofactor (MRTF) complex, which in turn to cause MRTF to translocate into the nucleus to activate MRTF-serum response factor (SRF) target genes. Increased actin polymerization also promotes the cytosolic retention of NF-κB complex, leading to the downregulation of NF-κB target genes [78]. On the contrary, cells subjected to soft matrices reduce the formation of actin bundles, promoting cytosolic MRTF localization and nuclear accumulation of NF- κB complex [78]. These findings indicate the novel link between mechanical signals and the modulation of gene expression.

1.6 YAP/TAZ and mechanotransduction

1.6.1 YAP/TAZ are downstream effectors of Hippo signaling pathway

The research on YAP/TAZ on multiple aspects of cell behaviours such as morphogenesis and organ-overgrowth can be traced back to the breakthrough studies of Yorkie, the Drosophila homolog of YAP [85]. In mammalian system, YAP (Yes-associated protein) and its paralog TAZ (transcriptional co-activator with PDZ-binding motif WWTR1) are highly related transcriptional cofactors and candidate oncogenes that play critical roles in cell growth and survival [85]. The sense and response of YAP/TAZ to various biochemical signals result in their translocation between the nucleus and cytoplasm. Activated YAP/TAZ are predominantly located in the nucleus where they utilize transcriptional factors TEA domain family members (TEAD) as a platform to bind distant enhancers of target genes and activate the genes encoding cell proliferation, migration, apoptosis, and stem cell self-renewal [85, 86].

Multiple mechanisms have been shown to regulate the activity of YAP/TAZ, including Hippo-dependent and Hippo-independent cascades. The Hippo pathway is an evolutionary conserved signalling pathway with core components of two protein kinases MST1/2 and LATS1/2, which represent the orthologues of Hippo and Warts in *Drosophila* respectively. MST1/2 bind to their partner protein Sav1 to form an active complex that phosphorylates and activates LATS1/2 and their co-factor MOB1. The activated LATS1/2-MOB1 complex in turn directly phosphorylates YAP/TAZ on Serine residues in five LATS1/2 target consensus motifs HXXRXS/T (four of these sites in TAZ) [86-88]. Among these phosphorylation sites, pS127 and pS381 are the most critical for YAP inhibition, as evidenced by the phosphorylation of YAP being blocked by the mutation of both S127 and S381. The pS127 and the flanking residues provide a binding motif for 14-3-3 proteins and the resulting interaction is responsible for cytoplasmic retention of YAP, while pS381 triggers subsequent phosphorylation on Ser384 and induces the interaction of YAP and β-TRCP that ultimately leading to the degradation of YAP [87-89]. Conversely, inhibition or mutation of Hippo components suppresses the phosphorylation of YAP and enhances their activity and nuclear accumulation [86, 90] (Figure 1.11).

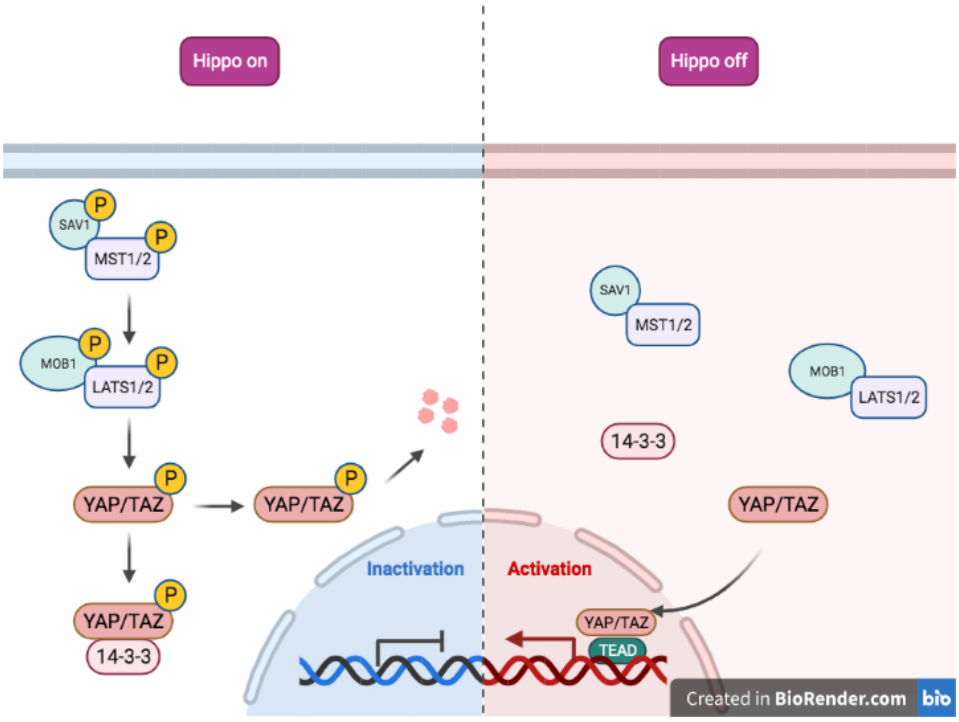

Figure 1.11 | Hippo pathway regulates YAP/TAZ activity

Schematic representation of the core module of the Hippo pathway that regulates YAP/TAZ subcellular localization and activity. Left: In 'Hippo on' state, the activated core kinase cascades such as MST1/2 and LATS1/2 phosphorylate YAP/TAZ, which ensuing YAP/TAZ proteosomal degradation or cytoplasmic sequestration through 14-3-3 protein binding. Right: In 'Hippo off' state, the core Hippo kinase cascades are inactivated, causing YAP/TAZ free from the inhibitory phosphorylation and enter the nucleus. YAP/TAZ then regulate expression of target genes through interaction with transcriptional factor TEAD.

1.6.2 YAP/TAZ play a role as mechanotransducers

Aside from canonical Hippo components, scores of recent reports have identified mechanotransduction as a critical determinant of YAP/TAZ regulation. ECM rigidity and topography, cell geometry, and stretching and strain forces have been shown to tightly regulate the subcellular localization and activity of YAP/TAZ (Figure 1.12). The ability to respond to various mechanical properties along with their co-transcriptional activity which determines multiple critical cell behaviours highlight the role of YAP/TAZ as universal mechanosensors and mechanotransducers. In this section we will review cellular mechanical responses through YAP/TAZ activity as well as the mechanisms underpinning the regulation of YAP/TAZ by mechanical properties.

Figure removed because of copyright

Figure 1.12 | Schematic representation of mechanical cues regulating YAP/TAZ subcellular localization and activity

A. YAP/TAZ are sequestered in the cytoplasm when there is no or low mechanical stimuli, while translocate to the nucleus and regulate gene expression when they are mechanically activated.
B. Schematic depiction of how YAP/TAZ subcellular localization and activity are regulated by mechanical stimuli such as cell geometry, ECM rigity and cell physical condition. The left panels represent the conditions when cells experience low mechanical stimuli that results in inhibition and cytoplasmic sequestration of YAP/TAZ. The right panels show the conditions when cells experience high mechanical cues that leads to YAP/TAZ activation and their translocation to the nucleus (indicated by red colour). Figure reproduced from Ref. [6]

1.6.2.1 Substrate rigidity and YAP/TAZ

In 2011, Dupont et al. first provided evidence of the correlation between mechanotransduction and YAP/TAZ [11]. That said, regulation of YAP/TAZ nuclear localization and activity is tightly related to mechanical signals exerted from cell substrate stiffness and topography. They found that YAP/TAZ remain in the cytoplasm when cells are plated on a soft substrate (0.7 kPa) but translocate into the nucleus when cells are grown on stiff ECM (40 kPa) [11]. The influence of substrate rigidity on the subcellular localiaztion of YAP/TAZ is not only limited in 2D culture but can also be observed in 3D cultures. Aragona et al. demonstrated that mammary epithelial cells cultured on 3D soft base membrane/collagen gel exhibit cytoplasmic YAP/TAZ along with the formation of growth-arrested acini. By contrast, cells seeded on stiff 3D gel display nuclear accumulation of YAP/TAZ and form larger spheroids with tubules and organoid-like structures [3]. In addition to the regulation of YAP/TAZ translocation between the nucleus and cytoplasm, substrate stiffness has been reported to modulate YAP/TAZ gene expression. Previous study indicated that YAP and TAZ mRNA significantly increase in human trabecular meshwork cells which experienced stiff micronvironment (75 kPa) in comparison to those in cells grown on soft gel (5 kPa) [91]. Similarly, alteration of YAP expression by mechanical stiffness was described by Meli et al., where total YAP protein level is downregulated in macrophage cultured on soft gel (fibrin) yet highly expressed in cells on stiff condition (glass) [92].

ECM is a highly dynamic structure which topography and physiological function is tightly relied on ECM remodeling, which is usually mediated by protease-dependent ECM degradation and collagen deposition [8, 93]. Importantly, a wealth of studies indicates that the change of ECM physical properties determines many facets of cell fate and pathological

progression through regulating the activation of YAP/TAZ. Liu et al showed that YAP/TAZ are highly accumulated in the nucleus of lung fibroblast cultured on pathologically stiff matrices and impose their profibrotic effects through promoting expression of plaminogen activator inhibitor-1 (PAI-1) and connective tissue gorwoth factor (CTGF) [94]. Remodeling of ECM is partly dependent on YAP/TAZ. Bertero et al. utilized a mouse model to demonstrate that ECM stiffening induces microRNA-130/131 in pulmonary vascular cells through activation of YAP/TAZ. Then the microRNA-130/131 promotes extensive collagen deposition and remodeling through PPARγ-APOE-LRP8 axis which in turn enhances YAP/TAZ through a mechanoactive feedback loop, furthur contributing the progression of pulmonary hypertension [95].

It is recognised that ECM stiffness regulates YAP/TAZ activity through cytoskeletal organization. Upon detecting mechanical properties at cell-ECM adhesion sites, integrins clustering and the subsequent activation of multiple focal adhesion molecules induces remodeling and contractility of stress fibre, therefore activates YAP/TAZ and their nuclear translocation) [6]. As cytoskeleton contractility is generated by sliding of myosin motor proteins on F-actin filaments [2], Inhibition of myosin or microfilament integrity have been found to suppress YAP/TAZ activity [3, 11]. Furthermore, activation of Rho GTPase activity by rigid substrate is a key factor to regulate cytoskeleton contractility and stability and in turn induces YAP/TAZ nuclear localization and function. These observation have been demonstrated by the Piccolo laboratory in which they showed that inhibition of Rho or F-actin stress fibre by drugs or genetic methods results in nuclear exclusion of YAP/TAZ [3, 11].

In addition, substrate rigidity have also been shown to drive mesenchymal stem cell (MSC) commitment through YAP/TAZ activtiy, which was evidenced that differentiation of MSC into osteoblast by stiff ECM is abrogated upon depletion of YAP and TAZ whereas mechanical repression of YAP was reported to promote adipogenesis in MSC [11, 96]. Furthermore, stiff ECM has been shown by Musah et al. to promote YAP nuclear retention and support long-term self-renewal properties of human pluripotent stem (hPS) cells [97]. However, compliant substrate prevents YAP nuclear localization and potentiates YAP to induce neuronal differentiation of hPS cells even with the presence of soluble pluripotency factors or without neurogenic factors, indicating the dominant role of ECM stiffness in determing cell fates through YAP activity [97].

1.6.2.2 YAP/TAZ are regulated by strain forces

The influence of mechanical strain on cell development, cytoskeletal organization and cell function has been analysed by several studies. Yan et al. showed that mechanical tensile strain imposed to mouse osteoblast cell line MC3T3-E1 promotes cell proliferation through integrin β1 and β5 -mediated ERK signalling pathway [98]. It has also been reported that exposure to strain forces retards cell migration yet enhances production of microtubule cytoskeleton in oligodendrocyte progenitor cells (OPCs) during oligodendrocyte differentiation [99]. Furthermore, mechanical loading conducted by equibiaxial cyclic strain is able to potentially offset aging-induced decline of cell regeneration and differentiation potential in mesenchymal stem cells, which was evidenced that strain forces increase self-renewal while inhibit adipogenesis in aging adipose tissue derived stromal cells (ADSCs) [100].

Recent reports have identified the role of YAP/TAZ as mechanical mediators in regulation of strain force-dependent cell response. Aragona et al. indicated that strain force overcomes YAP/TAZ inhibition and cell growth arrest by contact inhibition of proliferation (CIP), where they showed that mechanical strain induces the reentry of YAP/TAZ to the nucleus to sitmualte cell proliferation in confluent epithelial monolayer [3]. The effect of stretching on overriding CIP-induced suppression of YAP/TAZ activity and cell growth was also recapitulated by Benham-Pyle et al. The application of biaxial stretch on cell density-dependent quiescent epitheilial cells activates YAP and promotes its nuclear translocation, in which YAP mediates cell cycle reentry through its transciptional activity [101]. For further study on the mechanisms underlying strain force-mediated YAP/TAZ activity, Aragona et al. showed that strain force-induced reactivation of YAP/TAZ and cell proliferation are coupled with expansion of cell area as well as remodeling of F-actin cytoskeletal stress fibres, suggesting that mechanical strain regulats YAP/TAZ through cell geometry and cytoskeletal organization [3]. Meanwhile, a distinct mechanism behind the regulation of YAP by strain force was reported by Codelia et al., who showed that cyclic stretch enhances YAP nuclear retention and cell proliferation through JNK-mediated inhibition of Hippo signalling. They established a pathway showing that cyclic stretch activates JNK, which in turn phoshorylates LATS inhibitor, LIMD1, and increases the binding of LIMD1 to LATS. Thus, the reduced LATS activity by cyclic stretch consequently promotes YAP nuclear localization and activity [102].

1.6.2.3 YAP/TAZ sense cell geometry

It has been shown that the changes of cell geometry by mechanical cues emanated from ECM stiffness and cell density also regulate cell proliferation through YAP/TAZ. For example, the Piccolo laboratory showed that single cells display rounded shape with cytoplasmic

localization of YAP/TAZ when they are plated on a small micropatterned area (300 μm^2). On the contrary, when growing on large mocropatterned surface (1024~10,000 μm^2), cells show flattend and expanded geometry with active YAP/TAZ accumulated in the nucleus. The nuclear relocalization of YAP/TAZ by changes of geometry consequently alter cell proliferation, in which increased cell adhesive area by mechanical stretch regulates nuclear reentry of YAP/TAZ and promotes cell proliferation [3, 11]. The correlaton between cell morphology and subcellular localization of YAP is recapitulated by another study in which YAP is predominantly localized in cytoplasm in cells grown on a small adhesive area while significantly enriched in the nucleus in cells spread on a large surface [103]. Another prominent example of influence of cell geometry on cell behaviour is CIPs, a phenomenon of arrest of cell growth when they reach a critical cell density [104]. Mechanical forces derived from CIPs have been shown to induce drastically restricted cell spreading area, which suppresses YAP/TAZ nuclear distribution and cell proliferation [3]. These observations are consistent with the finding that dense cell monolayer inactivates YAP as cell spreading area is drastically restricted by high density [104], further supporting YAP/TAZ act as mechanosens or in response to changes of cell geometry.

The mechanism of how YAP/TAZ sense the changes of cell geometry has been intesively studied recently. It is widely recognised that cytoskeletal stress fibres and tensile actomyosin structures regulate YAP/TAZ activtiy downstream of cell geometry [11, 105]. Wada et al. indicated that cells show thick and abundant stress fibre with nuclear YAP in NIH3T3 at low density or grown on large microdomains (50 x 50 μm), while exhibite less evident stress fibres and cytosolic YAP in cells of high density or plated on small surface (20 x 20 μm). Disruption of F-actin stress fibres by filament inhibitors like cytochalasin D (CytoD) or cell detachment from culture dish results in cytoplasmic YAP [103]. Interestingly, the regulation of YAP subcellular localization by cell morphology was reported partially to rely on the Hippo component LATS. Disruption of stress fibres by CytoD has been found to cause rounded cell morphology and promote phosphorylation of YAP as well as its cytoplasmic localization. Coversely, knockdown of LATS2 maintains nuclear YAP even after stress fibres is reduced by treatment of CytoD, indicating the involvment of Hippo pathway in the regulation of YAP by cell morphology and stress fibres architecture [103].

Noteworthly, in epithelilal cells, cytoskeletal tension generated at adherens junction imposes a different mechanism in regulation of cell geometry-medaited YAP/TAZ activity. Furukawa et al. used MDCK epithelial cell line as a model to demonstrate that the formation

of a contracted circumferential actin belt at cell-cell junction at high density suppressed YAP/TAZ nuclear localization and protein activity [106]. The disruption of actomyosin tension at the circumferential actin belt by blebbistatin restores nuclear YAP/TAZ and increase proliferation. Importantly, they identified that one of Hippo signalling components, Merlin, acts as an adaptor downstream of density-mediated F-actin contraction to regulate the nuclear export of YAP/TAZ via its nuclear export signal (NES) sequence [106]. As Merlin strongly associates with E-cadherin but releases from adherens junction to cytoplasm at low- and high-cell density respectively, their finding implies that cell geometry-coupled mechanical force may lead to remodeling of protein complexes at cell-cell adhesion in epithelium.

Another study linking the role of adherens junction components in cell geometry-medaited regulation of YAP/TAZ was reported by Kim et al. [107]. Depletion of E-cadherin has been shown to inhibit YAP to be sequestered in the cytoplasm of confluent MDA-MB-231, while expression of E-cadherin rescues cell density-dependent regulation of nuclear YAP suppresion [107]. This study also indicated that cell geometry controls YAP activation in a Hippo dependent manner. Depletion of β-catenin reduces phosphoryaltion of YAP and enhances YAP nuclear accumulation in dense cell density, and the impact of downregulated β-catenin on YAP is similar to those of LATS ½ depletion [107]. These findings suggest a link conveying cell-cell adhesion and Hippo kinase cascade to cell geometry-medaited YAP/TAZ activation.

1.7 Project aims

Mechanical stimuli arising from ECM stiffness, cell stretching, cell density and fluid shear stress have been associated to multiple cell behaviours and pathological progression through mechanosensors such as YAP/TAZ. However, the regulators and mechanisms involved in mechanotransduction are still not fully understood. The relative subcellular distribution and particular function of YAP/TAZ in response to external mechanical cues inspired us to speculate that there could be other proteins with nuclear functions working in a similar way.

In this study, we aim to identify novel mechanoregulators, which can shuttle between the nucleus and cytoplasm in response to mechanical cues. The aims of this study are:

1. To develop a screen that allows the identification of novel mechanotransducers with nuclear functions.

2. To use this screen to identify novel potential mechanotransducers.
3. Based on the result of aim2, to investigate the role of the potential mechanical regulators with respect to their cellular function in mechanotransduction.

2. Chapter 2 – Materials and Methods

2.1 Cell culture

2.1.1 Cell line and culture condition

Table 2.1 | Reagents for mammalian cell culture

Reagents	Description	Suppliers
DMEM	DMEM (1X) + GlutaMAX™-Dulbecco's Modified Eagle Medium	Gibco®, Life Technologies™ (10569010)
DMEM/F12	Dulbecco's Modified Eagle Medium/Nutrient Mixture F-12	Gibco®, Life Technologies™ (11330032)
PBS	PBS pH7.4	Gibco®, Fisher Scientific (10010056)
Opti-MEM	Opti-MEM™ (1X) – Reduced Serum Medium	Gibco®, Life Technologies™ (11058021)
FBS	Fetal Bovine Serum, qualified, heat inactivated	Gibco®, Life Technologies™ (10500064)
HS	Horse Serum, New Zealand origin	Gibco®, Life Technologies™ (16050122)
Trypsin	Trypsin-EDTA (0.05%), Phenol red (1X)	Gibco®, Life Technologies™ (25300062)
Trypsin	Trypsin-EDTA (0.25%), Phenol red (1X)	Gibco®, Life Technologies™ (25200072)
Pen/Strep	Penicillin-Streptomycin (5,000U/mL) (100X) 5000units/mL of penicillin 5000µg/mL of streptomycin	Gibco®, Life Technologies™ (15070063)
Blasticidin S HCl	Antibiotic	Gibco®, Life Technologies™ (R21001)
Hygromycin B	Antibiotic	Gibco®, Life Technologies™ (10687010)
Zeocin™ Selection Reagent	Antibiotic	Gibco®, Life Technologies™ (R25001)
Puromycin	Antibiotic	Santa Cruz Biotechnologies (sc-108071)
Lipofectamine™ 2000	Lipofectamine™ 2000 Transfection Reagent	Invotrogen™, Fisher Scientific (11668019)
Poly-L-lysine	Poly-L-Lysine solution (0.1% (w/v) in H_2O)	Sigma-Aldrich® (P8920)

Table 2.2 | The mammalian cell lines, and culture condition used in this project

Cell line	Organism	Tissue origin	Morphology	Complete growth medium
Flp-In™T-REX™ HEK293	Human	Embryonic kidney	Epithelial/endothelial Adherent	DMEM-GlutaMax 10% FBS 1% Pen/Strep 100 μg/ml Zeocin 15 mg/ml Blasticidin S HCl
MCF10A	Human	Breast tissue	Epithelial Adherent	DMEM/F12 5% HS 20 ng/ml Epidermal growth factor 500 ng/ml Hydrocortisone 10 μg/ml Insulin 1% Pen/Strep
MDCK II	Canine	Kindney	Epithelial Adherent	DMEM-GlutaMax 10% FBS 1% Pen/Strep
HeLa	Human	Cervical cancer	Epithelial Adherent	DMEM-GlutaMax 10% FBS 1% Pen/Strep
Caco2	Human	Colon carcinoma	Epithelial Adherent	DMEM-GlutaMax 10% FBS 1% Pen/Strep
NIH3T3	Human	Embryo	fibroblast Adherent	DMEM-GlutaMax 10% FBS 1% Pen/Strep

Mammalian cell lines used in the project and corresponding reagents and culture medium was summarized in **Table 2.1** and **Table 2.2**. Cells were cultured in T-75 or 10-cm dish flasks and maintained in a humidified incubator at 37°C and 5% CO_2. The culture medium was refreshed every 2 days. All the cell culture procedure was conducted in a sterile cabinet to avoid contamination. When cells reached 80~90% confluency, they were passaged as described in **2.1.2**.

2.1.2 Subculture

Table 2.3 | Subculture for mammalian cell lines

Cell line	Incubation time	Centrifugation	Passaging ratio
Flp-In™T-REX™ HEK293	1 min	320 x g for 3 mins	1:10
MCF10A	5 mins	270 x g for 3 mins	1:8
MDCK II	5 mins	270 x g for 3 mins	1:8

HeLa	3 mins	320 x g for 3 mins	1:10~1:15
Caco2	5 mins	320 x g for 3 mins	1:6~1:8
NIH3T3	1 min	320 x g for 3 mins	1:6

Adherent cultures should be passaged before the cells reach the confluent stationary phase. Subculture is a procedure involves diluting cells and supplementing cells with fresh medium for continuous culture propagation. In brief, old culture medium was aspirated and cells were washed with 1x PBS to remove serum traces that could interfere the digestive activity of trypsin. 1 ml of Trypsin was added into the flasks and covered the whole cell layer by gently shaking the flasks. After incubation of the cells at 37°C for several minutes to ensure the sufficient detachment of cells, complete medium was added to neutralize trypsin and resuspend the cell solution. The cells in the suspension were pelleted by centrifugation at the speed indicated in **Table 2.3**. Supernatant was carefully removed, and the cell pellets were resuspended with 1 ml of complete medium. For subculture, cells with appropriate split ratio shown in **Table 2.3** were transferred into new culture vessel in which supplemented with complete medium to final volume of 10 ml. The cell suspension was mixed homogenously to ensure the uniform growth.

2.1.3 Cell counting and seeding

For some experiments, cells were seeded with particular amounts in the culture vessel. After detachment step as described in **2.1.2**, cell pellets collected from centrifugation were resuspended thoroughly in 10 ml of complete medium. Cells were counted by the means of haemocytometer under an inverted microscope. Cells of different amounts were seeded into various culture vessels based on the cell lines and intended application.

2.1.4 Cryopreservation of mammalian cell lines

Cryopreservation is a method for long-term storage of mammalian cells and serves as a way to avoid aging and genetic change through continuous culture of finite cell lines. Cryopreservation usually involves the application of cryoprotectant such as DMSO, which is used to prevent ice crystal formation within and outside the cells during freezing process. Before cryopreservation, cells should be checked for characterization and contamination. Only healthy and rapidly dividing cells should be frozen to ensure their viability after thawing. In order to prepare cell suspension for cryopreservation, cells were treated as for subculture described in **2.1.2**. After centrifugation step, the cell pellets were resuspended in fresh complete medium containing 10% DMSO and quickly transferred into cryovials. Cells from T-75 flask were aliquoted in two cryovials. The vials were then put in the wells of Mr. Frosty™

Freezing Container, which was designed to achieve a rate of cooling around -1°C/min, the optimal rate for cell preservation. The Mr. Frosty™ Freezing Container was placed in -80°C for a minimum of 4 hrs. The cells were moved to Liquid Nitrogen tank for long term storage.

2.1.5 Thawing cells

The procedure of thawing cells should be done quickly to reduce the time of exposure of the cells to DMSO. The vials of frozen cells taking from liquid nitrogen were thawed in a water bath of 37°C followed by the resuspension of cells in pre-warmed complete medium. Cells were centrifuged for 3 mins at the speed described in **Table2.3**. The supernatant was carefully removed, and cell pellets were resuspended in 10 ml of complete medium and transferred to desirable culture vessel. Cells were incubated at 37°C in 5% humidified CO_2 for overnight for attachment. The next day the culture medium was replaced by fresh complete medium to remove DMSO traces.

2.1.6 Cell transfection

Transfection is a process of introducing genetic material like DNA and dsRNA into eukaryotic cells for the purpose of gene expression (DNA transfection) or of gene inhibition (siRNA transfection). One day prior to transfection, cells of particular amounts were seeded in culture dishes as described in **Table 2.4**. Cells were allowed to attach the dish for at least 24 hrs and reached to around 60-70% of confluency before being transfected with nucleotide using Lipofectamine™ 2000 according to manufacturer's instructions. The nucleotide used in transfection was prepared in Opti-MEM. The culture medium was replaced with base medium without Pen/Strep antibiotics during the transfection. The minimum transfection period was 6 hrs and can be extended for overnight (~16 hrs) followed by replacement of the complete culture medium to the cells. The reagents and nucleotides used in transfection and incubation time are summarized in **Table 2.4**.

Table 2.4 | Reagents and nucleotides used for transfection of mammalian cell lines in this study
The amount of DNA or siRNA indicated represents the total amount for the transfection.

DNA transfection		
Flp-In™T-REX™ HEK293	4 x 10^5 cells/well in 6-well plate	For general DNA transfection: 150 µl Opti-MEM + 2.5 µl LF2000 150 µl Opti-MEM + 1 µg DNA Transfection: 6 hrs~16 hrs For generation of stable clone:

		150 µl Opti-MEM + 12.5 µl LF2000 150 µl Opti-MEM + 0.5 µg pcDNA5/FRT/TO-RhoA-Q63L + 4.5 µg pOG44 Transfection: 24hurs
MCF10A	2x 10^5 cells/well in 6-well plate	150 µl Opti-MEM + 2.5 µl LF2000 150 µl Opti-MEM + 1 µg DNA Transfection: 6 hrs~16 hrs

siRNA transfection		
Flp-In™T-REX™ HEK293	4 x 10^5 cells/well in 6-well plate	125 µl Opti-MEM + 2.5 µl LF2000 125 µl Opti-MEM + 50 pmoles siRNA - Day 1: 50 pmoles siRNA + 5 µl LF2000 in Opti-MEM, medium changed after 6 h - Day2: 50 pmoles siRNA + 5 µl LF2000 in Opti-MEM, medium changed after 6 h - Day3: continuing cell culture - Total siRNA transfection time: 72 h
MCF10A	1 x 10^5 cells/well in 6-well plate	125 µl Opti-MEM + 5 µl LF2000 125 µl Opti-MEM + 50 pmoles siRNA - Day 1: 50 pmoles siRNA + 5 µl LF2000 in Opti-MEM, medium changed after 6 h - Day2: 50 pmoles siRNA + 5 µl LF2000 in Opti-MEM, medium changed after 6 h - Day3: continuing culture - Total siRNA transfection time: 72 h

siRNA ID	Suppliers
siPCBP1-1	Invotrogen™, Fisher Scientific (HSS107633)
siPCBP1-3	Invotrogen™, Fisher Scientific (HSS107634)
siPTBP1-5	QIAGEN (SI00141638)
siPTBP1-18	QIAGEN (SI02649206)
Stealth RNAi™ siRNA negative control	Invotrogen™, Fisher Scientific (12935300)

2.2 Nucleic acid methods

The reagents and supplier information for RNA extraction and cDNA synthesis is listed in **Table 2.5.**

Table 2.5 | Reagents for nucleic acid methods

Reagents	Suppliers
RNaseZap™	Sigma-Aldrich (R2020)
RNeasy Plus Mini Kit (50)	QIAGEN (74134)
DNase I Amplification Grade	Invotrogen™, Fisher Scientific (18068015)
SuperScript™ II Reverse Transcriptase	Invotrogen™, Fisher Scientific (18064022)
dNTPs Mix (10 mM)	Thermo Scientific™ (R0191)
Random hexamers (5'-NNNNNN-3')	Sigma-Aldrich
UltraPure™ DNase/RNase-free distilled water	Invotrogen™, Fisher Scientific (10977049)

2.2.1 RNA extraction

RNA is well known prone to degradation than DNA due to its very structure and the ubiquitously existed ribonuclease (RNases), therefore, an RNase free environment is important when working with RNA samples. Before starting the experiments, the countertop, plastic surface, pipettes, tubes and gloves should be treated with RNaseZap™ to eliminate RNase contamination.

Total RNA of cells cultured for various experimental purpose was extracted and purified by the RNeasy Mini Kit according to manufacturer's instruction. The resulting RNA was essessed by NanoDrop Lite spectrophotometer (Thermo Scientific) to examine their concentration and purity. Ideally, the 260/280 ratio of ~2 is generally accepted as pure RNA. For storage, RNA samples were aliquoted in PCR microtubes and stored at -80°C. The reagents for RNA

2.2.2 DNase I treatment

Table 2.6 | Reagents and corresponding amounts for DNase I treatment of RNA sample

Components	Amount
RNA	1 μg
10x DNase I Reaction Buffer	1 μl
DNase I Amplification Grade (1U/μl)	1 μl
RNase-free water	Up to 101 μl

The resulting RNA from 2.2.1.1. were treated with DNase I to minimize residual genomic DNA contamination in the samples before cDNA synthesis. RNA samples were prepared in duplicates for positive and negative controls of reverse transcription procedure.

The reaction of DNase I treatment was described in **Table 2.6**. The samples were incubated at room temperature for 15 min followed by addition of 1 μl of EDTA 25mM to the reaction. Finally, samples were placed in 65°C for 10 min to heat-inactivate the enzymatic activity of DNase I.

2.2.3 cDNA synthesis

Table 2.7 | Reagents and corresponding amounts for cDNA synthesis

Reaction 1		
Components	**+RT**	**-RT**
Random hexamers (100μM)	1 μl	1 μl
DNase I-treated total RNA	11 μl	11 μl
dNTPs mix (10mM)	1 μl	1 μl

Reaction 2		
Components	**+RT**	**-RT**
5x First-strand Buffer	4 μl	4 μl
0.1M DTT	2 μl	2 μl

cDNA Synthesis describes the generation of complementary DNA (cDNA) from single-stranded RNA via reverse transcription. Before starting the procedure cDNA synthesis, the countertop, plastic surface, pipettes, tubes and gloves were treated with RNaseZap™. Clean filtered tips as well as the freshly autoclaved microtubes and PCR tubes were used for the experiment.

First-strand cDNA library from DNase I-treated total RNA was synthesized using SuperScript™ II Reverse Transcriptase along with short random hexamers (5'-NNNNNN-3') and oligo d(T) primers. Random primers are a mixture of any possible combination of six bases which serve to bind elsewhere in the genome and allow reverse transcriptase to fill up the gaps, while oligo d(T) binds to the poly-adenylated (poly-A) tail of RNA at the 3' end and then only transcribes RNA.

The components of two steps of cDNA synthesis were described in **Table 2.7**. A duplicate of each sample was made to incubate with reverse transcriptase (+RT) or with RNase-free water (-RT) as a negative control. First, the Reaction 1 listed in **Table 2.7** were incubated at 65°C for 5 mins and then chilled on ice for 2 min before spinning to collect the liquid at the bottom of the tube. The compounds described in **Table 2.7** were added to Reaction 1 and gently mixed. The tubes were incubated at 25°C for 2 mins followed by addition of 1μl (200

Units) of reverse transcriptase to +RT tube while 1µl of RNase-free water to -RT tube. Solutions were mixed by pipetting up and down gently and incubated at 25°C for 10 mins, then at 42°C for an hour. To stop the reaction, samples were incubated at 75°C for 15 mins. The resulting cDNA was aliquoted with small amounts to avoid degradation from repeated freeze-thaw cycles and stored at -20°C. Synthesized cDNA was used as the template in standard PCR to determine gene expression profile or in qPCR for quantification of gene expression level.

2.3 Molecular cloning

Molecular cloning is a technique that involves the insertion of a DNA sequence into a vector for propagation. In this project, DNA fragments used for molecular cloning were amplified by PCR or isolated from existing DNA plasmids.

2.3.1 Stranded Polymerase Chain Reaction (PCR)

2.3.1.1 Phusion™ High-Fidelity Polymerase

DNA fragments used for molecular cloning were amplified by PCR with Phusion™ High-Fidelity Polymerase as the DNA sequence needs to be correct after amplification. Characterized by *Pyrococcus*-like enzyme with a processivity-enhancing domain, the Phusion™ High-Fidelity Polymerase possesses 5' → 3' DNA polymerase activity and 3' → 5' exonuclease proofreading activity and will generate blunt-ended products with high accuracy.

Table 2.8 | Components and relevant amounts for PhusionTM High-Fidelity PCR

Reaction Components	Amount
5x Phusion Green HF buffer	10 µl
dNTP (10 mM)	1 µl
Forward primer (10 µM)	2.5 µl
Reverse primer (10 µM)	2.5 µl
Template DNA (plasmid DNA)	20 ng
Phusion™ High-Fidelity Polymerase (2U/ µl) *Added last	0.5 µl
ddH_2O	Up to 50 µl

Primers for the PCR were designed to be around 18-22 bases in length. In order to generate compatible ends for future cloning procedure, sequences recognized by specific restriction enzymes were also added to the 5' end of both PCR primers. The reagents for PCR were summarised in Table 2.8. Primer annealing temperature was determined using Tm calculator and instructions on ThermoFisher website. The PCR reactions were prepared as described in Table 2.8. Amplification of DNA fragments was performed in a thermocycler with the parameters listed in Table 2.9:

Table 2.9 | Parameters for Phusion™ High-Fidelity PCR

Cycle step	Temperature	Time	Cycles
Initial denaturation	98°C	30 sec	1
Denaturation **Annealing** **Extension**	98°C *x*°C < 70°C 72°C	10 sec 30 sec 30 sec/kb of plasmid length	35
Final extension	72°C	10 mins	1

2.3.1.2 GoTaq® DNA Polymerase

GoTaq® polymerase-conducted PCR was used to amplify small fragments of DNA (< 1kb). Despite the fact that GoTaq® Polymerase lacks the 3' → 5' exonuclease proofreading ability and may introduce small errors in the amplified sequence, it is still useful and convenient when screening large number of DNA amplicons in a short time. In this project, GoTaq® polymerase-conducted PCR was used to examine alternative splicing of cassette exons. Preparation of PCR components are described in Table 2.10, while the primers used in this study are listed in Table 2.11.

Table 2.10 | Components and relevant amounts for GoTaq® PCR

Reaction Components	Amount
5x Green GoTaq® Flexi buffer	4 µl
$MgCl_2$ (25 mM)	3.2 µl
dNTP (10 mM)	0.4 µl
Forward primer (10 µM)	1 µl
Reverse primer (10 µM)	1 µl

Template DNA (cDNA) *cDNA mixture from 1 µg of total RNA	2 µl
GoTaq® DNA Polymerase (5U/ µl) *Added last	0.1 µl
ddH_2O	Up to 20 µl

Table 2.11 | Primers used for examination of alternative splicing

These primers were designed based on reference indicated. All the primers were ordered and synthesized from Sigma-Aldrich.

Primer ID	FWD sequence (5'->3')	REV sequence (5'->3')	reference
AP1G2-E3	AGCTGGCCAAACTGCTCTAC	GTGCTCAAAGTGCACAAGGC	[108]
ARHGAP4-E9	TGGATCCTCCAGGGGACAAA	AATCAAGCACATCCCCGTCA	[108]
CTTN-E11	TGGTGTGCAGACAGACAGAC	CCATACTTCCCGCCGAATCC	[108]
WNK4-E2	GCTGCGTAAAGCAAGGGAAT	ACGTGGAATGGATAGGGCAA	[108]
TRPT1-E7	GCATGCGGTCCCATTGTGAA	GCTTGGGGCTACTCTGACAC	[108]
hCDK2-E5	GCTTTTGGAGTCCCTGTTCG	GGTCCCCAGAGTCCGAAAGA	[108]
TPM1-E6	CCCGTAAGCTGGTCATCAT	REV 1: TAATTGTTCTTCCAGCTGTCGG REV2: CCTGAGCCTCCAGTGACTTC	[109]
FAS-E6	GGAATGCACACTCACCAGCA	GTTGGAGATTCATGAGAACCTTGGT	[109]
NUMB-E9	AGGACCCCTTCTCATCTGCT	GCACCAGAAGATTGACCCCA	[109]
HITRA2-E7	GGAGGTGATTGGAGTGAA	GTCACATATAAGGTCAGT	[110]
EIF4G2-E9	ATCGCAGTTTGGAGAGATGG	CTGTCCCAGAGGTGGTGTTT	[111]
PPP5C-E5	ATGAGTACAGCGGACCCAAG	ATAGAACTGGCCATGGGTGT	[111]
FAM38A-E8	TGGATGTGTGTGGAGGACAT	ATGATGGCGATGAGGAAGAG	[111]
MPRL33-E3	TGTGGTCACCATGTTCCTCT	CCGCCCTCAGTCTTCTCTTT	[111]
EZH2-E17	AGAATGGAAACAGCGAAGGAT	AGGGCATTCACCAACTCCACAAA	[111]
MRPIP-E9	GAGGTCCCAGGTGATTGAAA	AGTCAGCCAGCCTTTCTTGA	[111]
PIP5K1A-E12	CAGGCTTCTACGCTGAACG	GTGAGAAACTGGGGTCAGGA	[111]

In GoTaq® polymerase-conducted PCR, melting temperature of each primer was determined using the Promega Tm Calculator web tool (www.promega.com/biomath). The optimal annealing temperature for a given primer pair was calculated as 3°C below the lowest melting temperature. Amplification of DNA fragments was performed in a thermocycler with the parameter listed in Table 2.12. PCR products were analysed by agarose gel.

Table 2.12 | Parameters for GoTaq® PCR

Cycle step	Temperature	Time	Cycles
Initial denaturation	95°C	3 mins	1

Denaturation **Annealing** **Extension**	95°C *x*°C < 70°C 72°C	45 sec 30 sec 1 min/kb of plasmid length	40
Final extension	72°C	10 mins	1

2.3.2 DNA purification and quantification

Purification of DNA from PCR products in order to remove unnecessary buffer, enzymes, nucleotides, and primers is essential for the following cloning procedure. In this project, DNA purification was carried out through DNA gel extraction and column purification.

2.3.2.1 DNA gel extraction

After PCR amplification, DNA of desired fragment was extracted and purified from agarose gel following agarose gel electrophoresis. DNA is negatively charged and moves toward the positive electrode by which the DNA fragments can be separated based on their length in base pairs. Agarose gel solution ideal for separation of DNA fragments with a range of 100 bp to 10 kb was prepared 1% in 1x TAE buffer (40 mM Tris, 20 mM acetic acid, 1 mM EDTA). Agarose was heated in the microwave until completely dissolved, then the agarose solution was cooled down to around 50°C. SYBR® Safe DNA gel stain was added to the agarose solution with a dilution ratio of 1:10000 to visualize DNA under the UV light. After solidifying at room temperature for about 30 mins, the agarose gel was put in the electrophoresis kit with 1x TAE buffer covered the whole gel. DNA samples (plasmid DNA) mixed or not (PCR products) with 6x Purple gel loading dye were carefully loaded into every other well on the agarose gel to avoid contamination of adjacent DNA when purification procedure was performed. An appropriate DNA ladder was loaded to assess the size of the DNA fragments. The agarose gel was run at 60-100 V until the lower dye reached 3/4 or 4/5 of the gel. DNA fragments can be visualized under a Blue LED Illuminator and the bands of interest were excised from the gel with a sterile scalpel. DNA was then further extracted using NucleoSpin® Gel and PCR clean-up Kit as description in **2.3.2.2**.

For the purpose to simply examine the size of DNA fragments without subsequent extraction and purification, gels were imaged using the Gel Doc™ EZ System after agarose gel electrophoresis.

2.3.2.2 Column purification

PCR products or restriction enzyme-treated DNA samples were purified by NucleoSpin® Gel and PCR clean-up Kit according to manufacturer's instructions to remove undesirable nucleotides, primers, dyes, and buffer salts. NucleoSpin® Gel and PCR clean-up Kit contains a silica resin that selectively binds DNA while impurities such as protein will be washed away after centrifugation. These columns are designed to yield up to 15 μg of purified DNA sized from 50 bp to 20 kb with a recovery of 70-95%.

2.3.2.3 Phenol-chloroform DNA purification

For stable transfection of target gene into host cells used in this work, the linearized plasmid DNA was purified by phenol-chloroform extraction procedure following restriction enzymes digestion. Phenol-chloroform extraction is widely used to remove proteins from DNA samples based on the idea that polar molecules and less polar compounds can be separated by aqueous phase and phenol phase. When DNA samples are mixed thoroughly with phenol-chloroform solution, two phases of light aqueous phase (upper layer) and dense phenol phase (lower layer) are formed based on different density. DNA with the negative charges on its phosphate backbone is very soluble in water rather than in phenol. However, the polarity of protein is flipped in phenol-DNA mixture, causing the less-polar residues from inside of protein structure to turn outside and become denatured in phenol environment. Then the aqueous DNA fraction can be separated from protein/phenol phase by centrifugation.

First an equal volume of Phenol: Chloroform: Isoamyl alcohol (ph8.0) from lower phase of the bottle was added to aqueous DNA solution. The microtube was inverted to mix thoroughly followed by centrifugation at maximum speed for 2 mins in a benchtop centrifuge. The top aqueous phase containing DNA was carefully transferred into a new 1.5 ml microtube. The centrifugation and extraction steps were repeated again. Then, 1/10 volume of 3 M Sodium acetate (pH 5.2) was added to and mixed thoroughly with the aqueous sample to neutralize the negative charges of DNA. The same volume of room temperature isopropanol was added to DNA sample and vortexed before being incubated at -80°C for 1~2 hrs or at -20°C for overnight. DNA pellet was obtained by centrifugation at 13000 x *g* for 30 mins at 4°C and then washed by 1 ml of 70% EtOH. After centrifugation at maximum speed at 4°C for 15 min, the supernatant was carefully discarded, and the DNA pellet was allowed to dry for a few minutes until being transparent. The DNA pellet was resolved in 20~50 μl of ddH2O. The DNA concentration and purity were then measured by a NanoDrop Lite spectrophotometer followed by immediate transfection procedure. Ideally, the 260/280 ratio of ~1.8 is generally

accepted as pure DNA. The purified DNA plasmid can also be store at -20°C if the DNA was circular.

2.3.2.4 Restriction enzyme digestion

Restriction enzymes are naturally occurring bacterial endonucleases that typically recognize 6-8 bp consecutive bases and cut DNA at or near these recognition sites. In the subcloning of a target gene from one vector into another recipient vector, double restriction enzyme (RE) digestion is performed to cleave DNA at recognition sites that are capable of being ligated together. In addition, restriction enzymes are widely used to generate PCR products for cloning purpose by adding restriction sequences to 5' end of both PCR primers. It is also applied to verify a plasmid by cutting the DNA into specific size and analysing the resulting fragments by gel electrophoresis, which is known as diagnostic digestion.

The restriction enzymes used in this project were selected only to cut DNA within the multiple cloning sites without causing any cleavage of the insert fragment. Optimal condition such as the choose of buffer and restriction enzymes compatibility were described in NEBtools Single/Double Digestion website (https://nebcloner.neb.com/#!/redigest). The digestion reaction was conducted at 37°C for 1~6 hrs according to the extended activity of selected restriction enzymes. Components prepared for restriction enzyme digestion were listed in Table 2.13. To prevent the digested recipient vector from self-ligation, 1 µl of CIP (Calf intestine alkaline phosphatase) was added to the reaction for another 30 min at 37°C to dephosphorylate the 5' -ends of DNA followed by inactivation procedure by incubating the reaction at 80°C for 20 min. The digested DNA was purified by gel extraction and column purification as described in 2.3.2.1 and 2.3.2.2 before ligation.

Table 2.13 | Restriction enzyme digestion reaction

The selection of 10x NEBuffer is dependent on the restriction enzyme used.

Components	Amount
10x NEBuffer	5 µl
DNA (PCR product or vector)	250 ng~5 µg
Restriction enzyme I *Added last	1 µl per µg of DNA to digest
Restriction enzyme II *Added last	1 µl per µg of DNA to digest
ddH_2O	50 µl

2.3.2.5 Ligation

In ligation procedure, RE-digested DNA inserts and recipient vector were jointed together through the formation of phosphodiester bond by T4 DNA ligase activity. For most standard cloning used in this work, the molar ratio of recipient plasmid to insert DNA was 1:5 while 50 ng of backbone was used in a 20 μl ligation reaction. The formula was shown as below:

$$ng\ of\ insert = ng\ of\ vector\ backbone \times \frac{length\ of\ insert\ (bp)}{length\ of\ backbone\ (bp)}$$

The components of ligation were prepared as listed in Table 2.14 and the reaction was conducted at room temperature for overnight. A parallel reaction with no DNA insert was used as control to check the unwanted background caused by incompletely digested vector. The recombinant plasmid after ligation reaction was then ready for bacterial transformation.

Table 2.14 | Ligation reaction

Reagents	DNA insert-inearized vector ligation	Self-circularization of linear vector (control)
10x T4 DNA Ligase buffer	2 μl	2 μl
Recipient vector	50 ng	50 ng
DNA insert	5:1 molar ratio over vector	–
T4 DNA Ligase (5 Weiss U/μL) * Added last	1 μl	1 μl
ddH_2O	Up to 20 μl	Up to 20 μl

2.3.2.6 Bacterial transformation

The purpose of bacterial transformation is to produce large copies of recombinant DNA by transferring exogenous DNA into a competent strain of bacteria. The bacteria then replicate the target gene in required amounts for further application. The procedure mainly consists of a heat-shock transformation, bacterial recovery and plating. All of steps were kept in a sterile environment near Bunsen Burner and carried out with autoclaved tips and microtubes.

In transformation procedure, a 50 μl aliquot of chemically prepared competent *E. coli* strain NovaBlue was thawed on ice for 10 mins. Particular amounts of DNA (e.g., 500 ng of validated plasmid or 7 μl of ligation reaction) was mixed with competent cells and placed on ice for 15

mins. The mixture was then placed at 42°C to create holes on bacteria, through which DNA can pass into the cells. The competent cells were put back on ice for 2 mins to restore membrane integrity and trapped DNA inside the cells.

For the bacterial recovery, 450 µl of antibiotic-free LB medium was added to competent cells and the tube was incubated at 37°C under constant shaking (230 rpm) for 1 hr. The bacterial culture was pelleted by centrifugation at 3615 x g for 2 mins. After discarding the supernatant, the pellet was resuspended with the remaining LB medium to create a bacteria suspension of around 100 µl. All of the transformed bacteria (with negative control DNA or ligation reaction) or various amounts of competent cells (10% of total culture for validated DNA) were plated on pre-warmed LB plate containing the appropriate antibiotics. The plates were then incubated upside down at 37°C for around 16 hrs before inspecting the formation of single colonies. The LB plates with bacterial colonies were sealed with Parafilm® and stored at 4°C until inoculation and can be kept for up to 4-6 weeks.

2.3.2.7 Plasmid isolation and purification Miniprep kit

After bacterial transformation with a ligation product, a sterile working environment was created, and a single bacterial colony was picked with a sterile loop and inoculated into a bacterial tube containing 5 ml of LB medium supplemented with appropriate antibiotics. The tube was incubated at 37°C under constant shaking (230 rpm) for around 16 hrs. After checking the bacterial growth, the culture was centrifuged at 1000 x g for 15 mins at 4°C to collect bacterial pellet prior to plasmid purification.

Plasmids were isolated and purified by GeneJET Plasmid Miniprep Kit according to manufacturer's instructions. DNA was eluted in 30 µl of ddH_2O and the concentration and purity were assessed by NanoDrop. To verify the insert, a diagnostic digest was performed with appropriate restriction enzymes. The digested DNA fragment was assessed by agarose gel electrophoresis and visualized by Gel Doc™ EZ System. Finally, the plasmid was validated by DNA sequencing.

2.3.2.8 DNA sequencing

DNA sequencing was used to determine the order of nucleotides in DNA and verify the constructs generated by molecular cloning. Sequencing was carried out at the University of Sheffield Core Genomic Facility using Applied Biosystems' 3730 DNA Analyser and the BigDyeTM Terminator v3.1 Cycle Sequencing Kit. Clean reads of DNA sequence of an average

of 700 bp were achieved with accordingly the primers based on the property of backbone. The resulting sequence was compared to the original gene using NCBI Nucleotide BLAST.

2.3.2.9 Plasmid propagation by NucleoBond® Xtra Midi kit

The validated plasmid DNA was then scaled up and purified for further experimental purpose. In brief, a sterile working environment was created and a single bacteria colony from an agar plate was inoculated in 5 ml of LB medium supplemented with appropriate antibiotics. The culture was incubated for 8 hrs at 37°C under constant shaking (230 rpm). The bacterial culture was then transferred into sterile flask containing 100 ml of LB medium and appropriate antibiotics and incubated in shaking incubator for overnight (~16 hours) at 37°C. The culture was centrifuged for 15 min at 4°C to collet bacterial pellet prior to the plasmid isolation procedure with NucleoBond® Xtra Midi kit according to manufacturer's instruction. The resulting DNA pellet was reconstituted in 200~300 µl of ddH_2O and the DNA concentration and purifty were assessed by NanoDrop.

2.4 Establishment of Flp-In™ T-REX™ HEK293 stable clone expressing mutant RhoA

In this project, Flp-In™ T-REX™ HEK293 is used to generate stable cell lines that ensure the homogenous expression of inducible constitutively active RhoA (CA-RhoA). The Flp-In™ T-REX™ HEK293 contains two plasmids: and pcDNA™6/TR. The pFRT/*lac*Zeo vector contains a single integrated FRT site which is inserted downstream of the ATG start codon of the *lacZ-Zeocin*™ fusion gene, while the pcDNA™6/TR stably expresses the Tet repressor under the control of the human CMV promoter. In order to keep the two unique plasmids in host cell line Flp-In™ T-REX™ HEK293 used in this project, the cells should be maintained and cultured in medium containing selection factors Zeocin and Blasticidin S HCl (Figure 2.1).

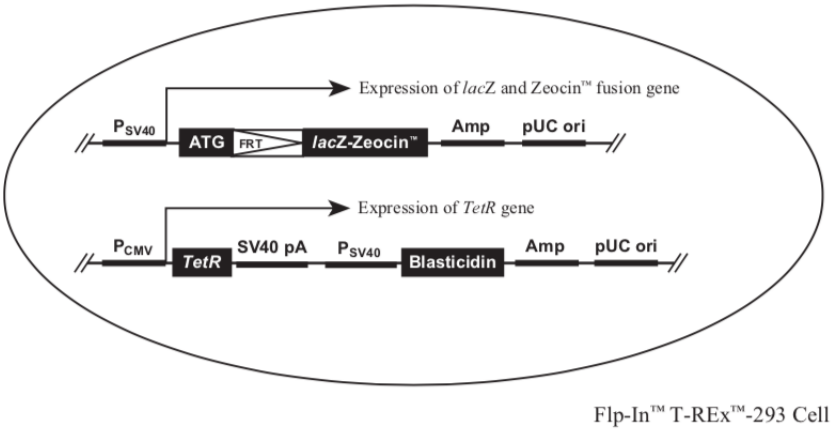

Figure 2.1 | Flp-InTM T-REXTM HEK293 system

Flp-InTM T-REX HEK293 contains two plasmids: pFRT/*lac*Zeo target site vector and pcDNA^{TM}6/TR. pFRT/*lac*Zeo displays Zeocin resistant gene a FRT site that serves as a binding and cleavage site of the Flp recombinase. pcDNA^{TM}6/TR is Blasticidin resistant and expresses tetracycline repressor (TetR) under the control of human CMV promoter.
Figure reproduced from https://www.thermofisher.com/order/catalog/product/R78007#/R78007.

Two other plasmids which are involved in the generation of Flp-In^{TM} T-REX^{TM} stable clone are pcDNA^{TM}5/FRT/TO and pOG44. Both of the plasmids were kindly provided by Professor Elizabeth Smythe. pcDNA^{TM}5/FRT/TO expression vector is used to construct recombinant plasmid containing GOI, which is under the control of a tetracycline-regulated, hybrid human cytomegalovirus promotor (pCMV/TetO_2). The vector contains a FRT site for its integration into pFRT/*lac*Zeo vector of host cells as well as displays a hygromycin resistant gene for further selection of resulting stable cell line. pOG44 functions to constitutively express the Flp recombinase that catalyses integration of pcDNA^{TM}5/FRT/TO with GOI into the genome of host cell line.

2.4.1 Mutant RhoA plasmid cloning

Table 2.15a | List of primers used for establishment of HEK293-tet-RhoA stable clone

Primer name	Sequence	Restriction enzyme	Tm (°C)
Q63L-RhoA FWD	5'-CTTAAGCTTGCCATGGTGAGCAAGGGC-3'	Hind III-HF	66
Q63L-RhoA REV	5'-CTTGCGGCCGCTCACAAGACAAGGCAACCAGATTTTT-3'	Not I-HF	66

Table 2.15b | List of plasmids used for establishment of HEK293-tet-RhoA stable clone

Plasmid	supplier
pcDNA3-EGFP-RhoA-Q63L	Addgene (Plasmids# 12968)
pOG44	Library of Professor Elizabeth Smythe Lab
pcDNA^{TM}5/FRT/TO	Library of Professor Elizabeth Smythe Lab

In our work, we utilized the Flp-In^{TM} T-REX^{TM} HEK293 system (gift from Professor Elizabeth Smythe) to generate stable clone in which the expression of the constitutively active RhoA (CA-RhoA) mutant can be induced by tetracycline. First, the EGFP-tagged CA-RhoA mutant was amplified from pcDNA3-EGFP-RhoA-Q63L by PCR with a pair of primers containing restriction enzyme (RE) site of HindIII-HF and NotI-HF at 5' end respectively. The primers used in this work are listed in Table 2.15a, while the plasmids used in this part can be found in Table 2.15b. The PCR product was purified as described in 2.3.2.1 and 2.3.2.2 followed by the quantification of DNA to determine the concentration. Then 1 μg of the PCR product as well as 2 μg of pcDNA^{TM}5/FRT/TO expression vector were digested by HindIII-HF and NotI-HF at 37 °C for 1 hr to create the ligating sites. To avoid self-ligation of linearized plasmid, pcDNA^{TM}5/FRT/TO vector was further treated with 1 μl of CIP at 37 °C for 30 min for the dephosphorylation at 5' and 3' end of DNA, followed by inactivation procedure at 80 °C for 20 minutes.

Restriction enzyme-treated PCR product and expression vector were purified again by gel extraction of DNA. Ligation was then performed for the cloning of EGFP-CA-RhoA to the HindIII-HF and NotI-HF site of pcDNA^{TM}5/FRT/TO to create recombinant plasmid pcDNA5/FRT/TO-RhoA-Q63L. The procedure of ligation is described in 2.2.3.5 whereas the reaction components are as listed in Table 2.14. The ligation reaction without insert DNA was used as a negative control.

For the purification of pcDNA5/FRT/TO-RhoA-Q63L, 7 μl of ligation mixture of each construct was introduced into 50 μl of Nova Blue *E. coli* competent cells. The transformation was performed based on the procedure in 2.2.3.6. After cell recovery period, the bacteria were plated on LB agar supplemented with 100 μg/ml of Ampicillin and cultured at 37 °C for overnight (~16 hrs). Three single colonies were then picked and inoculated respectively in 5

ml of LB medium containing 100 μg/ml of Ampicillin at 37 °C for 16 hrs. The plasmid construct was isolated and purified from bacteria by GeneJET Plasmid Miniprep Kit followed by DNA quantification. Restriction digestions of 500 μg of recipient vector by HindIII-HF and NotI-HF were applied as diagnostic digests to validate the construct. Resulting fragments were analysed by 1 % agarose gel electrophoresis before resorting to sequencing of the plasmid. The validated pcDNA5/FRT/TO-RhoA-Q63L plasmid was then scaled up by NucleoBond® Xtra Midi kit according to the description in 2.2.3.9.

2.4.2 Killing curve test of Flp-In™ T-REX™ HEK293

As the pcDNA™5/FRT/TO contains a hygromycin resistant gene, the hygromycin B antibiotic is used for the selection of resulting stable clone. Prior to generate stable cell line being able to express pcDNA5/FRT/TO-RhoA-Q63L, the killing curve test of parental Flp-In™ T-REX™ HEK293 was performed to determine the minimum effective dose of hygromycin that killed all non-resistant HEK293 cells. First, parental HEK293 were seeded in a 24-well plate at 1 x10^5 onto each well for 24 hours before the culture medium was replaced by selective medium supplemented with hygromycin. The concentration of hygromycin used for killing curve test was in a range from 100 μg/ml to 700 μg/ml. The selective medium was refreshed every two days, and the cell death was monitored daily. The minimum effective concentration of hygromycin B was 200 μg/ml as the dose was able to kill all non-resistant cells within 5 days.

2.4.3 Generation of HEK293-tet-RhoA stable cell line

The recombinant DNA pcDNA5/FRT/TO-RhoA-Q63L construct and pOG44 vector were co-transfected into Flp-In™ T-REX™ HEK293 parental cell line to generate a stable Flp-In™ T-REX™ cell line capable of expressing CA-RhoA mutant Q63L. One day prior to transfection, cells were seeded in a 6-well plate at 4 x 10^5 onto each well and allowed to grow to about 60~70 % of confluency. A mixture of plasmid DNA containing a 9:1 ratio (w/w) of pOG44:pcDNA5/FRT/TO-RhoA-Q63L was transfected into Flp-In™ T-REX™ HEK293 by Lipofectamine™ 2000 based on the procedure described in 2.1.6 and Table 2.4. One well of untransfected cells was as negative control. Another control was performed parallelly by transfecting the cells with pcDNA5/FRT/TO-RhoA-Q63L alone to ensure the integration of pcDNA5/FRT/TO-RhoA-Q63L was only under the mediation of Flp recombinase expressed by pOG44.

After 24 hrs of transfection, the medium was removed and replaced with fresh complete medium (DMEM culture medium + blasticidin) for another 24 hrs. Since the *lac*Zeo gene was interrupted by the integration of plasmid construct into the the FRT site, zeocin must be removed from culture medium after co-transfection of pcDNA5/FRT/TO-RhoA-Q63L and pOG44 because the transfectants were sensitive to zeocin. However, blasticidin should be remained in the selection medium for the maintenance of the pcDNA^{TM}6/TR plasmid. Before starting hygromycin B selection, cells were split into fresh selection medium supplemented with 200 μg/ml of hygromycin B to make low density culture of no more than 25 % confluency. The selection medium was replaced every two-three days until the visible colonies of true transfectants can be identified.

Given that the Flp-In^{TM} T-REX^{TM} HEK293 parental cell line displays a single integrated FRT site, the resulting stable clone HEK293-tet-RhoA was supposed to be an isogenic population with each cell would carrying only one copy of the RhoA-Q63L gene at the integrated site. After hygromycin B selection, the whole polyclonal population were pooled, expended for cryopreservation and further screening of tetracycline-regulated expression. The resulting stable clone was named HEK293-tet-RhoA.

2.5 Establishment of stable clones expressing proximity labelling system

In order to prepare nuclear protein samples for nuclear proteome analysis by Mass spectrometry, we used proximity labelling system as a means to isolate and purify nuclear components. The method is based on a previous study which generated two biotin ligase mutants TurboID and miniTurbo to catalyse the biotinylation of proteins of proximity in the presence of external biotin [112]. With a nuclear localization signal (NLS) tagged to the TurboID and miniTurbo constructs, the two biotin ligase mutants are supposed to be imported into the nucleus after translation. Therefore, only nuclear proteins will be biotinylated and able to be purified by streptavidin resins-conducted pulldown (PD) due to the strong interaction between biotin and streptavidin. The purpose of this part was to establish the stable clones expressing proximity labelling system for nuclear protein isolation.

2.5.1 Plasmid preparation

2.5.1.1 Construction pcDNA3.1-PuroR-3xHA-TurboID-NLS and pcDNA3.1-PuroR-3xHA-miniTurbo-NLS

Two biotin ligase mutant constructs used to generate stable cell lines were engineered by re-cloning TurboID or miniTurbo gene from donor plasmids 3xHA-TurboID-NLS_pCDNA3 and 3xHA-miniTurbo-NLS_pCDNA3 to recipient pcDNA3.1-Myc-PuroR expression vector. The plasmid information is listed in Table 2.16a. In brief, the digestion procedure of plasmids with restriction enzymes HindIII-HF and XbaI was followed the procedure of 2.3.2.4 while the digestion components were prepared as Table 2.16b. The linearized pcDNA3.1-Myc-PuroR plasmid was treated with 1 µl of CIP for 30 mins at 37 °C for the dephosphorylation at 5' and 3' end of DNA, followed by inactivation procedure for 20 mins at 80 °C.

The DNA fragments cutting from 3xHA-TurboID-NLS_pCDNA3 and 3xHA-miniTurbo-NLS_pCDNA3 as well as linear pcDNA3.1-Myc-PuroR were analysed by 1 % agarose gel electrophoresis to check the size before gel extraction. For ligation reaction, an 8:1 mass ratio of insert: expression vector was used for the cloning of TurboID and miniTurbo into pcDNA3.1-Myc-PuroR.

Table 2.16a | List of plasmids used for establishment of HEK293-tet-RhoA-TurboID stable clone

Plasmid	supplier
3xHA-TurboID-NLS_pCDNA3	Addgene (Plasmids# 107171)
3xHA-miniTurbo-NLS_pCDNA3	Addgene (Plasmids# 107172)
pcDNA3.1 (+) myc PuroR	Library of Dr Erdmann Lab

Table 2.16b | Restriction enzyme digestion reaction used for generation of HEK293-tet-RhoA-TurboID and HEK293-tet-RhoA-miniTurbol stable clone

Reagents	3xHA-TurboID-NLS-pCDNA3	3xHA-miniTurbo-NLS-pCDNA3	pcDNA3.1-Myc-PuroR
10x Buffer (CutSmart)	5 µl	5 µl	5 µl
Plasmid DNA	5 µg	5 µg	2 µg
*HindIII-HF	5 µl	5 µl	2 µl
*XbaI	5 µl	5 µl	2 µl
ddH2O	Up to 50 µl	Up to 50 µl	Up to 50 µl

*Restriction enzymes were added last.

To verify the resulting constructs pcDNA3.1-PuroR-3xHA-TurboID-NLS and pcDNA3.1-PuroR-3xHA-miniTurbo-NLS, 7 µl of ligation mixture of each construct was introduced into 50 µl of Nova Blue *E. coli* competent cells for bacterial transformation (see 2.2.3.6). Three single colonies from each construct were inoculated in 5 ml of LB medium supplemented with 100 µg/ml of Ampicillin and cultured for 16 hrs at 37°C. The purification of plasmids was conducted as described in 2.2.3.7. After DNA quantification, 500 ng of plasmid constructs were treated with HindIII-HF and XbaI followed by 1 % agarose gel analysis to verify DNA inserts. Plasmids with correct insert size were subjected to sequencing. The validated pcDNA3.1-PuroR-3xHA-TurboID-NLS and pcDNA3.1-PuroR-3xHA-miniTurbo-NLS plasmids were then scaled up by NucleoBond® Xtra Midi kit according to the description in 2.3.2.9.

2.5.1.2 Construction of pcDNA5-FRT-3xHA-TurboID-NLS

Another TurboID plasmid construct for the generation of stable clone through Flp-In HEK293 system was conducted by recloning TurboID from existing plasmid 3xHA-TurboID-NLS_pCDNA3 to pcDNA5/FRT. The restriction enzymes and related components used for the digestion of 3xHA-TurboID-NLS_pCDNA3 and pcDNA5/FRT are listed in Table 2.17. After the digestion reaction, the linearized pcDNA5/FRT expression vector was treated with 1 µl of CIP for 30 mins at 37 °C for the dephosphorylation at 5' and 3' end, followed by inactivation procedure for 20 mins at 80 °C. Both the digestion reactions were purified by gel extraction following verification with 1 % agarose gel electrophoresis. Next, an 8:1 mass ratio of insert: expression vector was used for ligation of 3xHA-TurboID-NLS into pcDNA5/FRT expression vector.

Table 2.17 | Restriction enzyme digestion reaction used for generation of HEK293-TurboID stable clone

Reagents	3xHA-TurboID-NLS-pCDNA3	pcDNA5/FRT
10x Buffer (Cut Smart)	5 µl	5 µl
Plasmid DNA	5 µg	2 µg
*HindIII-HF	5 µl	2 µl
* XhoI	5 µl	2 µl
ddH_2O	Up to 50 µl	Up to 50 µl

*Restriction enzymes were added last.

The resulting construct was named pcDNA5-FRT-3xHA-TurboID-NLS. For plasmid expansion of pcDNA5-FRT-3xHA-TurboID-NLS, 7 μl of ligation mixture was transformed into 50 μl of Nova Blue *E. coli* competent cells based on 2.3.2.6. Four single colonies were inoculated and cultured in 5 ml of LB supplemented with 100 μg/ml Amp medium for 16 hrs at 37 °C followed by purification of plasmids with Miniprep Kit as described in 2.3.2.7. After measurement of DNA concentration, 500 ng of plasmid constructs were treated with HindIII-HF and XhoI followed by 1 % agarose gel analysis to check DNA inserts. Plasmids with correct insert size were sorting to sequencing. The validated pcDNA5-FRT-3xHA-TurboID-NLS plasmid was then scaled up by NucleoBond® Xtra Midi kit according to the description in 2.3.2.9.

2.5.2 Killing curve test

2.5.2.1 For selection of HEK293-tet-RhoA-TurboID

The antibiotic puromycin was used to select HEK-Q63L cells carrying pcDNA3.1-PuroR-3xHA-TurboID-NLS or pcDNA3.1-PuroR-3xHA-miniTurbo-NLS after transfection. In order to determine the minimum selective dose of puromycin, killing curve test of HEK-Q63L cells was performed prior to transfection of cells with TurboID or miniTurbo construct. HEK-Q63L cells were seeded in a 24-well plate at $1x10^5$ onto each well for 24 hours before the puromycin selection with a concentration ranging from 0.5 μg/ml to 10 μg/ml. Cell death was monitored daily while refreshing the medium every two-three days. The minimum effective concentration of puromycin was 1.5 μg/ml as all non-resistant cells were killed by the dose within 5 days.

2.5.2.2 For selection of HEK293-TurboID

The concentration of Hygromycin used for the selection of resulting stable clone HEK293-TurboID Flp-In™ T-REX™ HEK293-based stable cell line had been described in 2.4.2. The killing curve test with the same antibiotic was performed as well to determine 150 μg/ml was the minimum effective dose that killed all non-resistant Flp-In™ T-REX™ HEK293.

2.5.3 Generation of HEK293-tet-RhoA-TurboID and HEK293-tet-RhoA-miniTurbo stable clones

The stable transfection performed here was aimed to generate HEK293-tet-RhoA-TurboID and HEK293-tet-RhoA-miniTurbo stable cell line that constitutively express TurboID-NLS or miniTurbo biotin ligase mutants. Stable transfections are more efficient when using linear

DNA, which bears free ends that are more likely to be integrated into the host genome. In addition, making linear DNA by cutting its specific site also avoid the introduction of plasmid with random breakage site disrupting the target gene.

Prior to stable transfection, pcDNA3.1-PuroR-3xHA-TurboID-NLS and pcDNA3.1-PuroR-3xHA-miniTurbo-NLS were linearized by treating with endonuclease ScaI-HF for 4 hrs at 37 °C. Reagents for plasmid linearization were listed in Table 2.18. The linear plasmids were further treated with 1 µl of CIP for 30 mins at 37 °C for the prevention of self-ligation followed by inactivation for 20 mins at 80 °C. The DNA was purified by Phenol-chloroform purification as described in 2.3.2.3 and was dissolved in 20 µl of ddH_2O for quantification. To verify the size of linear DNA, 250 µg of DNA sample was analysed by 1 % agarose gel electrophoresis.

Table 2.18 | Reagents for plasmid linearization

Reagents	pcDNA3.1-PuroR-3xHA-TurboID-NLS	pcDNA3.1-PuroR-3xHA-miniTurbo-NLS
10x Buffer (CutSmart)	20 µl	20 µl
Plasmid DNA	6 µg	6 µg
*ScaI-HF	3 µl	3 µl
ddH_2O	Up to 200 µl	Up to 200 µl

*Restriction enzymes were added last.

Stable transfection of 1 µg of each linearized plasmid into HEK293-tet-RhoA was conducted by Lipofectamine™ 2000 as described in 2.1.6. Cells without transfection were used as negative control. After 6 hrs, transfected cells were refreshed with complete medium and cultured for overnight. Cells were then split with 1:10 ratio and subcultured in 10 cm petri dish for overnight before starting the selection of true-transfectants with 1.5 µg/ml of puromycin. The selection medium was replaced every two-three days until the single colony can be visible.

The single colony from each transfectants was isolated by Scienceware® cloning discs (Sigma-Aldrich) and removed to each well of 96-well culture plate containing puromycin selection medium. Cells were continuously cultured in selection medium which was refreshed twice a week. Until 50% of confluency, cells were subcultured in larger culture plate for further propagation (ex: all cells from one well of 96-plate to one well of 24-plate). The

resulting stable cell line was cryopreserved and verified by the screening of TurboID and miniTurbo expression.

2.5.4 Generation of HEK293-TurboID stable clone

The recombinant pcDNA5-FRT-3xHA-TurboID-NLS plasmid and pOG44 vector were co-transfected into Flp-In™ T-REX™ HEK293 to generate stable cell lines that constitutively express TurboID biotin ligase. One day prior to transfection, cells were seeded in a 6-well plate at $4x10^5$ onto each well for overnight and to be about 60~70 % confluent. A mixture of plasmid DNA containing a 9:1 ratio (w/w) of pOG44:pcDNA5-FRT-3xHA-TurboID-NLS was transfected into Flp-In™ T-REX™ HEK293 by Lipofectamine™ 2000 based on the procedure described in 2.1.6. The cells without transfection or with pcDNA5-FRT-3xHA-TurboID-NLS alone were used as negative control.

After 24 hrs of transfection, the medium was removed and replaced with accordingly fresh complete medium (DMEM culture medium + blasticidin) for another 24 hrs. Cells then were split into fresh selection medium supplemented with 200 μg/ml hygromycin B to make low density culture of no more than 25 % confluency. The selection medium was replaced every two-three days until the visible colonies of true transfectants can be identified. The whole cell population were pooled, expended both for cryopreservation and further screening of TurboID expression. The resulting stable clone was named HEK293-TurboID

2.6 Protein methods

2.6.1 Protein preparation

The buffer and the relevant composition used for protein methods are listed in Table 2.19.

Table 2.19 | Buffer for protein assay and western blotting
*Added at the last

Buffer	Composition
1x PBS	137 mM NaCl, 2.7 mM KCl, 10 mM Na_2PO_4, 1.8 mM KH_2PO_4 pH7.4
RIPA buffer	50 mM Tris pH 7.5, 150 mM NaCl, 0.1% SDS, 0.5% Sodium deoxycholate, 1 mM EDTA, 1% NP-40 (v/v), *1x protease cocktail inhibitor *PhoSTOP™ phosphatase inhibitor (for Mass spectrometry analysis)
4x Laemmli Buffer	250 mM Tris-HCl pH6.8, 40% glycerol, 8% SDS, 20% β-mercaptoethanol, 1% bromophenol blue
10x SDS Running Buffer	192 mM Glycine, 25 mM Tris, 0.1% SDS (w/v)
1X SDS Running Buffer	10x dilution of 10x Running Buffer in dH_2O
10X Transfer Buffer	192 mM Glycine, 25 mM Tris
1x Transfer Buffer	10x dilution of 10x Transfer Buffer in dH_2O + 20% MeOH
1x PBST	0.05% Tween20, 1x PBS
10x TBST	137 mM NaCl, 20 mM Tris-HCl pH 7.6
1x TBST	10x dilution of 10x TBS in dH_2O + 0.1% Tween 20
Biotin solution	500 μM biotin in DMSO

2.6.1.1 Cell lysis

For total protein extraction, all procedures were kept on ice to prevent the protein from degradation. The buffers used in this section were listed in Table 2.19.

Prior to performance of cell lysis, cells were washed 3 times with ice-cold 1x PBS to remove residual phenol-red in culture medium. Then ice-cold RIPA buffer showed in Table 2.19 with 1x protease inhibitor was added to cell and stayed on ice for 10 min. Lysed cells were scrapped down by scraper and the lysate was homogenised by QIAShredder spin column (QIAGEN). The samples were then vortexed every 10 mins followed by centrifugation at 16600 x g for 20 mins at 4°C. The supernatant containing the total protein was transferred into a new ice-cold 1.5 ml microtube while the cell debris remaining in the pellet was discarded. Protein concentration was then quantified using DC assay as described in Section 2.6.1.3 and the samples were prepared with equal amounts of protein. 4x Laemmli Buffer was added to the protein samples to a final concentration 1X and the mixture was boiled for 5 mins at 98°C to denature proteins. The protein samples were then stored at -20°C until being detected by Western blot.

2.6.1.2 Streptavidin pull-down assay

Pull-down assay is a form of affinity purification to detect or confirm a physical interaction among multiple proteins. In streptavidin pull-down assay, streptavidin is covalently attached

to cross-linked agarose resins, which in turn to capture and purify biotinylated proteins from cell lysates due to the strong interaction between biotin and streptavidin.

In this project, nuclear proteins were isolated by streptavidin pull-down assays using biotin-streptavidin system. Stable cell line displaying constitutively expressed TurboID or miniTurbo biotin ligase were grown in 10 cm culture dishes until reaching high density. Cells were treated with 500 μM biotin for 20 mins at 37°C to allow the exogenous biotin covalently attached to the nuclear proteomes. After biotin labelling, cells were quickly cooled by placing the dishes on ice to stop biotinylation and washed 5 times with ice-cold 1x PBS to remove external biotin traces. The cell lysis procedure was performed with RIPA buffer as described in 2.6.1.1. As RIPA buffer was harsh enough to disrupt all cellular compartments including the nucleus, the long fragments of DNA were released and the whole lysate was made to a gooey substance. In order to cut the chromosome, the cell lysate was transferred into the QIAshredder spin column and centrifuged at maximum speed (16600 x g) for 2 mins at 4°C to homogenize cell lysate. The flow-through was collected in another clean ice-cold microtube for the rest steps of protein extraction.

Prior to biotin-streptavidin pull-down assay, 100 μl of slurry Pierce® Streptavidin Agarose Resins were equilibrated with ice-cold RIPA buffer by three times of washing and centrifugation steps. After the last wash, the supernatant was carefully removed without disturbing the resin pellet. Cell lysate was incubated with the equilibrated resins under constant rotation for overnight at 4°C to allow interaction of biotinylated nuclear proteins with the streptavidin immobilized on agarose beads. The resins were then precipitated by centrifugation at 1800 x g for 3 mins at 4°C. 5% of the supernatant was collected in a new ice-cold microtube and boiled with corresponding 4x Laemmli Buffer for 5 mins at 98°C. The fraction was referred to as unbound sample in which proteins did not bind to the streptavidin resin. The rest of supernatant was carefully discarded without disrupting the resin pellet. Streptavidin resins were washed with ice-cold RIPA buffer three time by the centrifugation at 1800 x g for 3 mins at 4°C. After the last wash, resins were resuspended in 60 ml of 2x Laemmli Buffer and boiled for 5 mins at 98°C. The resulting denatured protein released from streptavidin resins was regarded as pulldown sample. For protein detection, original lysate (input) as well as pulldown and unbound sample were analysed and visualized by western blot.

2.6.1.3 Assessment of protein concentration

Protein concentration in cell lysate was assessed using BIO-RAD DC protein assay kit, a colorimetric method that is modified from Lowry method. The procedure was conducted

based on the manufacturer's instruction and the readout was detected at 740 nm in FLUOstar Omega Multi-mode Microplate Reader (ISOGEN Life Science).

A standard curve was first created by the serial dilution of Albumin standard stock (2 mg/ml) in the same buffer as the protein samples in a range from 0 mg/ml to 1.5 mg/ml. The concentration of each albumin dilution and the corresponding absorbance value were plotted on X and Y axis respectively to generate a linear regression. If the R^2 value was above 0.98, then the concentration of protein sample was determined by the equation as below:

$$ABS_{740\text{nm}}\ (\text{y}) = a * concentration\ (\text{x}) + b$$

The absorbance measurement of each sample was performed in duplicates and the protein concentration was calculated based on the mean value of absorbance. Protein samples were adjusted to the same amount (20~60 μg) with the same lysis buffer for the preparation of samples.

2.6.2 SDS-PAGE

Protein samples were analysed by SDS-PAGE (sodium dodecyl sulphate polyacrylamide gel electrophoresis) based on their molecular weight. SDS-PAGE is a discontinuous electrophoresis technique consists of two types of polyacrylamide gel: stacking gel and resolving gel. These two types of gel vary in pH, polyacrylamide contents and pore sizes. Stacking gel contains the protein loading wells and functions to line up all the protein samples in the gel so they can enter the resolving gel at the same time. The resolving gel, by contrast, is to separate protein samples based on their molecular weight (Figure 2.2). The protein gels were prepared based on Table 2.20.

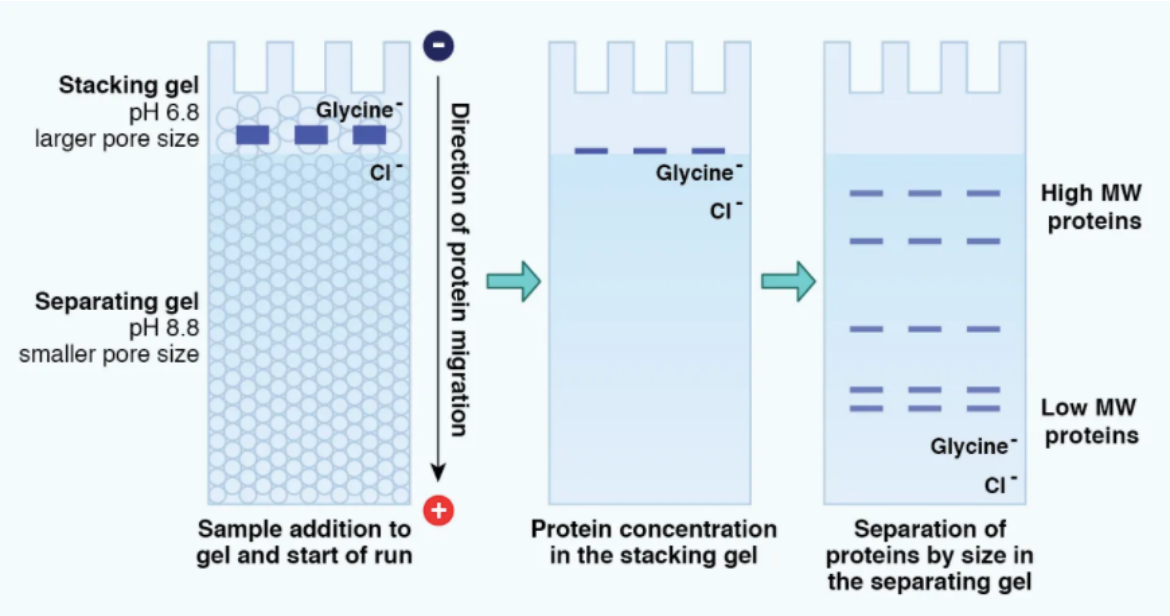

Figure 2.2 | Schematic representation of protein migration and separation by SDS-PAGE

Tris-Glycine SDS-PAGE consists of two distinct regions in the gel: the stacking and the resolving gel. The stacking gel contains 4% acrylamide and has lower pH (6.8 vs 8.8). The unique ion composition in stacking gel allows the protein sample to migrate in the gel between a high mobility leading ion (Cl^-) front and a low mobility trailing ion (glycine). As a result, the protein samples are lined up in a tight band and enter the resolving gel at the same time. The resolving gel, by contrast, contains higher concentration of acrylamide and higher pH (8.8). With the chemical properties closer to those of running buffer, resolving gel promotes protein to destack and migrate based on their molecular weight. Figure reproduced from https://www.antibodies.com/western-blotting

Table 2.20 | Buffer components of stacking and resolving gels for SDS-PAGE

Components	Stacking gel (10 ml)	Resolving gel (10 ml)	
	5%	8%	10%
ddH_20	5.7 ml	4.7 ml	4.1 ml
30% Acrylamide/Bis solution 37.5:1	1.7 ml	2.7 ml	3.3 ml
Tirs-HCl pH6.8	2.5 ml	–	–
Tirs-HCl pH8.8	–	2.5 ml	2.5 ml
10% SDS	100 µl	100 µl	100 µl
10% APS	50 µl	50 µl	50 µl
TEMED	10 µl	5 µl	5 µl

For SDS-PAGE, protein gels were cast with BioRad Mini-PROTEAN® Tetra Cell Casting Stand according to manufacturer's instructions. The acrylamide percentage of resolving gel was determined according to the molecular weight of proteins to detect: 8% for 50-200 kDa and 10% for 15-100 kDa. Protein samples were then loaded into wells of stacking gel along with a

Page Ruler ™ Prestained Protein Ladder (10-180 kDa) and run with 1x SDS running buffer. As described in 2.6.1.2, protein samples were prepared in Laemmli Buffer containing SDS and β-mercaptoethanol which denature the protein structure and make them uniformly negative charged, thus, the proteins are able to move through the gel toward positive electrode. During the stacking gel, the voltage was set to 70V to line up all the protein sample at stacking/resolving interphase. When proteins enter resolving gel, the voltage was increased to 120V for the entire run until the Laemmli Buffer completely left the gel. After the SDS-PAGE, the gel was carefully removed from glass plates and the proteins in the gel were then transferred onto a membrane for Western Blot.

2.6.3 Protein transfer

The proteins on SDS-gel were then transferred onto a nitrocellulose membrane (pore size of 0.2 μm) with Mini Trans-Blot® Electrophoretic Transfer Cells (BioRad) according to manufacturer's instructions. In brief, a sandwich pad was assembled in a transfer cassette as describe in Figure 2.3 before being inserted in the transfer tank. The transfer tank was filled with fresh 1x transfer buffer along with an ice pack to avoid overheat during the transfer process. The transfer was run at 250 mA for 90 mins. During the transfer, the negatively charged proteins migrate out of the SDS-PAGE and move toward the positively charged electrode. The transfer efficiency was estimated by the Prestained Protein Ladder.

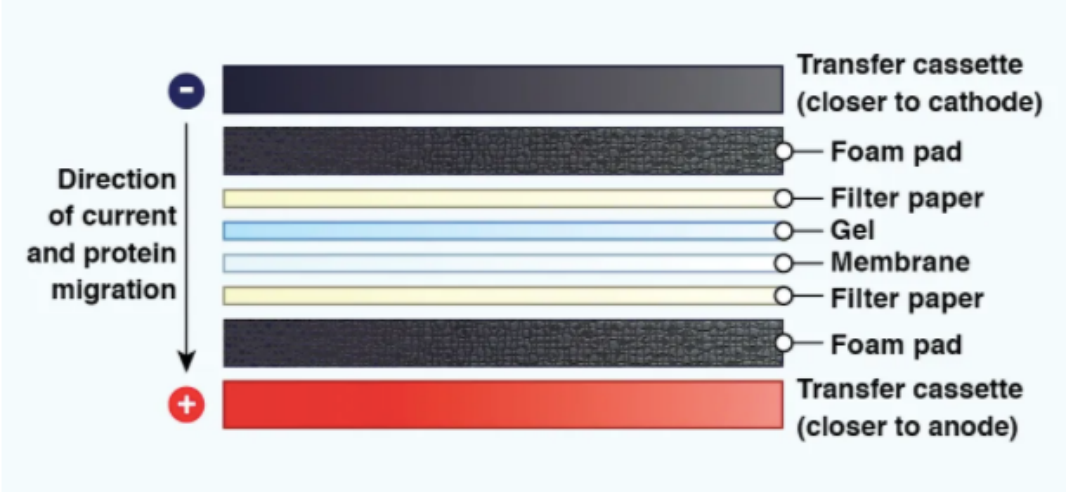

Figure 2.3 | The organization of transfer sandwich for protein transfer

The protein transfer sandwich is organized in the direction that allows negatively charged protein move out of gel and toward the positively charged electrode. In our study, foam pad represents the sponge while membrane indicates the nitrocellulose membrane. Figure reproduced from https://www.antibodies.com/western-blotting

2.6.4 Western blotting and protein detection

Table 2.21 | List of primary antibodies for western blotting

Antibody	Host species	Dilution ratio	Supplier
YAP	Mouse monoclonal	1:200	Santa Cruz Biotechnology (sc-101199)
PCBP1	Rabbit polyclonal	1:1000	ThermoFisher Scientific (PA5-86055)
PTBP1	Mouse monoclonal	1:500	ThermoFisher Scientific (32-4800)
Pitx2	Rabbit polyclonal	1:1000	Capra Science
CCT2	Mouse monoclonal	1:200	Santa Cruz Biotechnology (sc-374152)
Nucleolin	Mouse monoclonal	1:300	Santa Cruz Biotechnology (sc-8031)
GFP	Rabbit polyclonal	1:2000	Invitrogen™ (A-11122)
β-tubulin	Mouse polyclonal	1:5000	Sigma-Aldrich (M8064)
γ-adaptin	Mouse monoclonal	1:1500	Gift from Dr Andrew Peden Lab
NUMB	Rabbit monoclonal	1:1000	Cell Signalling Technology (2756)

Table 2.22 | List of secondary antibodies for western blotting

Antibody	Dilution ratio	Supplier
Donkey anti-rabbit IgG (H+L) Alexa Fluor® 680	1:5000	ThermoFisher Scientific (A-21109)
DyLight™800 4X PEG conjugate anti-mouse IgG (H+L)	1:5000	ThermoFisher Scientific (SA5-35521)

The proteins of interest on the membrane were detected by western blotting. After protein transfer, the membrane was carefully removed from transfer apparatus and cut to desired size according to the protein position on the membrane. The membrane was blocked in blocking buffer for 1 hr at room temperature. The selection of blocking buffer is dependent on the primary antibody and manufacturer's recommendation. The antibody and its dilution ratio used in this work are listed in Table 2.21 and Table 2.22. The membrane was incubated with a primary antibody diluted in associated buffer for overnight at 4°C. To remove excess and unbound antibody, the membrane was carefully washed 3 times in 1x PBST or 1x TBST with for 10 mins each. Next, the membrane was incubated with a specific fluorescent secondary antibody diluted in relevant buffer for 1 hr at room temperature before being washed 3 times in 1x PBST or 1x TBST for 10 mins each. The membrane was air dried for 20 mins in a dark environment.

The protein bands on membrane were imaged with Odyssey Sa® Infrared Imaging System of LI-COR with a 200μm resolution. Membrane were scanned with different infrared detection channel based on the species of secondary antibody: anti-rabbir-680nm and/or anti-mouse-800nm. Image StudioTM Lite software was used for quantification of protein bands.

2.7 Mass spectrometry proteomics

2.7.1 Mass spectrometry proteomics

The buffer used in preparation of samples for mass spectrometry analysis can be found in Table 2.23.

Table 2.23 | Buffer components for mass spectrometry proteomics

Buffer	Composition
SDS solution	2% SDS
RIPA buffer	50 mM Tris pH 7.5, 150 mM NaCl, 0.1% SDS, 0.5% Sodium deoxycholate, 1 mM EDTA, 1% NP-40 (v/v), *1x protease cocktail inhibitor *PhoSTOP™ phosphatase inhibitor (for Mass spectrometry analysis)
NaCl solution	250 mM Tris-HCl pH6.8, 40% glycerol, 8% SDS, 20% β-mercaptoethanol, 1% bromophenol blue
Urea/Tris-HCl	2 M Urea, 50 mM Tris-HCl pH8.0
Ammonium Bicarbonate solution	50 mM Ammonium Bicarbonate *Prepared in HPLC-grade dH_2O (Fisher Chemical W6-1)
TCEP	0.5 M Tris(2-caboxyethyl) phosphine hydrochloride *Prepared in HPLC-grade dH_2O (Fisher Chemical W6-1)
TFA	0.1%, 10% TFA (Trifluoroacetic acid) *Prepared in HPLC-grade dH_2O (Fisher Chemical W6-1)
TFA/ACN	0.1% TFA, 50% ACN (acetonitrile) *Prepared in HPLC-grade dH_2O (Fisher Chemical W6-1)

2.7.1.1 Preparation of protein sample

In this project, mass spectrometry was used to analyse nuclear proteome when cells experienced tetracycline-induced CA-RhoA. The stable cell line HEK293-tet-RhoA-TurboID was generated as described in 2.4.2.1. Nuclear proteins were labelled with biotin by treating HEK-Q63L-TurboID with 500 μM biotin for 20 mins at 37°C. The cell lysate was collected, and nuclear fraction was isolated and purified through streptavidin pull-down according to 2.6.1.2.

After streptavidin pull-down, the mixture of cell lysate/streptavidin resins were collected for the next washing procedure.

2.7.1.2 Washing procedure

The mixture of cell lysate/streptavidin agarose resins prepared according to 2.7.1.1 was carefully transferred to a Wizard^{R} Minicolumn (Promega). Wizard^{R} Minicolumn contains a filter at the bottom that allows the lysis buffer to flow through, but the agarose resins remain in the column. The resin column was washed with various buffer to remove non-specific bound proteins. The buffer for washing the resins was injected to the column with a syringe as the following order: 10 ml of 2% SDS, 10 ml of RIPA buffer, 10 ml of 0.5 M NaCl, 10 ml of 2 M Urea/50 mM Tris-HCl pH8, and 10 ml of 50 mM ammonium bicarbonate. All flow-through solution was discarded. After the washing procedure the resin can be stored at -20°C until on-bead digestion.

2.7.1.3 On-bead digestion

The proteins bound to streptavidin resin were then digested with trypsin to peptides. The resins were washed with 1 ml of freshly made 50 mM ammonium bicarbonate and centrifuged at 1800 x g for 3 mins at RT to remove the supernatant. The resins were resuspended with 1 ml of freshly made 50 mM ammonium bicarbonate and transferred to another clean 2ml tube for centrifugation at 1800 x g for 1 min at RT. After removal of supernatant, the resins were resuspended in 200 µl of freshly made 50mM ammonium bicarbonate and treated with 4 µl of 0.5 M TCEP (Tris(2-carboxyethyl) phosphine hydrochloride). The tube was incubated in a Thermomixer at 800 rpm for 15 mins at 37°C. Next, 4 µl of 0.5 M freshly made Iodoacetamide (IAA) was added to the sample followed by incubation in a Thermomixer at 800 rpm for 15 mins at 37°C. The sample was covered with tin foil to protect from light. Finally, the sample was treated with 1 µg of trypsin (10µl of 0.1mg/ml trypsin) and incubated in a Thermomixer at 800 rpm for overnight at 37°C

2.7.1.4 Desalting of the digested peptide

After trypsin digestion, peptides must de desalted to remove the salt and urea traces from digestion buffer as these salts would affect Orbitrap. First, the Pierce^{TM} C18 stage tips (Thermofisher Scientific) were equilibrated and washed twice by 10 µl of 0.1% Trifluoroacetic acid (TFA) to acidify the pH for better peptide binding. The digested sample was centrifuged at 1800 x g for 1 min at RT. The supernatant (the peptide fragments) was transferred to another tube to be acidified by 14 µl of 10% TFA to reach a pH of around 3. Next, the acidified

peptides sample was added to stage tip and slowly passed through stage tips. The flow-through was collected for repeating the same procedure 2 times. The stage tips were swashed 3 times with 100 µl of 0.1% TFA. Finally, the peptides were slowly eluted with 100 µl of 0.1% TFA/50% ACN (acetonitrile) into a clean Eppendorf.

2.7.1.5 Preparation of samples for Orbitrap injections

The desalted peptides sample was centrifuges in SpeedVac (Eppendorf) for 90 mins at 45°C with Eppendorf tube lid open to evaporate the solution and dry sample. The dried peptides were reconstituted in 0.5% formic acid and vortex gently at the lowest speed for 10 mins. Peptides sample was then transferred to a polypropylene vial and injected into Orbitrap.

2.7.1.6 LC-MS/MS analysis

The peptide sample was analysed by LC-MS/MS using Orbitrap Elite Hybrid Mass Spectrometer (Thermo Fisher). This procedure was operated by Dr Mark Collins (Senior Lecturer in the Department of Biological Science and Deputy Director of the Faculty of Science Mass Spectrometry Centre, University of Sheffield). The data analysis with Perseus software was conducted by Dr Mark Collins.

2.8 Fabrication of polyacrylamide gel

2.8.1 Fabrication of artificial ECM with mechanical properties

In order to generate the polyacrylamide (hereafter designated as PAA) hydrogel that can directly polymerize in polystyrene culture dishes, an acrylic-based photosensitive resin Loctite AA3525 was used to form an additional adhesive layer on the bottom of culture dish [113]. The polymerized Loctite resin then functioned as a 'glue' to attach PA hydrogel to plastic culture dishes. In our project, PAA gel was fabricated either in 35 mm dish for immunofluorescence staining or in 60 mm dish for the purpose of RT-PCR and western blotting.

2.8.1.1 Preparation of polystyrene culture dishes with adhesion substrate

First, recommended amounts of Loctite® AA3525 resin (hereafter designed as Loctite resin) based on previous study was deposited to culture dish and spreaded to cover the whole dish by a rubber spreader [113]. The Loctite material was overlaid by a cellulose acetate film to control its thickness and the flatness before being polymerized by the exposure to UV

radiation (γ=365 nm) for 1 min in a UV-crosslinker. Given that the Loctite resin must be completely cross-linked to prevent toxic noncured material from releasing into aqueous solution in later stage, two more post-curing procedures were performed after removing the cellulose film. The Loctite layer was exposed to UV for 5 min followed by another 5 min of UV exposure of upside-down resin layer.

In order to ensure an excellent adhesion between the Loctite material and hydrogel, the adhesive layer in 35 mm dish was activated by being incubated with 2 ml of ddH_2O (4 ml of ddH_2O for 60 mm dish) for 1.5 hrs. The water was removed completely, and the Loctite-coated dish was immediately exposed to UV radiation for 5 min right before the addition of hydrogel solution.

2.8.1.2 Fabrication of polyacrylamide (PAA) hydrogel in Loctite AA3525-coated dish

The fabrication of PAA hydrogel used in this work was based on previous literature [114]. In brief, preparation of PAA hydrogel with various stiffness was carried out by mixing particular amount of acrylamide and bis-acrylamide stock solution and inducing free radical polymerization. The components and the expected modulus of elasticity of PAA gel used in this study was listed in Table 2.24.

Table 2.24 | Components for PAA gel fabrication

Acrylamide (%)	Bis-acrylamide (%)	40% Acrylamide stock solution (ml)	2% Bis-acrylamide stock solution (ml)	Water (ml)	Expected elastic modulus *E* ± St. Dev. (KPa)
4	0.03	1	0.15	8.85	0.71 ± 0.24
5	0.03	1.25	0.15	8.6	1 ± 0.31
8	0.48	2	2.4	5.6	40.40 ± 2.39

Acrylamide stock solution (40%) and bis-acrylamide stock solution (2%) were mixed together in sterile 1x PBS followed by degas procedure by centrifuging at 2000 rpm for 20 min. Then 1/100 total volume of 10 % APS and 1/1000 total volume of TEMED were added to gel solutions and mixed thoroughly. To generate PA gel in culture dish, 850 µl and 2.5 ml of PAA gel solution was dispensed to freshly activated Loctite-coated 35 mm and 60 mm dishes respectively. The solution surface was immediately overlayed with parafilm of proper size.

The dish was sealed with parafilm to avoid the detriment of polymerization by free radical from oxygen. The PAA hydrogel was left to polymerize at room temperature for 2 hrs. After polymerization, the parafilm was carefully removed from the surface of hydrogel. The PAA hydrogel in each dish was first rinsed with ddH_2O then with 1x PBS three times with 20 minutes of each to adjust gel pH and salinity.

2.8.1.3 Protein conjugation

Before cells can attach to PAA gel, the ECM protein coating is prerequisite to guarantee cell adhesion and proliferation. Given that PAA gels do not readily adsorb proteins, we used a crosslinker solution composed of NHS-acrylate and free radical photoinitiator named Irgacure 2959 to functionalize the PAA gel surface before the ECM protein conjugation. Irgacure 2959 solution was freshly made in DMSO while NHS-acrylate stock in anhydrous DMSO was prepared in advance and stored at -80°C. To prepare the crosslinker solution, defined amounts of Irgacure 2959 and NHS-acrylate was mixed in 1x PBS as described in Table 2.25. The crosslinker solution was then dispensed onto PAA gel surface right before the exposure to UV radiation (γ=365 nm) for 15 min to covalently link the crosslinker mixture to PAA gel. NHS-acrylate contains a photoactivatable nitrophenylazide and functions as heterobifunctional crosslinker that reacts with primary amino groups in pH7-9 condition to form stable amino bonds. After functionalization of the PAA gel, excess crosslinker solution was removed and the PAA gel was washed gently with 1x PBS. ECM conjugated protein was prepared by series dilution of collagen type I solution stock. Collagen type I with concentration of 3 mg/ml was first diluted in cold 0.02 M Acetic acid to create 1mg/ml solution followed by second dilution in cold 1x PBS to generate 100 µg/ml working concentration. The diluted collagen type I solution was slowly added onto PAA gel. The conjugation procedure was carried out for overnight (~16 hrs) at room temperature or at 37°C.

Table 2.25 | Components for preparation of protein conjugation
The components and relevant amounts for PAA gel fabrication was according to a published work [114].

Culture dish	1x PBS	Irgacure 2959 (100 mg/ml)	NHS-acrylate (20 mg/ml)	Crosslinker mixture	Collagen type I solution (100 µg/ml)
35 mm dish	1.2 ml	120 µl	90 µl	1.4 ml	1.5 ml
60 mm dish	2.4 ml	240 µl	180 µl	2.6 ml	3 ml

2.8.1.4 Cell culture on hydrogel

Before cell culture on PAA gel, the gel surface must be equilibrated with culture medium at RT for better culture condition. The collagen-coated PAA gel was carefully washed 1 time with 1x PBS and then equilibrated in non-serum cell culture medium. At the same time, the PAA gel was sterilized by placing in a cell culture cabinet and exposed to UV for 1 hr. After sterilization, PAA gel was equilibrated with complete culture medium 2 times for 1hr each. During the last stage of equilibration, the PAA gel was moved to 37°C incubator before cells were seeded on the gel.

2.9 Inhibitory experiment

Inhibitory experiments were performed to investigate the influence of cytoskeleton on the phenotype of proteins of interests. The inhibitors used in this study can be found in Table 2.26. For examining the influence of cytoskeletal tension on proteins of interest, NIH3T3 fibroblasts were seeded in a 12-well plate at $1x10^5$ onto each coverslip/well for 24 hrs before treatment with 0.1 μM of Lat A, 25 μM of ML-7 and 25 μM of Y27632 for 30 mins to disrupt cytoskeleton tension and integrity. For testing the correlation between circumferential actin belt and selected proteins, high density cultured MCF10A and MDCKII were treated with 50 μM or 80 μM of Blebbistatin for 6 hours to relieve actomyosin tension at cell-cell junction. The phenotype of proteins of interest were analysed by immunofluorescence staining described in 2.10.

Table 2.26 | List of reagents used in inhibitory experiment

inhibitor	Function	Supplier
ML-7-Calbiochem	Inhibitor of myosin light chain kinase	Sigma-Aldrich (475880)
Latrunculin A	Inhibitor of F-actin	Santa Cruz Biotechnology (sc-202691)
Y27632-HCl	Inhibitor of Rho-kinase (ROCK)	Stratech Scientific (s1049)
±Blebbistatin-Calbiochem	Inhibitor of non-muscle myosin II	Sigma-Aldrich (203390)

2.10 Immunofluorescence staining

2.10.1 Immunofluorescence imaging

2.10.1.1 Coverslips coating

For performing immunofluorescence staining in some types of cells e.g., HEK293 and NIH3T3, the glass coverslips need to be coated with Poly-L-lysine prior to help cells attach on it without too much cell loss. The coverslips coating procedure was conducted under sterilized condition in cell culture cabinet. The Poly-L-lysine 0.1% was diluted 10-fold in ddH_2O, and 1 ml of diluted Poly-L-lysine solution (0.01%) was added to each well of a 12-well plate. The coverslips were incubated in Poly-L-lysine solution for 30 mins at RT. Then the solution was aspirated, and the coverslips were allowed to air dry in the cell culture cabinet (~30 mins). The Poly-L-lysine coated coverslips were washed 3 times with 1x PBS before cell culture.

2.10.1.2 Cell culture on micropatterned chips

For immunofluorescence staining of protein of interest regulated by various cell adhesive areas, we utilised fibronectin coated micropatterned chips (CYTOOchips™) for cell culture to control single cell spreading area. The procedure of seeding cells on micropatterned chips was according to manufacturer's instructions. In brief, the micropatterned chip was carefully taken out of the package and put in 35mm culture dish. The chip was gently rinsed once with 1x PBS and soaked in 1x PBS until the cells were plated on its surface. For cell culture on micropatterned chip, cells were trypsinized and diluted to a concentration of 30,000 cells per ml. Then the PBS was aspirated from the dish and 2 ml of cell suspension (60,000 cells) were slowly dispensed into the dish containing micropatterned chip. Ideally, around 10-30% of micropatterns will be occupied by a single cell.

2.10.1.3 Immunostaining

The buffer used in immunofluorescence imaging is listed in Table 2.27. The primary and secondary antibodies for immunofluorescence staining used in our study is summarised in Table 2.28a and Table 2.28b respectively.

Table 2.27 | Buffer for immunofluorescence imaging

Buffer	Composition
1x PBS	137 mM NaCl, 2.7 mM KCl, 10 mM Na_2PO_4, 1.8 mM KH_2PO_4 pH7.4

4% PFA (paraformaldehyde)	4% PFA in 1x PBS pH7.4
Quenching buffer	0.1 M Glycine in 1x PBS pH7.4
Permeabilization buffer	0.1% Triton in 1x PBS pH7.4
Blocking and antibody incubation buffer	0.5% FBS, 0.01% Tween 20 in 1x PBS pH7.4
1x Washing buffer	0.01% Tween 20 in 1x PBS pH7.4
Prolong Gold mounting medium	Invitrogen™ (p36930)

Table 2.28a | List of primary antibodies for immunofluorescence imaging

Antibody	Host species	Dilution ratio	Supplier
YAP	Mouse monoclonal	1:200	Santa Cruz Biotechnology (sc-101199)
YAP	Rabbit monoclonal	1:500	Cell Signalling Technology (14074)
PCBP1	Rabbit polyclonal	1:1000	ThermoFisher Scientific (PA5-86055)
PTBP1	Mouse monoclonal	1:500	ThermoFisher Scientific (32-4800)

Table 2-28b | List of secondary antibodies for immunofluorescence imaging

Antibody	Dilution ratio	Supplier
Goat anti-rabbit IgG (H+L) Alexa Fluor® 488	1:500	ThermoFisher Scientific (A-11034)
Goat anti-mouse IgG (H+L) Alexa Fluor® 488	1:500	ThermoFisher Scientific (A-11011)
Donkey anti-rabbit IgG (H+L) Alexa Fluor® 594	1:500	ThermoFisher Scientific (A-11012)
Donkey anti-rmouse IgG (H+L) Alexa Fluor® 594	1:500	ThermoFisher Scientific (A-11005)
Hoechst (for nucleotide staining)	1:1000	Invitrogen™ (H3570)

Cells were seeded on coverslips for various experiment purpose. When ready to stain with antibody, cells were gently washed 3 times with 1x PBS and then fixed with 4% PFA/1x PBS for 10 mins. Excess PFA solution was then removed by washing the cells 3 times with 1x PBS. To quench unreacted aldehyde, cells were incubated with 0.1 M Glycine/1x PBS for 5 mins. Cells were washed 2 times with 1x PBS before being permeabilized with 0.1% Triton/1x PBS for 15 mins. Cells were washed 3 times with 1x washing buffer (0.01% Tween20/1x PBS), then incubated in blocking buffer (0.5% FBS/0.01% Tween 20/1x PBS) for 1 hr at RT to reduce the nonspecific binding.

For immunostaining, all the antibody dilution was prepared in blocking buffer (Table 2.27). Cells were incubated with primary antibody in a humid chamber for either 2 hours at RT or overnight at 4°C then washed 3 times with 1x washing buffer. Next, fluorescent secondary

antibody and Hoechst was applied for an hour at room temperature. The coverslips were washed 3 times with 1x washing buffer and then mounted onto glass slides with 3 ml of Prolong gold anti-fade mounting medium. Glass slides were left for 24~48 hrs at room temperature in a dark environment then transferred to a slide box and stored at 4°C.

2.10.1.4 Microscopy

2.10.1.4.1 Epifluorescence microscope

Immunostained cells on coverslips were imaged with an epifluorescence microscope. The objective used was a 60x oil immersion objective. The images were acquired by Volovity software.

2.10.1.4.2 Olympus Fluoview 1000 Confocal

The subcellular localization of target protein in cells grown on polyacrylamide gel or coverslips were observed with an Olympus Fluoview 1000 Confocal microscope. The images of cells on PAA gel samples were acquired with a 60x water immersion objective, while the cells cultured on coverslips were observed with a 60x oil immersion objective. The images were obtained by FV10-ASW software.

2.10.1.4.3 Microscopy Image process

All the images acquired from Epifluorescence microscope and Olympus Fluoview 1000 confocal were further processed with Fiji-ImageJ software. All images from a same batch of experiment were processed with the same parameters. For quantification of fluorescence intensity of target proteins, the cell areas were manually selected, and the fluorescence intensity of protein of interest was assessed using Fiji software.

2.11 Statistical analysis

After acquiring quantitative data, graphs and statistical analysis were conducted using GraphPad Prism 9. Statistical analysis method is based on the dataset and indicated in each legend. Statistical significance is denoted by asterisks*: *p<0.05, **p<0.01, ***p<0.001 and ****p<0.0001.

3. Chapter 3 – Identification of potential molecular players in mechanotransduction

Growing evidence has suggested that mechanical signals critically influence cellular behaviours. Mechanical cues lead to changes on membrane and cortical cellular tension, largely caused by changes in the actomyosin contractility of the cytoskeleton. In order to identify potential protein mediators that regulate mechanotransduction, an efficient and reliable mechanical cue-mimicking cellular model was crucial for our project. In this part of the thesis, we developed a novel approach to analyse changes of the nuclear proteome upon changes in cellular actomyosin contractility.

3.1 Establishment of RhoA activity-inducing model

Upon perceiving mechanical cues from extracellular microenvironment (like ECM stiffness), cells generate pulling forces against their surroundings through the assembly of actomyosin contractile network and remodelling of cytoskeleton stress fibres [115]. Several articles have revealed that external mechanical stimuli activate RhoA and its downstream signalling pathways, which in turn induce actin reorganization and cell contractility [1, 72, 116] (also see 1.4.3). The cellular contractility and F-actin remodelling induced by Rho signalling also promote YAP nuclear localization [11], indicating the method of controlling RhoA signalling a promising strategy to induce contractile force without direct application of external mechanical forces to cells.

First, we generated a cell line that allowed to increase actomyosin contractility by controlling expression of constitutively active RhoA (CA-RhoA) using a tetracycline inducible system. Importantly, a previous study in which a similar system had been established demonstrating that activated RhoA leads to generation of cell contractile force and nuclear YAP localization [117], supporting our strategy used in this project. In this part, we engineered a construct encoding CA-RhoA and then introduced it into Flp-In™ T-REX™ HEK293 cell line to generate a stable clone HEK293-tet-RhoA in which the active RhoA can be regulated by tetracycline. This stable cell line will be used for the second step of experiments described in 3.2 and 3.3. The application of RhoA activity-inducing model in our study is overviewed in Figure 3.1.

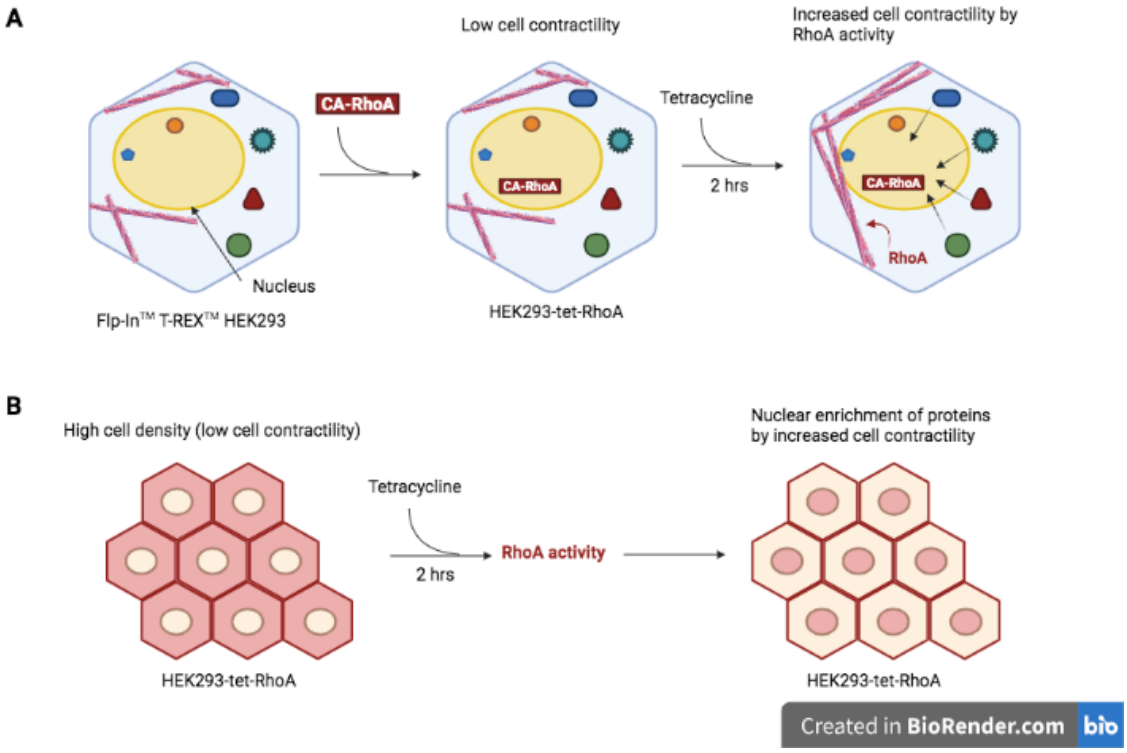

Figure 3.1 | Schematic representation of RhoA activity-inducing model for promotion of cell contractile force

(A) An engineered stable cell line HEK293-tet-RhoA can express constitutively active RhoA (CA-RhoA) under a tetracycline inducible promoter. The CA-RhoA increases cell contractility which may regulate nuclear translocation of particular proteins.
(B) Scheme of protein nuclear translocation by tetracycline in HEK293-tet-RhoA at high cell density.

3.1.1 YAP can be regulated by cell density in Flp-In™ TREX™ HEK293 cell

Before establishment a stable cell line through Flp-In™ T-REX™ HEK293 system in which the active RhoA can be regulated by tetracycline-inducible system, we examined the cell response to mechanical cues such as cell density. Change of mechanical stimuli from various cell density have been reported to regulate the subcellular localization of YAP, a mechanotransducer, in a variety of cell lines [11, 118]. Here we utilized YAP as positive control to test whether Flp-In™ T-REX™ HEK293 parental cell line displays a phenotype following the proof-of principle that YAP translocation is regulated by cell density-mediated mechanical cues. We first performed immunofluorescence qualitative assay to examine YAP subcellular localization across various cell densities. Flp-In™ T-REX™ HEK293 were grown at increasing cell confluence ranging from low to high cellular density before and subjected to

immunofluorescent staining for YAP. Our data showed that YAP was predominately located in the nucleus in sparsely cultured cells whereas gradually translocated to cytoplasm with increased cell density (Figure 3.2). The result was consistent with previous studies that cell density involved in YAP subcellular distribution, indicating that Flp-In™ T-REX™ HEK29 was able to correctly read mechanical cues derived from cell density and a suitable cell model in our following studies.

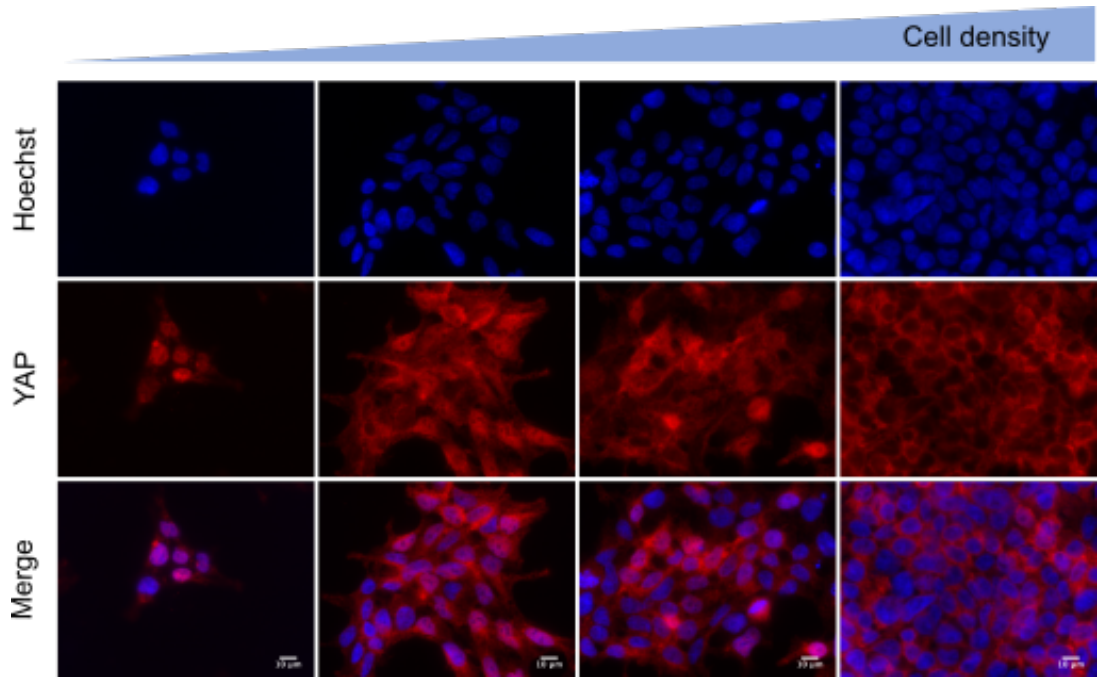

Figure 3.2 | Cell density regulates YAP subcellular localization

Immunostaining of YAP in Flp-In™ T-REX™ HEK293 shows the changes of YAP nuclear localization is regulated by cell density. YAP is mainly located in the nucleus at low cell density while translocated to cytoplasm when cells reach high density. Scale bars, 10 μm.

3.1.2 YAP subcellular translocation can be controlled by RhoA activtiy

Rho GTPase signalling has been shown to play a critical role in the formation of F-actin cytoskeletal bundles and actomyosin structures as a response to external forces [11]. Prior to the establishment of a mechanical application system that induce cell-generated force through RhoA signalling, we performed a preliminary test to examine the effect of RhoA activity on regulation of YAP cellular distribution. HeLa cells were cultured at low density and RhoA signalling was inhibited by 2 μg/ml of C3 before the immunofluorescence assay. As expected,

inhibition of RhoA reduced the proportion of cells displaying nuclear YAP in comparison with control cells, in which YAP was mostly located in the nucleus (Figure 3.3 A).

We next sought to determine whether RhoA signal could also directly drive YAP translocation under different cell density, in which the Hippo signalling pathway also exerts the control of YAP activity. Two RhoA mutants pcDNA3-EGFP-RhoA-T19N and pcDNA3-EGFP-RhoA-Q63L were transiently overexpressed in Flp-In™ T-REX™ HEK293 and the RhoA expression as well as YAP subcellular distribution were detected by immunofluorescence staining using anti-GFP and anti-YAP antibody respectively (Figure 3.3 B-C). The dominant negative (DN) RhoA T19N is a constantly inactive GDP-bound mutant whereas the constitutively active (CA) RhoA Q63L is a GTP-bound mutant. In low-density Flp-In™ T-REX™ HEK293, the majority of cells transfected with control GFP-vector displayed nuclear YAP. However, YAP nuclear localization was greatly suppressed in cells transiently expressing DN-RhoA (Figure 3.3 B). The reversion of cell density-mediated YAP translocation by RhoA activity was also observed in high-density Flp-In™ T-REX™ HEK293 displaying CA-RhoA. Endogenous YAP was sequestered in the cytoplasm of control cells whereas became significantly exclusive to the nucleus or to both cytoplasm and nucleus in CA-RhoA-transfected cells (Figure 3.3 C). Overall, our results suggested that RhoA-mediated contractility was capable to control cellular mechanics which was evidenced by YAP re-shuttling between the nucleus and cytoplasm. The phenotype of YAP regulated by RhoA shown in our data was consistent with previous study [11], supporting our working platform in which RhoA was utilized as intracellular mechanical force-generating model. In the following work, we focused on the further establishment of a screen for the identification of potential novel regulators of mechanotransduction exploiting activation of RhoA.

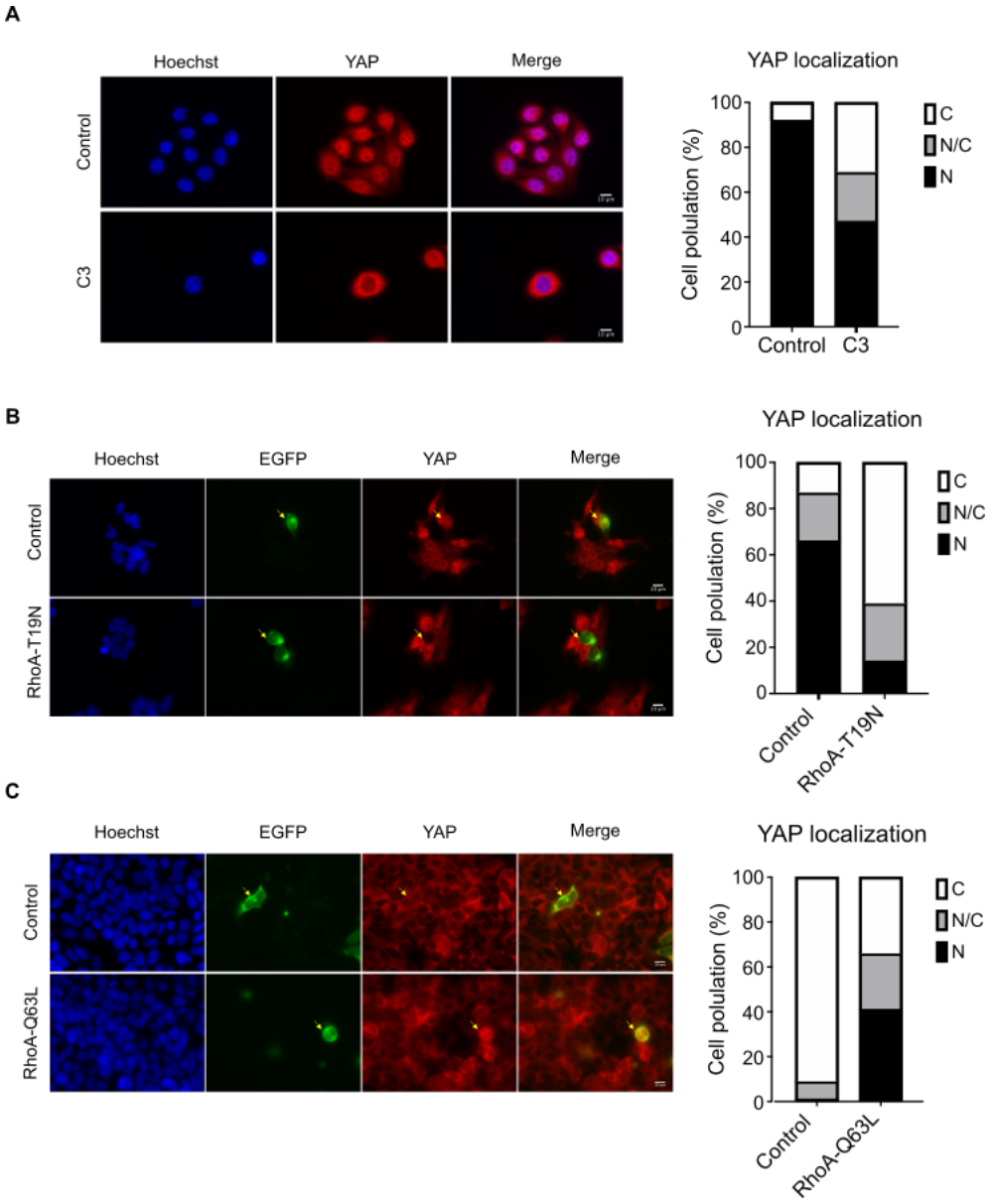

Figure 3.3 | YAP can be regulated by RhoA activity

(A) Immunofluorescence staining shows the change of YAP nuclear localiation in HeLa cells treated with 2 μg/ml of C3, Rho inhibitor, for 6 hrs. Graph provides quantifications of relative cell population displayed various YAP subcellular localization detected in HeLa cells. N: nuclear YAP; N/C: both nuclear and cytoplasmic YAP; and C: cytoplasmic YAP. Scale bars, 10 μm. The data was analysed by ordinary one-way ANOVA test (n=3).

(B) and (C) Immunofluorescence staining of YAP in Flp-In™ TREX™ HEK293 transiently transfected with dominant negative RhoA T19N and constitutively active RhoA-Q63L respectively. Yellow arrows indicate the transfected cells. Scale bars, 10 μm. Graph provides quantifications of relative cell population displayed various YAP subcellular localization in Flp-In™ TREX™ HEK293 cells. N: nuclear YAP; N/C: both nuclear/cytoplasmic YAP; and C: cytoplasmic YAP. The cell population was analysed by ordinary one-way ANOVA test (n=3).

3.1.3 Construction of stable cell line tetracycline induced RhoA through Flp-In™ TREX™ HEK293 system

In order to gain precise control over the RhoA expression within cells, we generated a stable cell line through Flp-In™ T-REX™ HEK293 system to express EGFP-tagged CA-RhoA under the control of a tetracycline (Tet)-inducible promoter [119]. Flp-In™ T-REX™ HEK293 was used as parental cell line for the generation of RhoA-expressing stable cell line. We first engineered a pcDNA5/FRT/TO expression vector which contained the gene encoding EGFP-Tagged CA mutant RhoA-Q63L and then introduced the construct along with pOG44 into Flp-In™ T-REX™ HEK293 parental cells. Given that both pcDNA5/FRRT/TO-EGFP-RhoA-Q63L and Flp-In™ T-REX™ HEK293 contain a single integrated Flp Recombination Target (FRT) site, only one copy of CA-RhoA construct was integrated into the genome of host cell line at the particular FRT site under the control of Flp recombinase expressed by pOG44. Thus, the resulting stable cell line HEK293-tet-RhoA represents an isogenic population with each cell carrying a single copy of CA-RhoA at the same genomic location (Figure 3.4 A).

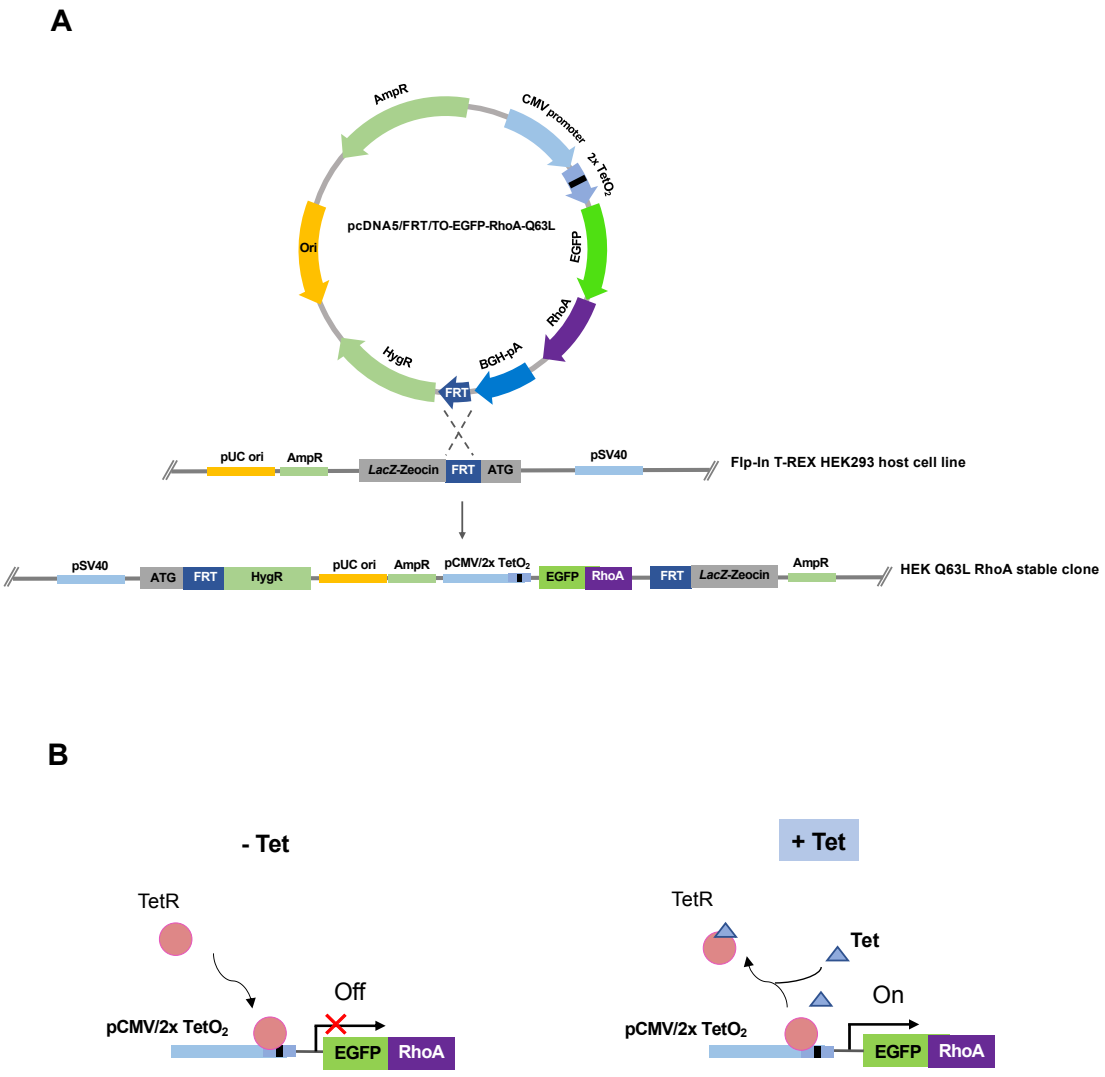

Figure 3.4 | Schematic representation of establishment of stable cell line HEK293-tet-RhoA

(A) The engineered pcDNA5/FRRT/TO-EGFP-RhoA-Q63L was integrated into genome of Flp-In™ TREX™ HEK293 through the FRT site, resulting stable clone HEK293-tet-RhoA.

(B) Expression of CA-RhoA protein in HEK293-tet-RhoA can be induced and regulated by tetracycline (Tet). The constitutively expressed tetracycline repressor (TetR) in cell binds to CMV promoter which inhibits expression of EGFP-CA-RhoA. The treatment of tetracycline neutralizes the inhibitory activity of TetR and promotes expression of EGFP-CA-RhoA.

Flp-In™ T-REX™ HEK293 constitutively expresses Tet repressor to bind to the Tet promoter and inhibits the expression of downstream target gene, as a result, the stable clone HEK293-tet-RhoA can only express CA-RhoA in the presence of tetracycline which neutralizes and reduces the inhibition of Tet repressor of target gene (Figure 3.4 B). To assess the induction of CA-RhoA by tetracycline, we treated HEK293-tet-RhoA with varying amounts of tetracycline for four hours before subjecting cell lysate for western blot analysis. Our result indicated that only after the treatment of tetracycline the cells began to express CA-RhoA.

Besides, expression level of CA-RhoA can be controlled by tetracycline concentration, which was confirmed by western blotting with anti-GFP antibody (Figure 3.5 A). Similarly, with the fixed amount of tetracycline (1 μg/ml), HEK293-tet-RhoA displayed a gradual increase of CA-RhoA protein levels in a time-dependent manner (Figure 3.5 B).

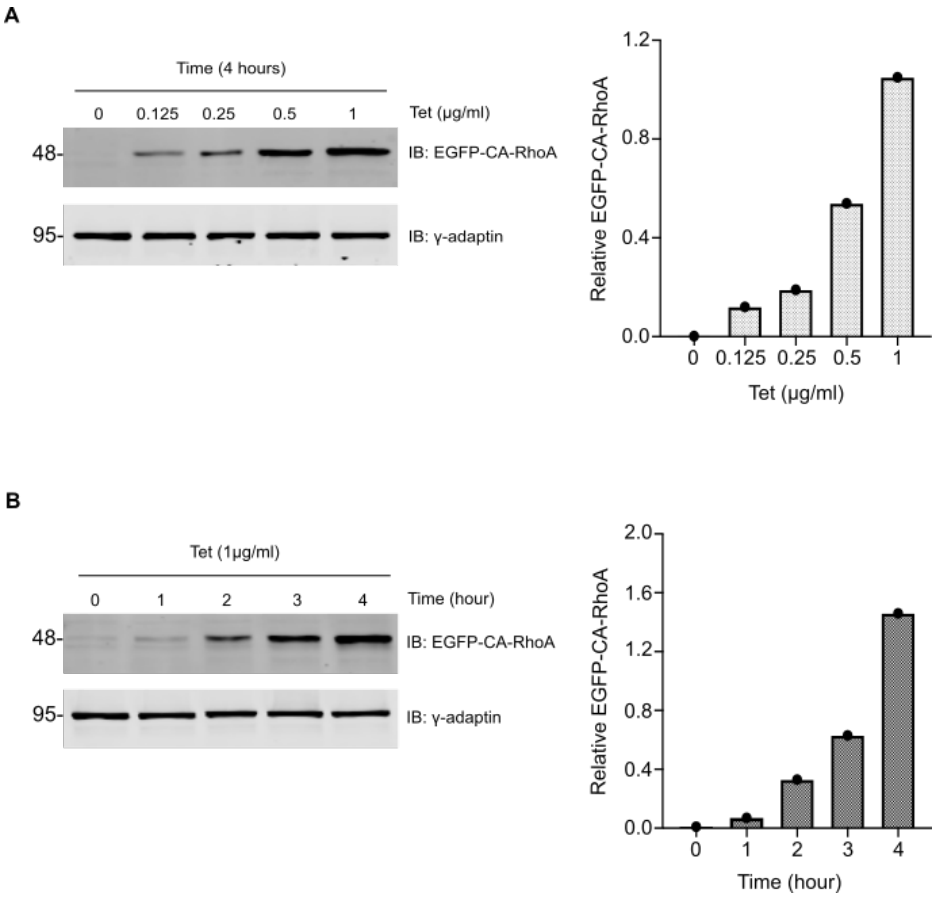

Figure 3.5 | Validation of stable clone HEK293-tet-RhoA

The induction and expression of CA-RhoA in HEK293-tet-RhoA can be regulated by tetracycline in a dose-dependent (A) or time-dependent (B) manner. Graphs provide quantification of the changes of relative EGFP-CA-RhoA expression displayed by western blotting at left side. EGFP-CA-RhoA of each blot was normalized against γ-adaptin loading control.

We next determined if we could manipulate cell response to tetracycline-induced CA-RhoA in HEK293-tet-RhoA stable cell line by examining YAP distribution. HEK293-tet-RhoA was placed at high density and CA-RhoA expression was induced by 1 μg/ml of tetracycline for two hours before subjecting to immunofluorescence assay. In comparison to control cells, HEK293-tet-RhoA experiencing two hours incubation of tetracycline exhibited nuclear localization of YAP as measured by the ratio of nuclear YAP over cytoplasmic YAP (Nuc/Cyt

YAP) (Figure 3.6). In addition, Tet-treated parental Flp-In™ T-REX™ HEK293 cells displayed the same phenotype of YAP as those observed in control cells, which allowed us to rule out the unknown influence of tetracycline on YAP regulation and confirmed that Tet-induced CA-RhoA contributed to control YAP subcellular distribution.

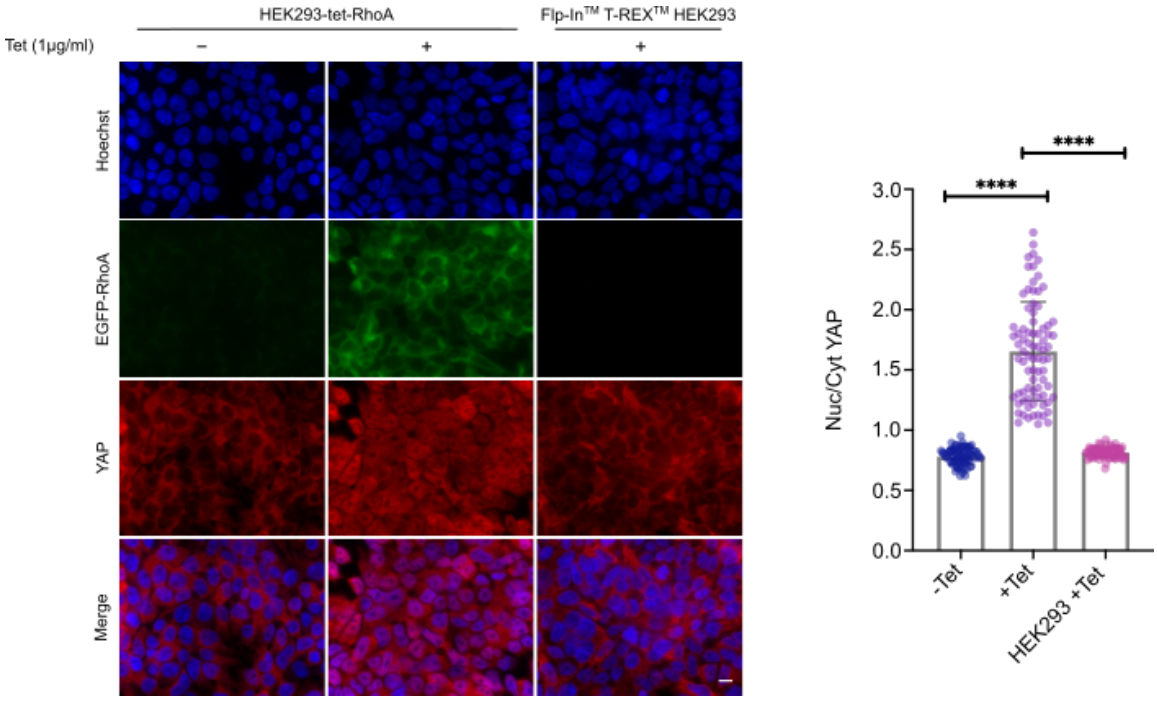

Figure 3.6 | Validation of stable clone HEK293-tet-RhoA

Immunofluorescence images showed that the subcellular translocation of YAP is regulated by Tet-induced CA-RhoA. Cells were placed at high density before CA-RhoA induction by tetracycline. The treatment of tetracycline promotes YAP nuclear localization in high density cultured HEK293-tet-RhoA. The Flp-In™ TREX™ HEK293 was used as negative control to prove that tetracycline itself has no impact on YAP translocation. Scale bars, 10μm. Graph provides quantification of ratio of Nuc/Cyt YAP. The immunofluorescent intensity of YAP of each cell was assessed by ImageJ. The data was analysed by ordinary one-way ANOVA test followed by Tukey's multiple comparisons test. Values are means ± s.d. (n=3). ****P<0.0001.

3.2 Establishment of proximity labelling system

In order to identify the molecular players which shuttle between the nucleus and cytoplasm as a response to RhoA activation, the development of a reliable and efficient method to isolate nuclear proteins is a critical step in our project. For this part we adopted a proximity labelling system to label nuclear proteomes as a strategy to isolate and purify nuclear components for

subsequent Mass spectrometry analysis. Importantly, this allowed us to avoid extensive mechanical handling of the cells using classical cell fractionation.

3.2.1 Generation of TurboID and miniTurbo biotin ligase constructs

A 2018 report demonstrating proximity labeling system in living cells and organisms with TurboID and miniTurbo provides us a unique alternative to conventional subcellular fractionation [112]. TurboID and miniTurbo are two promiscuous mutants of biotin ligase which catalyse proximity labelling of neighbouring proteins within a radius of about 10 nm with biotin. Then the biotin labelled proteins can be isolated through streptavidin resin-based purification as biotin exhibits a strong binding affinity for streptavidin [112]. The HA-tagged TurboID and miniTurbo used in this work are modified constructs containing three nuclear localization sequence (NLS) of SV40 large T antigen at C-terminal, ensuring nuclear localisation of the proteins. In this part, we utilized HEK293-tet-RhoA as a parental cell to establish another stable clone which allowed us to label nuclear proteomes with biotin through proximity labelling system. The schematic representation of the proximity labelling system used in our study is shown in Figure 3.7

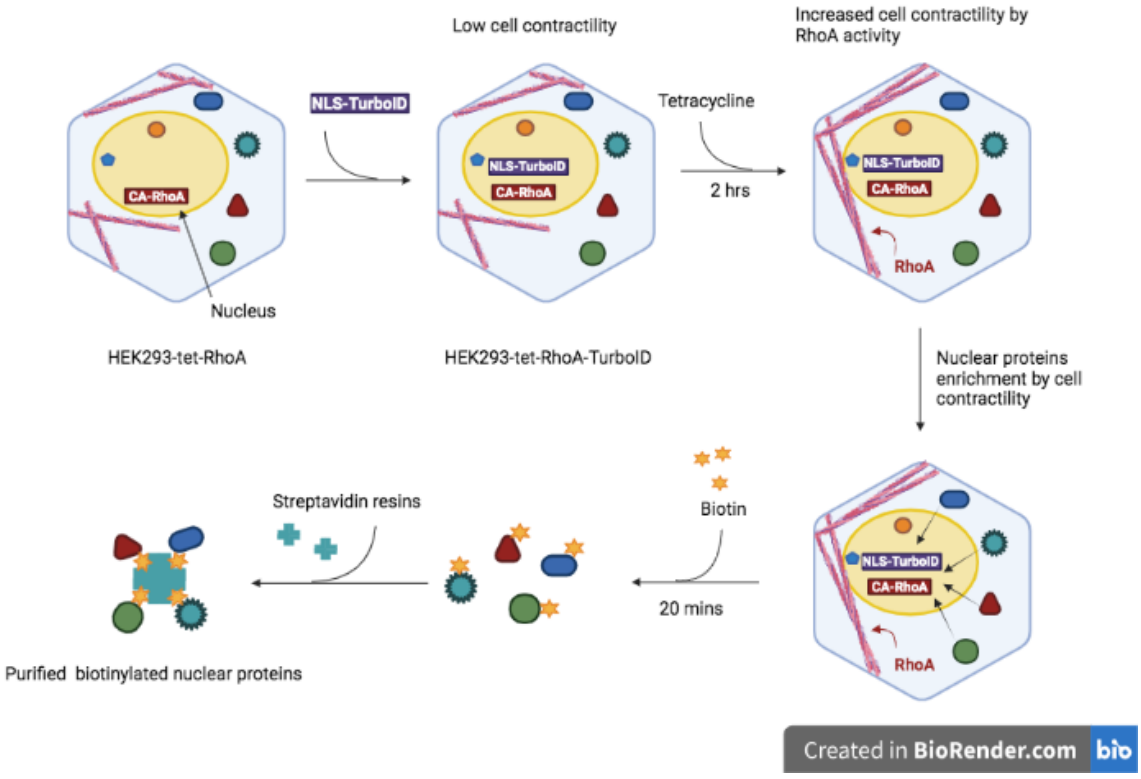

Figure 3.7 | Schematic overview of proximity labelling system

HA tagged TurboID-NLS or miniTurbo-NLS plasmid was introduced into HEK293-tet-RhoA to generate a stable cell line which catalyses biotinylation of nuclear proteins. The biotinylated nuclear proteins can be isolated and purified by incubation with streptavidin resins proteins through biotin-streptavidin interaction.

To establish the proximity labelling system for the isolation of nuclear proteomes, we cloned 3xHA-TurboID-NLS and 3xHA-miniTurbo-NLS into a pCDNA3-puromycin resistant working system in which the true transfectants can be selected by puromycin. We obtained two puromycin-resistant constructs 3xHA-pCDNA3.1/TurboID-NLS and 3xHA-pCDNA3.1/miniTurbo-NLS. To examine the location of protein expression of these two constructs, we introduced the HA-tagged TurboID or miniTurbo into HEK293-tet-RhoA transiently and performed immunofluorescence staining with anti-HA antibody to assess the subcellular localization of TurboID and miniTurbo (Figure 3.8 A). Our results showed that both TurboID and miniTurbo were located in the nucleus of the transfected cells, confirming the protein distribution of TurboID and miniTurbo encoded from these 3xHA-pCDNA3.1/TurboID-NLS and 3xHA-pCDNA3.1/miniTurbo-NLS were only limited to the nucleus.

We then tested the enzymatic function of TurboID and miniTurbo in HEK293-tet-RhoA. Cells were transiently transfected with TurboID or miniTurbo construct before initiating the labelling of nuclear proteomes with 50 μM of exogenous biotin for various time expansion. Whole cell lysate was subjected to the incubation with streptavidin resin to enrich biotinylated proteins. Biotinylated proteins were visualized by western blotting with fluorescent-labelled streptavidin antibody. The expression of HA-tagged TurboID or miniTurbo was detected by anti-HA antibody (Figure 3.8 B). Streptavidin blot indicated that biotinylation of endogenous proteins occurred in both TurboID and miniTurbo transfected cells in which the biotinylation degree increased with biotin exposure time. We observed that cells with overexpressed TurboID displayed stronger and more rapid biotinylation than miniTurbo, especially at earlier time points such as 10 minutes and 30 minutes after biotin treatment (Figure 3.8 B).

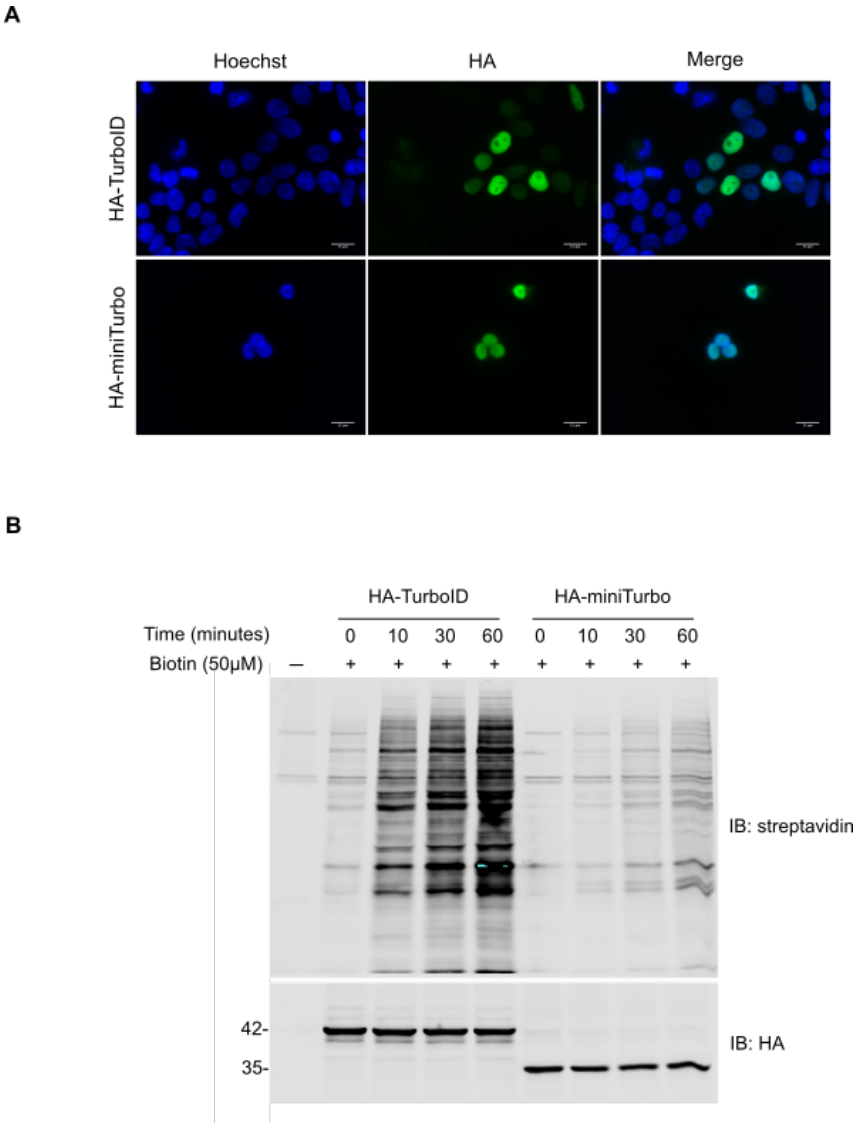

Figure 3.8 | Validation of TurboID and miniTurbo in HEK293-tet-RhoA.

(A) Immunofluorescence staining of HA showed the nuclear localization of TurboID and miniTurbo in cells after transient overexpression of HA-tagged TurboID or minTurbo in HEK293-tet-RhoA. Scale bars, 15μm.

(B) Western blotting for fluorescent-tagged streptavidin antibody indicated the different biotin-labelling ability between TurboID and miniTurbo-transfected cells. Anti-HA antibody represented the protein expression of TurboID and miniTurbo.

3.2.2 Establishment of TurboID and miniTurbo stable clones

For the purpose to analyse the changes of nuclear proteomes driven by RhoA expression, we next used our HEK293-tet-RhoA cell line as a parental cell line to develop another stable cell line containing TurboID or miniTurbo. We performed stable transfection of HEK293-tet-

RhoA with linearized 3xHA-pCDNA3.1/TurboID-NLS or 3xHA-pCDNA3.1/miniTurbo-NLS plasmid and selected the stably transfected cells with puromycin. The resulting stable clones were isolated and tested for the expression of HA-tagged TurboID or miniTurbo by western blot. All of the three resulting TurboID clones and six of total seven miniTurbo clones showed expression of the mutant biotin ligase, as detected by anti-HA antibody (Figure 3.9 A). To confirm whether these clones still maintained the property of inducible RhoA activity, we induced CA-RhoA expression by treating the stable clones with 1 μg/ml of tetracycline for two hours before cell lysis. Western blot showed that TurboID clones-A11 and B6 as well as miniTurbo clones-A5 and C3 exhibited comparative amount of CA-RhoA as those in HEK-Q63L control cells (Figure 3.9 B).

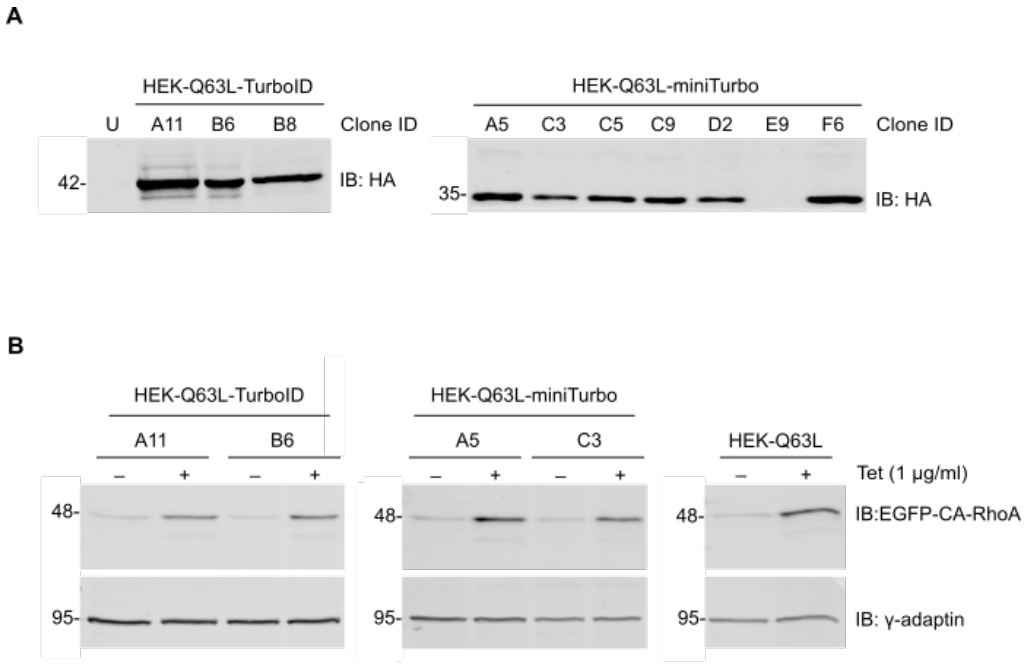

Figure 3.9 | Selection of TurboID and miniTurbo stable clones

(A) Various HEK293-tet-RhoA-TurboID and HEK293-tet-RhoA-miniTurbo clones were tested by immunoblot of HA to detect the expression of HA-tagged TurboID or miniTurbo biotin ligase.

(B) Immunoblot for EGFP-CA-RhoA in HEK-Q63L-TurboID clones (A11 and B6) and HEK-Q63L-mimiTurbo clones (A5 and C3) displayed tet-induced CA-RhoA expression. γ-adaptin was detected as loading control.

We next examined the effect of Tet-induced CA-RhoA on YAP translocation in these cell lines. HEK293-tet-RhoA clones TurboID-A11 and B6 as well as miniTurbo-A5 and C3 were cultured at high confluence before treatment with tetracycline to induce CA-RhoA. Both TurboID clones and miniTurbo-C3 displayed robust RhoA expression and nuclear YAP

translocation (Figure 3.10 A-B). By contrast, miniTurbo-5 showed visually less nuclear YAP under the same experimental condition (Figure 3.10 B). As a result, we selected TurboID clones-A11 and B6 and miniTurbo-C3 for the subsequent analysis.

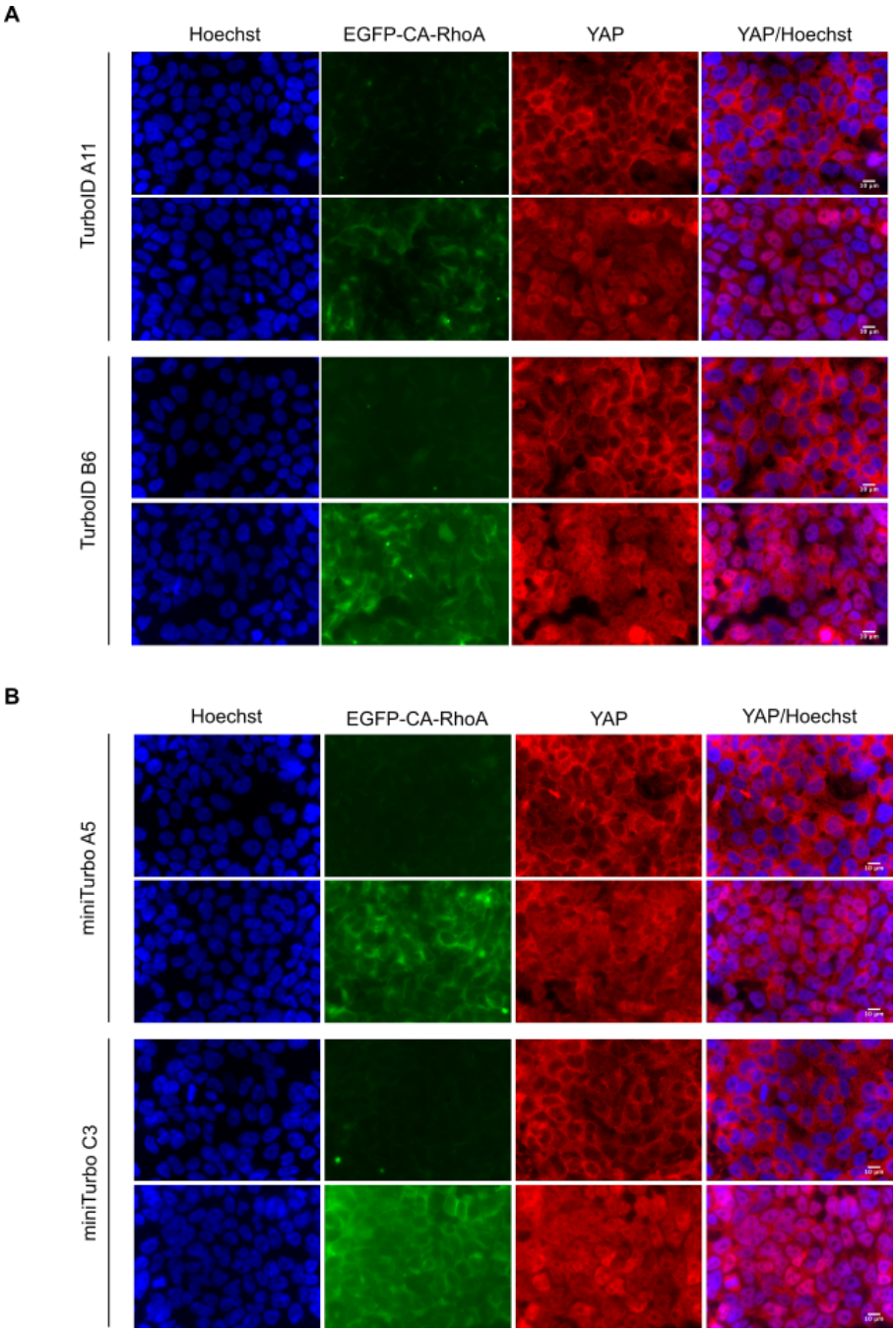

Figure 3.10 | Validation of TurboID and miniTurbo stable clones

Immunofluorescence imaging shows that Tet-induced CA-RhoA drives nuclear YAP accumulation in various TurboID (A) and miniTurboID (B) clones tested. Cells were placed at high density before the treatment of 1 μg/ml of tetracycline for 2 hours. Expression of EGFP-CA-RhoA represents the tetracycline-induced RhoA. All of the clones show the CA-RhoA dependent nuclear YAP enrichment. Scale bars, 10μm.

Considering that our previous results showed differences in levels of biotinylation between TurboID and miniTurbo transfected cells (Figure 3.8 B), we then tested the enzymatic activity of TurboID and miniTurbo biotin ligase in terms of their ability to label nuclear YAP with biotin. We carried out similar experiments to generate RhoA-mediated mechanical force by treating TurboID-A11, B6, and miniTurbo-C3 stable cell lines with tetracycline before labelling the nuclear components with biotin. The cell lysates were isolated and subjected to streptavidin pulldown for purification of biotin-labelled nuclear proteins. To compare the difference of TurboID and miniTurbo clones regarding biotinylating activity, we used fluorescent-labelled streptavidin antibody to visualize the isolated biotin-labelled nuclear proteins. Consisted with our transient overexpression experiment (Figure 3.8 B) and previous report [112], TurboID clones A11 and B6 displayed stronger enzymatic activity than miniTurbo clone C3 as they produced more biotinylated proteins than miniTurbo-C3, as monitored by streptavidin blot (Figure 3.11 A).

The phenotypic variation between TurboID and miniTurbo clones was also detected by nuclear YAP expression. Despite showing comparative YAP nuclear accumulation to the other two TurboID clones (Figure 3.10 B), miniTurbo-C3 exhibited less biotin-labelled nuclear YAP than TurboID-A11 and B6 after the streptavidin resin purification procedure (Figure 3.11 B). Given that our project aim was to identify molecular players that translocate between the nucleus and cytoplasm in responding to mechanical forces, the comprehensive and strong labelling ability of TurboID would give us more benefits in our work. Collectively, our results suggested that TurboID clones A11 and B6 not only exert cellular-generated force via Tet-induced CA-RhoA but are also capable to label and enrich nuclear components for subsequent purification, making the two clones promising cellular model for collecting nuclear proteomes.

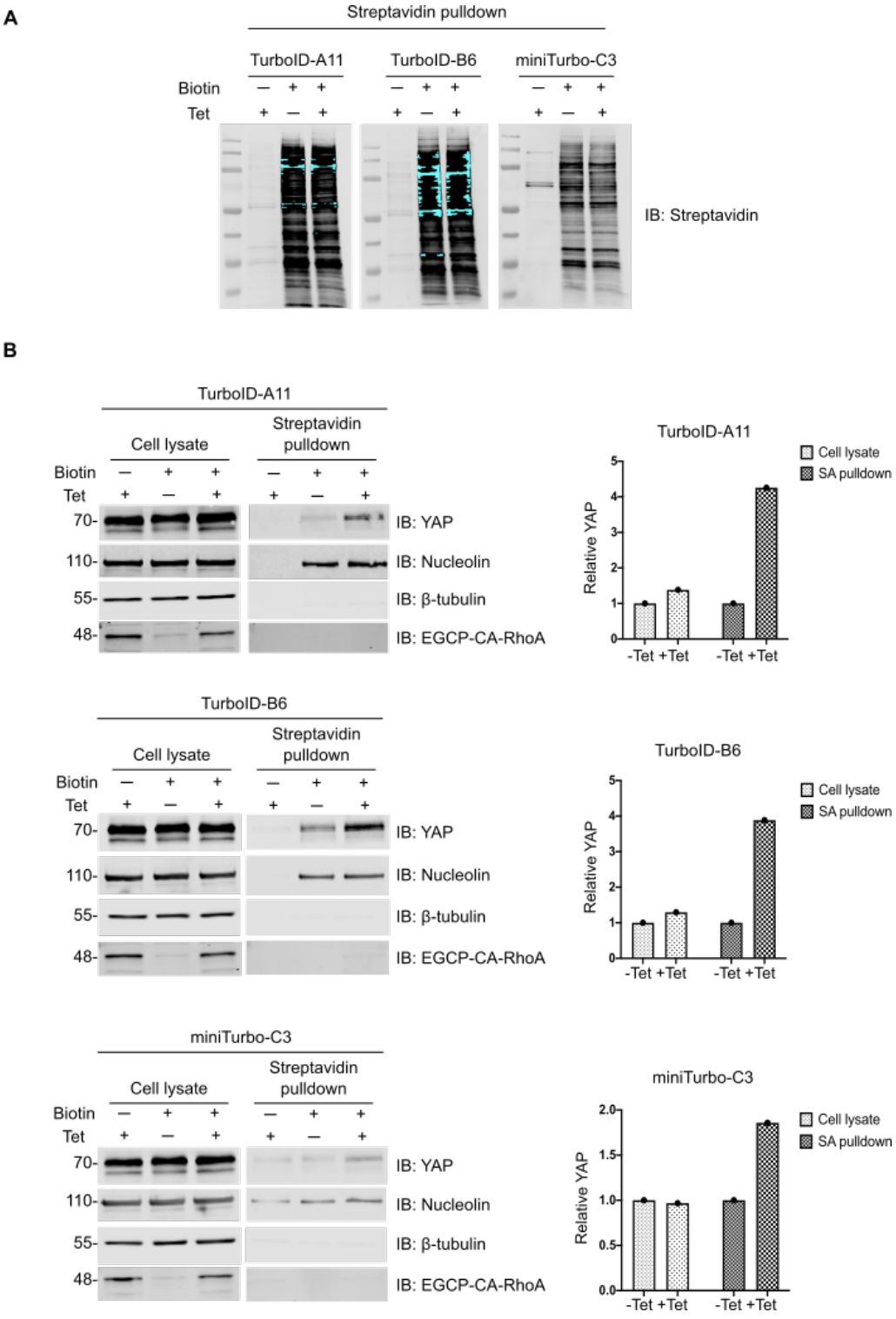

Figure 3.11 | Validation of TurboID and miniTurbo stable clones by western blot assay

(A) All TurboID and miniTurbo clones tested are capable to label nuclear proteins with biotin. The difference of biotinylated activity between TurboID clones A11 and B6 and miniTurbo clone C3 is visualized by western blot for streptavidin.

(B) Tet-induced CA-RhoA drives nuclear YAP accumulation in all TurboID and miniTurboID clones tested. Nucleolin and β-tubulin were act as nuclear and cytosolic marker respectively. YAP and

nucleolin are only detected in cells treated with both tetracycline and biotin. Graph summarized the relative amount of YAP in each TurboID or miniTurbo clones tested. YAP expression in total cell lysate or SA pulldown was first normalized to the expression of Nucleolin. Relative level of YAP in +Tet sample was normalized to -Tet sample.

3.3 Bioinformatic analysis of potential protein candidates involved in mechanotransduction

3.3.1 Detection and identification of active RhoA-mediated nuclear proteins by mass spectrometry

In our work, we aimed to identify the novel molecular players which potentially function as mechanotransducers. Here we adopted proximity-labelling system coupled with mass spectrometry to detect proteins enriched in the nucleus by increasing RhoA activity. We utilized the stable clone TurboID-A11 (hereafter designated as HEK293-tet-RhoA-TurboID). Its establishment and validation were described in 3.2.2. After setting up and validation of our screen approach, we collected nuclear fractions from five independent repeats and performed on-bead tryptic digestion to acquire peptide fragments which were then analysed by LC-MS/MS spectrometry (Figure 3.12 A). Each repeat comprised two groups of high density-cultured cells treated with tetracycline or vehicle (designated as +Tet or Tet respectively). In order to prove that our screen would allow us to identify possible mechanotransducers we immunoblotted for YAP (positive control), we also controlled the purity of our nuclear fraction by immunoblotting for the nuclear marker nucleolin and the cytosolic marker β-tubulin. Our result showed that YAP was enriched in the nucleus of cells treated with tetracycline after streptavidin pulldown while no β-tubulin was detected in the nuclear fraction (Figure 3.12 B), confirming these samples were suitable for subsequent mass spectrometry analysis.

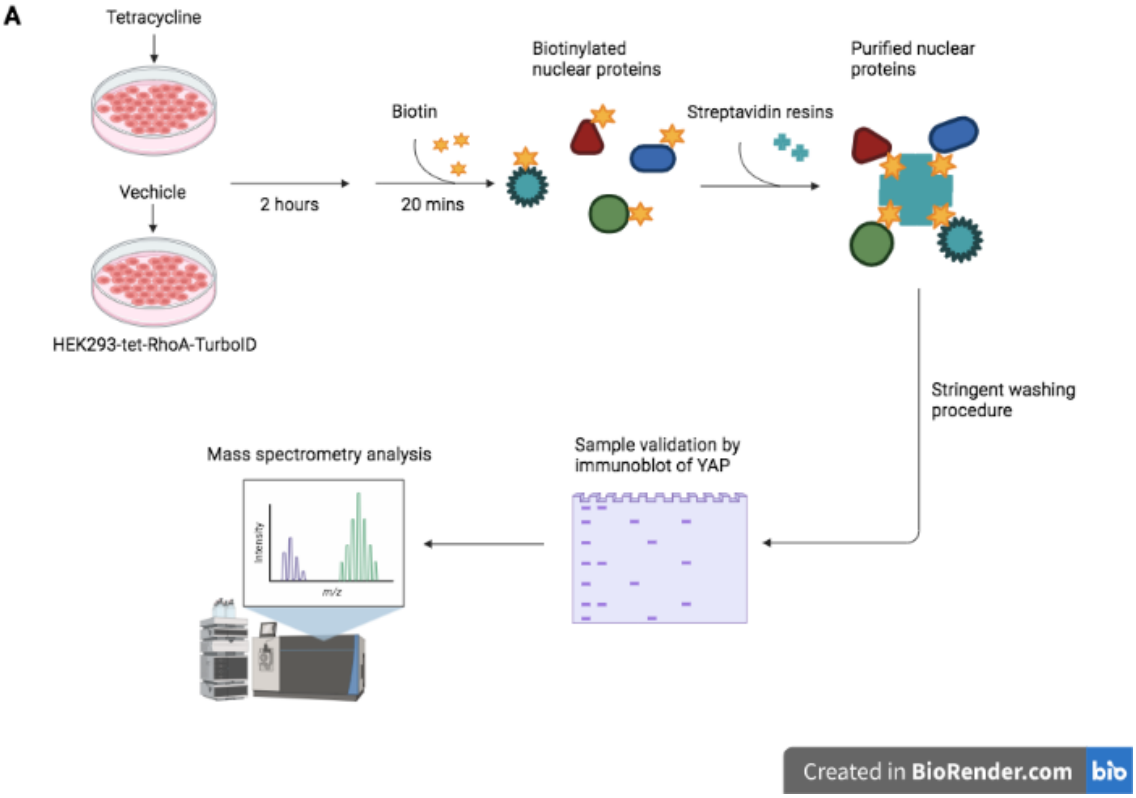

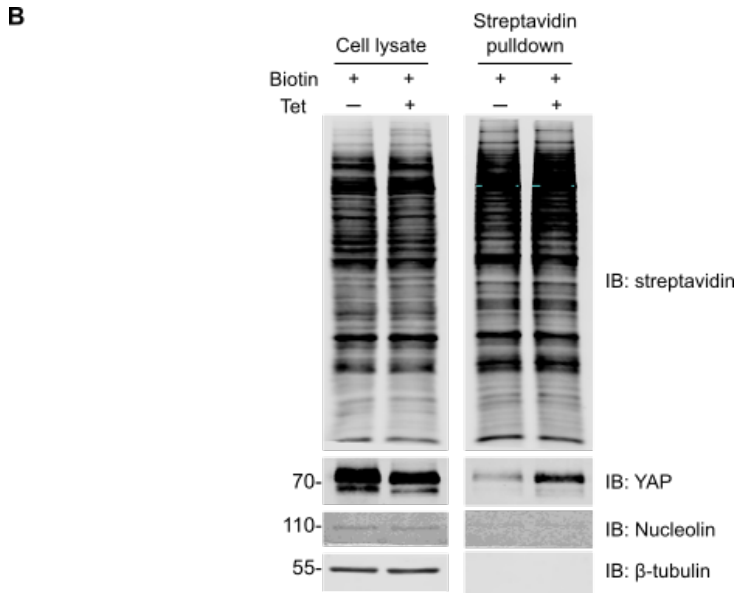

Figure 3.12 | Collection of nuclear proteins for mass spectrometry analysis
(A) Schematic overview of the screen procedure. Cells of high-density culture were treated with 1 μg/ml of tetracycline for 2 hours to induce CA-RhoA activity. The nuclear proteins were labelled with biotin for 20 minutes and subsequently purified by streptavidin pulldown. After trypsin

digestion and desalting procedure as described in 2.7.1, the samples were analyzed by mass spectrometry.
(B) Representative western blot of nuclear sample isolated from each experimental batch for mass spectrometry analysis.

Mass spec raw data was first sorted by Perseus to examine correlation between each biological repeat within the same group [120]. The correlation analysis indicated that +Tet-01, +Tet-02 and +Tet-03 of +Tet group showed strong relationship with each other while -Tet-01, -Tet-02, -Tet-04 and -Tet-05 from -Tet group were closely correlated (Pearson's r >0.95) (Figure 3.13 A-B). Thus, we selected these repeats of +Tet and -Tet group for further statistical analysis. The protein hits of these repeats were sorted by Perseus and analysed by two-sample t-test to compare their difference and corresponding significance between +Tet group and -Tet group. The statistical data was visualized by a volcano plot, revealing that 102 protein hits including YAP were significantly enriched whereas 797 proteins were downregulated in the nucleus in tetracycline treated samples (Figure 3.14).

A

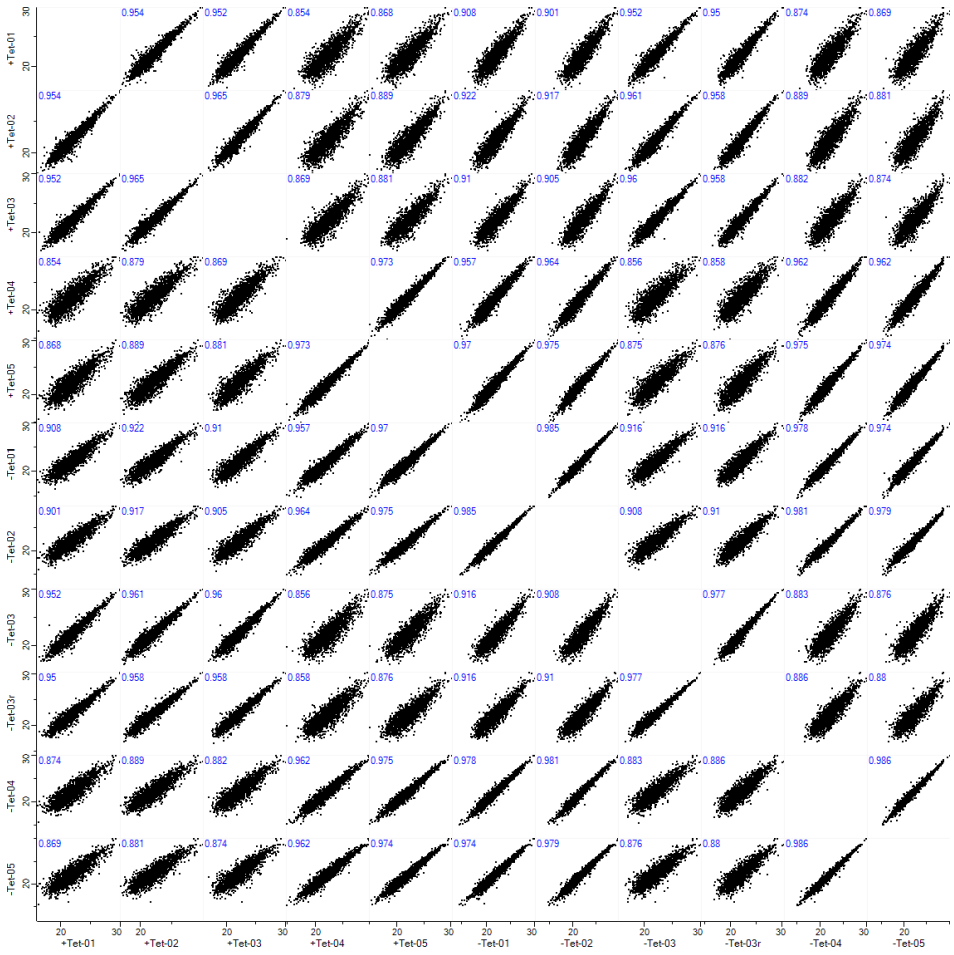

B

LFQ intensity +Tet-01	LFQ intensity +Tet-02	LFQ intensity +Tet-03	LFQ intensity -Tet-01	LFQ intensity -Tet-02	LFQ intensity -Tet-04	LFQ intensity -Tet-05	**Name**
NaN	0.9542175	0.9517787	0.9082981	0.9012935	0.8739702	0.8686486	LFQ intensity +Tet-01
0.9542175	NaN	0.9645137	0.9216884	0.9165679	0.8888911	0.8810076	LFQ intensity +Tet-02
0.9517787	0.9645137	NaN	0.9095135	0.9053265	0.8823966	0.8738747	LFQ intensity +Tet-03
0.9082981	0.9216884	0.9095135	NaN	0.9850712	0.9777908	0.9744061	LFQ intensity -Tet-01
0.9012935	0.9165679	0.9053265	0.9850712	NaN	0.9810804	0.9785691	LFQ intensity -Tet-02
0.8739702	0.8888911	0.8823966	0.9777908	0.9810804	NaN	0.985971	LFQ intensity -Tet-04
0.8686486	0.8810076	0.8738747	0.9744061	0.9785691	0.985971	NaN	LFQ intensity -Tet-05

Figure 3.13 | Selection of Mass Spec data by Perseus for further statistical analysis

(A) Correlation analysis of each biological repeats of the same group. Blue number in the plot indicated the Pearson's *r* value. The data was analysed by Dr Mark Collins (Senior Lecturer in the Department of Biological Science and Deputy Director of the Faculty of Science Mass Spectrometry Centre, University of Sheffield).

(B) Summary of correlation analysis showed in (A). Red and orange cells indicated the high correlation (Pearson's $r > 0.95$) between two corresponding replicates. The data was analysed

by Dr Mark Collins (Senior Lecturer in the Department of Biological Science and Deputy Director of the Faculty of Science Mass Spectrometry Centre, University of Sheffield).

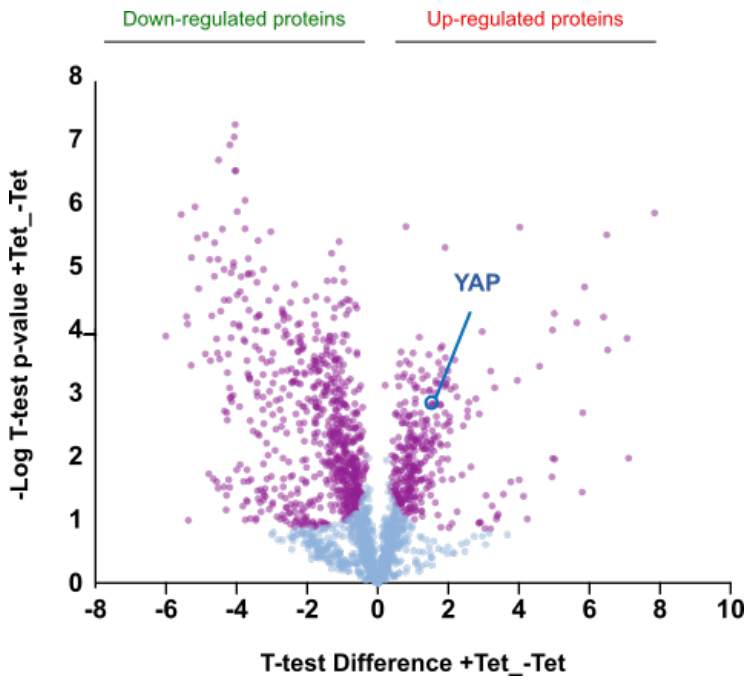

Figure 3.14 | Protein nuclear enrichment by tetracycline-induced RhoA in HEK293-tet-RhoA

Volcano plot showed the upregulated and downregulated nuclear protein hits after RhoA induction. YAP was identified in the screen with high confidence. The significance and difference of these differentially enriched proteins were analysed by two-sample t-test with FDR<0.05, log2 enrichment>1.5.

As our project aim is to identify potential mechanical regulators with nuclear function, we then focused on the investigation of protein candidates which were upregulated by tetracycline-induced CA-RhoA. The characteristics of the 102 significantly nuclear-enriched protein hits were examined based on Gene Ontology (GO). The protein enrichment was analysed by WEB-based GEne SeT AnaLysis Toolkit based on Gene Ontology cellular component (GOCC), which indicated that the majority of protein hits were originally located in the nucleus (83 over total 95 gene IDs in both user list and category) when compared to the number of proteins categorized to other compartments such as cytosol (42 over total 96 gene IDs), vesicle (19 over total 96 gene IDs) or cytoskeleton (13 over total 96 gene IDs) (Figure 3.15 A). Interestingly, GOCC analysis revealed 9 proteins distribute at cell-substrate interface such as focal adhesion and adherens junction (Figure 3.15 B), implying these proteins can be

transported into the nucleus triggered by tetracycline-induced RhoA signalling and may possess both nuclear and cytoplasmic function.

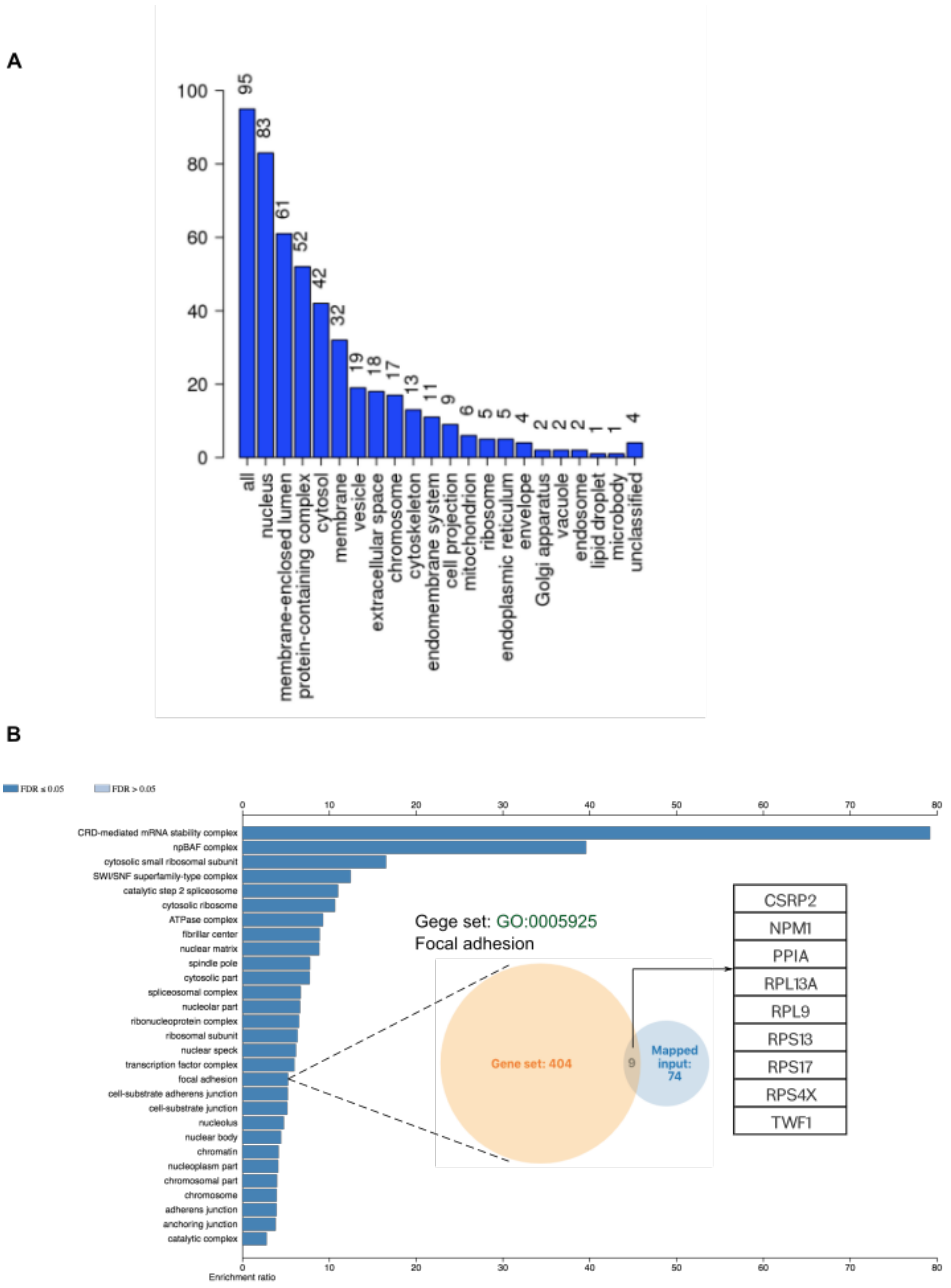

Figure 3.15 | Gene Ontology analysis of protein enrichment based on cellular components (GOCC)

(A) The number of proteins enriched in various cellular compartment were analysed by GOCC where 95 out of 102 user IDs were unambiguously mapped to 95 unique entrezgene IDs.

(B) GOCC revealed a group of proteins enriched in focal adhesions can be detected in the nucleus fraction in HEK293-tet-RhoA after CA-RhoA induction.

To further analyse these nuclear proteins by Gene Ontology based on biological process (GOBP), we found that most of the protein hits are involved in the regulation of RNA stability,

catabolic processes, metabolic processes and biosynthesis processes (Figure 3.16). In addition, GOBP also showed a group of proteins (including YAP) are implicated in the regulation of gene expression (Figure 3.17 A). In addition, there are 13 protein hits in this category including EIF4A3, GAPDH and a group of ribosomal proteins such as RPL13A, RPL9 and RPS13 engage in controlling peptide synthesis and protein translation (Figure 3.17 B). Taken together, our results indicated that RhoA-mediated signals may regulate multiple cellular functions at both transcriptional and post-transcriptional level.

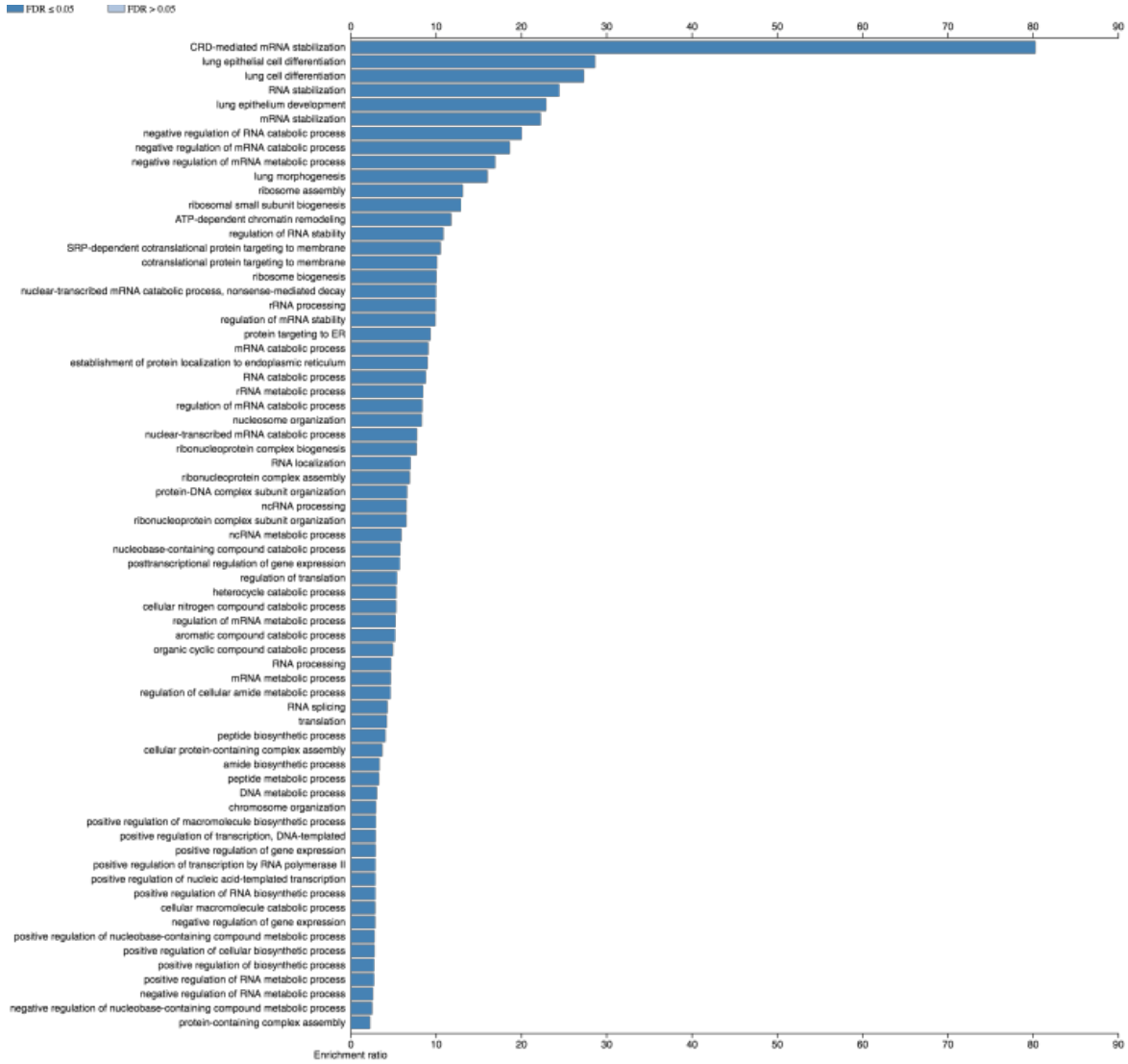

Figure 3.16 | Gene Ontology analysis based on biological process (GOBP)

GOBP analysis revealed that most of the proteins enriched in the nucleus by Tet-induced CA-RhoA are involved in the regulation of RNA stability, metabolic processes and biosynthesis processes.

Figure 3.17 | Gene Ontology analysis based on biological process (GOBP)

GOBP analysis showed that active RhoA-induced proteins involve in regulation of gene expression (A) and translation (B).

In order to validate our mass spectrometry results, we selected several candidates which were upregulated in the +Tet cell group for immunoblot analysis. These candidates have various biological functions such as RNA processing (PCBP1, PTBP1) [121, 122], promoting cell growth and invasiveness (CCT2) [123] and organ morphogenesis/transcription (Pitx2) [124]. Immunoblot analysis showed that all of the proteins tested were enriched in the nucleus after tetracycline-induced CA-RhoA signalling (Figure 3.18). Given that the level of YAP was also significantly elevated in the SA-pulldown sample, our data indicated that the subcellular distribution of these proteins were regulated by RhoA-activity, providing evidence of the authenticity of our screen strategy and the potential role of these protein candidates in mechanotransduction.

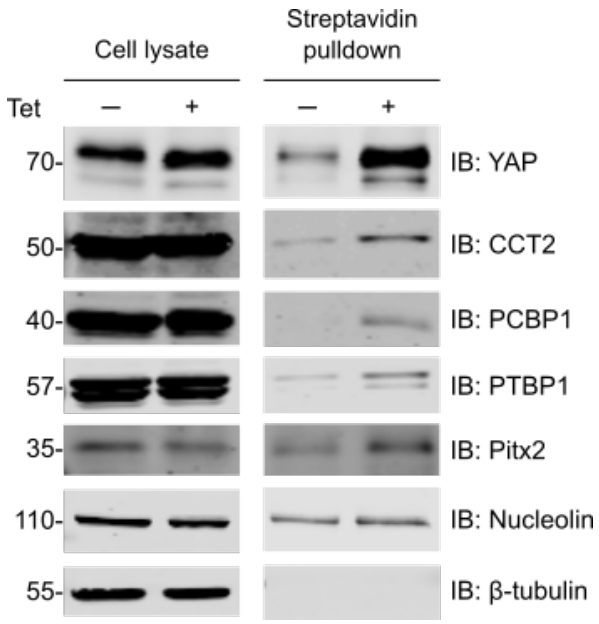

Figure 3.18 | Validation of potential protein candidates

Representative immunoblot from two independent biological replicates showing the nuclear enrichment of some protein candidates by tetracycline induced RhoA. YAP was as positive control while nucleolin and β-tubulin were used as nuclear marker and cytoplasmic marker respectively.

3.4 Summary

To enable us to identify potential novel mechanotransdcuers with a nuclear function, we engineered a stable cell line, HEK293-tet-RhoA-TurboID, which expresses CA-RhoA activity under a tetracycline-inducible promotor. In addition, this cell line expresses a biotin ligase in

the nucleus allowing us to isolate and purify nuclear proteins using proximity biotinylation followed by streptavidin affinity purification (Figure 3.11). The established mechanotransducer YAP was used as a positive control to optimise and validate our screen approach. A mass spectrometry analysis of our streptavidin pulldowns identified 102 proteins (including YAP) enriched in the nucleus in a RhoA dependent manner whilst 797 proteins were significantly downregulated under the same experimental conditions (Figure 3.14). Gene Ontology analysis of the identified proteins further revealed that most of the identified proteins are involved in RNA processing including RNA splicing and translation. Importantly, we validated our mass spectrometry results for a number of identified proteins including the splicing regulators PTBP1 and PCBP1 using western-blotting of nuclear fractions, confirming these proteins may translocate between the nucleus and cytoplasm as a response RhoA signalling (Figure 3.18).

4. Chapter 4 – Investigation of potential regulators in mechanotransduction

Our mass spectrometry analysis revealed that 102 proteins were significantly enriched in the nucleus after overexpression of CA-RhoA. Among these proteins, a group of RNA binding proteins (RBPs) including PCBP1, PTBP1 and EIF4A3 particularly intrigued our interest due to their role in RNA metabolism process such as regulating alternative splicing and translation of target transcripts (Figure 4.1) [122, 125, 126]. In the following work we focused on the investigation of PCBP1 and PTBP1. Both PCBP1 and PTBP1 contain nuclear localization signals (NLS) and are capable of shuttling between the nucleus and cytoplasm for specific biological function [122, 127]. Multiple mechanisms have been demonstrated underlying the nuclear/cytoplasmic shuttling of PCBP1 or PTBP1, however, the influence of mechanical forces on either subcellular localization or physiological function of these two proteins remains elusive. Here we hypothesized that PCBP1 and PTBP1 could be potential mechanotransducers which regulate cellular functions in responding to external mechanical signals. In this chapter we performed a series of experiments to verify the role of PCBP1 and PTBP1 in mechanotransduction.

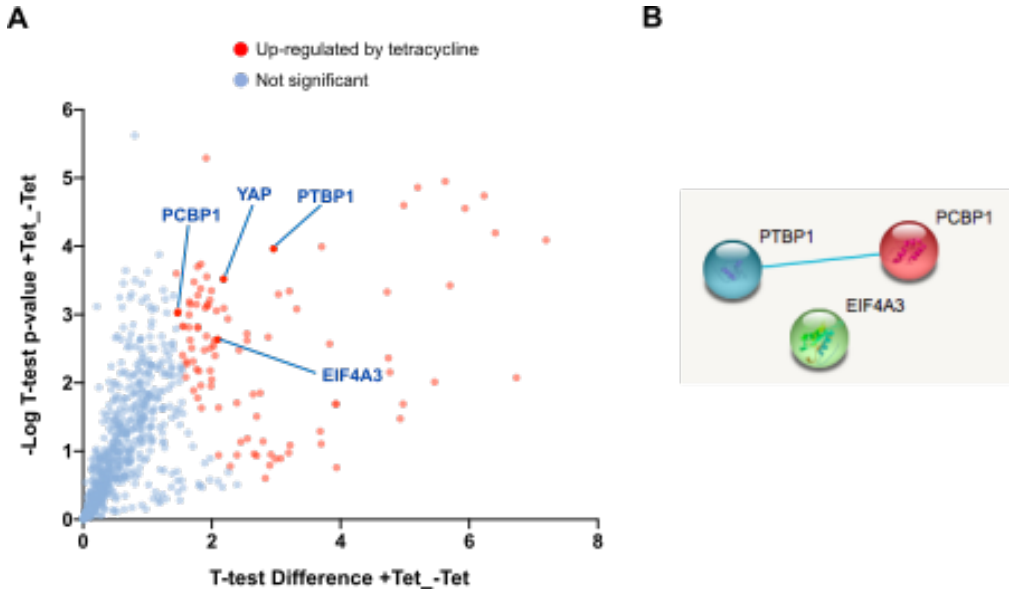

Figure 4.1 | PCBP1, PTBP1 and EIF4A3 are enriched in the nucleus by CA-RhoA activity.

(A) The significance and difference of PCBP1, PTBP1 and EIF4A3 between +Tet and -Tet group were visualized by volcano plot. YAP was presented as positive control. All of the four protein hits labelled in the plot were up-regulated by tetracycline-treated sample.

(B) Protein-protein interaction of PCBP1, PTBP1 and EIF4A3 analysed by STRING. The interaction was based on database (blue)

4.1 Subcellular localization of PCBP1 and PTBP1 is regulated by mechanical cues

4.1.1 Validation of PCBP1 and PTBP1 antibody

We first examined the specificity of PCBP1 and PTBP1 antibodies used in this work by siRNA mediated knockdown experiments. MCF10A cells were transfected with siRNAs targeting PCBP1 or PTBP1 for 72 hours before subjected to cell lysis and protein extraction. The siRNA used in this work are listed in **Table 2.4**. Western blot analysis indicated that siRNA-mediated knockdown induced around 75-80% reduction of total PCBP1 while 65-70% reduction of total PTBP1 (Figure 4.2 A-B). The protein expression pattern was also visualized by immunofluorescent staining, in which the PCBP1 or PTBP1 siRNA transfected MCF10A displayed overall reduction of these two proteins respectively (Figure 4.3 A-B). Our data confirm the specificity of PCBP1 and PTBP1 antibodies used in my PhD project.

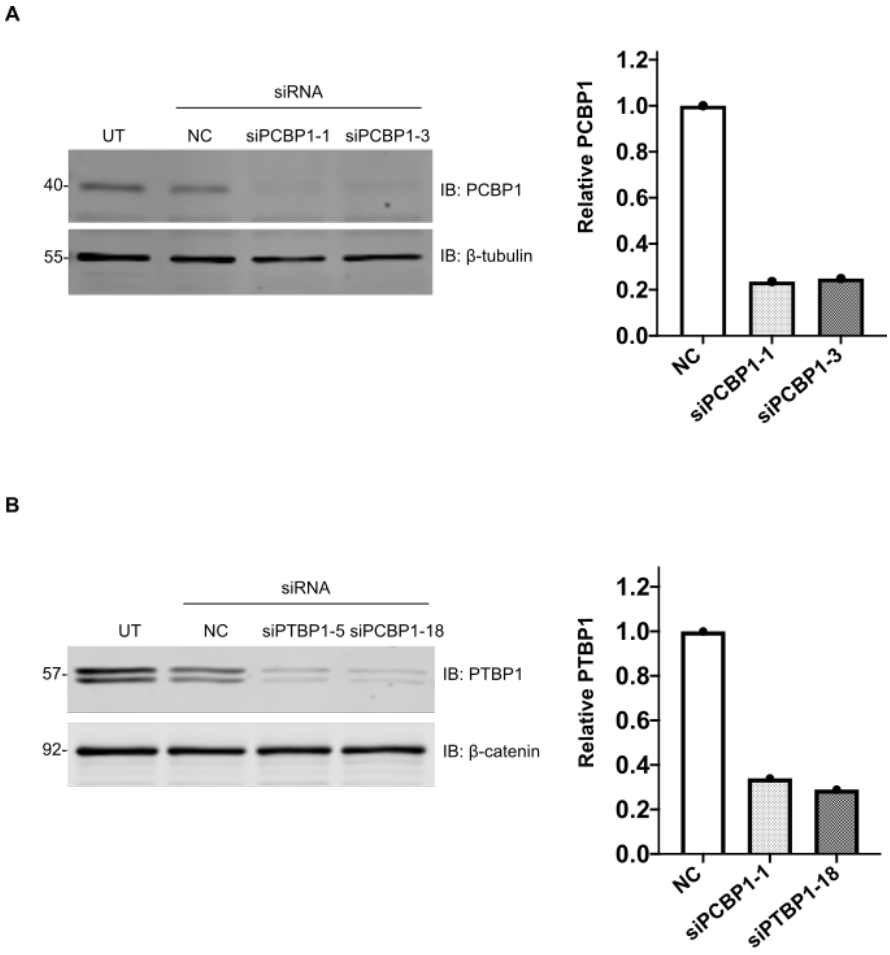

Figure 4.2 | siRNA-mediated knockdown of PCBP1 and PTBP1

(A) Left: Representative western blot of PCBP1 level in MCF10A treated with control siRNA (NC) or two different PCBP1 siRNA. NC represents the siRNA negative control. b-tubulin was used as a loading control. Right: Densitometric quantification of PCBP1 level presented in immunoblot showing the knockdown efficiency of this protein. PCBP1 level was normalized against β-tubulin loading control.

(B) Left: Representative western blot of PTBP1 level in MCF10A treated with control siRNA (NC) or two different PTBP1 siRNA. β-catenin was used as a loading control. Right: Densitometric quantification of PTBP1 level presented in immunoblot showing the knockdown efficiency of this protein. PTBP1 level was normalized against β-catenin loading control.

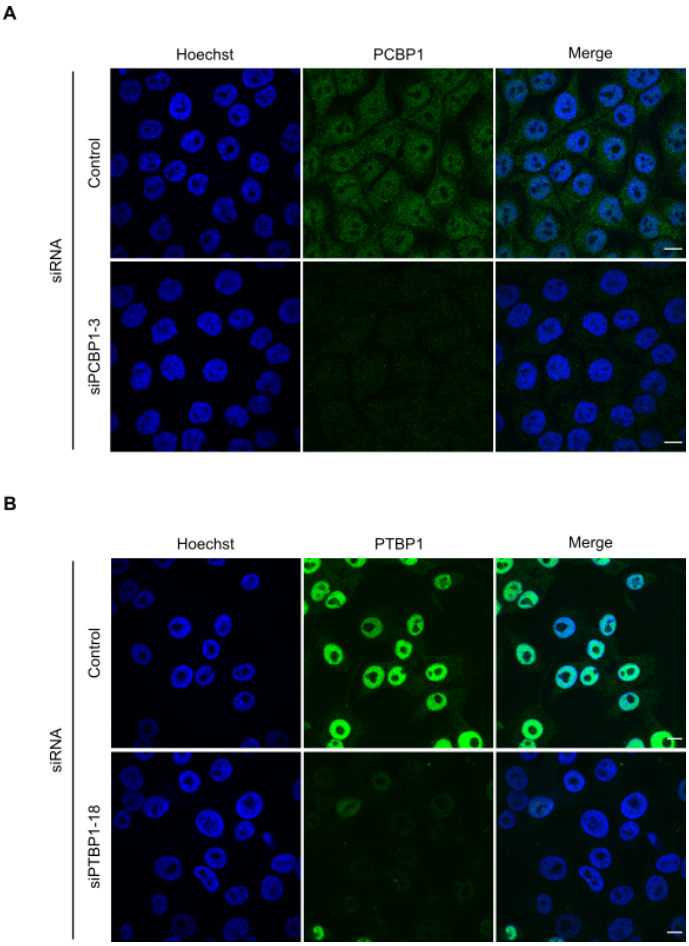

Figure 4.3 | siRNA-mediated knockdown of PCBP1 and PTBP1

Representative immunofluorescence images of siRNA-mediated knockdown of PCBP1 (A) and PTBP1 (B) in MCF10A. Cells were treated with indicated siRNA for 96 hours before immunofluorescence staining of PCBP1 or PTBP1. Scale bars, 10 μm.

4.1.2 Cell density regulated the subcellular translocation of PCBP1

Previous studies have demonstrated the impact of mechanical cues derived from cell density on YAP/TAZ translocation and protein activities [3]. To clarify the role of PCBP1 in mechanotransduction, we examined of the influence of cell density on the subcellular localization of PCBP1. Epithelial cell line MCF10A was placed at low or high density and YAP expression pattern was first tested as a positive control to monitor cell's ability to respond to cell density-dependent mechanical signals. As expected, YAP was predominantly located in the nucleus in sparsely cultured cells but largely excluded from the nucleus to cytoplasm when

cells reached high density (Figure 4.4 A). The cell density-dependent shift of YAP localization indicated this cell line's ability to respond to cell density.

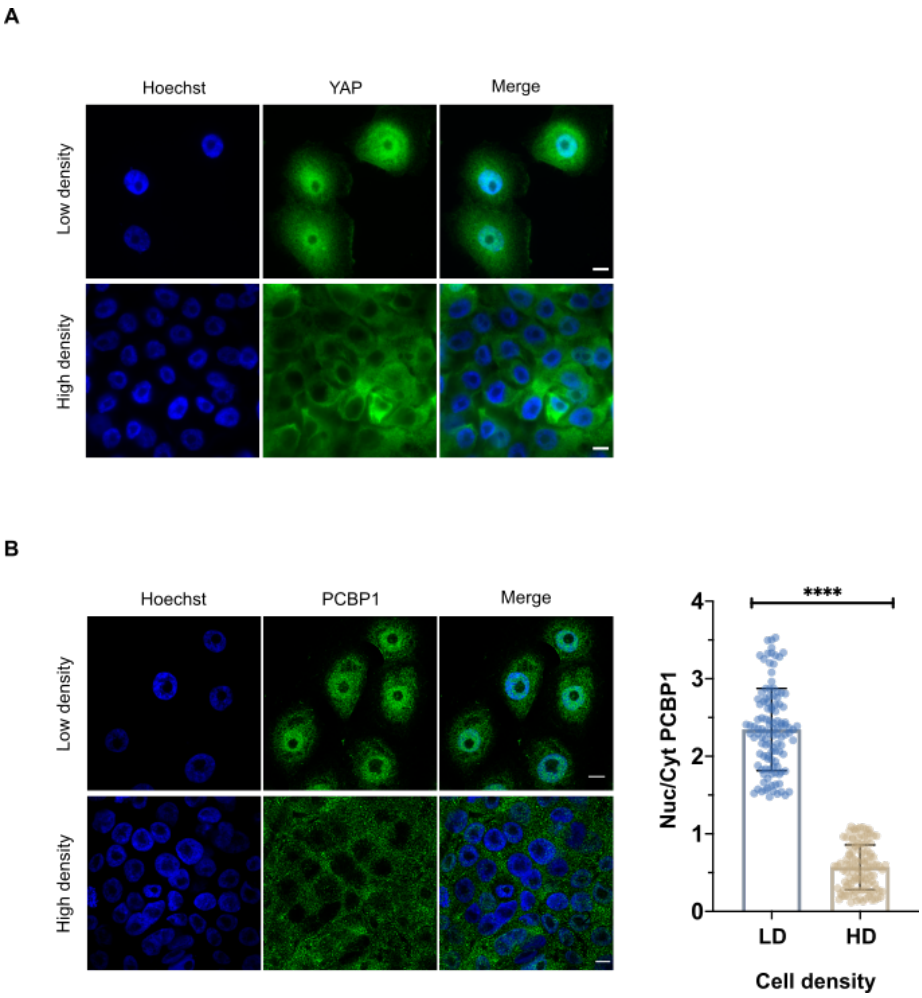

Figure 4.4 | Cell density regulates YAP and PCBP1 subcellular distribution in MCF10A

(A) MCF10A were plated at low (0.8 x 10^5/well) or high density (7 x 10^5/well) and subcellular translocation of YAP was visualized by immunofluorescence staining. Scale bars, 10 μm.

(B) Left: Immunofluorescence images of PCBP1 expression profile in MCF10A plated at low or high cell density. Scale bars, 10 μm. Right: Quantification of ratio of nuclear PCBP1 to cytoplasmic PCBP1. Fluorescence intensity of PCBP1 was assessed by ImageJ. Data was analysed by unpaired Welch's t-test (n=3). Values are means ± s.d. ****P<0.0001.

We then tested PCBP1 subcellular localisation in MCF10A cultured at low or high cell density. Similar to YAP, immunofluorescence staining showed that low density cultured cells displayed prominently nuclear PCBP1 (Nuc-PCBP1). On the contrary, dense cells showed much less Nuc-PCBP1 while accumulation of cytoplasmic PCBP1 (Cyt-PCBP1) (Figure 4.4 B). The quantification revealed a significant decrease in PCBP1 nucleus/cytoplasm ratio in high density

MCF10A (Figure 4.4 B). A similar cell density dependent-PCBP1 localization was also observed in another cell line, HEK293 (Figure 4.5 A-B).

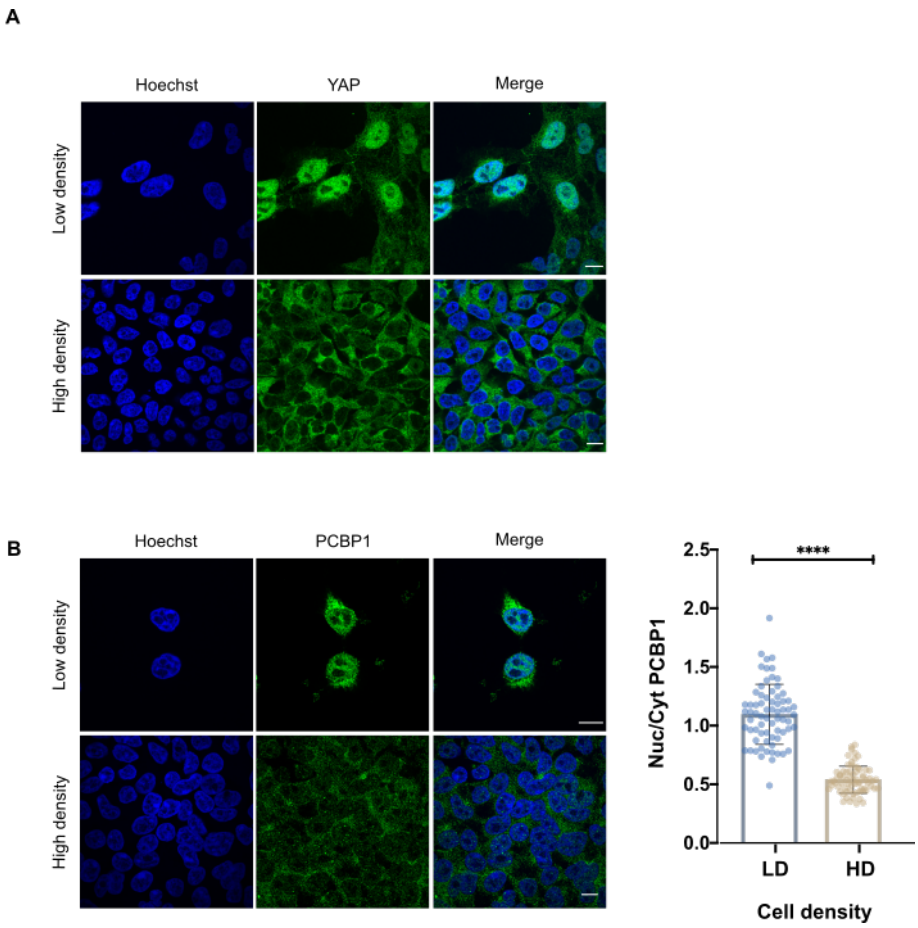

Figure 4.5 | Cell density regulates YAP and PCBP1 translocation in HEK293

(A) HEK293 were plated at low (1×10^5/well) or high density (6×10^5/well) and subcellular distribution of YAP was analysed by immunofluorescence staining. Scale bars, 10 μm.

(B) Left: representative Immunofluorescence images of PCBP1 in HEK293 plated at low and high cell density respectively. Scale bars, 10μm. Right: Quantification of ratio of nuclear PCBP1 to cytoplasmic PCBP1. Fluorescence intensity of PCBP1 was assessed by ImageJ. Data was analysed by unpaired Welch's t-test (n=3). Values are means ± s.d. ****P<0.0001.

To corroborate our immunofluorescence analysis with biochemical evidence, we utilized HEK293-TurboID stable cell line to analyse protein expression levels of PCBP1 and its presence in the nuclear fraction. HEK293-TurboID were designed to allow us to isolate nuclear protein through proximity-labelling system. The cell line was cultured at low or high density and nuclear proteins were labelled with 500 μM of biotin before isolation of nuclear proteins through streptavidin pulldown. The immunoblotting analysis indicated that PCBP1 increased in the nuclear fraction from low density-cultured cells when comparing to those from high

density culture (Figure 4.6). The total protein level of PCBP1 in cell lysate, however, were similar regardless of cell density (Figure 4.6). Our experiments showed that cell density did not affect endogenous PCBP1 level, suggesting that the increased nuclear localization of PCBP1 under low cell density condition would be mainly due to their shuttling from the cytoplasm to the nucleus.

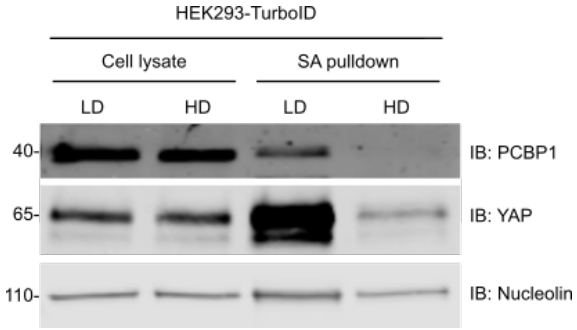

Figure 4.6 | Cell density regulates nuclear enrichment of PCBP1 in HEK293-TurboID

Immunoblotting for indicated proteins in HEK293-TurboID plated at low or high cell density. Nuclear fraction was isolated by streptavidin (SA) pulldown. Nucleolin was used as nuclear marker as well as the loading control.

4.1.3 Cell density-dependent subcellular localization of PTBP1 is cell type-dependent

We then determined whether another candidate, PTBP1, is also affected by cell density. The correlation between cell density and PTBP1 translocation was visualized by immunofluorescence staining, which showed a drastic shift in PTBP1 localization between the nucleus and cytoplasm by cell density in MCF10A. PTBP1 overwhelmingly remained in the nucleus of sparsely cultured MCF10A while Cyt-PTBP1 or both Nuc- and Cyt-PTBP1 mainly dominated in dense cells (Figure 4.7 A). Intriguingly, the influence of cell density on PTBP1 localization in HEK293-TurboID was not consistent with those observed in MCF10A. PTBP1 was only detected in the nucleus regardless of cell density in HEK293 (Figure 4.7 B). Although HEK293 displayed a visually reduced Nuc-PTBP1 in high density when compared to those observed in low density, neither total PTBP1 nor nuclear PTBP1 protein expression level was affected by cell density (Figure 4.7 C). Our data suggest that cell density-mediated PTBP1 relocalization would be cell type-dependent.

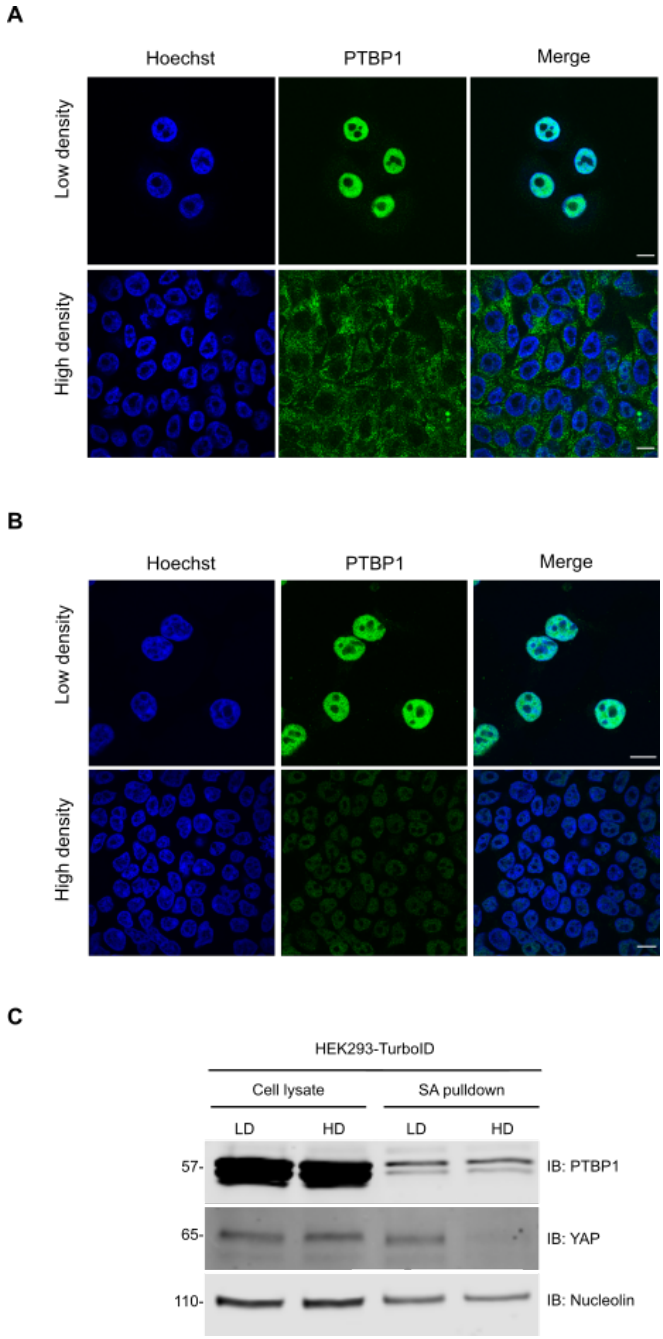

Figure 4.7 | Influence of cell density on PCBP1 expression pattern

(A) MCF10A were plated at low (0.8 x 10^5/well) or high density (7 x 10^5/well) and subcellular distribution of YAP was analysed by immunofluorescence staining. Scale bars, 10 μm.

(B) HEK293 were plated at low (1 x 10^5/well) or high density (6 x 10^5/well) and subcellular translocation of PTBP1 was detected by immunofluorescence staining. Scale bars, 10 μm.

(C) Immunofluorescence images of PTBP1 subcellular distribution in HEK293 of different cell density. Scale bars, 10μm.

4.1.4 Cell adhesive area regulates the subcellular localization of PCBP1 but not PTBP1

Given that changes of cell density involve alteration of cell adhesive area and cell morphology, which have been shown to regulate relocalization and activity of YAP/TAZ [11, 103], we asked whether the subcellular localization of PCBP1 and PTBP1 in MCF10A controlled by cell density is through the influence of cell adhesive area. We utilized fibronectin-coated micropattern to force cells to grow on an adhesive area of defined sizes and first examined the correlation between cell adhesive area and localization of YAP in MCF10A. To rule out the influence of cell-cell contacts on protein distribution, only the single cell of each micropatterned domain was selected to check the subcellular localization of target protein. The spreading degree of the single cell changed with domain size. Cell morphology was rounded when it was confined in smallest domain (300 μm^2) but started spreading in larger area (1024~10,000 μm^2), which was visualized by phalloidin staining for F-actin distribution (Figure 4.8). In addition, cell's response to various adhesive area was evidenced by YAP subcellular localization, that nuclear YAP was predominantly located in larger domains (1024~10,000 μm^2) (Figure 4.8). Such result was consistent with previous finding and confirmed our approach.

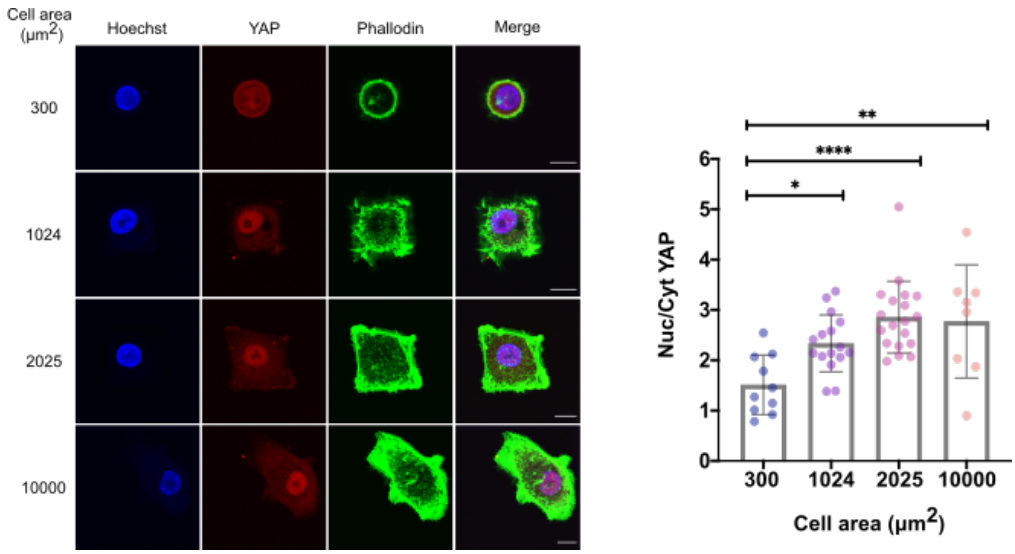

Figure 4.8 | Cell adhesive area regulates subcellular translocation of YAP in MCF10A

Left: Immunofluorescence images of YAP in single MCF10A cultured on fibronectin-coated domain of various defined sizes (μm^2). Scale bars, 10 μm. Right: Graph provides quantification of ratio of Nuc/Cyt YAP (n=1). Values are means ± s.d. * P<0.05, ** P<0.01, **** P<0.0001.

Similar to YAP's subcellular localisation, PCBP1 was diffusely distributed between both nucleus and cytoplasm in MCF10A cells frown at 300 μm^2, while the nucleus/cytoplasm ratio

of PCBP1 significantly increased in cells grown in larger domains (1024~10,000 μm^2) (Figure 4.9). PCBP1 was highly accumulated in the nucleus when cells grew on unpatterned area without defined size, with the nucleus/cytoplasm ratio similar to the quantification acquired in low density cultured cells (Figure 4.9). What we observed in this experiment implies that cell density-dependent change of nuclear PCBP1 level is through the influence of cell spreading area.

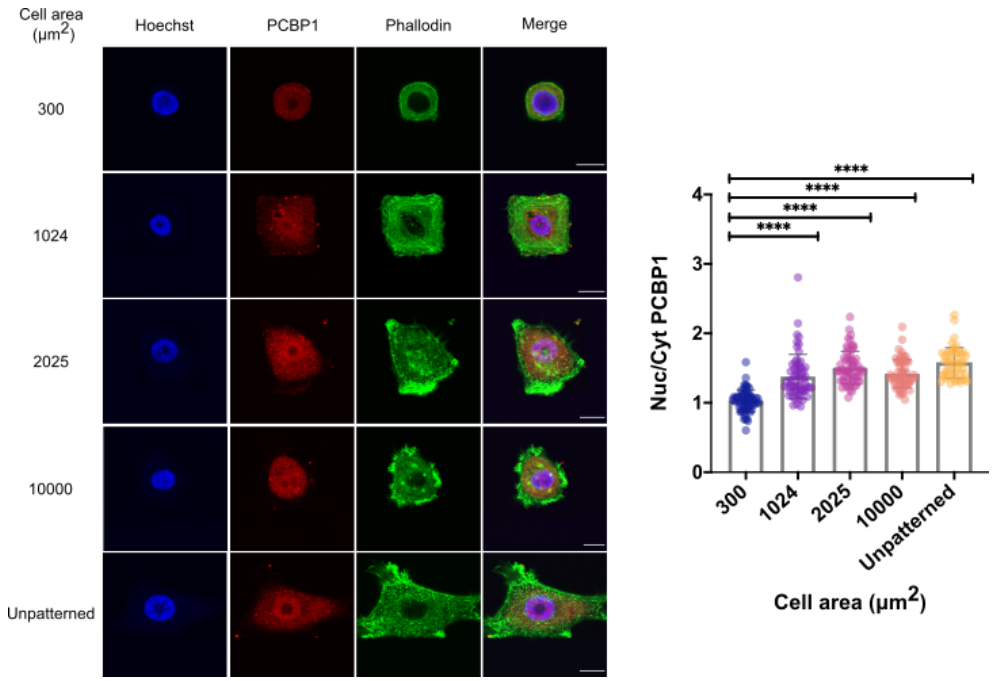

Figure 4.9 | Cell adhesive area regulates subcellular translocation of PCBP1 in MCF10A

Left: Immunofluorescence analysis of PCBP1 in single MCF10A plated on microdomain with defined sizes (μm^2). Scale bars, 10 μm. Right: Graph indicates quantification of ratio of Nuc/Cyt PCBP1. Data was analysed by ordinary one-way ANOVA followed by Tukey's multiple comparisons test. (n=3). Values are means ± s.d. ****P<0.0001.

The subcellular localization of PTBP1 in MCF10A growing in various domain area was also examined. Although our previous data showed that MCF10A exhibited cytoplasmic PTBP1 when they reached high cell density, here we observed that PTBP1 always remained in the nucleus throughout cell cultured in different domain sizes including unpatterned area. Moreover, there was no visible difference of nuclear PTBP1 expression level regardless of the degrees of cell spreading (Figure 4.10), indicating the nuclear localization of PTBP1 in MCF10A did not correlate with cell adhesive area.

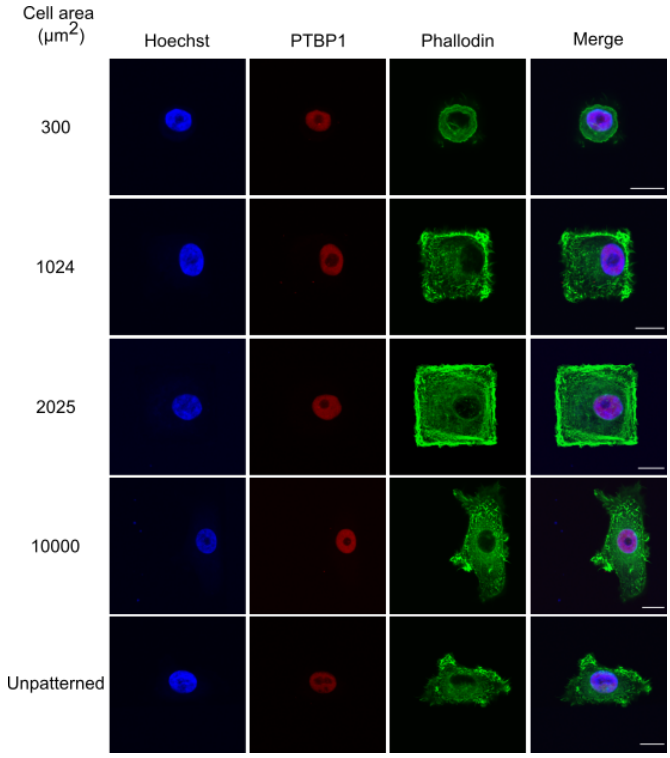

Figure 4.10 | PTBP1 is not affected by cellular confinement in MCF10A

Immunofluorescence analysis of single MCF10A plated on microdomain with defined sizes (μm^2). Cells were stained with anti-PTBP1 antibody. Scale bars, 10 μm.

4.1.5 ECM stiffness regulates subcellular localisation of PCBP1 and PTBP1

Previous studies have demonstrated the distinct impact of ECM stiffness on cell behaviour such as proliferation, migration and differentiation, in which YAP/TAZ play an important role in mechanical signal-mediated cellular function [11]. To investigate whether ECM rigidity engages in the regulation of PCBP1 and PTBP1, we utilized polyacrylamide hydrogels (hereafter designated as PAA gel) of varying stiffness to exert different physical properties to cells and tested the subcellular localization of PCBP1 and PTBP1. PAA gel has been widely used in the research of ECM stiffness-dependent cell biology due to its non-biodegradable, tuneable elastic properties [114, 128]. We fabricated PAA gel of soft (1 kPa or 0.7 kPa) and stiff (40 kPa) in culture dish and coated the gel with collagen prior to seeding the cells on top of the gels (Figure 4.11). In order to validate our PAA gel experiment system, we first checked YAP phenotype in MCF10A after being cultured on soft (1 or 0.7 kPa) and stiff (40 kPa) PAA gel for

24 hours. Of note, these parameters of PAA gel stiffness chosen in our work was based on previous study, in which a rigidity threshold of 5 kPa for YAP nuclear accumulation was identified [129]. Immunofluorescence experiments confirmed the correlation between ECM stiffness and YAP nuclear localisation in our experiments, that cells displayed more cytoplasmic YAP when cultured on soft ECM yet enriched nuclear YAP on stiff gel (Figure 4.12). Our data was consistent with the proof of principle that cells respond to various ECM stiffness through the translocation of YAP between the nucleus and cytoplasm. Moreover, the results also confirmed our PAA gel experiment system was able to provide distinctive mechanical cues to cells.

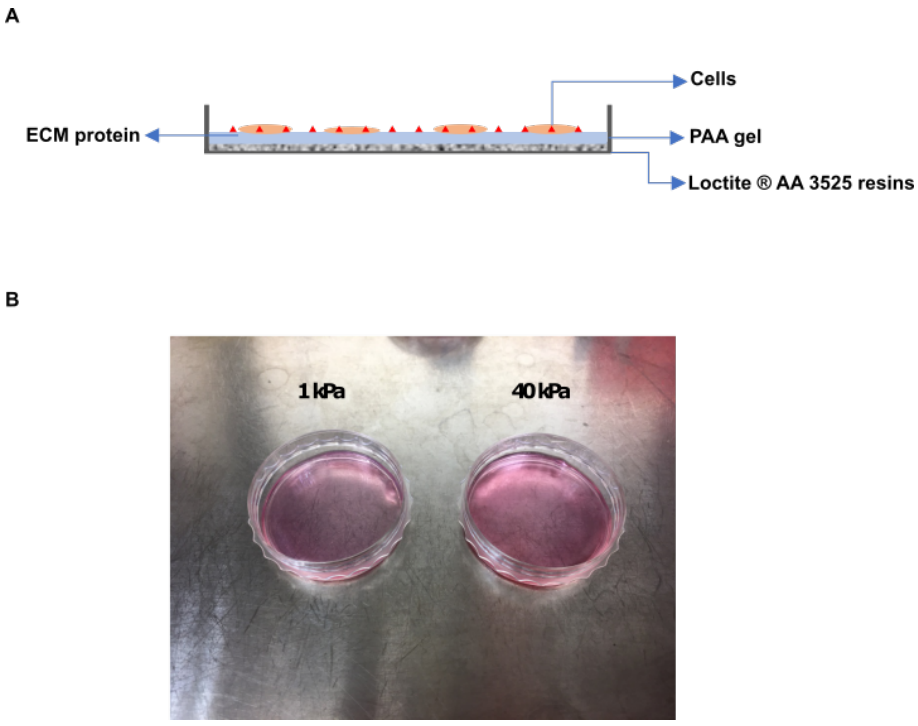

Figure 4.11 | Schematic representation of fabrication of polyacrylamide gel in plastic petri dish for cell culture

(A) Polyacrylamide gel was attached to petri dish by adhesive resin Loctite AA 3525 and coated with ECM protein (collagen type I in this experiment) on the surface for cell attachment and growth.
(B) Representative image of polymerized PAA gel in petri dish with cell culture medium.

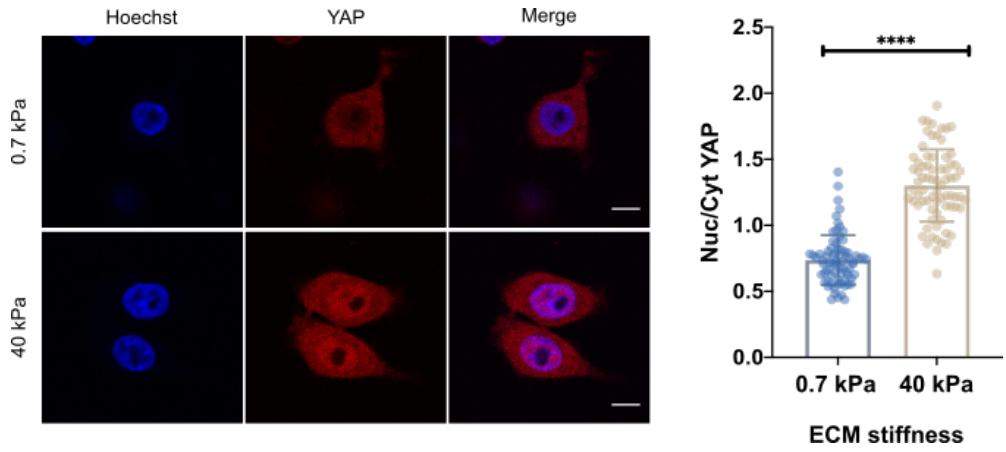

Figure 4.12 | ECM stiffness affects YAP subcellular translocation

Left: Immunofluorescence images of YAP in MCF10A grown on PAA gel with rigidity of soft (0.7 kPa) or stiff (40 kPa). YAP is mainly located in the cytoplasm on soft gel while enriched in the nucleus on stiff gel. Scale bars, 10 μm. Right: Quantification of ratio of Nuc/Cyto YAP. Data was analysed by unpaired Welch's t-test (n=3). Values are means ± s.d. ****P<0.0001.

We then examined the influence of ECM stiffness on PCBP1 subcellular localisation. Given that our IF data indicated that nuclear PCBP1 in MCF10A was significantly reduced by high cell density, in ECM stiffness experiments the cells were placed sparsely on PAA gel to rule out the impact of high cell density on the relocalization of the proteins being tested. We cultured MCF10A on soft (1 or 0.7 kPa) and stiff (40 kPa) PAA gel respectively for 24 hours before further examination of target proteins. By immunofluorescence staining of PCBP1, we observed that soft PAA gel promoted cytoplasmic localization of PCBP1. By contrast, PCBP1 was highly retained in the nucleus or distributed in both nucleus and cytoplasm in cells on stiff gel (Figure 4.13 A). Similar results were obtained in PTBP1 expression pattern when immunofluorescence staining visualized the changes of PTBP1 Nuc/Cyt ratio with PAA gel rigidity. MCF10A grown on soft gel exhibited diffused PTBP1 in both the nucleus and cytoplasm while this protein was significantly enriched in the nucleus by stiff gel (Figure 4.13 B). The changes of PCBP1 and PTBP1 in their subcellular localization under soft and stiff PAA gel supported the role of ECM stiffness-mediated mechanical cues in the translocation of these proteins.

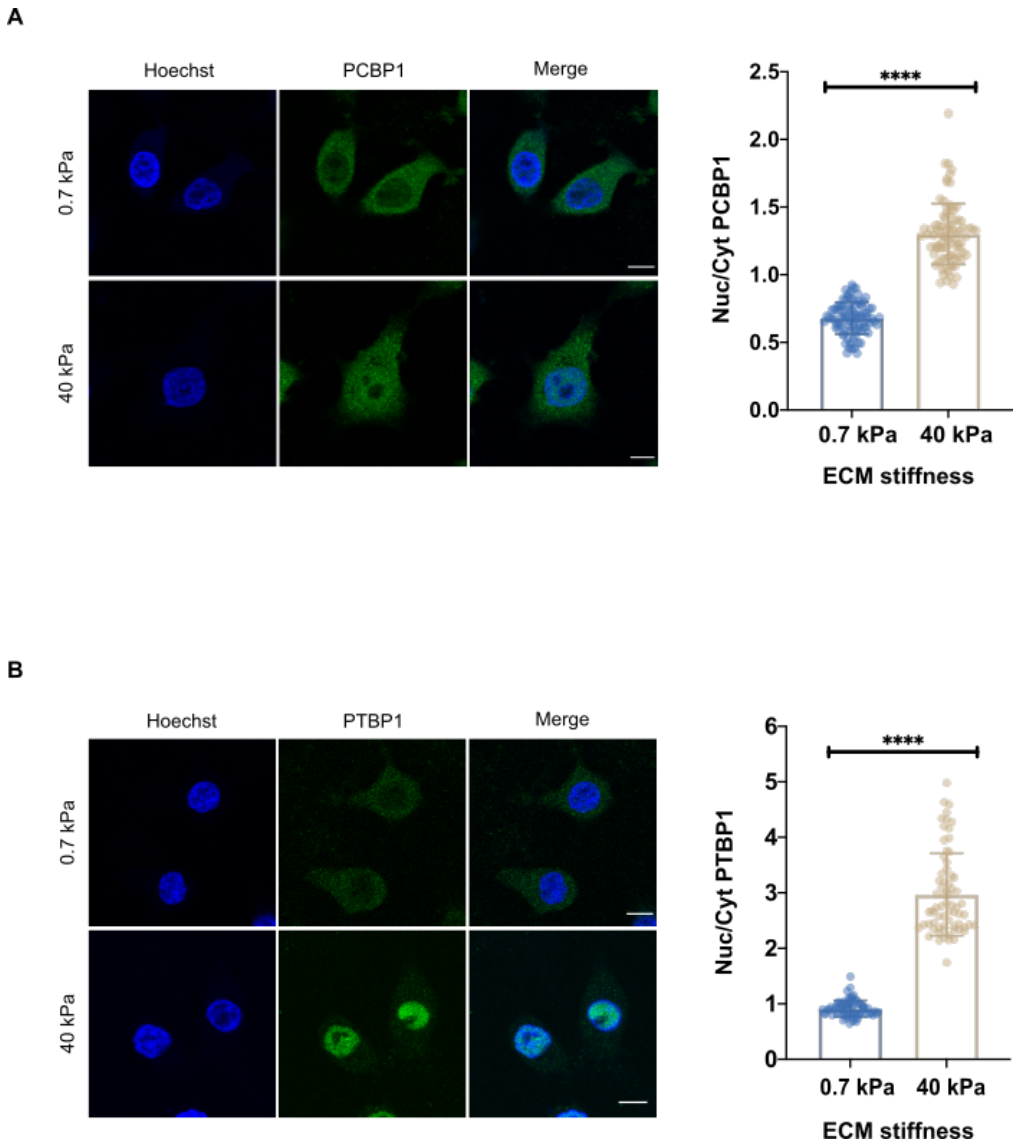

Figure 4.13 | ECM stiffness affects PTBP1 and PCBP1 subcellular translocation in MCF10A

(A) Left: Immunofluorescence images of PCBP1 expression profile in MCF10A plated on PAA gel with rigidity of soft (0.7 kPa) or stiff (40 kPa). 2.5 x 10^5 of cells were plated on PAA gel for 24 hours before immunofluorescence staining. Scale bars, 10 μm. Right: Graph provides quantification of ratio of Nuc/Cyt PCBP1. Immunofluorescence intensity of PCBP1 was assessed by ImageJ. Data was analysed by unpaired Welch's t-test (n=3). Values are means ± s.d. ****P<0.0001.

(B) Left: Immunofluorescence images of PTBP1 expression profile in MCF10A plated on PAA gel with rigidity of soft (0.7 kPa) or stiff (40 kPa). 2.5 x 10^5 of cells were plated on PAA gel for 24 hours before immunofluorescence staining. Scale bars, 10 μm. Right: Graph provides quantification of ratio of Nuc/Cyt PCBP1. Immunofluorescence intensity of PCBP1 was assessed by ImageJ. Data was analysed by unpaired Welch's t-test (n=3). Values are means ± s.d. ****P<0.0001.

To further clarify whether the ECM stiffness-dependent relocalization of PCBP1 and PTBP1 are also reproduced in other cell lines, we tested the subcellular localisation of these two

proteins in different cell lines such as HEK293, HeLa and Caco2 and found a similar phenotype. All of the cell lines tested in our work showed predominantly cytoplasmic PCBP1 on soft PAA gel yet nuclear PCBP1 on stiff gel. (Figure 4.14 A-C). A similar effect of ECM rigidity on PTBP1 localisation can be observed in these cell lines as well. Although PTBP1 was diffusely distributed in both nucleus and cytoplasm when cells were plated on soft gel, this protein was enriched in the nucleus of cells grown on stiff gel (Figure 4.15 A-B). Altogether, the results suggest a global impact of ECM stiffness on subcellular localisation of PCBP1 and PTBP1.

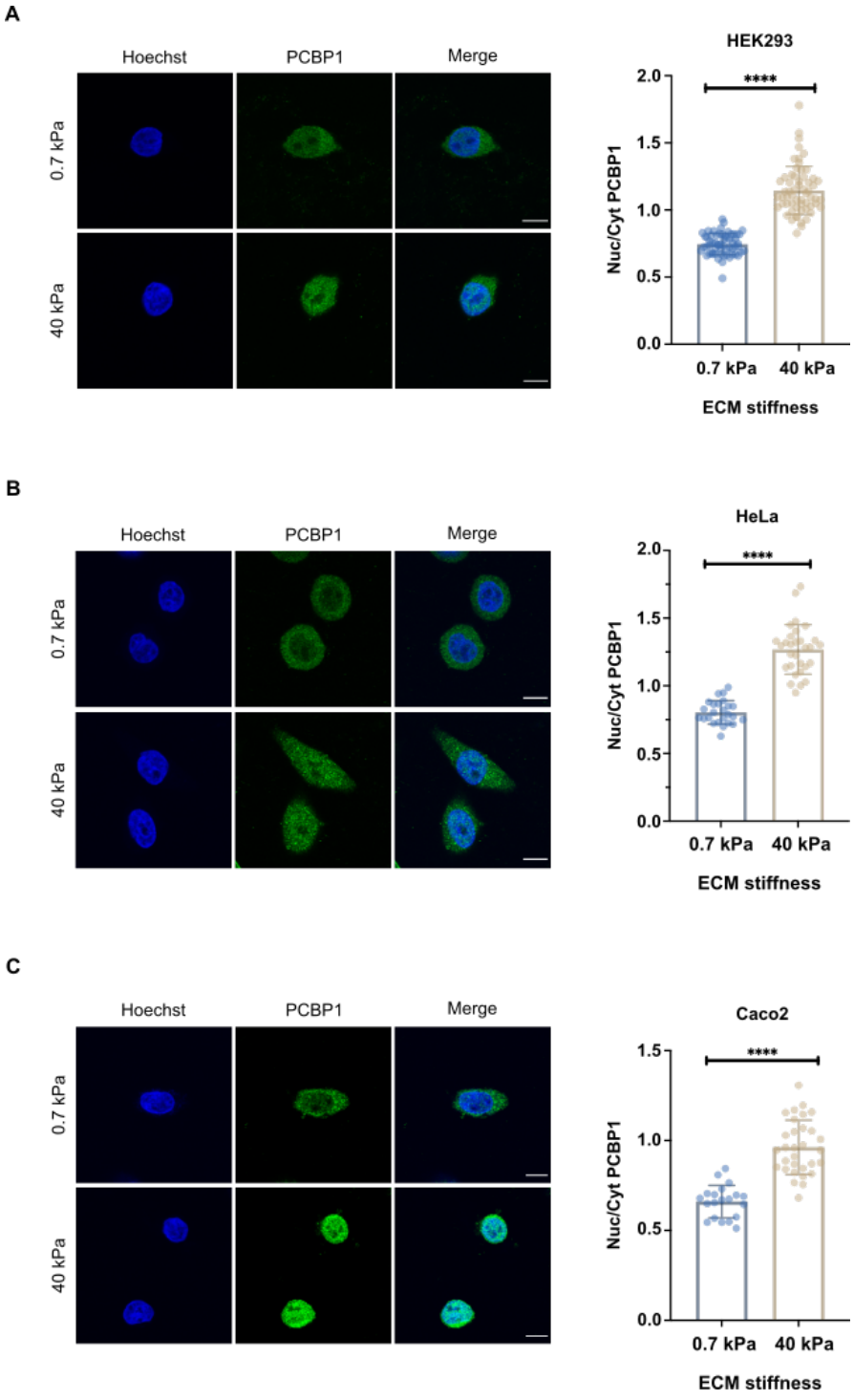

Figure 4.14 | ECM stiffness affects PCBP1 subcellular translocation in HEK293 (A), HeLa (B) and Caco2 (C)

Left: 2.5 x 10^5 of cells were plated on PAA gel for 24 hours before immunofluorescence staining of PCBP1. The immunofluorescence images show the subcellular distribution of PCBP1 based on ECM rigidity. Scale bars, 10μm.

Right: Graphs provide quantification of Nuc/Cyt ratio of PCBP1. Immunofluorescence intensity of PCBP1 was assessed by ImageJ. Data was analysed by unpaired Welch's t-test. The biological replicates of each cell line are: HEK293 (n=3), HeLa (n=2), Caco2 (n=1). Values are means ± s.d. ****P<0.0001.

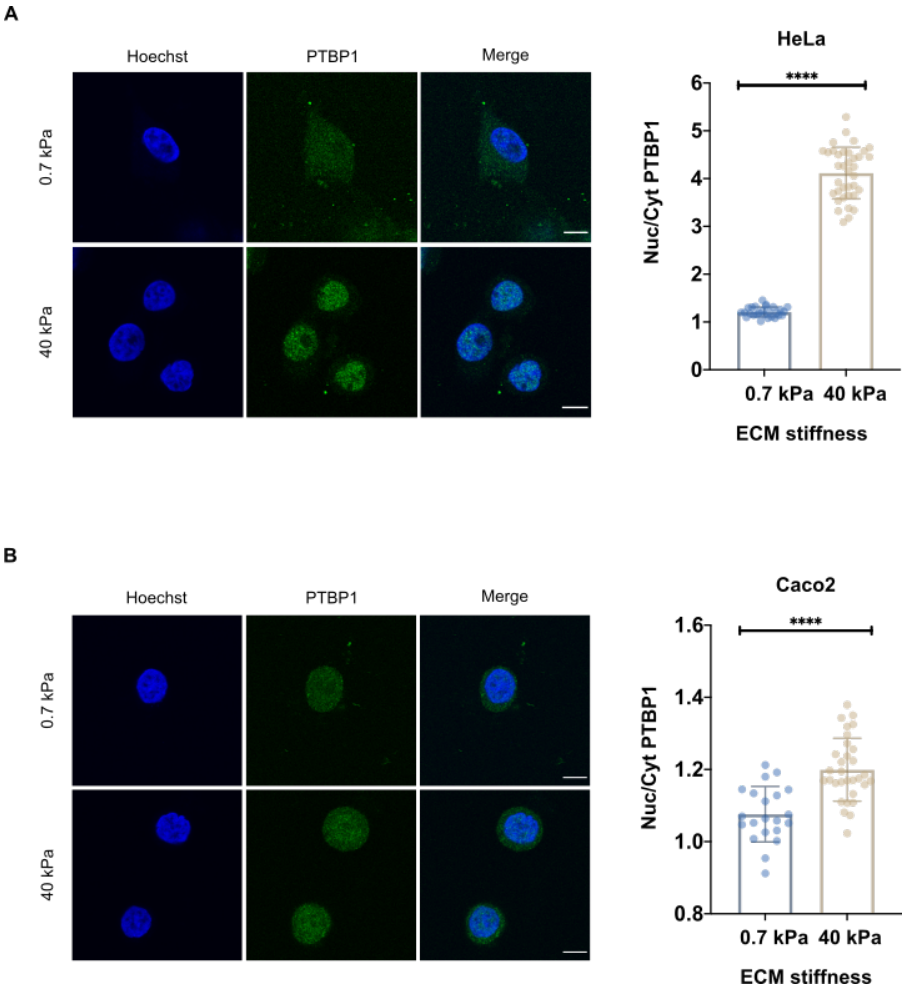

Figure 4.15 | ECM stiffness affects PTBP1 subcellular translocation in HeLa (A) and Caco2 (B).

Left: 2.5 x 10^5 of cells were plated on PAA gel for 24 hours before immunofluorescence staining with PTBP1 antibody. The immunofluorescence images show the subcellular distribution of PTBP1 based on ECM rigidity. Scale bars, 10μm.
Right: Graphs provide quantification of Nuc/Cyt ratio of PTBP1. Immunofluorescence intensity of PTBP1 was assessed by ImageJ. Data was analysed by unpaired Welch's t-test. The biological replicates of each cell line are: HeLa (n=1), Caco2 (n=1). Values are means ± s.d. ****P<0.0001.

We also investigated whether ECM stiffness has an effect on protein expression of PCBP1 and PTBP1. We carried out immunoblotting experiments in MCF10A grown on soft or stiff PAA gel. After 24 hours of cell culture, cell lysate was collected and subjected to protein extraction procedure. We checked the overall protein expression level of endogenous PCBP1 or PTBP1 affected by different ECM stiffness. We found a slight increase in PCBP1 and PTBP1 expression with fold change of 1.1 and 1.3 respectively. Our data implied that ECM stiffness has a marginal effect on endogenous PCBP1 and PTBP1 protein expression level (Figure 4.16).

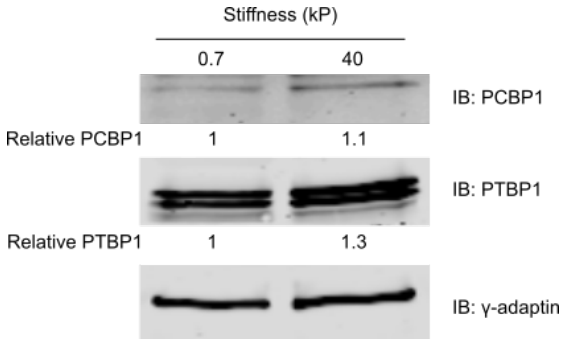

Figure 4.16 | The influence of ECM stiffness on PCBP1 and PTBP1 proteins expression

Immunoblotting of indicated proteins showed the change of endogenous protein level by ECM stiffness. The protein amounts were normalized to loading control γ-adaptin. For comparing the change of each protein by ECM stiffness, the relative levels of expression on stiff gel were normalized to the protein on soft gel.

4.1.6 PCBP2, a homologous protein of PCBP1, is not affected by ECM stiffness-mediated mechanical cues

PCBP1 is a retrotransposed derivative of PCBP2 and these two proteins have been shown to be highly homologous to each other in terms of nucleotide sequence [127]. Consequently, we investigated a possible regulation of PCBP2 by ECM stiffness-mediated mechanical. We performed the same experiments described in 4.1.5 on soft and stiff gel and analysed the corresponding subcellular localization of PCBP2. The immunofluorescence staining of PCBP2 showed that this protein was more distributed in the nucleus than PCBP1 irrespectively of PAA gel stiffness (Figure 4.17). Furthermore, the quantification showed no difference in the nucleus/cytoplasm ratio of PCBP2 between soft and stiff PAA stiffness (Figure 4.17). Our data implicated that despite highly homologous to PCBP1, subcellular localisation of PCBP2 was not affected by ECM rigidity.

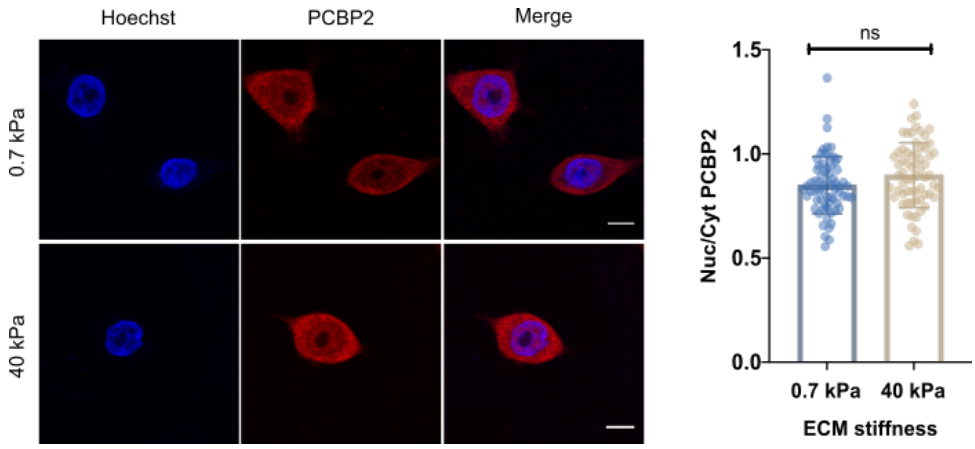

Figure 4.17 | ECM stiffness is not correlated with PCBP2 intracellular distribution

Left: 2.5 x 10^5 MCF10A were plated on soft and stiff PAA gel for 24 hours and PCBP2 subcellular localization was analysed by immunofluorescence staining. Immunofluorescence intensity of PCBP2 was assessed by ImageJ. Scale bars, 10 μm. Right: Graphs provide quantification of Nuc/Cyt ratio of PCBP2. Data was analysed by unpaired Welch's t-test (n=3). Values are means ± s.d. ns, not significant.

4.1.7 Cytoskeletal tension is involved in PCBP1 but not PTBP1 nuclear retention

It is recognized that cells rely on adjusting the tension and organization of cytoskeletal stress fibres to adapt to the rigidity of ECM and cell adhesive area. Cytoskeletal stress fibres have been shown to play a critical role in conveying mechanical signals and involve the regulation of YAP downstream of cell area and ECM stiffness [3, 11]. Since our data visualized the relocalization of PCBP1 and PTBP1 by cell density and ECM stiffness, we sought to determine whether the mechanical signals regulate PCBP1 and PTBP1 expression pattern through cytoskeletal stress fibres. In this experiment, we treated low density cultured NIH3T3 fibroblast with various inhibitors to disrupt microfilament organization and first evaluated YAP subcellular localization as a way to monitor cell's response to the changes of cytoskeleton organization. Cells treated with DMSO were used as negative control, in which YAP was mostly located in the nucleus (Figure 4.18). By contrast, YAP localisation was significantly changed towards the cytoplasm in the presence of inhibitors which disrupt cytoskeleton integrity: Lat A (F-actin), ML-7 (myosin light chain kinase) and Y27632 (Rho kinase) (Figure 4.18), confirming cell's reaction to mechanical cues transmitted through cytoskeleton stress fibres.

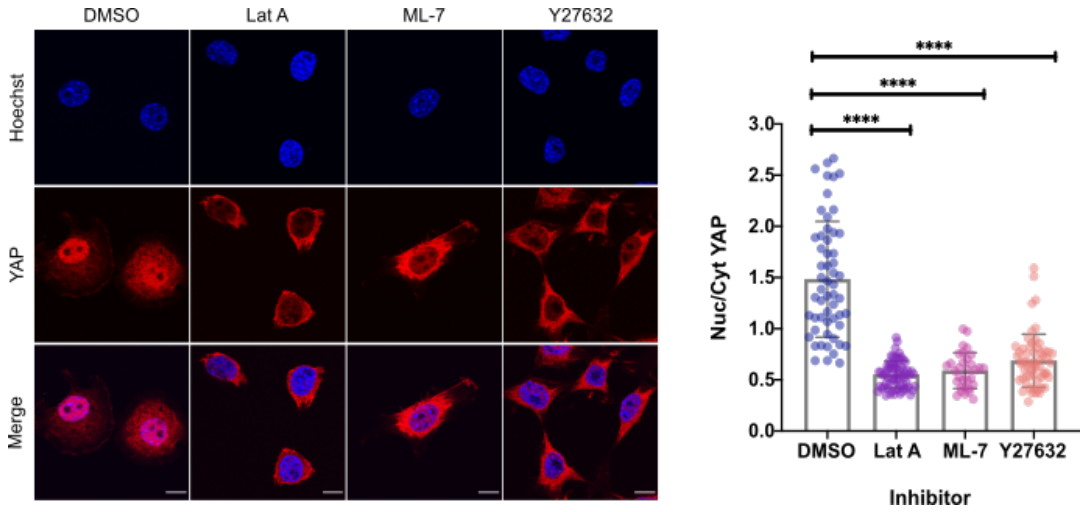

Figure 4.18 | Influence of cytoskeletal tension on YAP subcellular translocation in NIH3T3

On the top: images show the presence of cytoskeletal stress fibre promoted YAP nuclear localization. Cells were treated with 0.1 μM of Lat A, 25 μM of ML-7 and 25 μM of Y27632 for 30 minutes before immunofluorescence staining. Scale bars, 10 μm. Below: Graph summarizing the influence of various inhibitors or vehicle (DMSO) on the ratio of Nuc/Cyt YAP. Immunofluorescence intensity of YAP was assessed by ImageJ. Data was analysed by ordinary one-way ANOVA followed by Tukey's multiple comparisons test. (n=3). Values are means ± s.d. ****P<0.0001.

We then examined the effect of cytoskeletal stress fibres on PCBP1 localization in NIH3T3 by performing the same experiments. With the intact microfilament organization in controlled cells, PCBP1 was distributed in both the nucleus and cytoplasm (Figure 4.19). By contrast, when the cytoskeleton stress fibre was disrupted by various stress fibre inhibitors, PCBP1 was significantly reduced in the nucleus and accumulated in cytoplasm (Figure 4.19). However, the influence of cytoskeletal filaments was not observed for PTBP1. Cells exhibited nuclear PTBP1 irrespectively of the status of cytoskeletal stress fibre organization (Figure 4.20). Taken together, our data suggest that cytoskeletal tension is implicated in regulating PCBP1 but not PTBP1 subcellular localization.

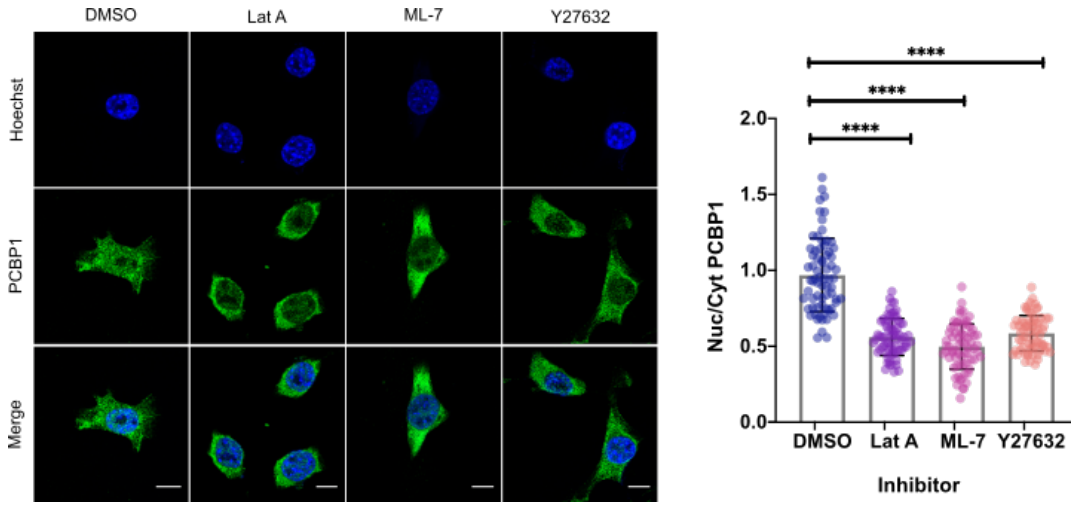

Figure 4.19 | Influence of cytoskeletal tension on PCBP1 subcellular translocation in NIH3T3

On the top: images show the presence of cytoskeletal stress fibre was essential for PCBP1 retained in the nuclear. Cells of low density were treated with 0.1 μM of Lat A, 25 μM of ML-7 and 25 μM of Y27632 for 30 minutes before immunofluorescence staining. Scale bars, 10 μm. Below: Graph summarizing the influence of various inhibitors or vehicle (DMSO) on the ratio of Nuc/Cyt PCBP1. Immunofluorescence intensity of PCBP1 was assessed by ImageJ. Data was analysed by ordinary one-way ANOVA followed by Tukey's multiple comparisons test. (n=3). Values are means ± s.d. ****P<0.0001.

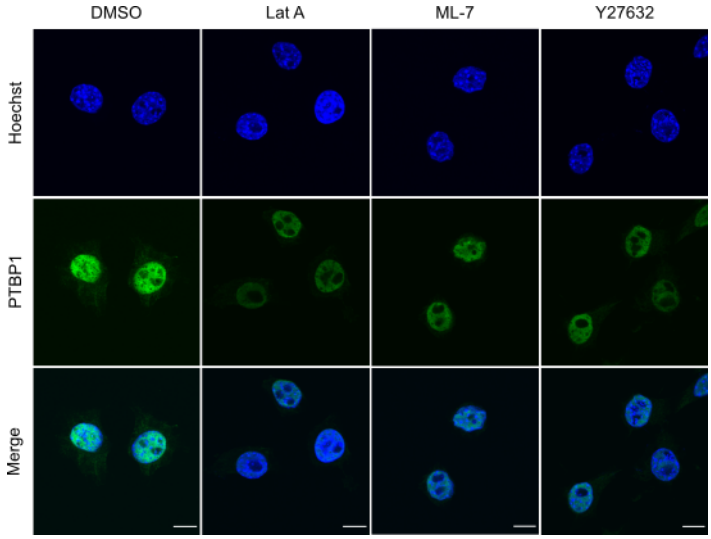

Figure 4.20 | Cytoskeleton stress tension is not related to PTBP1 subcellular localization in NIH3T3

Cells of low density were treated with 0.1 μM of Lat A, 25 μM of ML-7 and 25 μM of Y27632 for 30 minutes to disrupt cytoskeleton. Immunofluorescence images showed the nuclear retention of PTBP1 in the presence of all the drug tested. DMSO is as negative control. Scale bars, 10μm.

4.1.8 PCBP1 nuclear localization is regulated by circumferential actin belt

Given that mechanical tension exerted from adherens junctions in epithelial cells have been shown to suppress YAP/TAZ nuclear distribution through cortical actin-myosin network [106], we also tested whether PCBP1 phenotype is controlled by the epithelia-specific cytoskeletal stress fibre such as circumferential actin belt. For this part we cultured epithelial MCF10A at high density and treated the cells with blebbistatin, an inhibitor of myosin II that disrupts cortical actin-myosin tension, before immunofluorescence staining PCBP1. In this experiment, YAP was also tested as positive control. Our data showed that both YAP and PCBP1 were predominantly located in cytoplasm in control cells (Figure 4.21 A), which was consistent with our previous result that nuclear PCBP1 was suppressed in high density-cultured epithelial cells. However, the presence of blebbistatin promoted YAP and PCBP1 translocated from cytoplasm to the nucleus (Figure 4.21 A). Similar result was also found in another epithelial cell line MDCK II, where the subcellular localization PCBP1 was regulated blebbistatin (Figure 4.21 B). These findings supported our suggestion that PCBP1 is regulated by mechanical cues via cytoskeletal stress fibre.

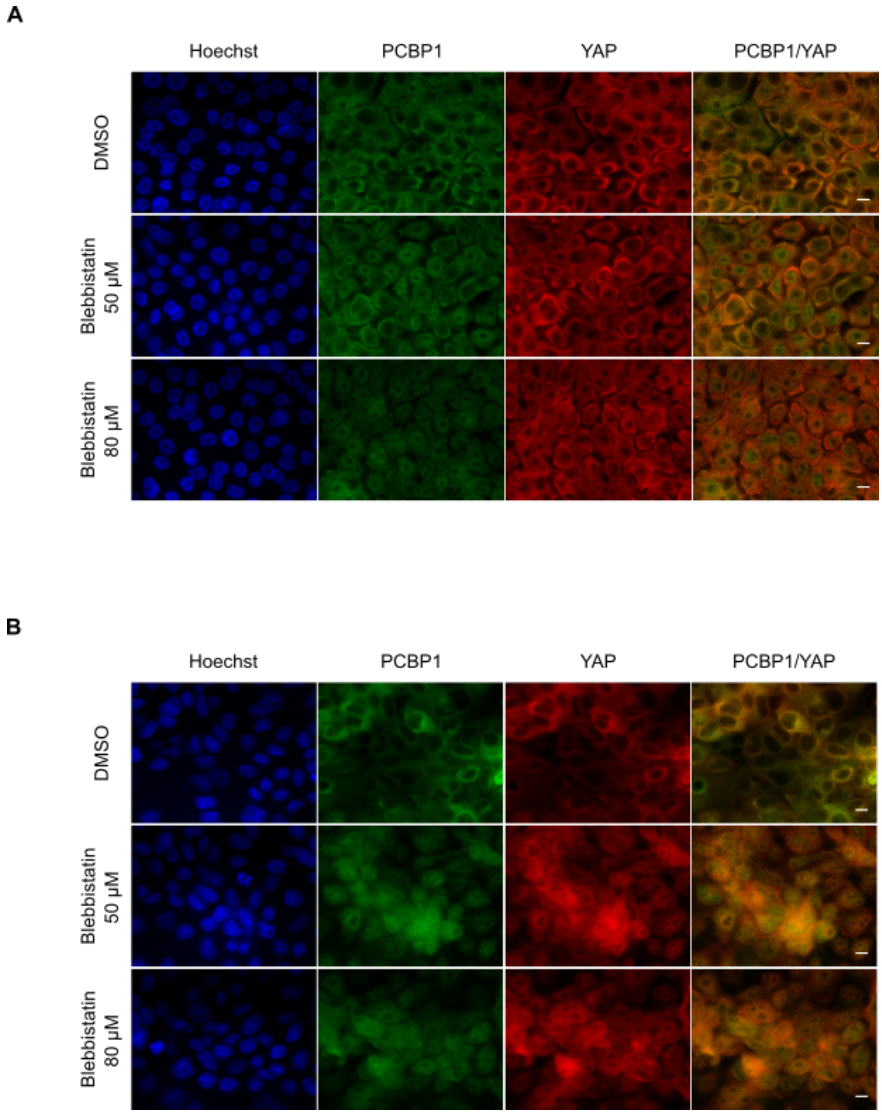

Figure 4.21 | Influence of circumferential actin belt on PCBP1 subcellular localization

Immunofluorescence images show that PCBP1 and YAP subcellular localization is affected by circumferential actin belt in MCF10A (A) and MDCK II (B). Cells of high density (7 x 10^5/well) were treated with blebbistatin of indicated concentration for 6 hours to disrupt circumferential actin belt. DMSO represents the negative control in this immunofluorescence analysis.

4.2 Alternative splicing regulated by ECM stiffness

4.2.1 ECM stiffness regulates alternative splicing of multiple transcripts

PCBP1 and PTBP1 are well known in their role of the regulation of RNA metabolism, including alternative splicing (AS) events in multiple mRNA transcripts [121, 122]. PCBP1 and PTBP1 have been shown to modulate AS of multiple genes involve in cellular process such as proliferation, motility and tumorigenesis [109, 130, 131]. Based on our finding that ECM stiffness promoted nuclear accumulation of PCBP1 and PTBP1, we hypothesized that the ECM stiffness involves regulation of alternative splicing through PCBP1 and PTBP1.

To answer the question, we explored whether mechanical signals derived from ECM stiffness regulate AS through PCBP1 and PTBP1. In order to examine AS events dependent on ECM stiffness, we first tried a preliminary test by culturing MCF10A on soft (1 kPa) and stiff (40 kPa) PAA gel for 72 hours before performing RNA extraction and the subsequent cDNA synthesis. We then checked the changes of cassette exons of multiple known transcript targets of PCBP1 or PTBP1 by RT-PCR with the corresponding primers which were designed according to previous studies [108-111]. The primers used in our work were listed in Table 2.11 and the cassette exons tested in each gene were listed in Table 4.1 and Table 4.2. Among these gene screened for AS events, we found that ECM stiffness promotes either inclusion or exclusion of several cassette exons. Expression of cassette exon was enhanced in AP1G2, CTTN, NUMB and ARHGAP4 yet reduced in FAS, PPP5C, MRPL33 and EIF4G2 (Figure 4.22 A-B). These genes vary in functions including protein sorting (AP1G2), stress fibre organization (ARHGAP4, CTTN), proliferation (NUMB, PPP5C, MPRL33, EIF4G2) and cell survival (FAS, MPRL33). The preliminary test suggested a correlation between ECM stiffness and alternative splicing.

Table 4.1 | List of RNA targets of PCBP1-regulated alternative splicing

The selection of RNA targets was based on previous study [108]. Exon ID: the cassette exon of each gene that is included or skipped by PCBP1-mediated alternative splicing. In Up/down column, '+' represents the inclusion level of cassette exon is enhanced by PCBP1 [108].

Gene symbol	Exon ID	Up/down
AP1G2	3	+
ARHGAP4	9	+
CTTN	11	+
WNK4	2	+
TRPT1	7	+
hCDK2	5	+

Table 4.2 | List of RNA targets of PTBP1-regulated alternative splicing

The selection of RNA targets was based on previous study [109-111] Exon ID: the cassette exon of each gene that is included or skipped by PTBP1-mediated alternative splicing. In Up/down column, '+' and '-' represents the inclusion level of cassette exon is enhanced or reduced by PTBP1 [109-111].

Gene symbol	Exon ID	Up/down
TPM1	6	–
FAS	6	–
NUMB	9	+
HITRA2	7	+
EIF4G2	9	–
CTTN	11	+
PPP5C	5	+
FAM38A	8	–
MPRL33	3	–
EZH2	17	+
MRPIP	9	+
PIP5K1A	12	–

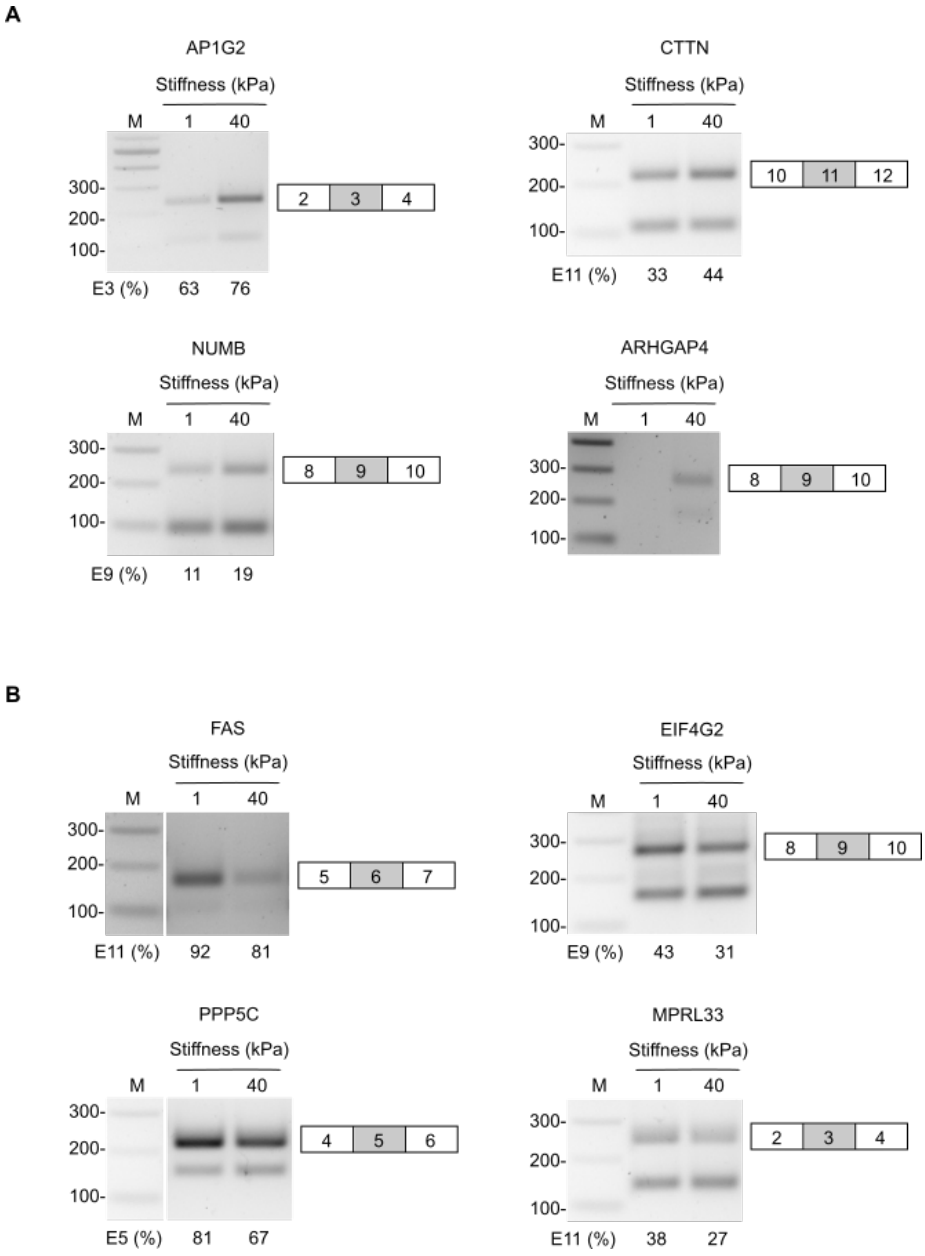

Figure 4.22 | Correlation between ECM stiffness and alternative splicing in MCF10A

RT-PCR analysis of indicated genes showed the promotion (A) and reduction (B) of cassette exons by stiff PAA gel. 1 kPa represents the soft gel while 40 kPa indicates the stiff gel. The splicing efficiency was calculated as the inclusion level (%) of the cassette exon in all splicing variants.

In order to define whether these gene candidates displayed ECM stiffness dependent AS, we repeated the experiments to see if the influence of ECM rigidity on expression of these cassette exons can be reproduced. We therefore cultured MCF10A on soft (0.7 kPa) and stiff (40 kPa) PAA gel for 72 hours and then performed RT-PCR of selected genes. There were at least three genes (NUMB, CTTN and AP1G2) whose AS patterns were consistent with what we

observed in the first trial (Figure 4.23 A). In such case we compared the inclusion level of cassette exons of each gene regulated by soft and stiff PAA gel. The quantification indicated that stiff gel promoted production of AP1G2 exon 3 by 1.89-fold, NUMB exon 9 by 2.6-fold and CTTN exon 11 by 1.56-fold when compared to those in cells cultured on soft gel (Figure 4.23 B). The change of cassette exon of various transcript between soft and stiff environment confirmed our hypothesis that ECM rigidity contributes to the regulation of alternative splicing.

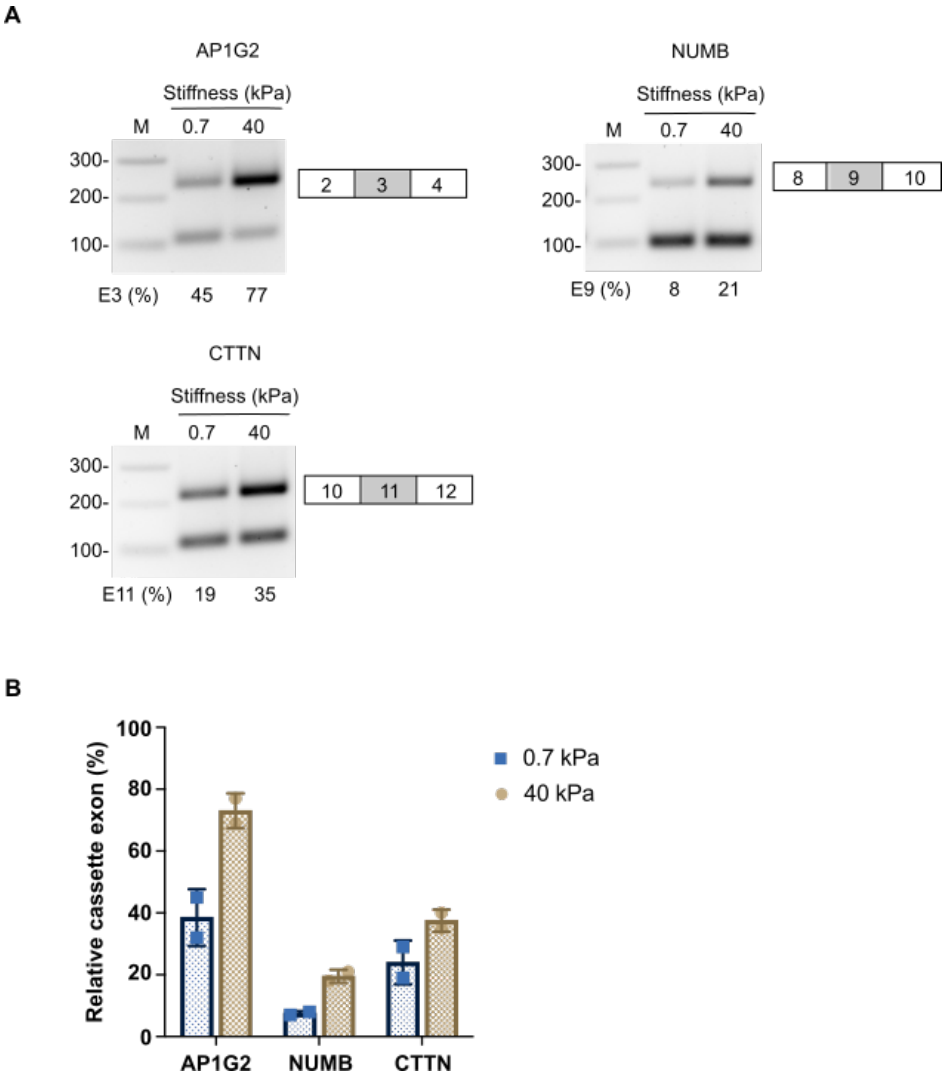

Figure 4.23 | ECM stiffness displays various effect on alternative splicing in MCF10A

(A) RT-PCR analysis showed the influence of rigid PAA gel on promotion of alternative splicing of indicated exons of AP1G2, NUMB and CTTN in MCF10A. The cassette exon inclusion was defined as the ratio of included exon isoform over the total level of included and excluded isoforms.

(B) Graph summarized the alternative splicing efficiency by ECM stiffness on genes indicated in (A) (n=2). Values are means ± s.d.

In light of our previous results indicated that cancerous epithelial cell lines HeLa and Caco2 also showed nuclear enrichment of PCBP1 and PTBP1 on stiff PAA gel, we also evaluated the AS events in these two cell lines. We cultured HeLa and Caco2 on soft (0.7 kPa) or stiff (40 kPa) gel respectively and tested several PCBP1 and PTBP1 transcript targets including NUMB, CTTN, AP1G2 and ARHGAP4 by RT-PCR. We found that the AS events of these transcripts by ECM stiffness in HeLa and Caco2 were quite different from those in MCF10A. No obvious change of

cassette exons of NUMB, CTTN and AP1G2 were observed in both HeLa and Caco2 regardless the gel rigidity (Figure 4.24 A). Another transcript ARHGAP4 whose isoform products can only be detected in MCF10A placed on stiff PAA gel, however, showed a stiffness-dependent shift of cassette exon 9 inclusion in HeLa (Figure 4.24 B). Taken together, the results suggested that ECM stiffness-mediated AS events were cell type-dependent.

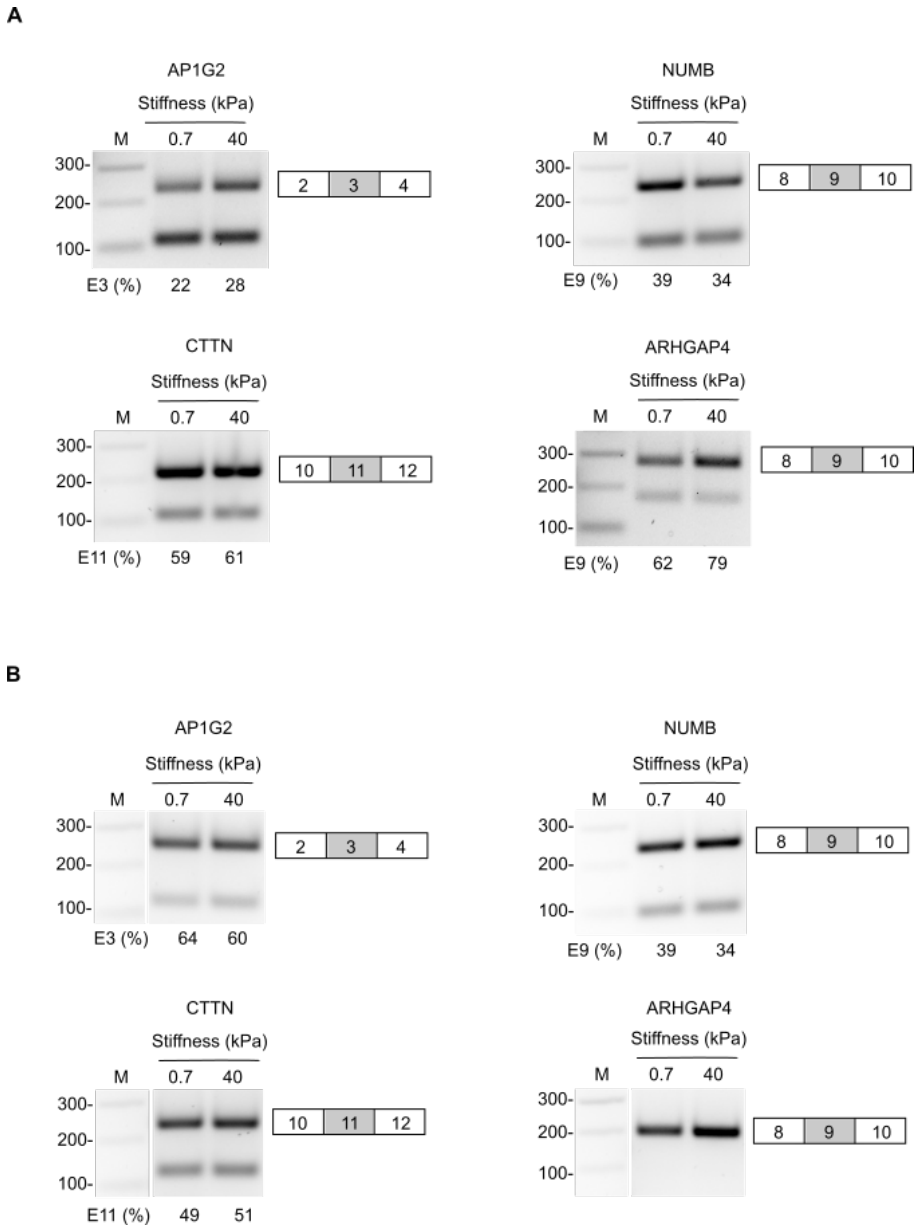

Figure 4.24 | Correlation between ECM stiffness and alternative splicing in HeLa and Caco2

Alternative splicing events of AP1G2, NUMB, CTTN and ARHGAP4 in HeLa (A) Caco2 (B) by ECM stiffness.

4.2.2 ECM stiffness regulates alternative splicing of NUMB exon 9 through PTBP1 activity

To clarify whether the cassette exon splicing of these three genes (NUMB, CTTN and AP1G2) are PCBP1 or PTBP1 dependent, we also tested their AS events with cDNA templates synthesized from RNA isolated from PCBP1 or PTBP1-depleted MCF10A. We performed siRNA-based approach to knock down PTBP1 in MCF10A grown in plastic culture dishes. The PCR data showed that PCBP1 knockdown reduced the inclusion of AP1G2 exon 3 by 1.3-fold, while depletion of PTBP1 suppressed NUMB exon 9 splicing by 1.9-fold (Figure 4.25 A), which is consistent with previous studies [108, 111]. Among the three genes, CTTN has been reported to be the RNA target of both PCBP1 and PTBP1 [108, 110]. Here we showed that knockdown of PCBP1 and PTBP1 resulted in CTTN exon 11 reduction by 1.22-fold and 1.16-fold respectively in comparison with control siRNA (Figure 4.25 A). Our results implied the possible involvement of PCBP1 or PTBP1 in the regulation of alternative splicing in AP1G2, NUMB and CTTN transcripts in MCF10A via ECM stiffness.

Given that the fold change of cassette exon in NUMB enhanced by stiff (40 kPa) PAA gel was highest among these three genes (NUMB, CTTN and AP1G2) tested in our study (Figure 4.23) we then focus on investigating the mechanism of ECM stiffness on alternative splicing of NUMB exon 9. It has been shown that splicing of NUMB exon 9 is regulated by several splicing factors including PTBP1 [132]. In addition, our knockdown experiments showed that NUMB is the target transcript of PTBP1 (Figure 4.25 A). We therefore attempted to understand whether PTBP1 associates with ECM stiffness-mediated alternative splicing of NUMB exon9. We cultured MCF10A on stiff (40 kPa) PAA gel and induced siRNA-based knockdown of PTBP1 before examining NUMB exon 9 expression profile. RT-PCR data indicated that the inclusion level of NUMB exon 9 was suppressed by PTBP1 siRNA, showing a 1.96-fold decrease of exon 9 when compared to the amplicons in parallel negative control siRNA-transfected cells (Figure 4.25 B). The shift of NUMB splice variants between PTBP1-KD and control cells implicated that ECM rigidity regulated NUMB exon 9 splicing through PTBP1-mediated alternative splicing activity.

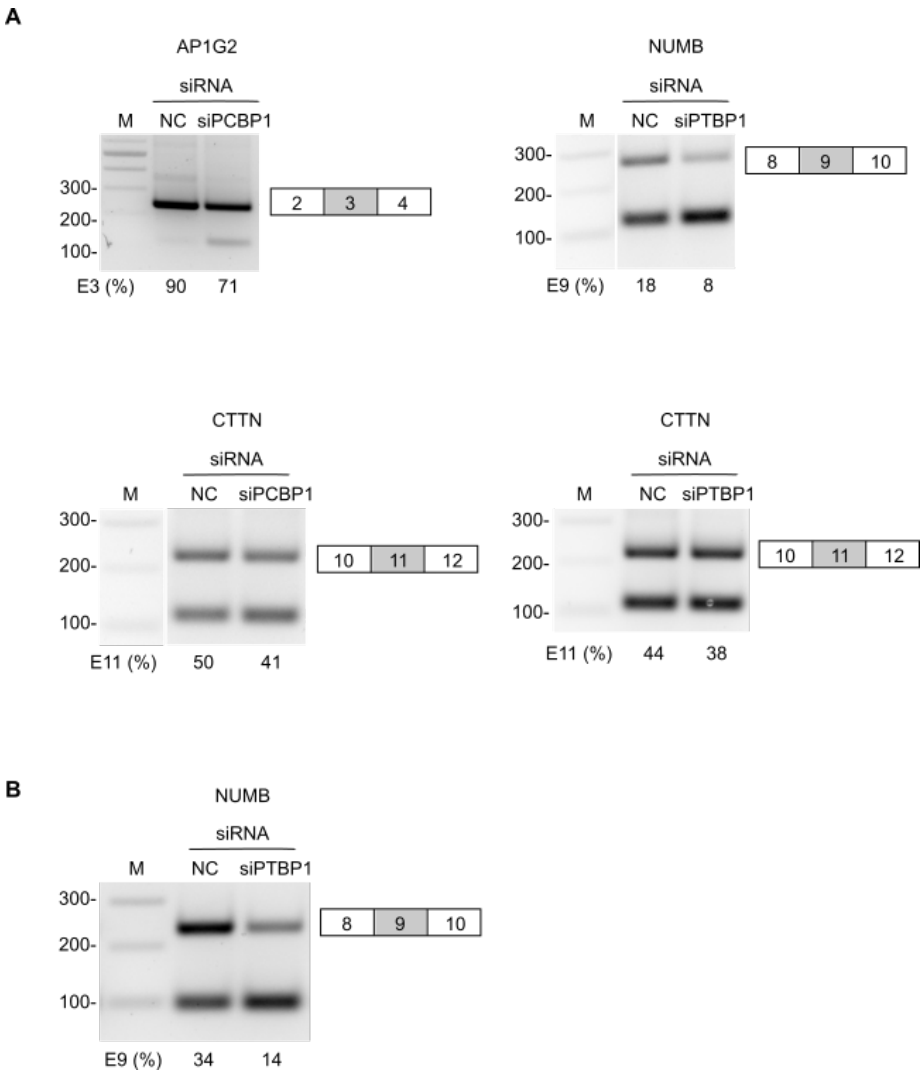

Figure 4.25 | PCBP1 and PTBP1 involve in the regulation of alternative splicing of several genes

(A) PCBP1 or PTBP1 knockdown reduced cassette exon splicing of AP1G2 and NUMB in MCF10A respectively. Both PCBP1 and PTBP1 involved in the regulation of CTTN exon 11 splicing. The splicing change was calculated as the relative level (%) of included cassette exon over the sum of total isoform variants.

(B) PTBP1 knockdown suppressed the inclusion of NUMB exon 9 in MCF10A plated on 40 kPa PAA gel. The cassette exon inclusion was determined as (A).

4.3 Regulation of NUMB isoforms by ECM stiffness-related mechanical signals

As our data showed that ECM rigidity regulated alternative splicing of NUMB exon 9 through PTBP1 activity, we next asked whether this change in NUMB transcript variants also reflected in their translational level. NUMB protein has been reported to consist of four isoforms which were produced by alternative splicing [132] (Figure 4.26 A). The alternative splicing of NUMB exon 9 results in two major isoforms with various length of their proline-rich region (PRR), including the exon 9 inclusion version (NUMB+E9, 72 kDa) and skipping version (NUMBΔE9, 66 kDa). In order to clarify the protein expression pattern of these two isoforms, we first knocked down PTBP1 by siRNA in MCF10A grown on petri dishes and checked NUMB expression by immunoblot. We observed two separated protein bands of similar intensity which respectively displayed predicted size of NUMB+E9 and NUMBΔE9 in negative control siRNA-transfected cells, however, the top band was significantly reduced in PTBP1-depleted cells (Figure 4.26 B). Considering that our RT-PCR data indicated the relationship between PTBP1 depletion and suppression of NUMB exon 9 splicing (Figure 4.25), the reduced top band by PTBP1 knockdown in our immunoblot was assumed the NUMB+E9 isoform while the lower band was referred to as NUMB+E9 isoform.

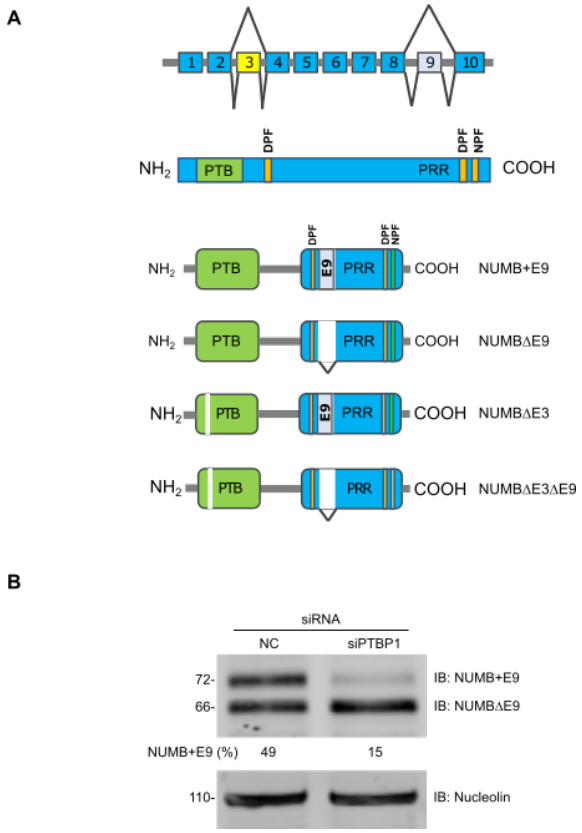

Figure 4.26 | Clarification of protein expression profile of NUMB isoform

(A) Schematic representation of NUMB isoforms produced from alternative splicing of exon 9 or exon 3.

(B) PTBP1 knockdown caused significantly reduction of NUMB+E9 isoform in MCF10A. The protein level was firstly normalized to loading control nucleolin. The relative amount of NUMB+E9 isoform of each sample was determined by calculating the ratio of NUMB+E9 variant over the sum of all isoforms expressed in each sample.

We then examined the impact of ECM stiffness on protein expression of these two NUMB isoforms. We cultured MCF10A onto PAA gel of soft and rigid stiffness (0.7 and 40 kPa) for 72 hours then collected protein sample for further analysis. To our surprise, no change in NUMB+E9 or NUMB+E9 isoform level was detected in cells irrespectively of ECM stiffness despite our previous PCR data suggested the increased exon 9 inclusion by stiff gel. Quantification showed that relative amount of NUMB+E9 isoform on both parameters of PAA gel stiffness used in our experiment was similar to each other. Moreover, cells cultured on soft gel also displayed NUMB+E9 isoform with similar protein level as that appeared in stiff gel (Figure 4.27 A), which was not consistent with our PCR result where soft gel caused only half expression of exon 9-containing isoform than stiff gel (Figure 4.23). Given this result, we

decided to preculture MCF10A on soft (0.2 kPa) PDMS substrate for 48 hours before transferring cells onto 0.7 and 40 kPa PAA gel respectively for another 72-hour culture and examined NUMB isoform expression. This strategy was taken in an attempt to offset the potential mechanical effect of hard dish on cell mechanosensing, based on the evidence that MCF10A possesses mechanical memory [133]. The immunoblot showed an overall reduction of both NUMB isoforms by soft gel in comparison with those by stiff gel (Figure 4.27 B). Nonetheless, densitometry analysis showed that the ratio of PRR^{L} and PRR^{S} isoforms appeared in cells grown on soft gel culture is still the same as those on stiff gel (Figure 4.27 B). Overall, our data suggested that ECM stiffness regulate NUMB isoforms at RNA level rather than protein expression level.

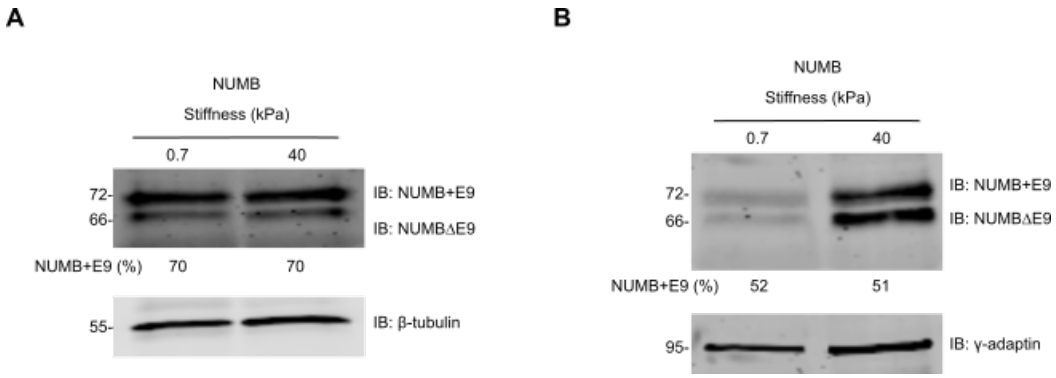

Figure 4.27 | Influence of ECM stiffness on NUMB protein expression

(A) Immunoblotting showed the expression of two major NUMB isoform in MCF10A plated on soft or stiff PAA gel. The protein intensity was normalized to loading control β-tubulin. The relative amount of NUMB+E9 isoform of each sample was determined by calculating the ratio of each variant over the sum of all isoforms.

(B) Immunoblotting showed the expression of two major NUMB isoform in MCF10A firstly plated on 0.2 kPa PDMS for 48 hours before being transferred to 0.7 and 40 kPa PAA gel. The protein intensity was normalized to loading control γ-adaptin. The relative amount of NUMB+E9 isoform of each sample was determined by calculating the ratio of each variant over the sum of all isoforms expressed in each sample.

4.4 Summary

Based on our screen results from chapter 3, we hypothesized two hnRNP proteins, PCBP1 and PTBP1, are potential candidates involved in mechanotransduction. In this chapter, we performed a series of experiments to investigate the influence of mechanical cues on the

subcellular localisation and function of PCBP1 and PTBP1. We demonstrated that the subcellular localization of PCBP1 and PTBP1 can be regulated by cell density and ECM stiffness. When cells were plated at high density or cultured on soft PAA gel, PCBP1 and PTBP1 were mainly located in the cytoplasm or distributed in both nucleus and cytoplasm. On the contrary, PCBP1 and PTBP1 were significantly enriched in the nucleus when cells were grown at low density or on stiff PAA gel (Figure 4.4, 4.5, 4.7, 4.13). In addition, PCBP1 nuclear accumulation was also affected by cytoskeleton integrity and ROCK activity. The disruption of actin stress fibre or inhibition of myosin II and ROCK by various inhibitors caused PCBP1 translocation from the nucleus to cytoplasm in NIH3T3 fibroblast (Figure 4.19). PCBP1 was also regulated at high cell density by the circumferential actin belt underlying adherens junction (Figure 4.21). We demonstrated that PCBP1 subcellular localization changed from cytoplasm to the nucleus when the actomyosin network was disrupted by blebbistatin in high density-cultures of MCF10A or MDCK II. We also examined the cellular function of PCBP1 and PTBP1 in alternative splicing under the influence of ECM stiffness. We found that rigid ECM promoted the inclusion of cassette exons of several PCBP1 and PTBP1 target transcripts, including NUMB (Figure 4.23). The knockdown experiments showed that ECM stiffness-dependent alternative splicing of NUMB exon9 was mediated by PTBP1 (Figure 4.25). Our results in this chapter suggest that PCBP1 and PTBP1 are potential mechanoregulators controlled by ECM stiffness.

5. Chapter 5 – Discussion and future perspectives

5.1 Establishment of our screen approach: the first step of identifying novel mechanotransducers

5.1.1 Rationale to use activation of RhoA in our screen

In order to detect potential mechanotransducers with nuclear functions, an efficient mechanical force-generating system is imperative to identify proteins, which show force-dependent subcellular localisation. Examples of force generating approaches include stretching of cells using integrated strain arrays, which caused relocalization of YAP and β-catenin to the nucleus which triggered cell cycle entry [101], or using atomic force microscope (AFM) cantilever to directly apply physical force to the nucleus which clarified the relationship between nuclear pore and molecular mechanical stability of YAP [129]. These experiments established valuable knowledge in terms of mechanosensing mechanisms and the correlation between mechanical force and cell behaviour. However, considering the aim of our project, which is to identify potential mechanotransducers that possess nuclear functions, via a mass spectrometry approach, the direct application of external physical force to cells was not practical [103, 129].

In this project, we utilized activation of RhoA as the basis of our screen for two reasons. Firstly, RhoA can be activated by mechanical cues such as ECM stiffness and cell tension at adherens junction. RhoA activation then subsequently induces actomyosin contractility through ROCK signalling or promotes actin polymerization through mDia, which contribute to the propagation of mechanical signals within the cells [134, 135] (also see Figure 1.10). Secondly, RhoA-dependent cytoskeleton remodelling in response to mechanical cues have been associated with multiple cell behaviour such as cell proliferation, migration and remodelling of ECM architecture [118, 134, 136, 137]. These important cellular processes also involve the participation of other mechanotransducers, e.g., YAP, which nuclear localization and function is regulated by RhoA [11]. Indeed, the manipulation of cellular forces through RhoA activity was also outlined in an elegant study by Valon and collegue, which utilized optogenetic tool to control the activation of RhoA by recruting it to the plasma membrane or mitochondiral membrane where the RhoA activator ARHGEF11 was immobolized [117]. They showed that RhoA is activated at the plasma membrane, inducing traction forces, stress fibres formation and

nuclear YAP. Their study provides another example of application of RhoA to control the production of cellular forces. Thus, our RhoA activity-dependent screen approach together with using the established mechanotransducer YAP as a positive control enabled us to detect potential candidates for mechanotransduction in the following experiments.

5.1.2 Control of RhoA expression using the Flp-In™ T-REX HEK293 system

RhoA exists in two different forms: active and inactive, which is regulated by its GTP or GDP-bound state [72] (also see Figure 1.9). The ability of RhoA to modulate cellular forces is dependent on its active state. Valon et al. showed that RhoA only causes cellular traction and nuclear YAP when it was activated at plasma memrbrane [117]. Therefore, a precise control of RhoA activity is critical. In our study, we adopted a genetic strategy to induce RhoA activity in cells. We utilized Flp-In™ T-REX™ HEK293 system to establish a stable cell line which expresses constitutively active RhoA (CA-RhoA) as a way to induce actomyosin contractility. With a tetracycline inducible promoter upstream of the CA-RhoA gene, the expression of CA-RhoA can be induced and precisely controlled by tetracycline in a time- and dose-dependent manner.

Although standard methods such as transient transfection of target genes can quickly produce large amount of protein, this also brings a downside such as highly variable protein expression levels throughout the population of cells and between each batch of experiments, which would negatively affect the accuracy and efficiency of our follow-up mass spectrometry analysis. The use of Flp-In™ T-REX™ HEK293 system, by contrast, gave us the advantage to create a stable clone being able to express CA-RhoA stably in an inducible and isogenic fashion. This strategy drastically reduces the possible variation of CA-RhoA expression levels caused by random integration of this gene into chromosomes of the host cells. Besides, there is no need to repeat transient transfection of CA-RhoA plasmid, which is not only highly variable but also expensive and inefficient for us to expand our experimental scale. The application of Flp-In™ T-REX™ system for the expression of specific genes of interest is also demonstrated in another study. Ward et al. showed that generation of a stable cell line using the Flp-In™ T-REX™ system allowed them to control expression of G protein-coupled receptors (GPCRs) by tetracycline/doxycycline treatment [119].

Importantly, in our pilot experiments we also examined the effect of various doses and time intervals of tetracycline treatment on RhoA expression and YAP nuclear translocation. As

described above, RhoA-mediated cellular contractility and cytoskeleton remodelling can promote YAP nuclear localization. Considering the function of YAP as co-transcriptional factor that regulates expression of genes involves in cell survival and proliferation [86], the accumulation of YAP in the nucleus by active RhoA can also trigger expression of its target genes that may change the subcellular localization of other force-independent proteins. Such background noise by YAP activity may reduce the accuracy of our screen approach. Therefore, in order to reduce the possible interruption by gene targets of YAP, we determined the minimal time interval and dose of tetracycline treatment in our screen approach.

5.1.3 Proximity biotinylation system offers an efficient isolation of nuclear proteins

For collecting nuclear proteins for proteomics analysis, we first tried standard methods such as utilizing various lysis buffers and a series of sonication and centrifugation in an attempt to isolate nuclear and cytoplasmic proteins. Though our data showed well separated nuclear and cytoplasmic fractions which was evidenced by detection of specific markers Lamin A/C and β-tubulin respectively, YAP nuclear distribution under different cell density conditions did not follow the proof of principle as cells displayed much fewer nuclear YAP than cytoplasmic YAP regardless of cell density (data not shown). Such results could be due to the disruption of cell-cell adhesion mediated mechanical cues by extensively mechanical handling of cells during the subcellular fraction procedure, which is supported by a previous study suggesting that YAP is constantly shuttling between the nucleus and cytoplasm independent of cell tension state, but the presence of tense cytoskeleton stress fibre promotes YAP nuclear retention [11]. Another evidence showed relevance between YAP subcellular translocation and direct application of physical force onto the nucleus [129], indicating the disruption of intracellular mechanical signals may change the nuclear proteome.

The fast dynamics of YAP regulation by mechanical forces means that we had to adopt a strategy other than the standard methods for subcellular fraction. The solution to the issue was the generation of a stable cell line being able to biotinylate specifically nuclear proteins for further purification. Our purpose was to analyse changes to the nuclear proteome, and our approach allowed only nuclear proteins to be labelled, which is critical to avoid false results arising from cross contamination with cytoplasmic proteins. In our work, we used HEK293-tet-RhoA as host cell line to generate a second cell line by stable transfection with a

recombinant plasmid containing nuclear localization sequence-harboured TurboID (NLS-TurboID) biotin ligase. This method is based on a previous study which developed TurboID and verified their role in labelling proteins with biotin [112]. TurboID is a mutated version of the well-used engineered biotin ligase BirA, which possesses more efficient capability to covalently attach biotin to proteins in close proximity. In addition, the NLS contained the TurboID in the nucleus allowing the biotinylation of only nuclear proteins. We confirmed that HEK293-tet-RhoA-TurboID cells can be used to isolate nuclear proteins and we validated in particular that YAP, our positive control, was indeed enriched in the nucleus in tetracycline treated cells compared to mock treated cells using a biochemical approach of streptavidin pulldown followed by western-blotting. Thus, given the scalability of our approach, this also confirmed that we were able to collect sufficient material for mass spectrometry.

5.2 Establishment of PAA gel for ECM stiffness experiments: the second layer for validation of potential candidates

In this PhD thesis, the mass spectrometry analysis revealed that around 102 proteins are enriched in the nucleus by tetracycline induced RhoA activity, making them possible molecular regulators in mechanotransduction. However, the major weakness of our RhoA activity-dependent screen approach is that we did not identify the physical properties directly induced by active RhoA, therefore, we lack the direct evidence that the nuclear accumulation of our protein hits is only contractile force-dependent. This concern is based on that although RhoA has been widely recognized as a regulator in mechanotransduction, RhoA is also involves in other signalling pathways. For example, RhoA/ROCK pathway has been associated with the phosphorylation and stimulation of PTEN (phosphatase and tensin homologue), a well-characterized tumour suppressor that regulates cell death and survival [138]. On the other hands, Liu et al showed that RhoA/ROCK signalling regulates nuclear translocation of ERK1/ERK2 which promotes mitogenesis of smooth muscle cells under the serotonin (5-HT) mechanism [139]. These effectors induced by RhoA/ROCK signalling could also lead to mechanical force-independent protein regulators translocate into the nucleus. As a result, a second layer of validation that provides more direct external mechanical cues is essential for investigating the role of our candidate protein hits in mechanotransduction.

Different substrate platforms such as PDMS (polydimethylsiloxane) and polyacrylamide (PAA) gel have been widely used in the study of mechanobiology. Each of the material has advantages and disadvantages. PDMS silicone elastomer is a viscoelastic material which can be easily fabricated to various stiffness by adjusting the ratio of crosslinker and polymer. PDMS is a nontoxic, optical transparent material of low costs. However, the major downside of PDMS is its hydrophobic surface that renders the material less biocompatible [140]. The other disadvantage of PDMS is its limitation to make very soft substrates. The present protocol for fabrication of PDMS can result in a polymer with a stiffness ranging from 5 kPa to 1.72 MPa [141]. Such rigidity range is not practical in our study when considering our use of mammary epithelial cell line MCF10A as a model to validate the potential protein candidates.

Given that most cells in a physiological condition are attached to a matrix with a range of tissue stiffness from very soft (e.g., neuron, ~0.1 kPa) to stiff (e.g., osteoblast, > 20 kPa) (Figure 5.1) [142], in our study we utilized polyacrylamide (PAA) gel to mimic different ECM stiffness and as a test model to validate the potential candidates due to its property can reach to a very soft substrate e.g., with stiffness of 0.5 kPa. Indeed, PAA gel is a popular material in the research of ECM stiffness-dependent cell biology owing to its multiple advantages. PAA gel is a non-biodegradable hydrogel with tuneable elastic property, which stiffness can be moulded to span a wide range that fits most tissue stiffness in a body. In addition, PAA gel are inexpensive and can be easily polymerized at lab by mixing different ratio of crosslinker (bis-acrylamide) to acrylamide [114, 128].

Figure removed because of copyright

Figure 5.1 | The mechanical property of physiological environment
The mechanical property in a physiological environment is tissue type-specific, and cells are tuned to the tissue stiffness of their matrix. Tissue stiffness is defined as elastic modulus which is measured in pascals (Pa). Mechanically compliant tissues like neuron and lung display low stiffness. By contrast, tissues such as bone and skeletal muscle that constantly experience mechanical loading display high stiffness. Stiffness of breast tissue is around 800~1000 Pa. Tumorigenesis e.g., breast cancer, is often paralleled with increased tissue and matrix stiffness. Figure reproduced from Ref. [142].

However, there are some disadvantages of PAA gel regarding its application in larger scale of experiments. Most studies involve PAA gel are about examination of protein of interest by culturing cells on PAA gel of defined stiffness and performing immunofluorescence staining of target proteins. Despite well-established protocols for cell culture on PAA gel, this method by far is predominantly limited to fabricate PAA gel on coverslips, where toxic chemicals like silanes (e.g., (3-Aminopropyl)triethoxysilane, APTES) needs to be used to functionalize the surface of glass coverslips [114]. In addition, it would be difficult to work with glass coverslips when we aim to conduct a broad range of biochemical experiments like detection of specific gene through PCR, quantification of proteins by western blot, or simply to collect large number of cells from the same culture environment. Although there are commercial products of culture dishes with matrix of various stiffness, their high cost and limited choice of materials and stiffness also hampers our study.

In our work, we adopted a method to directly fabricate PAA gel on petri dishes based on an article published in 2019 [113]. Given that it is very difficult to attach PAA gel to cell culture petri dish made of polystyrene, the usage of photosensitive adhesive resin, Loctite 3525, is a key point to adhere PAA gel to petri dish. Our results showed that with proper amounts and

thorough spreading of Loctite 3525 on the bottom of the petri dish PAA can well attach to the dish without shrinkage or distortion during gel polymerization (Figure 4.11). Our experiments confirmed that Loctite 3525 can promote the correct attachment and maintenance of PAA gel in plastic petri dishes.

Since PAA gel does not readily adsorb proteins, it is essential to coat a layer of ECM proteins onto the PAA gel for efficient cell attachment. Some protocols use the heterobifunctional crosslinker sulfo-SANPAH to covalently bind proteins to PAA gel [114, 128]. We used Acrylic acid N-hydroxysuccinimide ester (NHS-acrylate) along with a free radical photoinitiator Irgacure 2959 as crosslinker for ECM protein conjugation as previously published. With a chemical structure similar to sulfo-SANPAH, NHS-acrylate contains an amine-reactive N-hydroxysuccinimide (NHS) ester which allows NHS-acrylate efficiently to react with primary amino groups (-NH2) to form stable amide bonds in phosphate buffer at pH range 7-9. However, in our case we failed to reproduce what described in original protocol where they combined NHS-acrylate together with Irgacure 2959 and collagen in the same buffer for protein conjugation [113]. In order to improve the cell attachment efficiency, we tried to firstly activate PAA gel surface with a crosslinker solution of NHS-acrylate and Irgacure 2959 before collagen coating. Our data proved that this modified procedure of protein conjugation allowed us successfully to culture various cell lines including MCF10A, HEK293, HeLa and Caco2 on PAA gel in petri dishes for various biochemical analysis.

Given that our study aimed to investigate the role of potential mechanical regulators with ECM stiffness, the determination of PAA gel rigidity is crucial to discriminate cellular response to various mechanical forces. A previous study showed a rigidity threshold of 5 kPa for YAP nuclear enrichment [129], though the threshold is likely to be cell type specific. Importantly, it has been demonstrated that each tissue has a particular stiffness phenotype and their cellular components display unique stiffness optimum that can govern their development tendency [142]. Thus, the choice of ECM stiffness for studying mechanotransduction should take the stiffness optimum of the cells being tested into account. In our work, we chose MCF10A as a cell model to clarify the biological function of the potential protein candidates. MCF10A is an epithelial cell line originated from human mammary tissues with stiffness phenotype of around 0.8 kPa~1 kPa [142]. As a result, we fabricated PAA gel of 0.7 and 1 kPa as soft while 40 kPa as stiff substrate for testing our protein candidates.

Notably, although we did not measure the accurate rigidity of PAA gel by atomic force microscopy (AFM), these PAA gel of various stiffness used in our study was prepared based on existing protocol which guarantees excellent reproducibility in terms of mechanical stiffness control [114]. Moreover, we tested YAP nuclear retention as a positive control throughout our experiments to control the mechanoresponse to soft and stiff PAA gel. However, for more comprehensive understanding of impact of substrate rigidity on various physiological condition such as cell motility and cell growth, the fabrication of ECM substrate with accurate rigidity would be necessary to clarify the rigidity threshold that triggers critical cell behaviour.

One weakness of studying the role of the potential mechanical regulators with PAA gel in our work is that PAA gels are nearly purely elastic. However, in a physiological environment, most tissues display viscoelasticity or nonlinear elasticity [143]. Viscoelasticity has been identified in many living tissues such as brain, breast, liver, skin, embryonic tissues [144]. The biggest difference between purely elastic PAA gel and viscoelastic tissues is that viscoelastic tissues display a time-dependent mechanical response and can store and dissipate the energy from the mechanical load, while elastic material does not dissipate energy [143, 144]. Although PAA gels have been widely used to mimic the mechanical environment for the study of mechanobiology, the lack of precise mechanical properties of PAA gel may leave a gap in understanding the comprehensive biological function of our protein candidates. Thus, in vivo confirmation of our results is adamant.

5.3 Proteomic analysis reveals potential novel players involved in mechanotransduction

In search for specific factors involved in mechanotransduction, Dupont et al. conducted a bioinformatic analysis on genes differentially expressied upon external mechanical forces as well as performed a series of biochemical examination and therefore defined YAP/TAZ as sensors and mediators of mechanical cues [11]. In our work, we established an unbiased screen approach coupled with mass spectrometry to identify particular protein players involved in mechanotransduction. Our screen results and the subsequent statistical analysis on differentially enriched proteins revealed that 102 proteins were significantly enriched in the nucleus after RhoA induction. The cellular location of these proteins covered a broad range

of cell compartments including focal adhesions, cytosolic compartments such as Golgi and endoplasmic reticulum, cellular vesicles, and the nucleus. The wide distribution of protein hits implied that RhoA activity may mediate the accumulation of these proteins in the nucleus either by translocating the proteins between the nucleus and cytoplasm or in part by promoting their gene expression. In our screen approach, the optimized time interval for CA-RhoA induction by tetracycline was 2 hours, which was determined by the induced CA-RhoA protein level and its efficiency to promote YAP nuclear accumulation. However, as described in 5.2 that RhoA activity also induces other signalling pathways, the time interval of RhoA induction used in our study may involve gene expression of other nuclear proteins. Furthermore, the speed of translation in mammalian cells is approximately 1 min/protein (300 aa) [145], the fast dynamics of protein synthesis may also contribute to the size of protein hits of our screen results.

In addition, the well-defined mechanotransducer YAP was also detected in our screen with high confidence, which validated the overall approach. Based on Gene Ontology analysis, these protein hits play crucial roles in multiple biological processes including chromosome organization, gene expression, RNA processing and gene translation. Previous studies have illustrated that alteration of external mechanical cues affect stem cell migration and differentiation [4], regulate cell proliferation [101] and control cancer progression and reprogramming [146] [147], where YAP was particularly reported to integrate the mechanical signals to the corresponding cell behaviour. Beside the proteins involving in transcriptional regulation, a large group of RNA-binding proteins such as PCBP1, PTBP1, EIF4A3 and HNRNPU were detected in our screen, and all of the four proteins are known to play a role in RNA processing. Among these protein hits, nuclear enrichment of PCBP1 and PTBP1 in HEK293-tet-RhoA-TurboID after RhoA induction was also validated by immunoblotting (Figure 3.18), implying RNA processing such as alternative splicing conducted by PCBP1 and PTBP1 having a potential role in mechanotransduction. However, more evidence needs to be provided to support our assumption.

5.4 Are PCBP1 and PTBP1 potential mechanical sensors and regulators?

In order to detect potential mechanotransducers our screen for potential mechanotransducers revealed a small network of proteins including PCBP1 and PTBP1 enriched in the nucleus induced RhoA activity. PCBP1 and PTBP1 exhibit nuclear localization signals (NLS) which enable them to shuttle between the nucleus and cytoplasm, making the two proteins promising candidates in terms of regulators in mechanotransduction. Thus, we hypothesized PCBP1 and PTBP1 are potential candidates for mechanotransducers. In this part, we review biological functions of PCBP1 and PTBP1 and weigh the possibility linking such functions of mechanotransduction. We also discuss the possible mechanisms involving their role as mechanotransducers.

5.4.1 Biological function of PCBP1 and PTBP

PCBP1 and PTBP1 belong to Heterogeneous nuclear ribonucleoproteins (hnRNPs) superfamily. hnRNPs are multifunctional RNA-binding proteins which engage in multiple regulatory elements in nucleic acid metabolism such as packaging of nascent transcripts, alternative splicing, and transcriptional and translational regulation [148, 149]. Despite sharing general properties, hnRNPs vary in domain composition and post-translational modification, which contribute greatly to their functional diversity [148]. PCBP1 (poly (rC) binding protein 1, also known as hnrnpe1) are classified to a subgroup of hnRNPs containing three KH domains while PTBP1 (polypyrimidine tract binding protein 1, also known as hnRNP I or PTB1) contain four RNA recognition motifs (RRMs) (Figure 5.2). Through the interaction of the domains with the preference RNA sequence, PCBP1 and PTBP1 impose their function in regulating a broad range of cellular process [121].

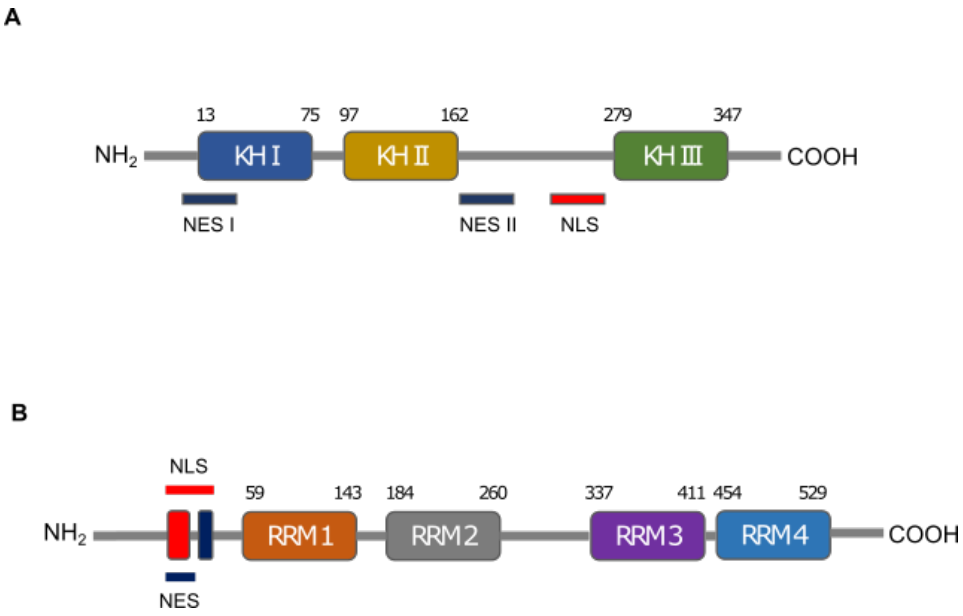

Figure 5.2 | Domain structure of PCBP1 and PTBP1

(A) Domain structure of PCBP1, which contains three KH domain for integration with RNA targets. Numbers indicate the position of amino acid residues relative to the domains. PCBP1 exhibits an NLS (nuclear localisation signal) between KH2 and KH3 domain, and two NES (nuclear export signal) which is respectively locates at N-terminal and region between KH2 and KH3 domains.

(B) Domain structure of PTBP1, which consists of four RRM for recognition and interaction with RNA targets. Numbers indicate the position of amino acid residues relative to the domains. PTBP1 contains a single NLS and NES at N-terminal that contribute to its shuttling between nuclear and cytoplasm.

5.4.1.1 PCBP1: a member of hnRNPs family with KH domains that recognize and bind poly(C) RNA

PCBP1 belongs to hnRNP E subgroup of the hnRNP superfamily characterized by a highly conserved triple repeat of the KH domain and poly(C)-binding specificity. The KH domain is defined as an ~70-amino acid domain which consists of a triple β-sheet platform supporting three α-helical segments [127]. KH domain has been shown to specifically interact with a target RNA through the consensus sequence VIGXXGXXI that maps to the middle of the KH domain [150]. Like other hnRNP E members, PCBP1 contains three KH domains; two are located at the N-terminus followed by a non-conserved region, and the third KH domain at C-terminus. It has been reported that KH1 and KH3 domains in PCBP1 are responsible for the binding to RNA, while the precise role of KH2 remains unknown [121]. PCBP1 exhibits a nuclear localization signal (NLS I) between KH2 and KH3 domains, making this protein capable of shuttling between

the nucleus and cytoplasm [127]. The domain structure of PCBP1 is demonstrated in Figure 5.2 A.

PCBP1 is highly homologous to the other hnRNP E member, PCBP2, with 89% similarity in amino acid sequences and 93% identical in KH domains [121, 127]. PCBP1 and PCBP2 are encoded by closely related mRNAs. Genomic analysis showed that PCBP2 is encoded by a gene with multiexon structure while PCBP1 is intronless and identical to its mRNA. PCBP1 has been suggested to be originally generated from a fully processed PCBP2 mRNA and occasionally retrotransposed into the genome as a pseudogene. Although pseudogenes are usually nonfunctional, PCBP1 has been defined as a multifunctional protein that mediates mRNA stability and expression [121]. Genomic sequence analysis has shown that PCBP1 is ubiquitously expressed and highly evolutionary conserved across various mammalian species including humans, mice, and rats [121, 151]. In addition, it has been estimated that the processed PCBP1 originated over 400 million years ago, right before the mammalian radiation. The unique conservation of PCBP1 suggests that the processed gene serves a nonredundant and critical role to the cells that vary from those of its PCBP2 origin [151]. Indeed, the difference in PCBP1 and PCBP2 function has been demonstrated by several groups. Shi et al. showed that PCBP1 attenuates cell proliferation and tumorigenesis by promoting p27 translation. Depletion of PCBP1 compromised p27 mRNA stability, causing reduced p27 protein levels and tumorigenesis. However, knockdown of PCBP2 had no significant effect on p27 mRNA and protein levels [152]. Another example of PCBP1 distinct function is demonstrated by Ghanem et al., which showed that PCBP1 and PCBP2 loci are individually essential for mouse embryony development. *PCBP1-null* alleles are lethal to embryo in the peri-implantation stage. *PCBP2-null* embryos show normal development until midgestation and are paralleled with hematopoietic defects [153]. This evidence indicates the specialized function of PCBP1.

PCBP1 has been shown to participate in a broad spectrum of the regulation of mRNA metabolism through the combination with other hnRNP proteins [121]. For example, PCBP1 acts as transcriptional activator by stimulating the transcription of mu opioid receptor (MOR) gene through the binding to a 26-nt, single-stranded polypyrimidine stretch in the proximal promoter with h PCBP2 and hnRNP K [121]. In addition, PCBP1 has been reported as both a translational coactivator and co-repressor. Pickering, B.M. et al. has indicated that PCBP1 along with polypyrimidine tract binding protein (PTB) increase the activity of an internal ribosome entry site (IRES) of *Bag-1* mRNA and consequently enhance mRNA translation [154]. PCBP1 is for example involved in the translational inhibition of *15-lipoxygenase* (*15-LOX*),

human papollilomavirus type 16 (HPV-16), *interleukin-like EMT inducer* (*ILEI*) and *disabled-2* (*Dab2*) mRNAs [121, 155].

PCBP1 also participates in the regulation of alternative splicing. A well-known PCBP-1 regulated splicing target is CD44 mRNA. The standard isoform CD44s contains only ten constant exons, while variant isoforms CD44v is encoded by a combination of ten constant exons and a mixed number of variable exons [156]. Zhang, T. et al. have reported that transient overexpression of PCBP1 represses multiple CD44v splicing as well as cell invasion in HepG2 [131]. Elevated nuclear PCBP1 stimulated by EGF is shown to accelerate TGF-β-induced EMT via regulation of CD44 splicing in MCF10A and HeLa, in which CD44s is significantly up-regulated over the production of CD44E (v8-10) [157]. Similar functions of PCBP1 were also described for pancreatic cancer cells [158]. Nuclear accumulation of PCBP1 induced by Fyn, a key member of Src family kinases, promotes alternative splicing of integrin β1 that switches a metastasis-associated isoform A to isoform C. Thus, reducing the invasion and migration of pancreatic cancer cells [158]. Furthermore, PCBP1 has been shown to suppress oncogenic STAT3α isoform via the regulation of alternative splice site in exon 23 of STAT gene and consequently, inhibited cell proliferation of breast cancer cells [130].

5.4.1.2 PTBP1: a member of the hnRNPs family that recognizes and binds polypyrimidine tracts through RRM domains

PTBP1 is a 57 kDa protein and belongs to the hnRNPs subgroup, hnRNPI. PTBP1 contains four RNA recognition motifs (RRMS) which are reported to mediate its binding to its RNA targets. RRMS are featured with widely conserved structural domains that comprise two α-helices and four stranded β-sheets which form a typical βαββαβ topology. N-terminal half of PTBP1 contains RRM 1 and 2 while C-terminal structure contains RRM3 and 4 [159]. Through these RRMs, PTBP1 binds to different sites of single-strand polypyrimidine-tract sequence on RNA such as UCUUC or CUCUCU that present in several discrete copies within intron and internal ribosome entry-site (IRES) where PTBP1 have been reported to regulate alternative splicing or translation initiation, respectively [160, 161]. Han et al. have reported that PTBP1 is not strictly pyrimidine specific, as evidenced by comutational models of PTBP1 binding sites that interspersed guanosine (G) within pyrimidine track are well tolerated for PTBP1-RNA interaction. Their finding may reveal new target splicing sites of PTBP1 [162]. PTBP1 contains an NLS that spans over 60 N-terminal amino acid residues while a separate nuclear export

signal (NES) occupies 25 residues of the N-terminus, implying this protein is capable of translocating between the nucleus and cytoplasm [163].

Like other hnRNPs, PTBP1 is involved in multiple cellular processes including mRNA stability and translation. For example, Ge et al. demonstrated that degradation of mRNA with long 3'UTR by nonsense-mediated RRMS decays (NMD) can be blocked by PTBP1 as PTBP1 prevents NMD protein UPF1 from associating to 3'UTR. Thus, PTBP1 positively regulates the stabilization of many human and retroviral transcripts [164]. PTBP1 is also reported to play an opposite role in controlling mRNA stability. A previous study indicated that the overexpression of the transmembrane receptor tyrosine kinase AXL in many cancer was correlated with cancer cell metastasis and survival. However the binding of PTBP1 to 5'-UTR of AXL mRNA decreased the stability of AXL mRNA and promoted apoptosis in lung cancer cells [165]. PTBP1 is also known for its cytoplasmic function such as stimilation of translation. It has been shown that PTBP1 binds to the internal ribosomal entry site (IRES) at the 5'UTR of viral mRNA [166]. In addition, Knoch et al. demonstrated that gluose induces translocation of PTBP1 from the nucleus to cytoplasm, where PTBP1 binds to mRNA encoding proteins of secretory granules (SGs), enhancing translation of SGs [167]

Besiede mRNA stability and translation, PTBP1 has been widely studied in its role of alternative splicing, especially the regulation of alternative splicing of oncogenes. Takahash et al. showed that PTBP1 strongly expressed in tumor tissue where this protein promoted splicing of PKM2 isoform (exon 10-included isoform). As a result, PKM2 isoform was dominantly expressed in cancer cells [168]. Importantly, PKM2 (pyruvate kinase muscle isozyme M2) plays a central role in cancer metabolism and tumour growth. Many tumour cells use aerobic glycolysis for glucose metabolism, a process which is an essential step for tumorigenesis and requires PKM2 catalytic activity [169, 170]. The upregulated PKM2 isoform by PTBP1 can increase rate of lactate production which favors cancer cell proliferation and can confers resistance to drugs [171]. Another example of the role of PTBP1 in controlling oncogene isoforms was demonstrated by Wang et al.. They showed that expression of cortactin isoform-a was PTBP1-dependent and correlated with cell invasion in colorectal cancer cells [110]. PTBP1 is also known to regulate alternative splicing during oncogene-induced senescence (OIS), where Georgilis et al. showed that overexpression of PTBP1 promotes splicing of short EXOC7 isoform (EXOC7-S, lacking exon 7) and induces a senescence-associated secretory phenotype (SASP). Conversley, depletion of PTBP1 resulted in opposite results [172].

5.4.1.3 PCBP1 and PTBP1 subcellular localization and cell function is controlled by phosphorylation on specific threonine and serine residues

It has been shown that phosphorylation of PCBP1 and PTBP1 is highly correlated with their subcellular localization and cellular function. Meng et al. demonstrated that PCBP1 shuttles between the nucleus and cytoplasm in a signal-dependent manner. In their study, they showed that EGF-mediated p21-activated kinase 1 (PAK1)-signalling phosphorylates PCBP1 on Thr-60 and Thr-127 residues, disrupting its binding to a DICE sequence in the 3'UTR of *15-LOX* mRNA and causing the reversal of its translational inhibitory function [125]. The phosphorylation of PCBP1 by PAK1 also induces its nuclear retention where PCBP1 regulates RNA processing like alternative splicing [125]. Similarly, Chaudhury and colleagues showed that phosphorylation of PCBP1 by TGF-β-dependent Akt2 on Ser 43 resulted in its release from a BAT RNA element and restored translational activation of EMT gene *Dab2* and *ILEI* [155].

For regulation of PTBP1 subcellular distribution, previous study showed that phosphorylation negatively controls nuclear retention of PTBP1. Xie et al. demonstrated the signal-dependent subcellular localization of PTBP1 by conducting in vitro and in vivo experiments, showing that a conserved Ser 16 flanked by two sets of basic residues in the N-terminus of PTBP1 are required for its efficient nuclear localization. 3',5'-cAMP-dependent protein kinase A (PKA) directly phosphorylates PTBP1 on Ser 16 within the NES, making this protein sequestered in cytoplasm [173]. These studies suggest that subcellular localization of PCBP1 and PTBP1 are dynamically regulated upon diverse triggers. Thus, we speculated that mechanical cues like cell density or ECM stiffness could potentially also be regulators of subcellular localization for PCBP1 and PTBP1.

5.4.2 Mechanical cues can regulate subcellular localization of PCBP1 and PTBP1

In this thesis, we showed that ECM stiffness and cell density can control PCBP1 and PTBP1 subcellular localization. The nuclear accumulation of PCBP1 and PTBP1 caused by rigid ECM or low cell density was mainly due to a transition of these protein from the cytoplasm into the nucleus because we only found small changes in overall expression levels of PCBP1 and PTBP1 (Figure 4.16). As described in **5.3.1** the diverse function of PCBP1 and PTBP1 are executed within specific cellular compartments. The changes in subcellular localization of PCBP1 and PTBP1 induced by mechanical cues like ECM rigidity could consequently affect their cellular function in terms of the regulation of RNA processing.

5.4.2.1 PCBP1 is regulated by cell density as well as cell confinement

We showed that cell density regulates PCBP1 subcellular localization in two different cell lines, MCF10A and HEK293. Our results indicated predominantly nuclear PCBP1 at low cell density while mainly cytoplasmic PCBP1 at high density, which was consistent with the phenotype of YAP under different cell density-mediated mechanical signals. Considering that cell density of various degrees of cell-cell contacts involves activation of the biochemical signallings such as Hippo pathway or TGF-β signalling which controls downstream factors like YAP or SMAD [3, 174], further investigation of the correlation between cell density-mediated mechanical cues and PCBP1 subcellular localization at single cell level is necessary to exclude the influence of cell-cell contact-dependent signalling pathways.

To investigate the effect of cell size on PCBP1 subcellular localization, we utilized microdomains of defined size for growing single cells to simulate the physiological condition where cell adhesive area is controlled by cell confinement. The influence of mechanical cues from cell confinement area on YAP has been reported by previous study and in our thesis, that cells display prominant nuclear YAP on large microdomains but more cytoplasmic YAP on small microdomains [11, 118] (also see Figure 4.8). The regulation of YAP nuclear localization by cell size is mainly dependent on the promotion of actin stress bundles by large adhesive area [103, 175]. In our work, we found that nuclear enrichment of PCBP1 is also correlated with the size of cell adhesive area. PCBP1 is distributed in both the nucleus and cytoplasm in cells grown on smallest domains, however, the nuclear PCBP1 is increased when cells grown on large domains (Figure 4.9). Thus, the change of PCBP1 subcellular localization by the mechanical condition known to regulate YAP provides an evidence that PCBP1 could be a potential mechanotransducer.

5.4.2.2 Is PTBP1 subcellular distribution regulated by cell density via adherens junction?

With regards to the relationship between cell density and PTBP1, our data indicated that cell density altered PTBP1 subcellular distribution in a cell type-specific manner. We showed that cells exhibited overwhelmingly nuclear PTBP1 in sparse but largely cytoplasmic PTBP1 in dense MCF10A cells. However, such regulation by cell density was not detected in HEK293. However, one of our lab members found that cell density-dependent regulation of PTBP1 can be reproduced in HCT116 but not in MDA-MB-231 (data not shown).

Among these cell lines tested, MCF10A and HCT116 are of epithelial origin with expression of adherens junction marker E-cadherin while MDA-MB-231 is more mesenchymal which lacks E-cadherin [176, 177]. Although HEK293 cells are assumed to be epithelial in origin but this cell line displays much lower levels of E-cadherin than epithelial cell line [178]. Combining these information with the observed cell-to-cell variability of the PTBP1 phenotype, we speculate that the changes of PTBP1 subcellular localization by cell density is limited to epithelial cells expressing adherens junction. The possible mechanism may involve the cortical actin-myosin networks. The contractile actin-myosin networks are coupled to adherens junction in columnar epithelial cell layers, playing a role to mediate forces transmission between adjecent cells. Of note, previous study also showed that cortical actin-myosin network can regulate YAP nuclear translocation. Furukawa et al demonstrated that MDCK at high cell density displayed tensed cortical actin-myosin network which inhibited YAP/TAZ nuclear localization. However, disruption of F-actin tension with blebbistatin, an inhibitor of non-muscle myosin II, caused YAP/TAZ nuclear translocation carried by Merlin [106]. Such mechanism may also regulate PTBP1 subcellular distribution in a similar way.

Interestingly, our microdomain experiments showed that PTBP1 remained localizaed in the nucleus of single MCF10A cells even when the cell was growing in the smallest domain. Given that epithelial cells cannot develop adherens junctionswhen in sparse culture conditions, our microdomain experiment result may support the speculation of the relationship between PTBP1 and adherens junction, because it is in line our observed cell density-independence of PTBP1 translocation in HEK293 and MDA-MB-231. However, more experiments are needed to clarify if cell density regulates PTBP1 subcellular translocation via adherens junctions. For this part, we may egineer a stable HEK293 clone in which the expression of a full length of E-cadherin can be induced to mimic the phenotype of adherens junction. We will compare subcellular localization of PTBP1 in high density-cultured HEK293 expressing E-cadherin or control plasmid to test the role of E-cadherin in the regulation of PTBP1 cellular distribution.

5.4.2.3 ECM rigidity regulated PCBP1 and PTBP1 translocation

PCBP1 subcellular localization has been shown to be regulated by EGF and serum dependent PAK1- signalling or by TGF-β stimulated Akt pathway [125, 155], while the nucleocytoplasmic transport of PTBP1 has been reported to be controlled by 3',5'-cAMP-dependent protein kinase A (PKA) [173]. These signalling pathways play a key role in determining biological function of PCBP1 or PTBP1 at transcriptional or translational regulatory

level. However, to our knowledge, there is no evidence thus far implying mechanical cues in regulating PCBP1 or PTBP1.

In our study, we showed that subcellular distribution of PCBP1 and PTBP1 correlated with PAA gel rigidity. Unlike previous studies which treated cells with EGF or TGF-β or PKA expression vector to induce particular signalling to promote PCBP1 or PTBP1 subcellular translocation [125, 155, 173], we cultured cells on PAA gels of various rigidity. Thus, in our experiments,ECM stiffness was the only changing parameter to control the phenotype of PCBP1 and PTBP1. Furthermore, PCBP1 and PTBP1 behaved very similar to the known mechanotransducer YAP. Finally, we also confirmed that the change of PCBP1 and PTBP1 subcellular localization by ECM stiffness was not limited to MCF10A cells but can be found also in mutiple other cell lines including HEK293, HeLa and Caco2, indicating that ECM stiffness appears to have an impact on PCBP1 and PTBP1 subcellular localization in a wide range od cell lines of different tissue origin. Together this supports a view that PCBP1 and PTBP1 may be potential mechanotransducers.

5.4.2.4 Cytoskeletal stress fibres are involved in the regulation of PCBP1 subcellular localization

Given that cytoskeletal reorganization and remodelling propagate external mechanical forces throughout the cell [3, 11, 103], clarification of their role in regulating PCBP1 and PTBP1 subcellular localization was important. In this thesis, we demonstrated that PCBP1 nuclear localization was regulated by cytoskeletal stress fibre in NIH3T3 fibroblast, in which the presence of various microfilament inhibitors diminished PCBP1 nuclear retention. Among these inhibitors used in this study, latrunculin A (Lat A) binds to monomeric G-actin and causes depolymerization of actin filaments, ML-7 inhibits myosin light chain kinase (MLCK) to block phosphorylation of myosin regulatory light chain (MRLC), and Y27632 inhibits ROCK to prevent actomyosin contractility as well as activation of LIM domain kinase [6, 179]. Previous research also used these microfilament inhibitors to attenuate cell tension as a way to support the role of the mechanical regulators YAP/TAZ [11]. Similarly, disruption of architecture of cytoskeletal stress fibre by F-actin severing proteins has been shown to play an essential role to inhibit YAP/TAZ activity in cells experiencing low mechanical forces [3]. The cytoskeletal tension-dependent regulation of PCBP1 as suggested by our inhibitor study provides additional strong evidence that PCBP1 can act as potential mechanotransducer.

Interestingly, despite F-actin tension has been widely shown to promote YAP/TAZ nuclear localization, the mechanical forces exert upon cell-cell junctions reversely regulate YAP/TAZ nuclear localization and function. Furukawa et al. demonstrated that treatment of high density-cultured MDCK with blebbistatin, an inhibitor of myosin II, relieved F-actin tension in circumferential actin belt and enhanced nuclear YAP/TAZ distribution [106]. In our work, we also showed that PCBP1 and YAP changed from cytoplasm to the nucleus by blebbistatin in two high density epithelial cell lines (Figure 4.21), which was consistent with the idea that mechanical stresses mediated by epithelia-specific circumferential actin belt underlying adherens junctions may represent an independent signalling pathway from those emanating from ECM-cell junctions [106]. Thus, with a phenotype similar to YAP which can be regulated by adherens junction-mediated mechanical forces, the changes of PCBP1 subcellular localization upon disruption of circumferential actin belt provides another evidence that PCBP1 is a potential regulator of mechanotransduction.

5.5 Does ECM stiffness regulate the cell's through PCBP1 and PTBP1?

Elevated ECM stiffness is highly associated with several cell behaviours including enhanced cell growth and cell migration through the activation of RhoA/ROCK and remodelling of actin cytoskeleton as well as the downstream effectors e.g., YAP [118, 137]. As we aimed to identify molecular regulators of nuclear function that integrate mechanical signals into specific cell behaviour, investigation of the effects of ECM stiffness on RNA processing such as alternative splicing was important to clarify the role of potential mechanotransducers.

5.5.1 ECM stiffness may regulate alternative splicing through PCBP1 or PTBP1

In this thesis, we show that ECM stiffness is involved in the regulation of alternative splicing of several PCBP1 and PTBP1 target transcripts. Alternative splicing is a crucial process to give rise to different protein isoforms of various cellular function. The influence of mechanical forces on alternative splicing is still a very poorly investigated area. However, there are few examples suggesting that mechanical cues have the potential to regulate alternative splicing [180]. For example, Inoue et al. showed that fluid shear stress induces FosB gene variants *FosB*

and Δ FosB at both mRNA and proteins levels. This regulation is dependent on Ca2+ influx and downstream effector ERK1/2 [181]. Regarding the correlation between ECM stiffness and alternative splicing, to our knowledge, there is so far only one paper demonstrating the correlation between ECM stiffness and alternative splicing. Bordeleau et al. showed that stiff matrix increased the production of fibronectin extra domain-B (EDB-FN) splice variant in endothelial cells. This process is regulated by Rho/ROCK mediated cell contractility, which consequently induces the phosphorylation of splicing factor SRp40 through PI3K/AKT signalling [182]. Interestingly, the phosphorylation of SRp40 by stiff matrix also promotes the splicing of antiangiogenic VEGF 165b [182]. As our work here shows that elevated ECM stiffness is accompanied by nuclear accumulation of two splicing factors PCBP1 and PTBP1 in several cell lines, our data provides strong evidence that PCBP1 and PTBP1 potentially link ECM stiffness with alternative splicing changes.

Interestingly, the role of PCBP1 and PTBP1 in alternative splicing has been reported in the context of various disease models [109, 110, 130, 131, 158]. The identification of direct RNA targets and their interacted motif sites recognized by PCBP1 or PTBP1 were conducted by high throughput RNA-seq coupled with transcriptome mapping in cancer cell lines [108, 111]. These genes whose alternative splicing regulated by PCBP1 or PTBP1 are involved in a broad range of molecular and cellular function including cell death and survival, cell proliferation, motility, and RNA post-transcriptional modification [108, 110, 111]. In these studies, depletion of PCBP1 or PTBP1 by siRNA-mediated knockdown resulted in enhanced or suppressed splicing of multiple cassette exons [108, 110, 111]. Although our data showed that the changes of ECM stiffness only slightly altered the endogenous level of PCBP1 and PTBP1 (Figure 4.16), the exclusion and enrichment of nuclear PCBP1 and PTBP1 by soft and stiff ECM respectively may represent similar condition where PCBP1 and PTBP1 are depleted or not. As a result, our finding of ECM rigidity-dependent splicing of PCBP1 and PTBP1 target RNA supports the idea that ECM stiffness regulates alternative splicing through PCBP1 and PTBP1 function.

5.5.2 ECM stiffness-mediated alternative splicing could be cell type-dependent

PCBP1 and PTBP1 have been reported to regulate alternative splicing of multiple transcripts [108, 111]. However, we found that the splicing patterns of these genes caused by knockdown of PCBP1 or PTBP1 were not always consistent with these published works. For example, Ji et al. demonstrated that splicing of STAT2 exon 18 was significantly reduced by depletion of PCBP1 in K562 cells, however, our preliminary test showed that PCBP1 knockdown enhanced

inclusion of STAT2 exon 18 [108] (data not shown). This could be because previous studies used cancer cell lines to clarify PCBP1 or PTBP1-mediated alternative splicing while we used non-cancerous epithelial cell lines, in which the expression of some particular genes may vary from those of cancer cell lines used in previous studies.

The diversity of alternative splicing of the same RNA transcript across different cell lines also can be seen in our ECM stiffness experiments. We found that the splicing of cassette exons of AP1G2, NUMB and CTTN in MCF10A enhanced by rigid ECM were not reproduced in cancer cell lines such as HeLa and Caco2. The possible reasons behind such phenomenon could be cell type-dependent protein levels of PCBP1 or PTBP1, in which previous reports have demonstrated that PTBP1 was overexpressed in multiple tumour tissue while PCBP1 was found down-regulated in several cancers [110, 165, 183, 184]. However, more work is needed to clarify the PCBP1 and PTBP1 protein expression levels as well as the corresponding alternative splicing events in normal and cancer cell lineage.

5.5.3 Does ECM stiffness play a role in controlling alternative splicing of NUMB exon 9?

5.5.3.1 ECM stiffness may regulate splicing of NUMB exon 9 transcript

Our results indicated that several PCBP1 and PTBP1 target transcripts such as NUMB was mechanically regulated by ECM stiffness. We particularlly focused on the investigation of alternative splicing of NUMB because its splicing variants are already functionally characterised. NUMB has been identified to play a role in cell development and cell fate decision [185]. NUMB is an endocytic adaptor protein comprising four isoforms produced by alternative splicing [132, 186]. The two prevalent isoforms, NUMB p72 and NUMB p66, differ by the inclusion or exclusion of exon 9 (E9) respectively that causes various length of their proline-rich region (PRR), a domain that functions as an Src homology 3-binidng site [132, 187]. Previous studies have indicated that NUMB E9-included (NUMB+E9) and E9-excluded (NUMBΔE9) isoforms exerted opposing effects on multiple cellular functions (Figure 5.3). For example, Wei et al. demonstrated that NUMB regulates endocytosis in an isoform dependent manner. In their study, NUMB isoform including E9 promotes receptor recycling while E9-excluded isoform directs receptor lysosomal degradation [188]. The isoform specific role of NUMB in controlling cell proliferation and metastasis was also reported. It has been shown that expression of E9-included isoform is associated with enhanced cell proliferation and

invasion for different cancer cell lines. However. E9-excluded isoform displayed the opposite effect regarding this cell behaviour [189, 190].

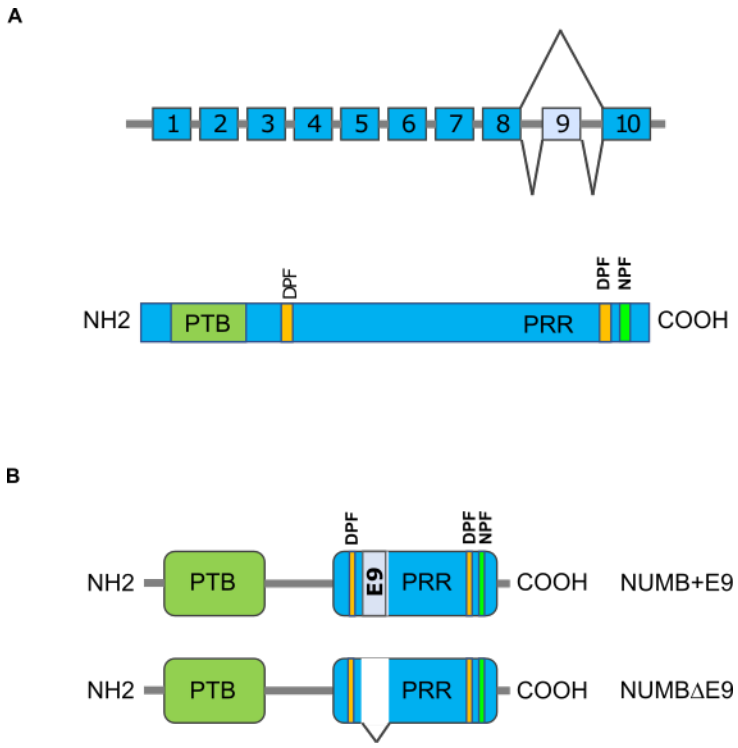

Figure 5.3 | Domain structure of NUMB variants

(A) Top: the structure of NUMB pre-mRNA, with exon 9 depicted as cassette exon. Bottom: schematic representation of fully encoded NUMB protein which contains an N-terminal phosphotyrosine-binding (PTB) domain, a proline-rich region (PRR), two aspartic acid-proline-phenylalanine (DPF) motifs and an asparagine-proline-phenylalanine (NPF) motif.
(B) Two major splice variants of NUMB which are formed from alternative splicing of exon 9 (E9): E9-included isoform p72 (NUMB+E9) and E9-skipped isoform p66(NUMBΔE9).

Here, we have shown as far as we know for the first time that rigid ECM promotes splicing of NUMB E9 (NUMB+E9) transcript in MCF10A cells (Figure 4.23). Based on previous studies, we suggested that the elevated NUMB+E9 transcript isoform by stiff ECM may favour cell proliferation. Our finding is consistent with the concept that elevated ECM stiffness enhanced cell growth [191, 192]. Furthermore, NUMB+E9 isoform has been shown to regulate the recycling of anaplastic lymphoma kinase (ALK), whose aberrant activation is associated with several forms of cancer [188]. As a result, our finding provides an important insight that ECM

rigidity may govern cell growth and tumorigenesis through controlling the ratio of NUMB splice variants.

We identified PTBP1 as the regulator in ECM stiffness-mediated alternative splicing of NUMB where PTBP1 promoted inclusion of NUMB E9 in MCF10A grown on rigid ECM. The role of PTBP1 in controlling NUMB splice variants was also detected in previous study. Rajendran et al. indicated that PTBP1 and ASF/SF2 have opposing effects on NUMB E9 splicing, in which PTBP1 enhanced E9 inclusion while ASF/SF2 increased E9 skipping in HEK293T and A549 [132]. High expression of NUMB+E9 protein isoform have been shown in a number of cancer cells though in which other splicing factors involved E9 splicing were studied [189, 190]. In addition, it has been reported that PTBP1 is overexpressed in multiple tumour tissues and is responsible for proliferation and maintainence of metastatic properties of cancer cells [165, 193, 194]. These publications suggest that elevated PTBP1 in solid tissue e.g., tumour tissue, promotes NUMB E9 splicing. By contrast, our data showed that stiff ECM only slightly increased endogenous PTBP1 expression (Figure 4.16), indicating the change of NUMB exon 9 splicing by ECM stiffness is not through overall PTBP1 protein. Considering our evidence that rigid ECM drives significant enrichment of nuclear PTBP1, our results suggest that the increased NUMB E9 isoform by rigid ECM was via the accumulation of PTBP1 in the nucleus where alternative splicing events occur.

5.5.3.2 Does ECM stiffness regulate NUMBΔE9 protein isoform through other factors?

Notably, although our data of knockdown inhibition of PTBP1 showed the switch between NUMB+E9 and NUMBΔE9 isoforms at both RNA and protein level, the ECM stiffness-mediated ratio change in these two NUMB transcript variants was not reflected in their downstream protein expression level. Desipte the increased protein production of NUMB+E9 isoform by rigid ECM was consistent with its change in RNA expression, we found that soft ECM resulted in significant decrease in both NUMB+E9 and NUMBΔE9 protein although much higher amounts of NUMBΔE9 was detected at RNA level when compared with NUMB+E9 splice variant.

The differential expression of NUMBΔE9 isoforms between RNA and protein level on soft gel was probably due to unidentified mechanisms that regulate translation of NUMB by ECM stiffness. For example, there could be factors involve in the suppression of NUMB translation by soft ECM. Our IF data showed that most PCBP1 was sequestered in the cytoplasm on soft gel (Figure 4.13). In addition, cytoplasmic PCBP1 has been reported to inhibit translation of

several genes such as *Dab2* and *ILEL* [155]. Thus, we speculate that cytoplasmic PCBP1 by soft ECM may play a role in repressing translation of NUMBΔE9 protein isoform. To clarify the effect of cytoplasmic PCBP1 on NUMB protein expression, an investigation towards the changes of protein expression of NUMB isoforms in the presence or absence of PCBP1 would be important.

5.6 Possible mechanisms linking mechanical cues to regulation of subcellular localization of PCBP1 and PTBP1

5.6.1 Does ECM stiffness regulate PCBP1 and PTBP1 subcellular localization through phosphorylation of these two proteins?

It is not clear how ECM stiffness drives PCBP1 or PTBP1 into the nucleus for regulation of alternative splicing of their transcript targets. Several studies described in chapter 5.4.1.3 indicate that nucleocytoplasmic transport of PCBP1 and PTBP1 as well as their cellular function relied on specific signal transduction such as PAK-1, TGF-β or PKA-mediated signalling pathway [125, 155, 173]. Further research showed that EGF signalling promoted PCBP1 nuclear localization where this protein worked with TGF-β mediated SMAD3 to enhance alternative splicing of CD44s isoform [157]. Another example demonstrating the role of phosphorylation in alternative splicing regulation was recently published by Bordeleau et al. They showed phosphorylation of SRp40 by the PI13K/AKT pathway was necessary for matrix stiffness-modulated production of EDB-FN splicing variants [182].

Linking together with what we found in our work with previous reports, we speculate that ECM stiffness may regulate PCBP1 and PTBP1 subcellular distribution and their function e.g., alternative splicing, via phosphorylation of these two proteins on specific residues. The speculation is based on two reasons: 1), ECM stiffness-mediated mechanotransduction has been shown to activate multiple kinases like Rho/ROCK or the integrin/FAK/ERK pathway, which may regulate phosphorylation of downstream factors [195, 196]; 2), previous studies described in 5.4.1.3 indicates that the phosphorylation status of PCBP1 and PTBP1 can control their subcellular localization. This information prompted us to consider whether

phosphorylation of PCBP1 and PTBP1 induces protein conformational change and causes exposure or hinderance of their NLS or NES, as a result, mediates their nucleocytoplasmic transportation.

To test such a model, we will examine whether ECM stiffness cues leads to phosphorylation of PCBP1 or PTBP1 by performing Phos-tag SDS-PAGE to compare protein mobility between soft and stiff ECM. Phos-tag SDS-PAGE is a phosphate-affinity electrophoresis technique that separates phosphorylated and non-phosphorylated proteins by SDS-PAGE. During electrophoresis, the phosphorylated proteins bind to Phos-tag immobilized in the gel and form slower migration than those without being phosphorylated (https://labchem-wako.fujifilm.com). Based on the different migration behaviour, we can distinguish if PCBP1 and PTBP1 are phosphorylate by ECM stiffness.

We will also utilize mass spectrometry to analyse phosphorylation of amino acids regulated by various ECM stiffness. With the database such as PhosphoSitePlus® that provides the information about phosphorylated sites of particular proteins and the involved kinases, we will further investigate whether ECM stiffness regulates phosphorylation of PCBP1 and PTBP1 through particular kinase signalling pathway. Based on our findings, we will perform knockdown of particular kinase to evaluate its role in regulation of ECM stiffness-dependent PCBP1 and PTBP1 subcellular localization.

5.6.2 Does the nuclear pore mechanical restriction regulate PCBP1 and PTBP1 nuclear translocation?

In addition to induce biochemical signalling pathway that regulates varying phenotype of target proteins, mechanical cues also exert their influence on cells in a physical manner, e.g., through cytoskeletal tension. Actin-dependent regulation is highly conserved in mechanotransduction, which has been demonstrated by multiple groups studying the role of YAP in mechanotransduction [3, 11, 103, 106]. Our result showed that F-actin integrity and actomyosin contractility regulated PCBP but not PTBP1 subcellular localization (Figure 4.19 & 4.20), implying that there could be other mechanisms independently regulate these two potential mechanotransducers.

Rigid ECM has been reported to establish a physical connection between the cytoskeleton and the nucleus through Nucleoskeleton and Cytoskeleton (LINC) complex. LINC is a protein

complex featured with SUN domain of SUN proteins and KASH domain of nesprin proteins LINC. With various nesprin isoform, LINC connect different types of cytoskeletons to SUN, which spans inner nuclear membrane [2] (also see 1.5). Thus, mechanical forces arising from focal adhesion can be directly transmitted to the nucleus, stretching nuclear pores and increasing YAP nuclear import [129]. Thus, we speculate that such force transmission to the nucleus also plays a role in ECM stiffness-mediated nuclear accumulation of PCBP1 and PTBP1. To test this hypothesis, we will overexpress a KASH domain only construct to disrupt the linker of Nucleoskeleton and Cytoskeleton (LINC) complex and examine if ECM rigidity regulates PCBP1 and PTBP1 subcellular localization through mechanical coupling between the cytoskeleton and the nucleus. We could also test ECM stiffness-dependent PCBP1 and PTBP1 nuclear import and export kinetics to clarify if the mechanically stretched nuclear pores play a role in mediating PCBP1 and PTBP1 subcellular translocation. These further investigations will help us to understand if ECM stiffness regulates PCBP1 and PTBP1 nucleocytoplasmic transportation by directly converting physical force into changes in nuclear molecular import rates.

5.7 Future perspectives

Our developed original screen for identifying novel player of mechanotransduction has resulted in the identification of PCBP1 and PTBP1 as strong candidates. To our knowledge, a connection between PCBP1, PTBP1 and mechanotransduction has not previously been demonstrated. This thesis not only provides evidence suggesting that PCBP1 and PTBP1 are mechanotransducers, but also opens a wide range of questions which needs to be addressed.

1) **Examining of influence of ECM stiffness on global alternative splicing events**

In this thesis, we examined the impact of ECM stiffness on alternative splicing of several PCBP1 and PTBP1 target transcripts in MCF10A. However, the choice of genes used in our work is based on previous studies which tested the alternative splicing events by depletion of PCBP1 or PTBP1 in various cancer cell lines [108, 111]. Since our data showed that the ECM stiffness-mediated alternative splicing is cell type-dependent, a broad examination of alternative splicing events is important to identify the target genes which undergo alternative splicing controlled by ECM stiffness. In order to achieve this purpose, we may perform RNA-seq to check the changes of RNA isoforms by ECM stiffness in a genome-

wide manner. Based on the results, we would be able to target the key genes which alternative splicing may play critical role in controlling cell behaviour such as proliferation and migration.

2) **Establishing in vivo model for investigation of the role of PCBP1 and PTBP1 in mechanotransduction**

In this thesis, we used several epithelial cell lines to clarify the possible role of PCBP1 and PTBP1 in mechanotransduction. As we understand, the physiological condition is much more complex in *in vivo* environment. For example, we cultured the cells on PAA gel of various rigidity to allow the cells experience mechanical cues underneath their substrate. In a 3D like *in vivo* condition, however, cells are very likely to sense mechanical stimuli from all three dimensions, which may have different mechanisms to regulate molecular mechanosensors. Notably, PCBP1 and PTBP1 have been shown to impose critical function in pathological model, where PCBP1 and PTBP1-medaited alternative splicing of several oncogenes is related to cell survival and metastasis [109, 110, 130, 158]. Thus, the establishment of *in vivo* models is important to help us to get a more complete understanding of the role of PCBP1 and PTBP1 in mechanotransduction. For this part, we may establish mouse or zebrafish models and conduct xenograft experiments or study tumorigenesis, as a model to simulate a physiological-relevant condition and test the correlation between PCBP1, PTBP1 and mechanotransduction.

3) **Investigating other cell behaviour in vitro and in vivo regulated by mechanical cues through PCBP1 and PTBP1**

Here we showed that ECM stiffness-mediated mechanical cues may regulate alternative splicing through PCBP1 and PTBP1. Interestingly, PCBP1 and PTBP1 also regulate other RNA metabolic steps such as gene translation and RNA stability. The nucleocytoplasmic translocation of PCBP1 and PTBP1 by external mechanical stimuli may also involve in other important cellular function, e.g., gene translation in the cytoplasm. The further investigation of a broad range of cell behaviour such as proliferation, endocytosis and metastasis that is regulated by mechanical forces may provide further insights on how mechanical forces would govern cell function.

5.8 Concluding remarks

In this thesis, we established an unbiased screen approach coupled with LC-MS/MS to identify novel molecular players that shuttle between the nucleus and cytoplasm upon activation of RhoA signalling. This thesis provides evidence, for the first time, that PCBP1 and PTBP1 act as potential regulators in mechanotransduction. Our work revealed that the subcellular localization of PCBP1 and PTBP1 can be mechanical cues dependent. We also demonstrated that the nucleocytoplasmic translocation of PCBP1 and PTBP1 by ECM stiffness played a role in the regulation of alternative splicing as a way to convert external mechanical cues into biochemical cellular changes. As many of PCBP1 and PTBP1 target transcripts are defined as oncogenes which alternative splicing pattern is associated with various pathological progression such as cancer proliferation and metastasis, this thesis provides new insights into a so far poorly investigated mechanotransduction pathway.

Reference

1. Ohashi, K., S. Fujiwara, and K. Mizuno, *Roles of the cytoskeleton, cell adhesion and rho signalling in mechanosensing and mechanotransduction.* The Journal of Biochemistry, 2017. **161**(3): p. 245-254.
2. Martino, F., et al., *Cellular Mechanotransduction: From Tension to Function.* Frontiers in Physiology, 2018. **9**: p. 824.
3. Aragona, M., et al., *A Mechanical Checkpoint Controls Multicellular Growth through YAP/TAZ Regulation by Actin-Processing Factors.* Cell, 2013. **154**(5): p. 1047-1059.
4. Hadden, W.J., et al., *Stem cell migration and mechanotransduction on linear stiffness gradient hydrogels.* Proceedings of the National Academy of Sciences, 2017. **114**(22): p. 5647.
5. Vogel, V. and M. Sheetz, *Local force and geometry sensing regulate cell functions.* Nature Reviews Molecular Cell Biology, 2006. **7**(4): p. 265-275.
6. Panciera, T., et al., *Mechanobiology of YAP and TAZ in physiology and disease.* Nature Reviews Molecular Cell Biology, 2017. **18**: p. 758.
7. Gkretsi, V. and T. Stylianopoulos, *Cell Adhesion and Matrix Stiffness: Coordinating Cancer Cell Invasion and Metastasis.* Frontiers in oncology, 2018. **8**: p. 145-145.
8. Bonnans, C., J. Chou, and Z. Werb, *Remodelling the extracellular matrix in development and disease.* Nature reviews. Molecular cell biology, 2014. **15**(12): p. 786-801.
9. Jansen, K.A., P. Atherton, and C. Ballestrem, *Mechanotransduction at the cell-matrix interface.* Seminars in Cell & Developmental Biology, 2017. **71**: p. 75-83.
10. Schiller, H.B. and R. Fässler, *Mechanosensitivity and compositional dynamics of cell–matrix adhesions.* EMBO reports, 2013. **14**(6): p. 509-519.
11. Dupont, S., et al., *Role of YAP/TAZ in mechanotransduction.* Nature, 2011. **474**(7350): p. 179.
12. Hynes, R.O., *Integrins: Bidirectional, Allosteric Signaling Machines.* Cell, 2002. **110**(6): p. 673-687.
13. Liddington, R.C. and M.H. Ginsberg, *Integrin activation takes shape.* Journal of Cell Biology, 2002. **158**(5): p. 833-839.
14. Takagi, J., et al., *Global Conformational Rearrangements in Integrin Extracellular Domains in Outside-In and Inside-Out Signaling.* Cell, 2002. **110**(5): p. 599-611.
15. Tadokoro, S., et al., *Talin Binding to Integrin ß Tails: A Final Common Step in Integrin Activation.* Science, 2003. **302**(5642): p. 103.
16. Puklin-Faucher, E. and M.P. Sheetz, *The mechanical integrin cycle.* Journal of Cell Science, 2009. **122**(2): p. 179-186.
17. Provenzano, P.P. and P.J. Keely, *Mechanical signaling through the cytoskeleton regulates cell proliferation by coordinated focal adhesion and Rho GTPase signaling.* Journal of Cell Science, 2011. **124**(8): p. 1195-1205.
18. Zhong, C., et al., *Rho-mediated contractility exposes a cryptic site in fibronectin and induces fibronectin matrix assembly.* The Journal of cell biology, 1998. **141**(2): p. 539-551.
19. Han, Y.L., et al., *Cell contraction induces long-ranged stress stiffening in the extracellular matrix.* Proceedings of the National Academy of Sciences, 2018. **115**(16): p. 4075.
20. Zaidel-Bar, R., et al., *Functional atlas of the integrin adhesome.* Nature Cell Biology, 2007. **9**(8): p. 858-867.

21. Horton, E., et al., **Definition of a consensus integrin adhesome and its dynamics during adhesion complex assembly and disassembly.* Nature cell biology, 2015. **17**.
22. Kanchanawong, P., et al., *Nanoscale architecture of integrin-based cell adhesions.* Nature, 2010. **468**(7323): p. 580-584.
23. Mitra, S.K., D.A. Hanson, and D.D. Schlaepfer, *Focal adhesion kinase: in command and control of cell motility.* Nature Reviews Molecular Cell Biology, 2005. **6**(1): p. 56-68.
24. Zhou, J., et al., *Mechanism of Focal Adhesion Kinase Mechanosensing.* PLoS computational biology, 2015. **11**(11): p. e1004593-e1004593.
25. Dahl, K.N., et al., *The nuclear envelope lamina network has elasticity and a compressibility limit suggestive of a molecular shock absorber.* Journal of Cell Science, 2004. **117**(20): p. 4779-4786.
26. Sawada, Y., et al., *Force sensing by mechanical extension of the Src family kinase substrate p130Cas.* Cell, 2006. **127**(5): p. 1015-1026.
27. Schaller, M.D., *Paxillin: a focal adhesion-associated adaptor protein.* Oncogene, 2001. **20**(44): p. 6459-6472.
28. Turner, C.E., *Paxillin and focal adhesion signalling.* Nature Cell Biology, 2000. **2**(12): p. E231-E236.
29. Petit, V., et al., *Phosphorylation of tyrosine residues 31 and 118 on paxillin regulates cell migration through an association with CRK in NBT-II cells.* The Journal of cell biology, 2000. **148**(5): p. 957-970.
30. Critchley, D.R., *Biochemical and Structural Properties of the Integrin-Associated Cytoskeletal Protein Talin.* Annual Review of Biophysics, 2009. **38**(1): p. 235-254.
31. Yao, M., et al., *The mechanical response of talin.* Nature communications, 2016. **7**: p. 11966-11966.
32. del Rio, A., et al., *Stretching Single Talin Rod Molecules Activates Vinculin Binding.* Science, 2009. **323**(5914): p. 638.
33. Humphries, J.D., et al., *Vinculin controls focal adhesion formation by direct interactions with talin and actin.* The Journal of cell biology, 2007. **179**(5): p. 1043-1057.
34. Ziegler, W.H., R.C. Liddington, and D.R. Critchley, *The structure and regulation of vinculin.* Trends in Cell Biology, 2006. **16**(9): p. 453-460.
35. Case, L.B., et al., *Molecular mechanism of vinculin activation and nanoscale spatial organization in focal adhesions.* Nature cell biology, 2015. **17**(7): p. 880-892.
36. Dumbauld, D.W., et al., *How vinculin regulates force transmission.* Proceedings of the National Academy of Sciences, 2013. **110**(24): p. 9788.
37. Hirata, H., H. Tatsumi, and M. Sokabe, *Zyxin emerges as a key player in the mechanotransduction at cell adhesive structures.* Communicative & integrative biology, 2008. **1**(2): p. 192-195.
38. Hirata, H., H. Tatsumi, and M. Sokabe, *Mechanical forces facilitate actin polymerization at focal adhesions in a zyxin-dependent manner.* Journal of Cell Science, 2008. **121**(17): p. 2795-2804.
39. Uemura, A., et al., *The LIM domain of zyxin is sufficient for force-induced accumulation of zyxin during cell migration.* Biophysical journal, 2011. **101**(5): p. 1069-1075.
40. Yoshigi, M., et al., *Mechanical force mobilizes zyxin from focal adhesions to actin filaments and regulates cytoskeletal reinforcement.* The Journal of cell biology, 2005. **171**(2): p. 209-215.
41. Crawford, A.W., J.W. Michelsen, and M.C. Beckerle, *An interaction between zyxin and alpha-actinin.* The Journal of cell biology, 1992. **116**(6): p. 1381-1393.

42. Feng, Y., et al., *α-actinin1 and 4 tyrosine phosphorylation is critical for stress fiber establishment, maintenance and focal adhesion maturation.* Experimental cell research, 2013. **319**(8): p. 1124-1135.
43. Meacci, G., et al., *α-Actinin links extracellular matrix rigidity-sensing contractile units with periodic cell-edge retractions.* Molecular biology of the cell, 2016. **27**(22): p. 3471-3479.
44. Gumbiner, B.M., *Regulation of cadherin-mediated adhesion in morphogenesis.* Nature Reviews Molecular Cell Biology, 2005. **6**(8): p. 622-634.
45. Takeichi, M., *Dynamic contacts: rearranging adherens junctions to drive epithelial remodelling.* Nature Reviews Molecular Cell Biology, 2014. **15**(6): p. 397-410.
46. Kovacs, E.M., et al., *Cadherin-Directed Actin Assembly: E-Cadherin Physically Associates with the Arp2/3 Complex to Direct Actin Assembly in Nascent Adhesive Contacts.* Current Biology, 2002. **12**(5): p. 379-382.
47. Harris, A.R., A. Daeden, and G.T. Charras, *Formation of adherens junctions leads to the emergence of a tissue-level tension in epithelial monolayers.* Journal of cell science, 2014. **127**(Pt 11): p. 2507-2517.
48. Shewan, A.M., et al., *Myosin 2 is a key Rho kinase target necessary for the local concentration of E-cadherin at cell-cell contacts.* Molecular biology of the cell, 2005. **16**(10): p. 4531-4542.
49. Priya, R., et al., *Feedback regulation through myosin II confers robustness on RhoA signalling at E-cadherin junctions.* Nature Cell Biology, 2015. **17**(10): p. 1282-1293.
50. Ladoux, B., et al., *The mechanotransduction machinery at work at adherens junctions.* Integrative biology : quantitative biosciences from nano to macro, 2015. **7**(10): p. 1109-1119.
51. Yonemura, S., et al., *α-Catenin as a tension transducer that induces adherens junction development.* Nature Cell Biology, 2010. **12**(6): p. 533-542.
52. Shigenobu, Y., *A mechanism of mechanotransduction at the cell-cell interface.* BioEssays, 2011. **33**(10): p. 732-736.
53. Seddiki, R., et al., *Force-dependent binding of vinculin to α-catenin regulates cell-cell contact stability and collective cell behavior.* Molecular biology of the cell, 2018. **29**(4): p. 380-388.
54. Fletcher, D.A. and R.D. Mullins, *Cell mechanics and the cytoskeleton.* Nature, 2010. **463**(7280): p. 485-492.
55. Tang, D.D. and B.D. Gerlach, *The roles and regulation of the actin cytoskeleton, intermediate filaments and microtubules in smooth muscle cell migration.* Respiratory Research, 2017. **18**(1): p. 54.
56. Parent, C.A., *Making all the right moves: chemotaxis in neutrophils and Dictyostelium.* Current Opinion in Cell Biology, 2004. **16**(1): p. 4-13.
57. Sun, Z., S.S. Guo, and R. Fässler, *Integrin-mediated mechanotransduction.* The Journal of cell biology, 2016. **215**(4): p. 445-456.
58. Kline-Smith, S.L. and C.E. Walczak, *Mitotic Spindle Assembly and Chromosome Segregation: Refocusing on Microtubule Dynamics.* Molecular Cell, 2004. **15**(3): p. 317-327.
59. Strelkov, S.V., H. Herrmann, and U. Aebi, *Molecular architecture of intermediate filaments.* BioEssays, 2003. **25**(3): p. 243-251.
60. Herrmann, H., et al., *Intermediate filaments: from cell architecture to nanomechanics.* Nature Reviews Molecular Cell Biology, 2007. **8**(7): p. 562-573.
61. Geiger, B., J.P. Spatz, and A.D. Bershadsky, *Environmental sensing through focal adhesions.* Nature Reviews Molecular Cell Biology, 2009. **10**(1): p. 21-33.

62. Houdusse, A. and H.L. Sweeney, *How Myosin Generates Force on Actin Filaments.* Trends in biochemical sciences, 2016. **41**(12): p. 989-997.
63. Tojkander, S., G. Gateva, and P. Lappalainen, *Actin stress fibers – assembly, dynamics and biological roles.* Journal of Cell Science, 2012. **125**(8): p. 1855-1864.
64. Hotulainen, P. and P. Lappalainen, *Stress fibers are generated by two distinct actin assembly mechanisms in motile cells.* Journal of Cell Biology, 2006. **173**(3): p. 383-394.
65. Maninová, M. and T. Vomastek, *Dorsal stress fibers, transverse actin arcs, and perinuclear actin fibers form an interconnected network that induces nuclear movement in polarizing fibroblasts.* The FEBS Journal, 2016. **283**(20): p. 3676-3693.
66. Maninova, M., J. Caslavsky, and T. Vomastek, *The assembly and function of perinuclear actin cap in migrating cells.* Protoplasma, 2017. **254**(3): p. 1207-1218.
67. Tavares, S., et al., *Actin stress fiber organization promotes cell stiffening and proliferation of pre-invasive breast cancer cells.* Nature Communications, 2017. **8**(1): p. 15237.
68. Parsons, J.T., A.R. Horwitz, and M.A. Schwartz, *Cell adhesion: integrating cytoskeletal dynamics and cellular tension.* Nature Reviews Molecular Cell Biology, 2010. **11**(9): p. 633-643.
69. Yamashita, H., et al., *The role of the interaction of the vinculin proline-rich linker region with vinexin α in sensing the stiffness of the extracellular matrix.* Journal of Cell Science, 2014. **127**(9): p. 1875-1886.
70. Balaban, N.Q., et al., *Force and focal adhesion assembly: a close relationship studied using elastic micropatterned substrates.* Nature Cell Biology, 2001. **3**(5): p. 466-472.
71. Heasman, S.J. and A.J. Ridley, *Mammalian Rho GTPases: new insights into their functions from in vivo studies.* Nature Reviews Molecular Cell Biology, 2008. **9**(9): p. 690-701.
72. Lessey, E.C., C. Guilluy, and K. Burridge, *From Mechanical Force to RhoA Activation.* Biochemistry, 2012. **51**(38): p. 7420-7432.
73. Garcia-Mata, R., E. Boulter, and K. Burridge, *The 'invisible hand': regulation of RHO GTPases by RHOGDIs.* Nature Reviews Molecular Cell Biology, 2011. **12**(8): p. 493-504.
74. Guilluy, C., et al., *The Rho GEFs LARG and GEF-H1 regulate the mechanical response to force on integrins.* Nature cell biology, 2011. **13**(6): p. 722-727.
75. Burridge, K., *Focal adhesions: a personal perspective on a half century of progress.* The FEBS journal, 2017. **284**(20): p. 3355-3361.
76. Amano, M., et al., *Phosphorylation and Activation of Myosin by Rho-associated Kinase (Rho-kinase) **.* Journal of Biological Chemistry, 1996. **271**(34): p. 20246-20249.
77. Ohashi, K., et al., *Rho-associated Kinase ROCK Activates LIM-kinase 1 by Phosphorylation at Threonine 508 within the Activation Loop **.* Journal of Biological Chemistry, 2000. **275**(5): p. 3577-3582.
78. Uhler, C. and G.V. Shivashankar, *Regulation of genome organization and gene expression by nuclear mechanotransduction.* Nature Reviews Molecular Cell Biology, 2017. **18**: p. 717.
79. Lombardi, M.L., et al., *The Interaction between Nesprins and Sun Proteins at the Nuclear Envelope Is Critical for Force Transmission between the Nucleus and Cytoskeleton.* The Journal of Biological Chemistry, 2011. **286**(30): p. 26743-26753.
80. Isermann, P. and J. Lammerding, *Nuclear Mechanics and Mechanotransduction in Health and Disease.* Current biology : CB, 2013. **23**(24): p. 10.1016/j.cub.2013.11.009.

81. Gruenbaum, Y. and R. Foisner, *Lamins: Nuclear Intermediate Filament Proteins with Fundamental Functions in Nuclear Mechanics and Genome Regulation.* Annual Review of Biochemistry, 2015. **84**(1): p. 131-164.
82. Lovett, D.B., et al., *Modulation of Nuclear Shape by Substrate Rigidity.* Cellular and molecular bioengineering, 2013. **6**(2): p. 230-238.
83. Buxboim, A., et al., *Matrix Elasticity Regulates Lamin-A,C Phosphorylation and Turnover with Feedback to Actomyosin.* Current Biology, 2014. **24**(16): p. 1909-1917.
84. Guilluy, C., et al., *Isolated nuclei adapt to force and reveal a mechanotransduction pathway within the nucleus.* Nature cell biology, 2014. **16**(4): p. 376-381.
85. Huang, J., et al., *The Hippo Signaling Pathway Coordinately Regulates Cell Proliferation and Apoptosis by Inactivating Yorkie, the Drosophila Homolog of YAP.* Cell, 2005. **122**(3): p. 421-434.
86. Piccolo, S., S. Dupont, and M. Cordenonsi, *The Biology of YAP/TAZ: Hippo Signaling and Beyond.* Physiological Reviews, 2014. **94**(4): p. 1287-1312.
87. Zhao, B., et al., *The Hippo–YAP pathway in organ size control and tumorigenesis: an updated version.* Genes & Development, 2010. **24**(9): p. 862-874.
88. Zhao, B., et al., *A coordinated phosphorylation by Lats and CK1 regulates YAP stability through SCFβ-TRCP.* Genes & Development, 2010. **24**(1): p. 72-85.
89. Sudol, M., D.C. Shields, and A. Farooq, *Structures of YAP protein domains reveal promising targets for development of new cancer drugs.* Seminars in Cell & Developmental Biology, 2012. **23**(7): p. 827-833.
90. Yu, F.-X. and K.-L. Guan, *The Hippo pathway: regulators and regulations.* Genes & Development, 2013. **27**(4): p. 355-371.
91. Thomasy, S.M., et al., *Substratum stiffness and latrunculin B modulate the gene expression of the mechanotransducers YAP and TAZ in human trabecular meshwork cells.* Experimental Eye Research, 2013. **113**: p. 66-73.
92. Meli, V.S., et al., *YAP-mediated mechanotransduction tunes the macrophage inflammatory response.* Science advances, 2020. **6**(49): p. eabb8471.
93. Winkler, J., et al., *Concepts of extracellular matrix remodelling in tumour progression and metastasis.* Nature Communications, 2020. **11**(1): p. 5120.
94. Liu, F., et al., *Mechanosignaling through YAP and TAZ drives fibroblast activation and fibrosis.* American Journal of Physiology-Lung Cellular and Molecular Physiology, 2014. **308**(4): p. L344-L357.
95. Bertero, T., et al., *Matrix Remodeling Promotes Pulmonary Hypertension through Feedback Mechanoactivation of the YAP/TAZ-miR-130/301 Circuit.* Cell reports, 2015. **13**(5): p. 1016-1032.
96. Oliver-De La Cruz, J., et al., *Substrate mechanics controls adipogenesis through YAP phosphorylation by dictating cell spreading.* Biomaterials, 2019. **205**: p. 64-80.
97. Musah, S., et al., *Substratum-induced differentiation of human pluripotent stem cells reveals the coactivator YAP is a potent regulator of neuronal specification.* Proceedings of the National Academy of Sciences, 2014. **111**(38): p. 13805.
98. Yan, Y.-x., et al., *Mechanical strain regulates osteoblast proliferation through integrin-mediated ERK activation.* PloS one, 2012. **7**(4): p. e35709-e35709.
99. Makhija, E., et al., *Mechanical Strain Alters Cellular and Nuclear Dynamics at Early Stages of Oligodendrocyte Differentiation.* Frontiers in Cellular Neuroscience, 2018. **12**: p. 59.
100. Huang, S.-C., et al., *Mechanical strain modulates age-related changes in the proliferation and differentiation of mouse adipose-derived stromal cells.* BMC Cell Biology, 2010. **11**(1): p. 18.

101. Benham-Pyle, B.W., B.L. Pruitt, and W.J. Nelson, *Mechanical strain induces E-cadherin–dependent Yap1 and β-catenin activation to drive cell cycle entry.* Science, 2015. **348**(6238): p. 1024.
102. Codelia, V.A., G. Sun, and K.D. Irvine, *Regulation of YAP by mechanical strain through Jnk and Hippo signaling.* Current biology : CB, 2014. **24**(17): p. 2012-2017.
103. Wada, K.-I., et al., *Hippo pathway regulation by cell morphology and stress fibers.* Development, 2011. **138**(18): p. 3907-3914.
104. Zhao, B., et al., *Inactivation of YAP oncoprotein by the Hippo pathway is involved in cell contact inhibition and tissue growth control.* Genes & Development, 2007. **21**(21): p. 2747-2761.
105. Marjoram, R., E.C. Lessey, and K. Burridge, *Regulation of RhoA Activity by Adhesion Molecules and Mechanotransduction*. Vol. 14. 2014.
106. Furukawa, K.T., et al., *The Epithelial Circumferential Actin Belt Regulates YAP/TAZ through Nucleocytoplasmic Shuttling of Merlin.* Cell Reports, 2017. **20**(6): p. 1435-1447.
107. Kim, N.-G., et al., *E-cadherin mediates contact inhibition of proliferation through Hippo signaling-pathway components.* Proceedings of the National Academy of Sciences of the United States of America, 2011. **108**(29): p. 11930-11935.
108. Ji, X., et al., *αCP binding to a cytosine-rich subset of polypyrimidine tracts drives a novel pathway of cassette exon splicing in the mammalian transcriptome.* Nucleic acids research, 2016. **44**(5): p. 2283-2297.
109. Bielli, P., et al., *The Splicing Factor PTBP1 Promotes Expression of Oncogenic Splice Variants and Predicts Poor Prognosis in Patients with Non–muscle-Invasive Bladder Cancer.* Clinical Cancer Research, 2018. **24**(21): p. 5422.
110. Wang, Z.-N., et al., *High expression of PTBP1 promote invasion of colorectal cancer by alternative splicing of cortactin.* Oncotarget, 2017. **8**(22): p. 36185-36202.
111. Xue, Y., et al., *Genome-wide Analysis of PTB-RNA Interactions Reveals a Strategy Used by the General Splicing Repressor to Modulate Exon Inclusion or Skipping.* Molecular Cell, 2009. **36**(6): p. 996-1006.
112. Branon, T.C., et al., *Efficient proximity labeling in living cells and organisms with TurboID.* Nature Biotechnology, 2018. **36**: p. 880.
113. Díaz-Bello, B., et al., *Method for the Direct Fabrication of Polyacrylamide Hydrogels with Controlled Stiffness in Polystyrene Multiwell Plates for Mechanobiology Assays.* ACS Biomaterials Science & Engineering, 2019. **5**(9): p. 4219-4227.
114. Tse, J.R. and A.J. Engler, *Preparation of Hydrogel Substrates with Tunable Mechanical Properties.* Current Protocols in Cell Biology, 2010. **47**(1): p. 10.16.1-10.16.16.
115. Schwarz, U.S. and M.L. Gardel, *United we stand – integrating the actin cytoskeleton and cell–matrix adhesions in cellular mechanotransduction.* Journal of Cell Science, 2012. **125**(13): p. 3051.
116. Huveneers, S. and E.H.J. Danen, *Adhesion signaling – crosstalk between integrins, Src and Rho.* Journal of Cell Science, 2009. **122**(8): p. 1059.
117. Valon, L., et al., *Optogenetic control of cellular forces and mechanotransduction.* Nature communications, 2017. **8**: p. 14396-14396.
118. Nardone, G., et al., *YAP regulates cell mechanics by controlling focal adhesion assembly.* Nature Communications, 2017. **8**(1): p. 15321.
119. Ward, R.J., E. Alvarez-Curto, and G. Milligan, *Using the Flp-In™ T-Rex™ System to Regulate GPCR Expression*, in *Receptor Signal Transduction Protocols: Third Edition*, G.B. Willars and R.A.J. Challiss, Editors. 2011, Humana Press: Totowa, NJ. p. 21-37.

120. Tyanova, S., et al., *The Perseus computational platform for comprehensive analysis of (prote)omics data.* Nature Methods, 2016. **13**(9): p. 731-740.
121. Chaudhury, A., P. Chander, and P.H. Howe, *Heterogeneous nuclear ribonucleoproteins (hnRNPs) in cellular processes: Focus on hnRNP E1's multifunctional regulatory roles.* RNA (New York, N.Y.), 2010. **16**(8): p. 1449-1462.
122. Zhu, W., et al., *Roles of PTBP1 in alternative splicing, glycolysis, and oncogensis.* Journal of Zhejiang University. Science. B, 2020. **21**(2): p. 122-136.
123. Showalter, A.E., et al., *Investigating Chaperonin-Containing TCP-1 subunit 2 as an essential component of the chaperonin complex for tumorigenesis.* Scientific Reports, 2020. **10**(1): p. 798.
124. Franco, D. and M. Campione, *The Role of Pitx2 during Cardiac Development: Linking Left–Right Signaling and Congenital Heart Diseases.* Trends in Cardiovascular Medicine, 2003. **13**(4): p. 157-163.
125. Meng, Q., et al., *Signaling-dependent and coordinated regulation of transcription, splicing, and translation resides in a single coregulator, PCBP1.* Proceedings of the National Academy of Sciences, 2007. **104**(14): p. 5866.
126. Mazloomian, A., et al., *Pharmacological systems analysis defines EIF4A3 functions in cell-cycle and RNA stress granule formation.* Communications Biology, 2019. **2**(1): p. 165.
127. Chkheidze, A.N. and S.A. Liebhaber, *A novel set of nuclear localization signals determine distributions of the alphaCP RNA-binding proteins.* Molecular and cellular biology, 2003. **23**(23): p. 8405-8415.
128. Fischer, R.S., et al., *Stiffness-controlled three-dimensional extracellular matrices for high-resolution imaging of cell behavior.* Nature Protocols, 2012. **7**(11): p. 2056-2066.
129. Elosegui-Artola, A., et al., *Force Triggers YAP Nuclear Entry by Regulating Transport across Nuclear Pores.* Cell, 2017. **171**(6): p. 1397-1410.e14.
130. Wang, X., et al., *PCBP1 inhibits the expression of oncogenic STAT3 isoform by targeting alternative splicing of STAT3 exon 23.* International Journal of Biological Sciences, 2019. **15**(6): p. 1177-1186.
131. Zhang, T., et al., *PCBP-1 regulates alternative splicing of the CD44 gene and inhibits invasion in human hepatoma cell line HepG2 cells.* Molecular Cancer, 2010. **9**(1): p. 72.
132. Rajendran, D., et al., *Regulation of Numb isoform expression by activated ERK signaling.* Oncogene, 2016. **35**(39): p. 5202-5213.
133. Nasrollahi, S., et al., *Past matrix stiffness primes epithelial cells and regulates their future collective migration through a mechanical memory.* Biomaterials, 2017. **146**: p. 146-155.
134. O'Connor, K. and M. Chen, *Dynamic functions of RhoA in tumor cell migration and invasion.* Small GTPases, 2013. **4**(3): p. 141-147.
135. Paul, R., et al., *Propagation of Mechanical Stress through the Actin Cytoskeleton toward Focal Adhesions: Model and Experiment.* Biophysical Journal, 2008. **94**(4): p. 1470-1482.
136. Provenzano, P.P. and P.J. Keely, *Mechanical signaling through the cytoskeleton regulates cell proliferation by coordinated focal adhesion and Rho GTPase signaling.* Journal of Cell Science, 2011. **124**(8): p. 1195.
137. Zegers, M.M. and P. Friedl, *Rho GTPases in collective cell migration.* Small GTPases, 2014. **5**(3): p. e983869.
138. Li, Z., et al., *Regulation of PTEN by Rho small GTPases.* Nature Cell Biology, 2005. **7**(4): p. 399-404.

139. Liu, Y., et al., *Rho Kinase–Induced Nuclear Translocation of ERK1/ERK2 in Smooth Muscle Cell Mitogenesis Caused by Serotonin.* Circulation Research, 2004. **95**(6): p. 579-586.
140. Chuah, Y.J., et al., *Simple surface engineering of polydimethylsiloxane with polydopamine for stabilized mesenchymal stem cell adhesion and multipotency.* Scientific Reports, 2015. **5**(1): p. 18162.
141. Palchesko, R.N., et al., *Development of Polydimethylsiloxane Substrates with Tunable Elastic Modulus to Study Cell Mechanobiology in Muscle and Nerve.* PLOS ONE, 2012. **7**(12): p. e51499.
142. Butcher, D.T., T. Alliston, and V.M. Weaver, *A tense situation: forcing tumour progression.* Nature Reviews Cancer, 2009. **9**(2): p. 108-122.
143. Chaudhuri, O., et al., *Effects of extracellular matrix viscoelasticity on cellular behaviour.* Nature, 2020. **584**(7822): p. 535-546.
144. Huang, D., et al., *Viscoelasticity in natural tissues and engineered scaffolds for tissue reconstruction.* Acta Biomaterialia, 2019. **97**: p. 74-92.
145. Shamir, M., et al., *SnapShot: Timescales in Cell Biology.* Cell, 2016. **164**(6): p. 1302-1302.e1.
146. Panciera, T., et al., *Reprogramming normal cells into tumour precursors requires ECM stiffness and oncogene-mediated changes of cell mechanical properties.* Nature Materials, 2020. **19**(7): p. 797-806.
147. Kaukonen, R., et al., *Normal stroma suppresses cancer cell proliferation via mechanosensitive regulation of JMJD1a-mediated transcription.* Nature Communications, 2016. **7**(1): p. 12237.
148. Geuens, T., D. Bouhy, and V. Timmerman, *The hnRNP family: insights into their role in health and disease.* Human Genetics, 2016. **135**(8): p. 851-867.
149. Han, Siew P., Yue H. Tang, and R. Smith, *Functional diversity of the hnRNPs: past, present and perspectives.* Biochemical Journal, 2010. **430**(3): p. 379-392.
150. Grishin, N.V., *KH domain: one motif, two folds.* Nucleic Acids Research, 2001. **29**(3): p. 638-643.
151. Makeyev, A.V., A.N. Chkheidze, and S.A. Liebhaber, *A Set of Highly Conserved RNA-binding Proteins, αCP-1 and αCP-2, Implicated in mRNA Stabilization, Are Coexpressed from an Intronless Gene and Its Intron-containing Paralog.* Journal of Biological Chemistry, 1999. **274**(35): p. 24849-24857.
152. Shi, H., et al., *PCBP1 depletion promotes tumorigenesis through attenuation of p27Kip1 mRNA stability and translation.* Journal of Experimental & Clinical Cancer Research, 2018. **37**(1): p. 187.
153. Ghanem, L.R., et al., *The Poly(C) Binding Protein Pcbp2 and Its Retrotransposed Derivative Pcbp1 Are Independently Essential to Mouse Development.* Molecular and cellular biology, 2015. **36**(2): p. 304-319.
154. Pickering, B.M., et al., *Polypyrimidine tract binding protein and poly r(C) binding protein 1 interact with the BAG-1 IRES and stimulate its activity in vitro and in vivo.* Nucleic acids research, 2003. **31**(2): p. 639-646.
155. Chaudhury, A., et al., *TGF-β-mediated phosphorylation of hnRNP E1 induces EMT via transcript-selective translational induction of Dab2 and ILEI.* Nature Cell Biology, 2010. **12**(3): p. 286-293.
156. Chen, C., et al., *The biology and role of CD44 in cancer progression: therapeutic implications.* Journal of Hematology & Oncology, 2018. **11**(1): p. 64.
157. Tripathi, V., et al., *Direct Regulation of Alternative Splicing by SMAD3 through PCBP1 Is Essential to the Tumor-Promoting Role of TGF-β.* Molecular Cell, 2016. **64**(3): p. 549-564.

158. Jiang, P., et al., *Fyn/heterogeneous nuclear ribonucleoprotein E1 signaling regulates pancreatic cancer metastasis by affecting the alternative splicing of integrin β1.* International journal of oncology, 2017. **51**(1): p. 169-183.
159. Simpson, P.J., et al., *Structure and RNA Interactions of the N-Terminal RRM Domains of PTB.* Structure, 2004. **12**(9): p. 1631-1643.
160. Pilipenko, E.V., et al., *Cell-specific proteins regulate viral RNA translation and virus-induced disease.* The EMBO journal, 2001. **20**(23): p. 6899-6908.
161. Chou, M.-Y., et al., *Multisite RNA Binding and Release of Polypyrimidine Tract Binding Protein during the Regulation of c-src Neural-Specific Splicing.* Molecular Cell, 2000. **5**(6): p. 949-957.
162. Han, A., et al., *De Novo Prediction of PTBP1 Binding and Splicing Targets Reveals Unexpected Features of Its RNA Recognition and Function.* PLOS Computational Biology, 2014. **10**(1): p. e1003442.
163. Li, B. and T.S.B. Yen, *Characterization of the Nuclear Export Signal of Polypyrimidine Tract-binding Protein *.* Journal of Biological Chemistry, 2002. **277**(12): p. 10306-10314.
164. Ge, Z., et al., *Polypyrimidine tract binding protein 1 protects mRNAs from recognition by the nonsense-mediated mRNA decay pathway.* eLife, 2016. **5**: p. e11155.
165. Cho, C.-Y., et al., *PTBP1-mediated regulation of AXL mRNA stability plays a role in lung tumorigenesis.* Scientific Reports, 2019. **9**(1): p. 16922.
166. Kafasla, P., et al., *Polypyrimidine Tract Binding Protein Stabilizes the Encephalomyocarditis Virus IRES Structure via Binding Multiple Sites in a Unique Orientation.* Molecular Cell, 2009. **34**(5): p. 556-568.
167. Knoch, K.-P., et al., *Polypyrimidine tract-binding protein promotes insulin secretory granule biogenesis.* Nature Cell Biology, 2004. **6**(3): p. 207-214.
168. Takahashi, H., et al., *Significance of Polypyrimidine Tract–Binding Protein 1 Expression in Colorectal Cancer.* Molecular Cancer Therapeutics, 2015. **14**(7): p. 1705.
169. Christofk, H.R., et al., *The M2 splice isoform of pyruvate kinase is important for cancer metabolism and tumour growth.* Nature, 2008. **452**(7184): p. 230-233.
170. Dong, G., et al., *PKM2 and cancer: The function of PKM2 beyond glycolysis.* Oncology letters, 2016. **11**(3): p. 1980-1986.
171. Calabretta, S., et al., *Modulation of PKM alternative splicing by PTBP1 promotes gemcitabine resistance in pancreatic cancer cells.* Oncogene, 2016. **35**(16): p. 2031-2039.
172. Georgilis, A., et al., *PTBP1-Mediated Alternative Splicing Regulates the Inflammatory Secretome and the Pro-tumorigenic Effects of Senescent Cells.* Cancer cell, 2018. **34**(1): p. 85-102.e9.
173. Xie, J., et al., *Protein kinase A phosphorylation modulates transport of the polypyrimidine tract-binding protein.* Proceedings of the National Academy of Sciences, 2003. **100**(15): p. 8776.
174. Nallet-Staub, F., et al., *Cell density sensing alters TGF-β signaling in a cell-type-specific manner, independent from Hippo pathway activation.* Developmental cell, 2015. **32**(5): p. 640-651.
175. Schwartz, M.A., *Integrins and extracellular matrix in mechanotransduction.* Cold Spring Harbor perspectives in biology, 2010. **2**(12): p. a005066-a005066.
176. Mbalaviele, G., et al., *E-Cadherin Expression in Human Breast Cancer Cells Suppresses the Development of Osteolytic Bone Metastases in an Experimental Metastasis Model.* Cancer Research, 1996. **56**(17): p. 4063.

177. Conacci-Sorrell, M., et al., *Autoregulation of E-cadherin expression by cadherin-cadherin interactions: the roles of beta-catenin signaling, Slug, and MAPK.* The Journal of cell biology, 2003. **163**(4): p. 847-857.
178. Noren, N.K., et al., *Cadherin Engagement Regulates Rho family GTPases.* Journal of Biological Chemistry, 2001. **276**(36): p. 33305-33308.
179. Matsui, T.S. and S. Deguchi, *Spatially selective myosin regulatory light chain regulation is absent in dedifferentiated vascular smooth muscle cells but is partially induced by fibronectin and Klf4.* American Journal of Physiology-Cell Physiology, 2019. **316**(4): p. C509-C521.
180. Liu, H. and L. Tang, *Mechano-regulation of alternative splicing.* Current genomics, 2013. **14**(1): p. 49-55.
181. Inoue, D., S. Kido, and T. Matsumoto, *Transcriptional Induction of FosB/ΔFosB Gene by Mechanical Stress in Osteoblasts **.* Journal of Biological Chemistry, 2004. **279**(48): p. 49795-49803.
182. Bordeleau, F., et al., *Tissue stiffness regulates serine/arginine-rich protein-mediated splicing of the extra domain B-fibronectin isoform in tumors.* Proceedings of the National Academy of Sciences, 2015. **112**(27): p. 8314.
183. Zhang, X., et al., *Multilevel regulation and molecular mechanism of poly (rC)-binding protein 1 in cancer.* The FASEB Journal, 2020. **34**(12): p. 15647-15658.
184. Guo, J. and R. Jia, *Splicing factor poly(rC)-binding protein 1 is a novel and distinctive tumor suppressor.* Journal of Cellular Physiology, 2019. **234**(1): p. 33-41.
185. Bani-Yaghoub, M., et al., *A switch in numb isoforms is a critical step in cortical development.* Developmental Dynamics, 2007. **236**(3): p. 696-705.
186. Bechara, Elias G., et al., *RBM5, 6, and 10 Differentially Regulate NUMB Alternative Splicing to Control Cancer Cell Proliferation.* Molecular Cell, 2013. **52**(5): p. 720-733.
187. Dho, S.E., et al., *Characterization of Four Mammalian Numb Protein Isoforms: IDENTIFICATION OF CYTOPLASMIC AND MEMBRANE-ASSOCIATED VARIANTS OF THE PHOSPHOTYROSINE BINDING DOMAIN **.* Journal of Biological Chemistry, 1999. **274**(46): p. 33097-33104.
188. Wei, R., et al., *NUMB regulates the endocytosis and activity of the anaplastic lymphoma kinase in an isoform-specific manner.* Journal of Molecular Cell Biology, 2019. **11**(11): p. 994-1005.
189. Lu, Y., et al., *Alternative splicing of the cell fate determinant Numb in hepatocellular carcinoma.* Hepatology (Baltimore, Md.), 2015. **62**(4): p. 1122-1131.
190. Zhang, Y., et al., *Isoform-specific functions of Numb in breast cancer progression, metastasis and proteome remodeling.* bioRxiv, 2021: p. 2021.02.01.429237.
191. Wells, R.G., *The role of matrix stiffness in regulating cell behavior.* Hepatology, 2008. **47**(4): p. 1394-1400.
192. Schrader, J., et al., *Matrix stiffness modulates proliferation, chemotherapeutic response, and dormancy in hepatocellular carcinoma cells.* Hepatology, 2011. **53**(4): p. 1192-1205.
193. He, X., et al., *Involvement of polypyrimidine tract-binding protein (PTBP1) in maintaining breast cancer cell growth and malignant properties.* Oncogenesis, 2014. **3**(1): p. e84-e84.
194. Wang, X., et al., *PTBP1 promotes the growth of breast cancer cells through the PTEN/Akt pathway and autophagy.* Journal of Cellular Physiology, 2018. **233**(11): p. 8930-8939.

195. Keely, P.J., *Mechanisms by which the extracellular matrix and integrin signaling act to regulate the switch between tumor suppression and tumor promotion.* Journal of mammary gland biology and neoplasia, 2011. **16**(3): p. 205-219.
196. Lv, H., et al., *Mechanism of regulation of stem cell differentiation by matrix stiffness.* Stem cell research & therapy, 2015. **6**(1): p. 103-103.